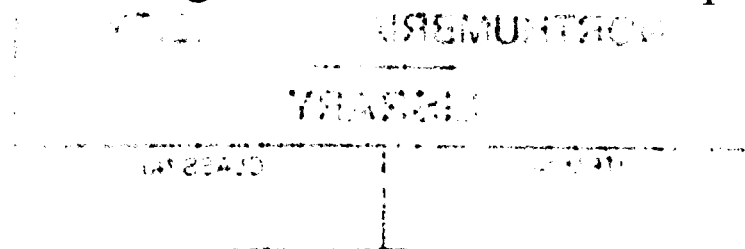# Northumbria Research Link

Increased Bandwidth Microstrip Antennas for Road Tolling Applications

Huw Evans

School of Engineering and Technology

University of Northumbria at Newcastle

A thesis submitted in partial fulfilment of the requirements

of the University of Northumbria at Newcastle for

the degree of Doctor of Philosophy

October 2004

Abstract

This thesis provides the results of research that has been carried out in order to develop the microstrip patch antennas required by a high speed digital communication link for road traffic applications. The operating frequency is 5.8GHz.

Although a single compact broad band radiating element is developed for use within the   vehicle, the main focus of the research is increasing the frequency bandwidth of the antenna arrays used within the road side unit of such a system. This is achieved by investigation into radiating element design, the orientation of the radiating elements within the array and the arrays feed networks geometry.

A single layer circularly polarised dual feed microstrip patch antenna is optimised for use within the array. Using a genetic algorithm to aid design of the dual feed network, the input impedance at the dual feed point is increased beyond what can normally be achieved when a tradition design process is adopted. This results in a more compact structure that allows thinner tracks to be used in the arrays feed network.

These radiating elements are sequentially rotated to form the array. The traditional corporate feed network is replaced by a series feed network and the effect this has upon the performance of a two, three and four element array is investigated. The four element array is suited to a vehicle access control application; due to the complexity the feed network an adaptation of simulated annealing is required to both generate and optimise the series feed line sections of this array. Not only does the new series feeding method result in doubling the VSWR 2:1 bandwidth of the four element array to over 10%, it also produces a more compact structure. Both mathematical modelling and experimental measurement are used to confirm the performance of these new arrays.

The four element array is then sequentially rotated to form a larger sixteen element array, that adopts the same series feeding method, suitable for motorway tolling applications. This new array demonstrates a VSWR 2:1 bandwidth of 14.7% and a 3 dB axial ratio bandwidth of 12.4%, an improvement factor of two over the same array

using a traditional corporate feed. The side lobes of this larger array are reduced by modifying the power distribution within the series feed network.

A single compact circularly polarised wide band microstrip patch antenna for use within the in-vehicle equipment is developed using an adaptation of the cavity model. The radiating patch is excited by a single feed line via a cross slot aperture. Air is used for the antenna substrate, increasing frequency bandwidth while simplifying the fabrication process hence reducing the manufacturing costs of the in-vehicle equipment. The inclusion of the wide band radiating element within the series fed four element array is also investigated. This new structure results in a VSWR 2:1 bandwidth of at least 22.8% and 3 dB axial ratio bandwidth of 17.5%, a significant improvement over traditional designs.

As a result of this research papers have been published in the IEE Electronic Letters (2000), the IEE Electronic Letters (2003) and Microwave and Optical Technology Letters (2003). Papers have been accepted and presentations have been made at the Ansoft microwave workshop in London (2001) and Los Angeles (2001). This work has also contributed towards publications in the IEE Electronic Letters (2000) and in the IEE Transactions on Antenna and Propagation (2001).

The antenna arrays developed during the course of this research have been used within a commercially viable traffic management system and installed at a large shopping centre. It is pleasing to note that the fruits of this research have been used in a 'real life' situation.

Acknowledgements

I would like to express my sincere thanks to my director of studies Professor Alistair Sambell for his faith, guidance and technical support.

Thanks are also due to my second supervisor Dr Sean Danaher and Mark Leach for their help with the mathematics.

I would also like to express my appreciation to Mr Peter Gale for his invaluable help and guidance with the practical work.

Finally I wish to thank my wife, Sandra Evans for her patience, support and encouragement throughout the course of my studies.

Abbreviations

BER	Bit Error Rate
CEPT	Conference of Europe Posts and Telecommunications
CW	Carrier Wave
DPSK	Differential Phase Shift Key
DSRC	Digital Short Range Communication link
ERIP	Effective Isotropic Radiated Power
LHCP	Left Hand Circular Polarisation
MGA	Multi-objective Genetic Algorithm
MoM	Method of Moments
MPIE	Mixed-Potential Integral Equation
NRZ	Non Return to Zero
OBU	On Board Unit
PC	Personal Computer
PCB	Printed Circuit Board
PSK	Phase Shift Key
Q	Quality factor
RHCP	Right Hand Circular Polarisation
RSU	Road Side Unit
SA	Simulated Annealing
VSWR	Voltage Standing Wave Ratio

Table of Contents

CHAPTER 1

INTRODUCTION AND OVERVIEW OF THESIS

1.1 Background

Throughout the developed world there has been a large increase in road use which in turn has led to an increase in both road traffic congestion and driver frustration. This also raises environmental concerns about the increased demand for new roads and the amount of pollution generated by grid-locked vehicles.

Within the United Kingdom the car population is likely to increase by up to 50% in the next thirty years [1] increasing the congestion on already overcrowded motorways. This is not only confined to motorways; for many years now, in response to urban congestion, there has been a trend towards pedestrianised 'car free' city centers and park and ride schemes. Further, in the 2000 Transport Act and the integrated transport white paper July 1998 that gave rise to it, there is a requirement for local authorities to further reduce traffic in urban areas by at least 10%.

Pedestrianised city centers will require some form of automated access control for emergency vehicles, public transport, taxis and deliveries. In addition, there is commercial interest in vehicle access control for automated car parks used by universities, hotels and other private and public authorities. The requirement for access control extends further to restricted areas within secure installations such as government buildings, police stations and MOD sites.

Consequently, traffic management systems are required to optimise traffic flow through some form of fee collection, redistributing traffic from congested areas, allowing access or priority travel for public services in urban environments and also producing traffic information so that drivers can avoid, not contribute to, traffic congestion [2].

Currently, the most popular method for automatic fee collection is a two-way high speed Digital Short Range Communication link (DSRC) between a On Board Unit (OBU) placed behind the windscreen of a vehicle and a Road Side Unit (RSU) [3] as seen in Figure 1-1.
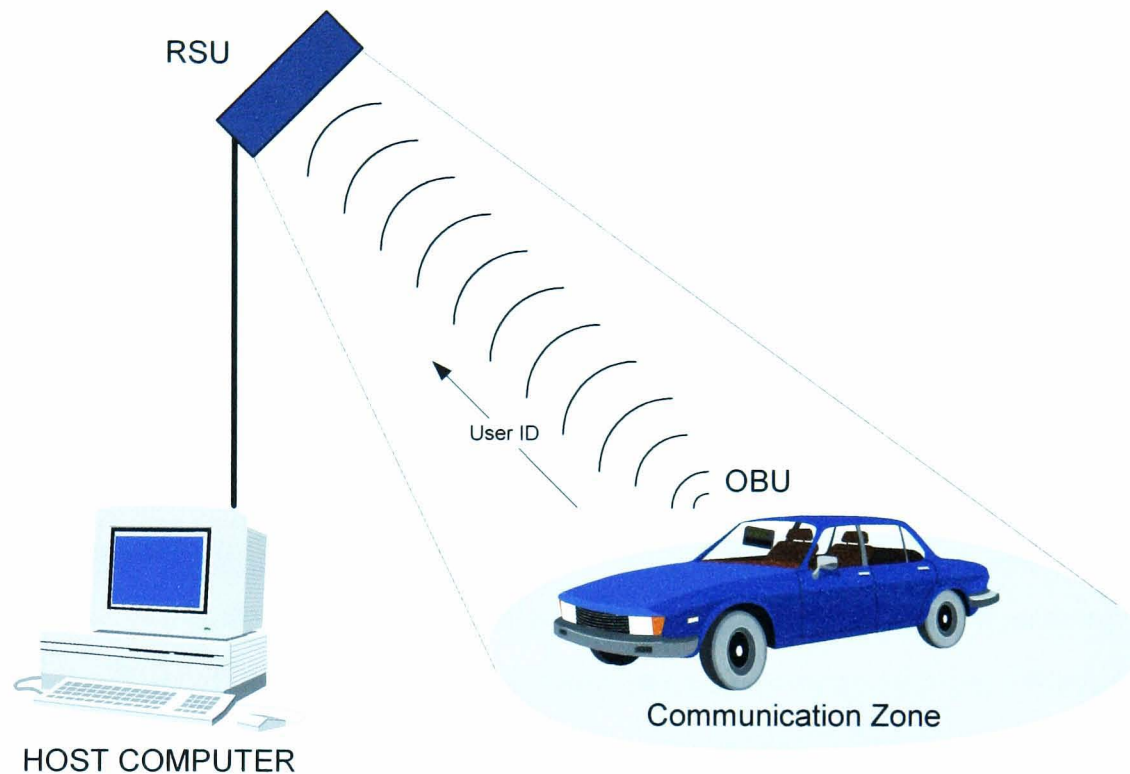
Figure 1-1: Vehicle DSRC system.

The DSRC system uses a 5.8 GHz microwave carrier frequency allocated by the Conference of Europe Posts and Telecommunications (CEPT) for road transport and traffic applications. Circular polarisation is used as it allows the OBU to be placed in any orientation behind the windscreen and helps to discriminate between reflected signals. As the vehicle enters the communication zone the OBU wakes from a low power sleep state and transmits a unique ID to the RSU. This ID is sent to a back office for data processing enabling some form of fee collection. A fully comprehensive description of the DSRC traffic management system can be found in Appendix A.

Within the UK road user charging has been mainly restricted to tunnels and bridges. However the first urban toll was introduced in Durham City during 2002 and the UK's first implementation of motorway tolling occurred on a 27 mile duplicate section of the M6 motorway which connects Junction 11 in Staffordshire with

Junction 4 in Warwickshire in December 2003. Furthermore, the Department for Transport is currently running an extensive DSRC test trial near Leeds to assess the feasibility of implementing full scale road user charging on UK motorways.

Globally, there has already been a large increase in the use of DSRC for road user charging; both in direct response to rising congestion and automating existing toll collection facilities [4]. This in turn has led to a great deal of recent academic research [5,6,7,8] and commercial interest in this area.

The development of traffic management systems has been of particular interest at the University of Northumbria at Newcastle for some time. In June 1994, Tak Kong Chan presented a thesis entitled 'Development of a two-way microwave communication system for traffic applications' [9]. This detailed the results of research that had been carried out in order to realise a DSRC system suitable for motorway tolling. A basic system was developed, including a circularly polarised 4x4 planar patch antenna array for use in the RSU. The effects of mutual coupling and investigation into side lobe levels were presented. The antennas used in this system had limited frequency bandwidth. In 1997 in 'Modelling and application of a cross aperture coupled single feed circularly polarised patch antenna'[10], Tamas Valasit presented research that had been carried out in order to increase the bandwidth of the OBU's antenna using a single cross slot aperture coupled patch antenna, operating at 2.4GHz. A strip slot foam inverted patch construction method was used to improve the axial ratio bandwidth performance and loosen the requirement for tight manufacturing tolerances. However this new multi-layer structure increased manufacturing complexity leading to an increase in fabrication cost. For future work he suggested, *inter alia*, using air for the antenna's substrate with the OBU's plastic case as the patch's superstructure and cross aperture coupled patch arrays.

Today, there are two distinct application scenarios: vehicle access control and motorway tolling. In a vehicle access control application, there is a logistical requirement for the range between the OBU and the RSU to be restricted to the length of one vehicle. Furthermore a wider communication zone is advantageous as lane discipline cannot always be guaranteed at a barrier entry. For motorway use, greater range is required allowing the RSU to be mounted above the carriageway on an

overhead gantry. In a motorway application it is also important that the communication zone is restricted to a single lane.

While a common OBU is preferred for both applications, the communication zone requirements differ. These requirements can be satisfied using RSU antenna arrays that meet the specifications defined in Table 1-1.

RSU Application	OBU Read range	3 dB Beam width	Operating frequency	Gain	Main / Side lobe isolation
Access control	5 meters	40 degrees	5.8 GHz	12 dBi	12 dB
Motorway tolling	12 meters	20 degrees	5.8 GHz	18 dBi	20 dB

Table 1-1: Specification for RSU antenna arrays.

The microstrip patch antenna is an attractive choice for use within a traffic management system due to the low profile, physically robust structure and ease of manufacture. Moreover, the required beam shape for each application may be readily achieved using different arrays of microstrip elements.

A significant disadvantage of microstrip antennas is the narrow operational bandwidth, which increases fabrication costs due to the requirement for tighter manufacturing tolerances. Furthermore, a DSRC traffic management system with a narrow operational bandwidth will lack long term stability, be less tolerant to varying environmental conditions and more sensitive to the de-tuning effect of the vehicle's windscreen. This leads to a reduction in system reliability, which is unacceptable in this application since financial transactions are involved. Therefore, this thesis investigates new microstrip antenna structures with enhanced frequency bandwidth performance for use within the RSU and the OBU of a traffic management system.

A novel array feed structure, employing sequential rotation with serial feed, is proposed and investigated. Physical or sequential rotation of radiating elements within a circularly polarised array, with an appropriate offset in feed phase, has been shown to increase array bandwidth [11]. This technique can be applied to the arrays used

within the RSU. It has been shown that a dominant factor affecting the performance of such an array is the relationship between internal reflections within the feed network of the array [12]. The relationship between these internal reflections is highly dependant upon the particular choice of feed geometry. Previous research into using this technique has been directed towards arrays employing some form of corporate feed network. Series feed networks have the advantage of being less complex, more compact, having lower insertion loss, and lower line losses when compared to corporate feeds [13]. Traditionally, a series fed array exhibits a narrower frequency bandwidth than a corporate fed array, as the distance between each radiating element and the feed point is not equal. However, the unequal feed length also applies to a corporate feed when used in sequentially rotated array because of the requirement for phase delays in radiating element excitation. Therefore this thesis investigates the frequency performance of a new sequentially rotated array using a series feeding system.

The use of an aperture coupled antenna structure to enhance the bandwidth of the radiating element in the OBU is also investigated. As the OBU is mounted behind the windscreen of a vehicle, it needs to be compact and have a low profile to avoid obscuring the driver's view. Due to the close proximity of the vehicle's windscreen and unpredictable environmental conditions, robust frequency performance is required to ensure reliable operation. These requirements can be satisfied by a single broadband antenna. Aperture coupling results in the antenna having a wider bandwidth [14,15]. A further advantage of aperture coupling is that it is possible to optimise the radiation mechanism by using a low permittivity material for the antenna substrate and high permittivity low loss material for the feed network [16]. This thesis considers the modelling and design of a 5.8GHz single feed circular polarised cross aperture coupled antenna, where the radiating patch is supported above the aperture using the OBU's enclosure, allowing the use of air for the antenna's substrate while simplifying the manufacturing process. The potential to apply the cross aperture coupled antenna within the series fed sequentially rotated array is also explored.

1.2 Aims and objectives

The aim of this research is to increase the frequency bandwidth of the antennas used in a 5.8 GHz DSRC system. This will be achieved by developing two novel arrays for

use within the RSU that satisfy the two application scenarios and a single broadband element for use within the OBU.

This will involve:

- Optimising the design of a planar dual feed circular polarised radiating element for use in the RSU arrays.
- Investigating the benefit of using a series feeding system in sequentially rotated arrays for bandwidth enhancement.
- Optimising the design of a four-element series fed sequentially rotated array for use in a RSU suited to an access control application.
- Sequentially rotating this four element array to form a larger 16 element array, which shares the same series feeding technique, suited to a motorway tolling application.
- Developing a single broadband radiating element for use within the OBU operating at 5.8 GHz using air for the antenna substrate.

1.3 Overview of thesis

This thesis contains a total of nine chapters. Microstrip patch antennas are introduced in Chapter 2 where a brief historical background and review of current research into this area is presented. The radiation mechanism is described and the various excitation techniques identified and appraised. Circular polarisation is presented and methods for its generation described. The various operational parameters of patch antenna are presented with other issues of interest to an antenna designer such as losses. Techniques for modelling patch antenna are introduced, these cover both simple models that give a good physical insight into the operation of the antenna and the more complex modelling and simulation techniques that can provide a higher degree of accuracy. Microstrip arrays are introduced and the advantages and disadvantages of various feed geometries discussed. The principle of sequential rotation of radiating elements within arrays is described including a literature survey of current research in this area.

Chapter 3 studies the optimised design of a dual feed circularly polarised patch antenna for use in an array. A traditional dual feed design approach is detailed including the various design equations necessary for determining the dimensions of

the radiating patch and the realisation of the microstrip feed line sections that make up the dual feed network. A model for the antenna is developed using a transmission line model to represent the radiating patch and the dual feed network. Physical restrictions within the traditional design approach are identified and the consequences of these upon the antenna quantified. A genetic algorithm is then used to optimise the design parameters of the dual feed network, increasing the input impedance at the feed point of the antenna beyond what is traditionally possible, making it more desirable for use in an array as thinner tracks can be used within the array's feed network. Undesirable step discontinuities between the feed sections are also minimised. This work has contributed towards an IEE Electronic Letter that presents the use of a genetic algorithm to optimise the design of the dual feed network [17]. Experimental measurement validate the integrity of the model and this optimised design.

In Chapter 4, modelling and experimental work provide the basis for an investigation into the frequency performance of sequentially rotated arrays that employ a series feeding system. The concept of sequential rotation is presented with current generic mathematical models used to assess potential array performance. It is shown that these models are inadequate as they do not cater for specific array geometry which is shown to have a significant effect on array performance. The design and frequency performance of two, three and four element series fed sequentially rotated arrays are presented. A comparison is made between the performance of these arrays using the new series feed structure and the same arrays using a more traditional corporate feeding system. Comparative performance between the use of both dual and single fed radiating elements in the series fed arrays is also assessed and quantified. Experimental measurement validates the integrity of the model and verifies the performance of the new series fed arrays.

Chapter 5 concentrates on the optimal design of a four-element series fed array suitable for use within the RSU in an access control application. The large number of feed design variables makes manual generation of these variables problematic. An adaptation of Simulated Annealing (SA) is developed to both generate and optimise the values of the individual feed sections. Optimum choice of dual feed radiating element in this array is assessed by comparing the performance of the optimised design presented in Chapter 3 with a traditional dual feed design. As a direct result of

7

this work an IEE Electronic Letter that presents the optimisation of the series feed network has been published [18]. The performance of the optimised four element array is confirmed using both full wave simulation and practical measurement.

In Chapter 6 a larger sixteen element antenna array for use within the RSU in a motorway tolling application is presented. The optimised 2x2 sub-arrays presented in Chapter 5 are themselves sequentially rotated to form a larger sixteen element 4x4 array that adopts the same series feeding method. Radiation pattern control is achieved by varying the distribution of power across the array. The resulting reduction in side lobes helps restrict the communication zone of the RSU to a single lane. As a direct result of this work an IEE Electronic Letter that presents the performance of this new 4x4 array has been published [19]. Full wave simulation and experimental measurement confirm the performance of this new array.

Chapter 7 presents the design of a single broadband radiating element suited for use within the OBU. Energy from a microstrip feed line is coupled through a cross-shaped aperture to a nearly square patch. A low loss material is used for the feed substrate and air is used as a thicker low permittivity antenna substrate allowing the radiating patch to be supported by the OBU's enclosure. An adaptation of the cavity model is used to aid and optimise this design. This work has contributed to a paper published in the IEE Transactions on Antennas and Propagation that presents this model [20]. This broadband radiating element is then used within the four element array presented in Chapter 4 and the resulting frequency performance quantified. A paper detailing the performance of this new wideband array has been published in the Microwave and Optical Technology Letters [21]. The integrity of this novel design is confirmed by both full-wave simulation and experimental measurement.

In Chapter 8 a review and summary of this research work is presented along with suggestions for further work.

1.4 Summary of published work

1. Aljibouri B., Lim E.G., Evans H, and Sambell A. `Multiobjective genetic algorithm approach for a dual feed circular polarised patch antenna design', Electron. Lett. vol 36, No 12, pp.1005-1006, March 2000.

2. Evans H., Gale P., Aljibouri B., Lim E.G., Korolkiewicz E and Sambell A.:'Application of simulated annealing to the design of serial feed sequentially rotated 2x2 antenna array', Electron. Lett., vol 36, No 24, pp.1987-1988, November 2000.

3. Evans H.:'Performance and application of a 5.8GHz 2x2 sequentially rotated patch array with a serial feed'. Ansoft 'No Boundries' microwave workshop, Bracknell, October 2000.

4. Evans H.:'Optimum Design of a Sequentially Rotated 2x2 Circular Polarised Patch Array.", UNN research seminar, December 2000.

5. Evans H.:'Increasing the bandwidth of a 2x2 sequentially rotated patch array with a serial feed'. Ansoft HFSS/Ensemble users microwave workshop, Los Angeles, CA, January 2001.

6. Aljibouri B., Evans H., Lim E. G., Korolkiewicz, E.K., and Vlasits, T.:'Cavity Model of circularly polarised cross-aperture-coupled microstrip antenna', IEE Proc. Antennas Propag. vol 148, No 3, pp.147-152, June 2001.

7. Evans H., Gale P. and Sambell A.:'Performance of a 4x4 Sequentially Rotated Patch Antenna Array Using a Series Feed.', Electron. Lett, vol 39, No 6, pp.493 – 494, March 2003.

8. Evans H., and Sambell A.:'Wideband 2x2 sequentially rotated patch antenna array with a series feed'. Microwave and Optic Technology Lett. vol 40, No 4, pp.293 – 294, February 2004.

CHAPTER 2

MICROSTRIP PATCH ANTENNAS

2.1 Introduction

Following a comprehensive review of current literature, this chapter presents the basic principles of microstrip patch antenna. Following a brief historical introduction, the electrical and physical characteristics are introduced including the radiation mechanism and alternative feeding techniques. The concept of circular polarisation is presented and methods for generating this reviewed. The key operational parameters which characterise the antenna performance are presented. Techniques of analysis for microstrip antenna are also described. Finally, various array configurations and feed line geometries used in microstrip patch arrays are presented and discussed.

2.2 Microstrip patch antennas

Patch or microstrip antennas were first presented in the 1950s [22,23] but it was not until the 1970s that serious attention was paid to this type of radiating element, it first being realised by Munson [24]. There are many variations in patch shape, feeding techniques, substrate configurations and array geometries. The basic configuration of a patch antenna consists of a metallic patch printed onto a grounded dielectric substrate. Substrates commonly used for microstrip antennas are usually in the range of $2.2 \leq \varepsilon_r \leq 25$ with a loss tangent from 0.0001 to 0.004 [25]. Patch antennas have a very low profile, are mechanically robust and are easily manufactured using traditional printed circuit board techniques. This leads to a low profile conformable structure that can be fabricated at low cost.

Due to the low profile (0.01 - 0.05 free space wavelength) and light weight, patch antennas are ideal for mounting on plane surfaces such as aircraft and missiles as they have no significant affect on the aerodynamics. They are easily integrated with associated circuit elements and it is relatively easy to achieve the various wave polarisations which different applications may require. Due to these physical attributes patch antennas are ideally suited for use within a traffic management

system. The small size and low profile of the antenna allows an unobtrusive OBU when mounted behind the vehicles windscreen. The ease of manufacture and resulting low cost is an important consideration if large quantities of OBUs are required in large scale motorway tolling applications. The compact and robust nature of microstrip antenna arrays makes them ideal for use in the RSU where access for maintenance can be problematic especially when mounted to a gantry over a live road carriageway.

To date, patch antennas have also been used in a wide variety of alternative applications such as: satellite ground stations, telecommunications, satellites for television broadcasting, mobile phone communications, aeronautical applications, marine applications and GPS systems for detection and identification [26].

However, the patch antenna has several operational disadvantages. These include narrow frequency bandwidth of typically $2 - 3\%$ [27], spurious feed radiation, limited power handling capability and poor polarisation purity. The majority of research to date has been aimed at trying to overcome these problems.

2.3 Radiation mechanism

The antenna is driven with a voltage between the feed point and the ground plane. This excites current on the patch and a vertical electric field between the patch and the ground plane. The patch element resonates when its length is near $\lambda/2$, leading to relatively large current and field amplitudes.

The electromagnetic radiation mechanism occurs between the two edges of the patch antenna and the ground plane. The patch is considered as a perfect conductor so it is assumed that there is no electric field on the patch surface. These edges are not a perfect open circuit, since the dielectric substrate is usually electrically thin ($< 0.05\lambda$) compared to the wavelength at the design frequency. Consequently fringing fields appear at the edges of the patch as shown in Figure 2-1.
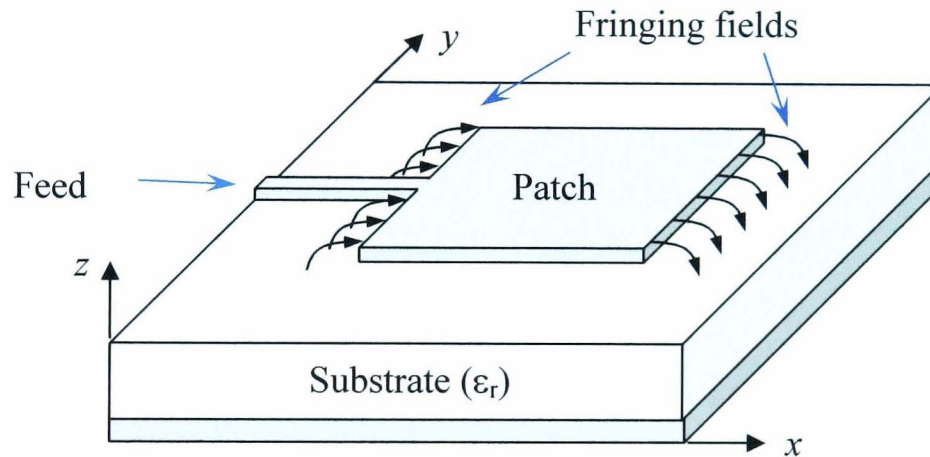
Figure 2-1: Fringing fields from patch antenna fed by a microstrip line.

These fringing fields can be split into normal and tangential components with respect to the ground plane. The normal components are 180 degrees out of phase, as the patch length is $\lambda/2$, therefore cancel out in the far field in the broadside direction. The tangential components (those parallel to the ground plane) are in phase, thus the fields combine to give maximum radiated field normal to the surface of the patch antenna [28].

The extent of the fringing fields depends on the dimensions of the patch and the height of the substrate. For the principal E-plane, fringing is a function of the ratio between the length of the patch L and the height of the substrate h (L/h) and the

dielectric constant of the substrate ε_r. Since the length of a patch is much greater than its height fringing is small, however it must be considered as it influences the resonant frequency of the antenna.

The Quality factor (Q) of a patch antenna on a thin substrate is large and the bandwidth is small. The bandwidth increases with an increase in substrate thickness and a decrease in substrate permittivity. Consequently, patch antennas operate best when the substrate is thick with a low dielectric constant, as it requires loosely bound fields for radiation into space. Furthermore, a lower dielectric constant reduces the generation of surface waves. However, a thin substrate with a high dielectric constant is preferred for the microstrip lines that make up the feed network, as they require tightly bound fields to prevent undesired radiation or coupling. As both feed and antenna are often fabricated on the same substrate, a compromise must be made between good feed and radiating element performance [29].

2.4 Excitation Techniques

2.4.1 Direct feed

Early patch antennas all used a direct feeding method, either through a microstrip line as seen in Figure 2-2 (a) or through a coaxial probe as seen in Figure 2-2 (b).

(a)

(b)
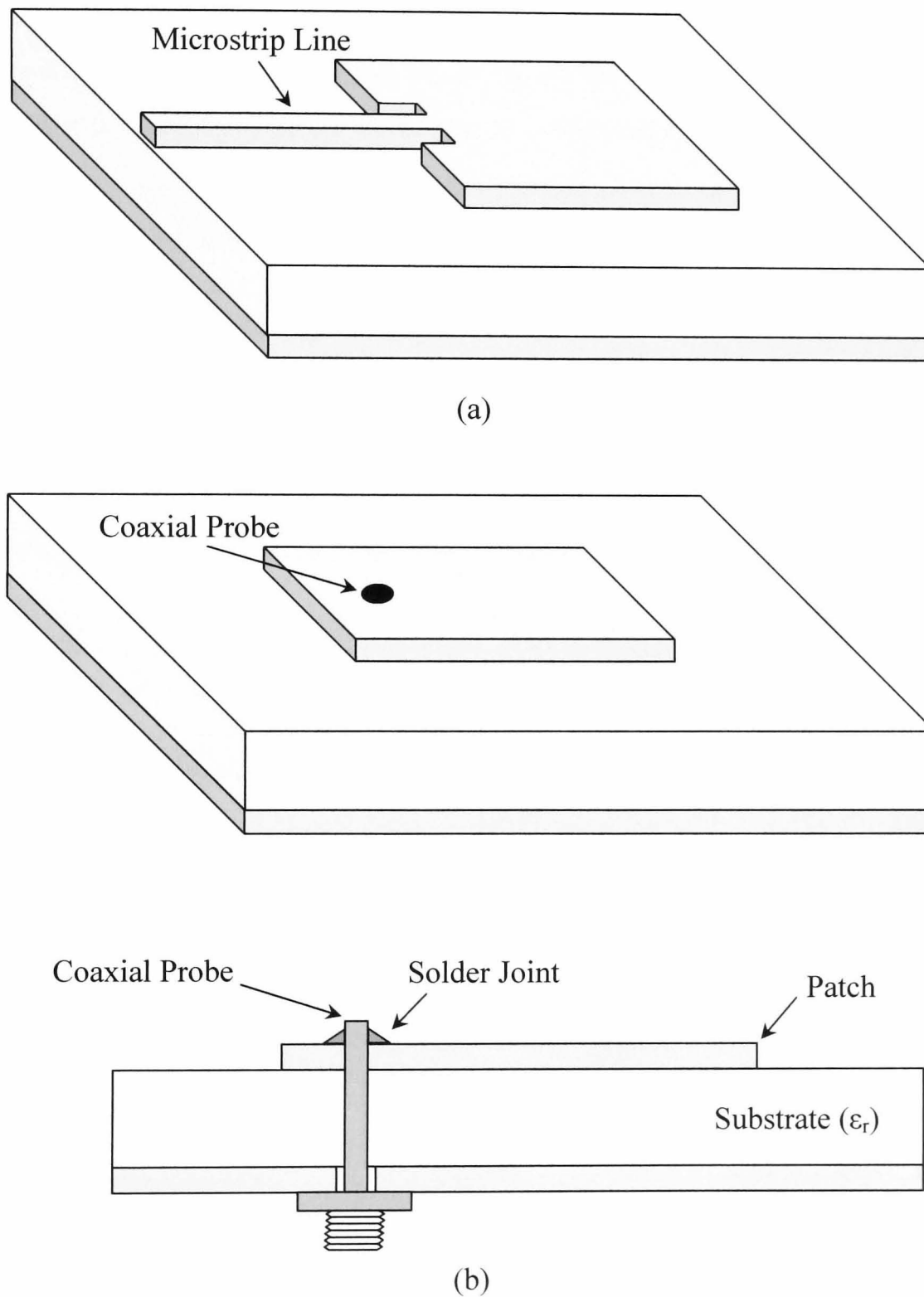
Figure 2-2: (a) Offset microstrip feed line (b) Coaxial probe feed including side elevation.

Direct contact feeding methods have the advantage of simplicity, but often have a limited bandwidth and increased feed inductance [30]. With coaxial line feeds the inner conductor of the coax is attached to the radiating patch while the outer conductor is connected to the ground plane. Although impedance matching can be simply achieved, as described later, manufacture becomes far more complex and antenna reliability is decreased significantly by the necessity for solder joints [26], particularly if used in arrays. The advantage of using microstrip feed lines is that they preserve the desirable features which are attributed to the radiating patch. Ease of manufacture is maintained as the feed network is fabricated during the same photo etching process as the radiating patch; furthermore this feeding method leads to the most robust structure with lowest profile.

2.4.2 Aperture Coupling

The aperture coupled patch antenna [31] consists of separate feed and patch substrates which are separated by a ground plane as seen in Figure 2-3. On the bottom side of the lower substrate there is a feed line whose energy is coupled to the patch through a slot in the ground plane that separates the two substrates.
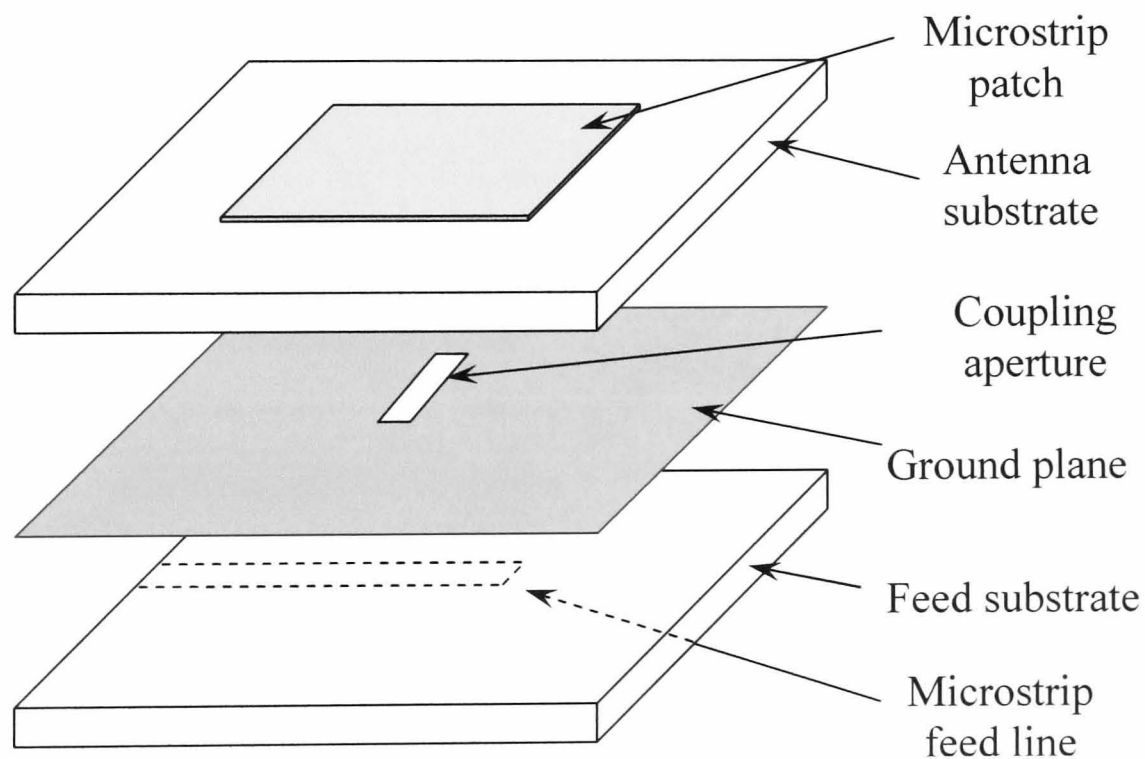
Figure 2-3: Aperture coupled feed arrangement.

Input impedance matching is performed by controlling the length of the slot and the width of the feed line, which is extended beyond the aperture thereby acting as a tuning stub removing any residual reactance from the aperture.

Compared with direct feed system, the aperture coupled feed arrangement offers a number of advantages. As the feed network and radiating patch are implemented on separate substrates, both the thickness and dielectric properties of each substrate can be independently optimised catering for their conflicting requirements. The patch is isolated from the feed network by a ground plane, minimising the contribution of spurious feed radiation to the main radiation pattern. Furthermore, as the aperture is positioned below the centre of patch, the excitation symmetry ensures good polarisation purity. A disadvantage is that this structure is usually more complex to fabricate. A more detailed study of aperture coupled patch antennas is presented in Chapter 7.

2.4.3 Proximity coupling

The proximity or electromagnetically coupled patch antenna uses a two layer substrate with a microstrip feed line on top of the lower substrate, terminating in an open ended stub. The patch is printed on the upper substrate as seen in Figure 2-4.
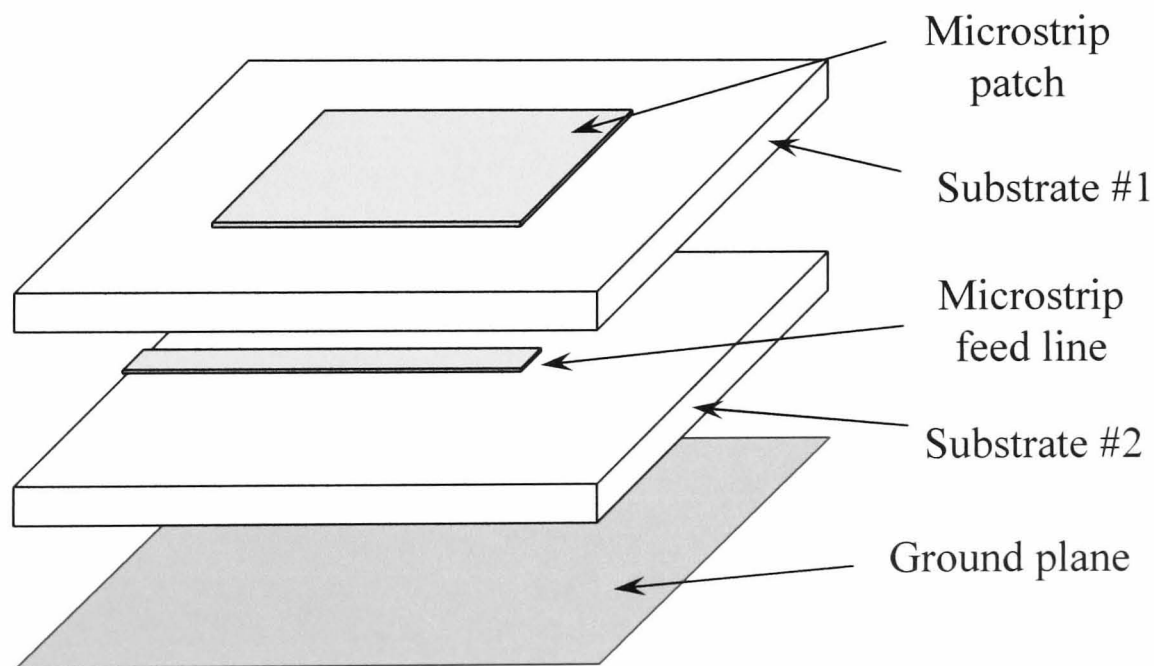
Figure 2-4: Proximity coupled feed arrangement.

Originally developed for printed dipoles [32], this technique was later used to increase the bandwidth of patch antennas [33,34,35,36] demonstrating bandwidths of up to 13%. The length of the feed stub and the patch width to feed line width ratio controls the input impedance. This method has also been used in arrays [37].

Like aperture coupling, proximity coupling also has the advantage of allowing the patch substrate to be relatively thick allowing much greater bandwidth, while the feed line effectively sees thinner substrate reducing spurious radiation. Thus a reduction in the area of the feed network, hence overall antenna system, is achieved. Furthermore, spurious radiation due to discontinuities in the feed lines is reduced considerably. However, due to the need for reasonable accuracy in the alignment of the feed and patch, fabrication is made more difficult.

2.5 Circular Polarisation

2.5.1 Wave polarisation

The electric field vector for a traveling wave propagating in the positive z direction has the form

$$E = E_x \sin(\omega t - \beta z)\hat{i} + E_y \sin(\omega t - \beta z + \phi)\hat{j} \qquad (2.1)$$

where βz is phase shift and ϕ is the phase difference between E_x and E_y. If $E_x = 0$ then the electric field is orientated in the y direction only and the wave is linearly polarised as seen in Figure 2-5 (a).

(a)   (b)   (c)
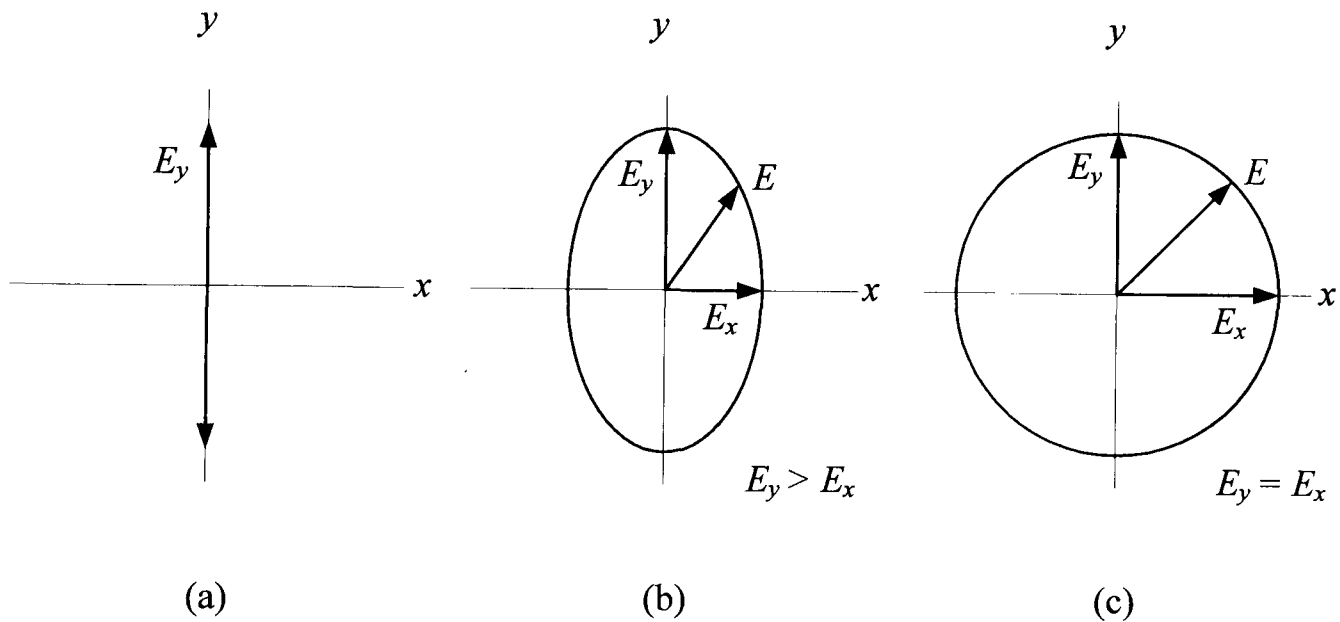
Figure 2-5: States of wave polarisation. (a) Linear polarisation (b) Elliptical polarisation (c) Circular polarisation.

If $E_x \neq 0$ and $E_y \neq 0$ then the wave has two components as shown in Figure 2-5 (b), the electric field vector traces out an elliptical locus and the wave is termed elliptically polarised. If the x and y directed field components are equal in amplitude and the phase angle between them is 90 degrees, the locus of the wave vector traces a circular path making one complete revolution during one period of the wave. This wave is said to be circular polarised as shown in Figure 2-5 (c).

If $\phi = +90°$ the rotation of the field vector, looking in the direction of propagation, is anti-clockwise and the wave is defined as being Left Hand Circular Polarised (LHCP). If $\phi = -90°$ the rotation of the field vector is clockwise and is defined as being Right Hand Circular Polarised (RHCP).

An advantage of using circular polarisation is that the rotational orientation of a transmitter and receiver are unimportant in relation to received signal strength. In a vehicle tagging application, circular polarisation allows the OBU to be placed in any orientation behind a vehicles windscreen. Furthermore, when a circularly polarised wave is reflected from a metallic surface, such as from a vehicle's bonnet or an adjacent vehicle, the sense of polarisation reverses from left hand to right hand (and vice versa). This allows the system to discriminate between reflected signals.

Four distinct sources of error that degrade polarisation purity have been identified [38].

1. Amplitude error: both linearly polarised components must be of equal amplitude.
2. Phase error: the phase shift between the two linear polarised components must be 90 degrees.
3. Orthogonality error: the two linear polarised components have to be orthogonal.
4. Polarisation error: the two orthogonal components must be linear polarised with no cross-polarisation.

The first two errors usually depend on the characteristics and electrical design, while the latter two depend on the physical design of the antenna.

2.5.2 Feeding techniques for circular polarisation

Circular polarised radiation can be generated if two orthogonal modes are both equal in magnitude and have a 90 degree phase shift between them. This can be achieved using a single patch with a dual or single feed mechanism. Two orthogonal modes can be generated by two linearly polarised patches placed orthogonally in space [39]. The main problem with this method is that polarisation purity degrades away from broadside because the phase centers of the patches are displaced.

2.5.2.1 Dual feed

Circular polarisation can be achieved using a square or circular patch fed at two adjacent sides [40, 41], quadrature phase difference can be achieved by altering the length of one of the feeds or by using a 90 degree hybrid as seen in **Figure 2-6**.

(a)   (b)
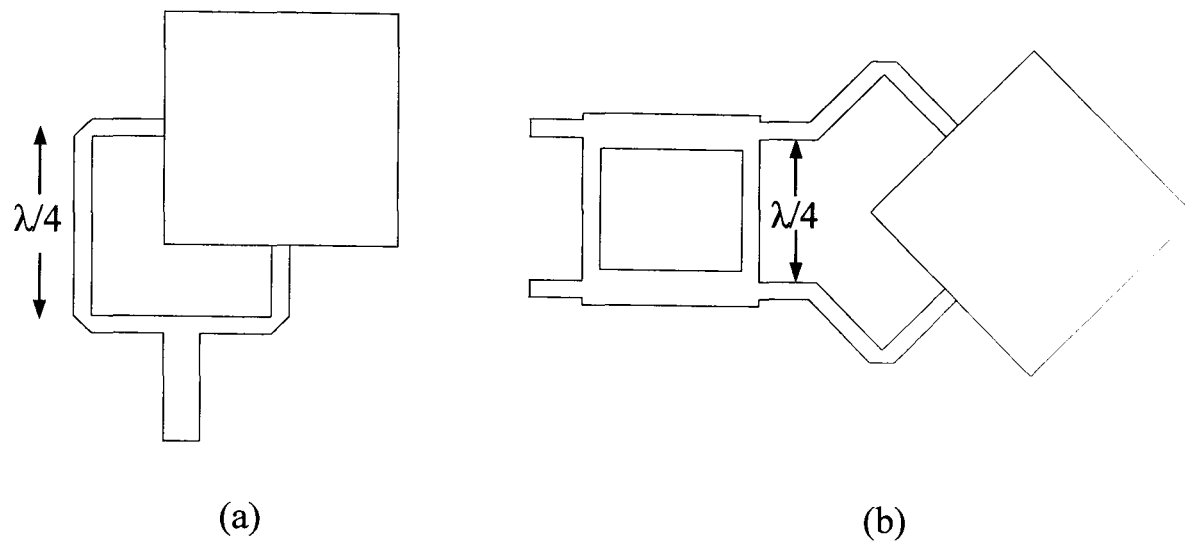
Figure 2-6: Dual feed patch driven at adjacent sides (a) through an offset power divider, (b) through a 90 degree hybrid coupler.

In the non-isolated feed network seen in Figure 2-6 (a) reflections from the mismatched patch, away from design frequency, tend to cancel out at the input terminal due to the 90 degree phase difference between the feeds. Consequently, the input match remains acceptable over the bandwidth of a single mode. Unfortunately, due to the lack of isolation between the ports, the polarisation purity of one mode is degraded by reflected power from the other [42]. For the isolated feed, seen in Figure 2-6 (b), good axial ratio and input match can be achieved as reflected power is absorbed in a matched load on the other input port of the hybrid coupler. The two input ports also allow for the radiated field to be in either left or right hand circular polarisation. However this advantage is offset by the additional real estate required by this geometry.

2.5.2.2 Single feed

A single feed or degenerate mode patch is regarded as one of the simplest radiators of circularly polarised radiation. Some common examples can be seen in Figure 2-7.

<p style="text-align:center">(a)   (b)   (c)</p>
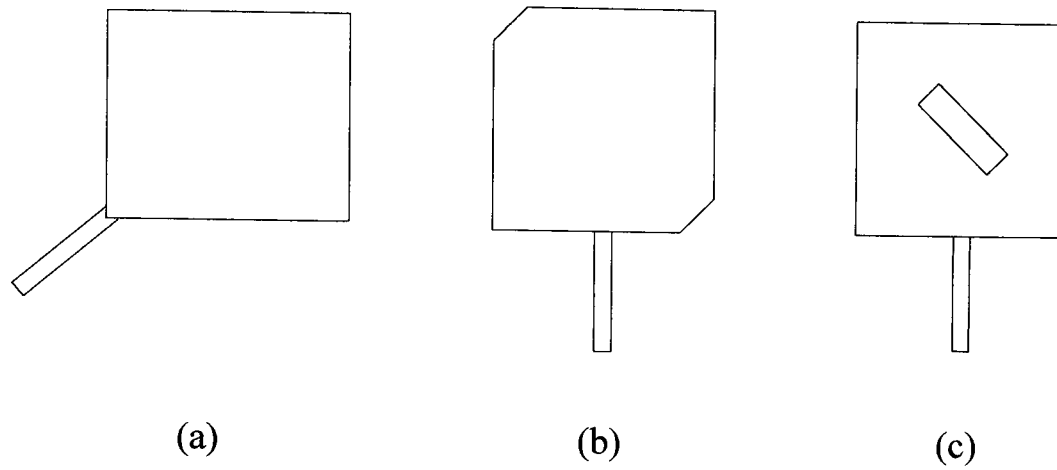
Figure 2-7: Nearly Square [43,44], Truncated Corner [45], Slotted Square [46].

The generated mode can be separated into two orthogonal modes, Mode 1 and 2. The radiated fields excited by these modes (TM_{010} and TM_{001}) are orthogonally polarised in the broadside direction. The amplitude and phase of these modes can be seen in Figure 2-8.

<p style="text-align:center">(a)</p>
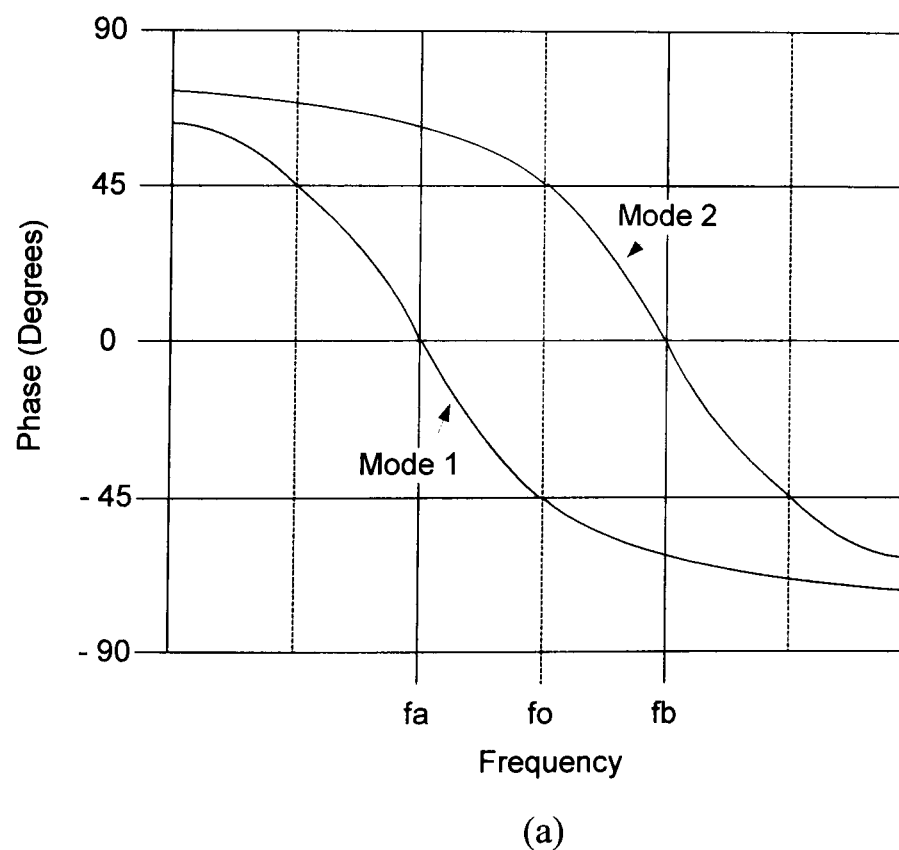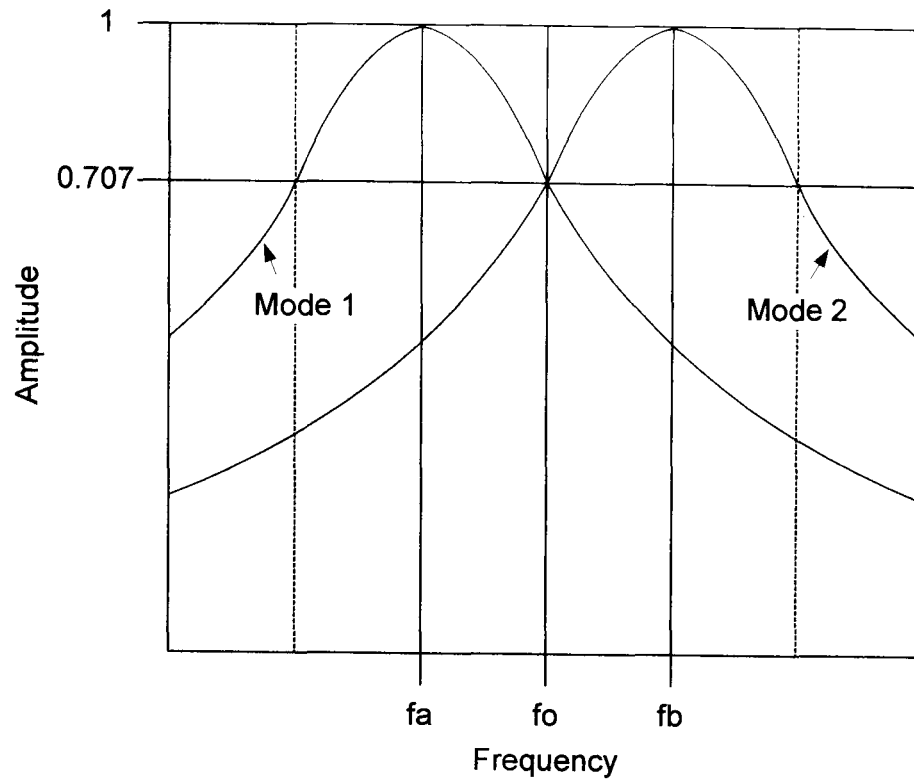
Figure 2-8: (a) Amplitude and (b) phase of orthogonal modes in single feed circular polarised patch antenna [47].

The perturbation segment is adjusted so that the two modes are equal in magnitude and 90 degrees out of phase at the design frequency. Consequently, circular polarised radiation is achieved without the use of an external polariser.

Performance is similar to the non-isolated dual feed arrangement seen in Figure 2-6 (a), with the axial ratio degrading fairly rapidly away from design frequency while the input VSWR remains acceptable [48]. The drawback to this type of radiating element is the sensitivity of the perturbation segment's dimensions, requiring very tight manufacturing tolerances and greater sensitivity to mutual coupling when used in an array [49].

2.6 Operational parameters

Operational parameters of interest in microstrip antenna design are as follows.

2.6.1 Resonant frequency

The resonant frequency is defined as the frequency at which the input impedance is purely resistive and most of the power fed to the antenna is radiated. The dominant resonant frequency can be determined using [50]

$$f_r = \frac{c}{2L_{eff}\sqrt{\varepsilon_{eff}}} \tag{2.2}$$

where c is the speed of light in free space, where L_{eff} is the effective length of the patch and ε_{eff} is the effective permittivity of the antenna substrate (discussed further in Chapter 3).

The patch can also resonate at higher resonant frequencies or higher order resonant TM modes, both along the length and width of the patch, as seen in Figure 2-9.

(a)

(b)

(c)

(d)
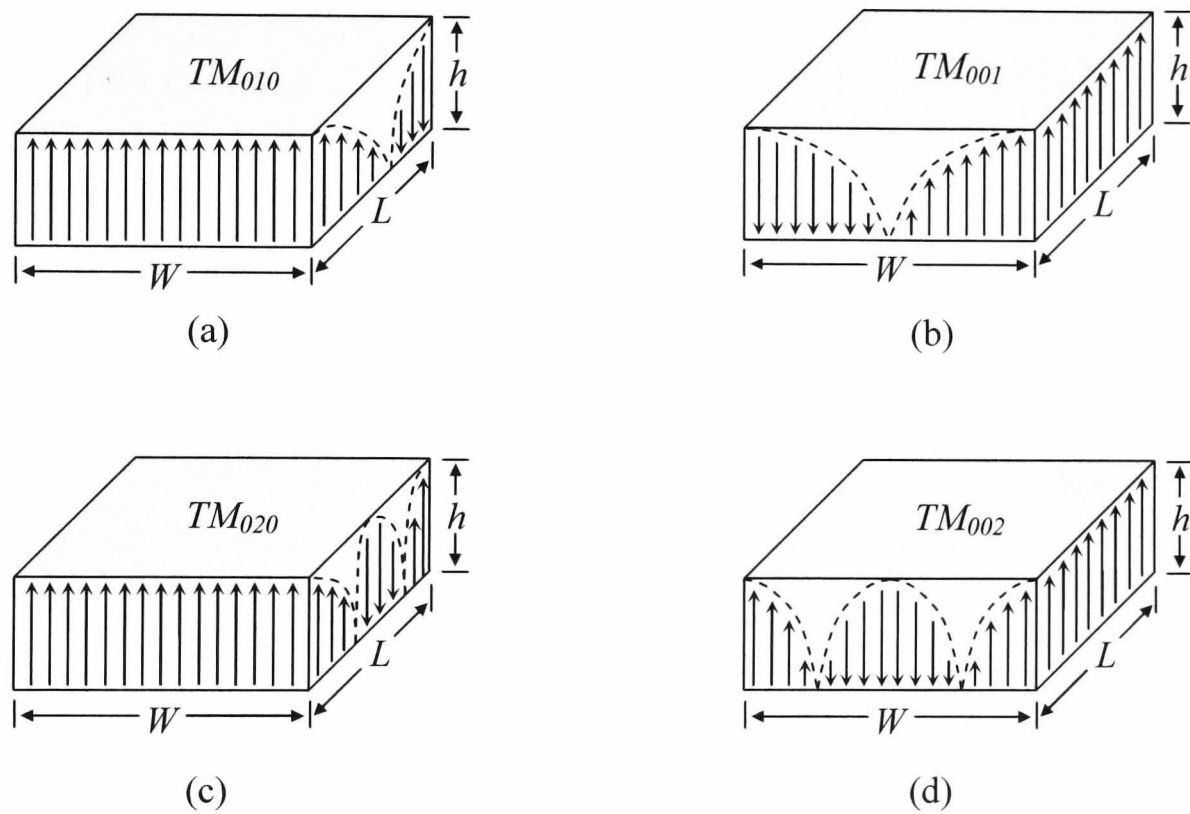
Figure 2-9: E-field distribution of resonant modes within rectangular patch antenna.

The mode with the lowest resonant frequency is the dominant mode. For all patch antenna, the height is much less than both the length and the width. Assuming $L > W$ the dominant mode will be the TM_{010} mode as seen here in Figure 2-9 (a). If $L > W > L/2$ the next higher order mode will be the TM_{001} mode, seen in Figure 2-9 (b). However, If $L/2 > W$ then TM_{020} will be the second order mode as seen in Figure 2-9 (c).

2.6.2 Input impedance

Input impedance is defined as the impedance presented by the antenna at its input feed point. For a feed point at a radiating edge the voltage is at a maximum and the current is at a minimum, so the input impedance is at a maximum, typically between 150-350 ohms [26]. As the patch length is approximately $\lambda/2$, if the feed point were at the centre of the patch the voltage is zero while the current is at a maximum so the input impedance is zero. Therefore adjusting the position of the feed point can vary the input impedance to the antenna.

An input impedance of 50 ohms is traditionally required at the feed point of an antenna. This value is a compromise between the characteristic impedance of an air filled coaxial line where attenuation (77Ω) is at a minimum and power capacity (30Ω) is at a maximum [51]. Altering the feed position to achieve this value is easily achieved with a probe feed. With a microstrip feed line the feed is offset (as seen in Figure 2-2 (a)) which creates a physical notch that in turn introduces a junction capacitance. This will influence the resonant frequency which would typically vary by about 1% [52]. Alternatively, a quarter wave section of microstrip feed line can be used to match this impedance to the periphery of the radiating patch.

At resonance the input impedance to the antenna is purely resistive, the antenna and feed are matched and no power is reflected back into the antenna's feed network. Away from resonance the antenna and feed are no longer matched and some of the power is reflected. A good measure of this mismatch is the Voltage Standing Wave Ratio (VSWR) which is equal to one under matched conditions. The VSWR is given by

$$VSWR = \frac{1+|\Gamma|}{1-|\Gamma|} \qquad \text{where} \qquad 1 \leq VSWR \leq \infty \qquad (2.3)$$

where Γ is the reflection coefficient, defined in terms of the input impedance Z_L of the antenna and the characteristic impedance of the feed line Z_0 with the relationship

$$\Gamma = \frac{Z_L - Z_0}{Z_L + Z_0} \tag{2.4}$$

The reflection coefficient is equal to zero under matched conditions as no power is reflected.

2.6.3 Axial ratio

The polarisation purity of a circularly polarised antenna is characterised by its axial ratio. The axial ratio is defined as the ratio between the major and minor axis, as defined in Figure 2-10, and is given by equation (2.5) [50]. This represents the ratio of the maximum to minimum signal strength of the electric field vector components.

$$AR = \frac{MajorAxis}{MinorAxis} = \frac{OA}{OB} \qquad 0 \le AR \le \infty \tag{2.5}$$

where

$$OA = E_x^2 + E_y^2 + \sqrt{E_x^4 + E_y^4 + 2E_x^2 E_y^2 \cos 2\theta} \tag{2.6}$$

and

$$OB = E_x^2 + E_y^2 - \sqrt{E_x^4 + E_y^4 + 2E_x^2 E_y^2 \cos 2\theta} \tag{2.7}$$

E_x and E_y are the magnitude of the radiated field components and θ is the phase difference between them.
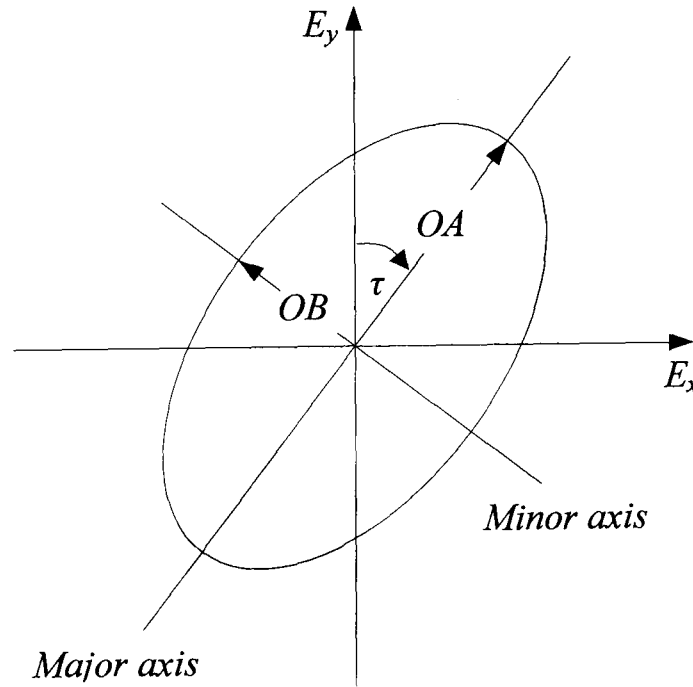
Figure 2-10: Rotation of a plane electromagnetic wave and its polarisation ellipse.

τ is the azimuth angle of the major axis, as described further in Appendix C.

In terms of magnitude and phase difference of the radiated field components, AR is given by

$$AR = 10 Log \left[\frac{E_x^{\ 2} + E_y^{\ 2} + \sqrt{E_x^{\ 4} + E_y^{\ 4} + 2E_x^{\ 2}E_y^{\ 2}\cos 2\theta}}{E_x^{\ 2} + E_y^{\ 2} - \sqrt{E_x^{\ 4} + E_y^{\ 4} + 2E_x^{\ 2}E_y^{\ 2}\cos 2\theta}} \right] \qquad (2.8)$$

This parameter is usually expressed in dB. For perfect circular polarisation $OA = OB$ and the axial ratio is 1. An axial ratio of 3 to 6 dB is acceptable for most practical applications [53] although axial ratio performance as low as 1 dB can be required by applications such as small satellite ground stations [54].

2.6.4 Bandwidth

The bandwidth of an antenna is defined as the range of frequencies within which the performance of an antenna, with respect to some specified characteristic, conforms to a specified standard [50]. Input impedance bandwidth is often specified over the range of frequencies where the VSWR at the feed point is less than 2, which corresponds to a return loss of 9.5 dB or 11% reflected power. More stringent applications may require the VSWR to be less than 1.5 (which corresponds to a return loss of 14 dB or 4% reflected power). Axial ratio bandwidth is commonly quoted as the range of frequencies where axial ratio is less than 3 dB. When describing the bandwidth of a patch antenna, the bandwidth is often expressed as a percentage of the resonant frequency.

2.6.5 Gain

Assuming no direction is specified, the relative gain of an antenna is defined as [50]

$$G = \frac{\text{Maximum radiation intensity}}{\text{Maximum radiation intensity from a reference antenna with same power}}$$

The power input must be the same for both antennas; the reference antenna is usually a lossless isotropic source. The antenna gain is measured in dB and for microstrip antennas the gain is typically in the region of 5 - 6 dB broadside.

2.6.6 Radiation Pattern

The radiation pattern of an antenna is determined in the far field region and is a graphical representation of the radiation properties. Figure 2-11 (a) shows a typical radiation pattern for LHCP square microstrip antenna. Antenna gain is plotted in dB against ϕ where $\theta = 0$ and $\theta = 90$ as defined by the coordinate system seen in Figure 2-11 (b).

(a)   (b)
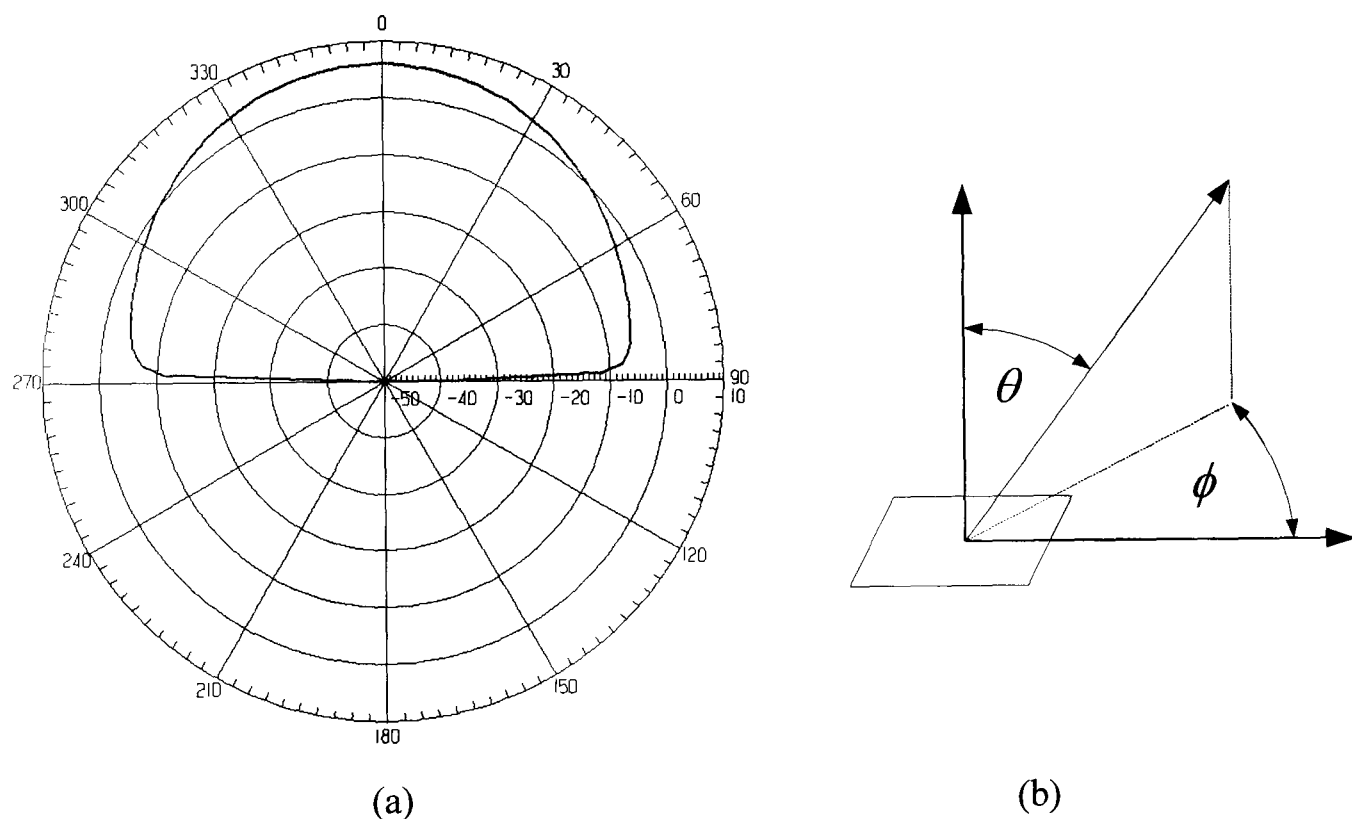
Figure 2-11: (a) Typical radiation pattern (b) Coordinate system.

2.6.7 Beamwidth

Antenna beamwidth usually refers to the angle between two points on the main lobe 3 dB below the maximum point.

2.6.8 Quality factor and Antenna losses

The quality factor or Q of a microstrip antenna is inversely proportional to the gain bandwidth. It is defined in terms of resonant frequency f_r and 3 dB bandwidth '$2\Delta f$' as

$$Q_t = \frac{f_r}{2\Delta f} \qquad (2.9)$$

The quality factor also represents the antenna losses. In terms of the power loss factor the total Q factor Q_t is given by

$$\frac{1}{Q_t} = \frac{1}{Q_d} + \frac{1}{Q_c} + \frac{1}{Q_r} \qquad (2.10)$$

where Q_r is the radiation loss factor, Q_c is the conductance loss factor and Q_d is the dielectric loss factor. The individual 'Q' terms in equation (2.10) are defined as follows

The dielectric loss Q-factor Q_d represents energy lost by heat generated in the dielectric and can be determined using

$$Q_d = \frac{1}{\tan \delta} \qquad (2.11)$$

Which is independent of the dimensions of the antenna, $tan\ \delta$ is the loss tangent of the dielectric.

The copper loss Q-factor is given by

$$Q_c = h\sqrt{\mu_0 \pi f_r \sigma_c} \qquad (2.12)$$

Where σ_c is the conductivity and h is the height of the metal used.

The radiation loss Q-factor is given by

$$Q_r = \frac{\pi}{4 G_r Z_0} \qquad (2.13)$$

Where G_r is the self conductance and Z_0 is the characteristic impedance of the patch. The following three relationships for G_r have been shown [26]

$$G_r = \frac{W_e}{120\lambda_0} - \frac{1}{60\pi^2} \qquad 0.35\lambda_0 \le W_e \le 2\lambda_0 \qquad (2.14)$$

W_e is the effective width of the patch and μ_0 is the free space wave length.

The antenna can excite surface waves that bond to the dielectric substrate and, as this power does not contribute to the main radiation pattern, these waves can be regarded as a loss mechanism. They are transmitted from the antenna into the dielectric and remain trapped there by repeated internal reflections between the ground plane and air-dielectric interface. The generation of surface waves increases with both substrate thickness and permittivity, however for thin substrates, the losses due to surface waves are very small and can be neglected [55].

2.7 Modelling planar patch antennas

At microwave frequencies, the dimensions of the radiating patch and feed network are crucial and small variations can have significant affect on performance. Antenna analysis is therefore a very important part of the design process as it reduces the amount of expensive and time consuming trial and error attempts, particularly when the antenna is to be optimised over a number of design parameters.

The simple physical structure of a microstrip patch antenna might suggest a straight forward mathematical model. This is not in fact not the case, the determination of the electromagnetic fields of the antenna being a complex problem. Full wave analysis requires the determination of the electromagnetic field structure within a microstrip structure; Maxwell's equations must be solved under the appropriate boundary conditions. This is problematical for a number of reasons. Due to the inhomogeneous nature of the structure, the fields propagate in the contiguous media of air and dielectric. The air-dielectric interface is partially covered with metal so different boundary conditions apply at different points of the interface. Further, the transverse dimensions of the ground plane and substrates are finite.

Due to the difficulty involved in a rigorous analysis, two simplified models have been developed which can provide useful information especially in the more basic microstrip structures, namely the transmission line and cavity model. These models are especially good for practical design as well as providing a good physical insight into antenna operation.

The transmission line model of a rectangular patch antenna was the first model used in microstrip antenna analysis [56,57,58].This is the simplest model to be analysed and has limited accuracy. A number of improvements have been made [59,60,61] which improve the model's accuracy and versatility. This model is described further in Chapter 3.

The cavity model can easily be applied to regular shaped patches [62,63]. The space under the patch and above the ground plane is regarded as a lossy resonant cavity bound by magnetic walls at the edges and electric walls top and bottom. The fields under the patch, derived from microwave cavity theory [64], can be considered as resonant TM modes as seen in Figure 2-9. The actual length of the patch is slightly smaller than the cross section of the equivalent cavity. This is due to fringing fields, therefore the resonant frequency of an actual patch must be determined taking these fields into account. A radiation and loss resistance must be introduced as without this the resonant cavity would not radiate and the input impedance would be purely resistive. Both input impedance and resonant frequency can be determined from this analysis and have been shown to compare well with measurements [65]. The multi port network model is also a generalisation of the cavity model [66,26]. An adaptation of the cavity model is used later in Chapter 7.

Full-wave analysis is a rigorous modelling technique in which the current distribution on the conducting elements is established. The currents produce electromagnetic fields which must satisfy certain boundary conditions determined by the antenna structure. The electromagnetic fields are determined from Maxwell's equations which relate the fields, current sources and charges. This is most commonly achieved using the exact Green's function for the dielectric substrate. Utilising Green functions in a Moment of Methods (MoM) solution results in versatile and accurate analysis that can incorporate space wave radiation, surface wave models. dielectric loss and mutual

coupling into the analysis. Maxwell's equations can be expressed in either differential or integral form, and the vector field and current densities can be given in time-varying or time harmonic form. The consequence is more accurate results for input impedance and resonant frequency, however the model is complex, computational cost is high and it does not lend itself to optimisation so readily.

Today commercial software designed to simulate patch antenna structures using full wave simulation is widely available. Not only is accuracy high but these packages also have additional benefits such as drawing interfaces and the ability to export designs in a format suited to the Printed Circuit Board (PCB) fabrication process. A highly respected market leader in this field is a product from Ansoft called Ensemble®.

Ensemble® can deal with irregular shapes, multiple layers and finite ground planes with a high degree of accuracy. Once the designer has defined thickness, material and properties of dielectric substrate(s), the design can be imported into the package or entered using a graphical interface. The structure's surface is then automatically 'meshed' or broken down into simple geometric shapes. A volume mesh is not generated inside the model because at high frequencies the skin depth is so small that a surface mesh is sufficient. To generate a solution from which S-parameters can be computed, Ensemble® employs the Mixed-Potential Integral Equation (MPIE) method. The MoM is applied to the MPIE to obtain the current distribution on the surface mesh. The S-parameters and radiated fields are calculated from the surface currents.

2.8 Microstrip Arrays

In many microstrip antenna applications a single patch will meet the necessary system requirements. However some systems require a higher gain while maintaining a low profile structure. For these applications, microstrip arrays offer several advantages relative to other types of antenna arrays: low weight, low profile with conformability and low manufacturing cost. These attractive features lead to many military, space and commercial applications [67] using microstrip arrays instead of conventional high gain antenna arrays such as horns, helices, slotted waveguides and parabolic reflectors. These advantages are offset by microstrip antenna arrays inherent drawbacks, namely small bandwidth (usually less than 5%), relatively high feed line loss and power handling capability [68].

2.8.1 Feed network

Most single element excitation techniques can be applied to microstrip arrays. The feed network is one of the most important aspects of an array as it occupies valuable space, radiates spurious signals and consumes power through dielectric and ohmic losses. As the size of the array increases so does the average distance between the feed point and the patch radiators. Therefore these problems increase with array size as the length of the microstrip lines increase and probe fed arrays require more solder joints. Alternative methods such as parasitic coupling are one response to these problems. By parasitic coupling several patches to a driven patch, it is possible to transfer some of the power division tasks from the feed network to the radiating elements. This has been demonstrated with up to fifteen elements, only one being driven by the feed network [69]. A 1280 element array was constructed from 256 clusters of five elements, the centre element of each cluster being aperture coupled from the feed network [70]. However, there is little freedom of alter the patch spacing and hence manipulate the resulting radiation pattern of such an array.

Microstrip feed lines are an attractive choice of feed method as they maintain the desirable features normally associated with the patch radiators (light weight, low profile with conformability and low cost due to manufacturing simplicity). Additionally, using microstrip feed lines allows for easy control of the feed section's characteristic impedance, providing a degree of freedom not so easily obtained using

32

other feed methods such as waveguides. Major disadvantages of using microstrip lines as a feeding method within arrays are the losses such as the copper loss, dielectric loss and radiation loss sometimes contributing to the radiation pattern [71].

One of the difficulties encountered in designing planar microstrip arrays is the limitation of space [26]. Therefore, when using microstrip feed lines in an array, particular attention must also be paid when physically fitting the feed lines around the radiating elements themselves, as mutual coupling between the feed lines and patch radiators increases as the physical distance between them decreases.

The physical advantages of a microstrip feed network can be maintained while the undesirable losses and coupling due to a lack of physical space can be minimised by correct choice of microstrip feed line geometry.

2.8.1.1 Series feed

In a series feed configuration, multiple elements are arranged linearly and fed serially by a single transmission line. Two configurations of a series feed can be seen in Figure 2-12.
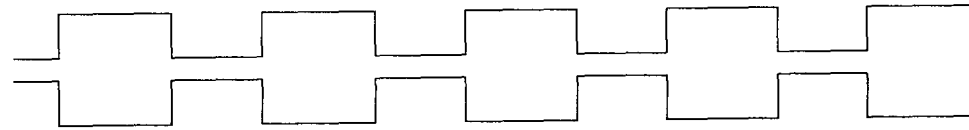
(a)
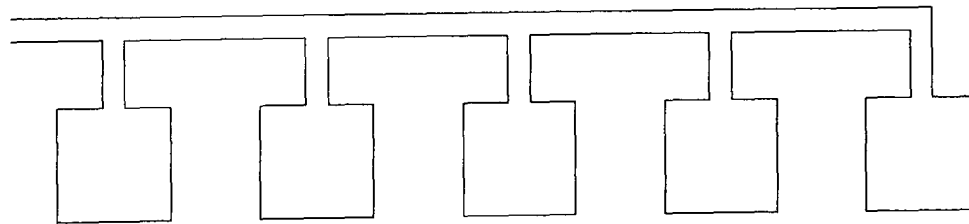
(b)

Figure 2-12: (a) in-line series feed (b) out-of-line series feed.

The in-line feed uses two port patches while the out-of-line feed uses one port patches. The in-line feed [72,73] has the feed transmission line and radiating elements arranged in the same line, while the out of line series feed [74] has the feed line arranged parallel to the radiating elements. The in-line feed occupies the least space and has the lowest insertion loss, but generally has the least polarisation control and the narrowest bandwidth. It is also more suited to linear polarisation, rather than circular polarisation generation. The phase difference between the patches is not only a function of line length, but also the patch's input impedance; therefore it has the narrowest bandwidth. Since the patches are amplitude weighted differently with different input impedances, the phase will be different for different elements and will change more drastically as frequency changes, due to the narrow band characteristic of the patches.

The series fed arrays can also be classified into standing wave (resonant) and travelling wave (non-resonant) arrays [75]. In a resonant array, the elements are spaced at multiple integrals of one wavelength so that reflected power will radiate into space in correct coherence. The line junctions and radiating elements do not have to be matched because the elements are spaced at a single or multiples of one wavelength, the beam of a resonant array is always pointing broadside. This spacing also leads to a very narrow bandwidth, generally less than 1%, since as the frequency changes, a one wavelength difference in excitation no longer exists and reflected waves no longer radiate coherently, but instead travel back to the input port as mismatched energy. Furthermore, these internal reflections within the standing wave series feed lead to a higher insertion loss [76]. Both in-line and out-of-line feed arrays can be designed as a resonant type.

In a travelling wave array, the transmission lines are matched to the radiating elements. The array can be designed so that the last element radiates all the remaining power. Alternatively, the remaining power can be absorbed by a matched load or can be reflected back in phase for broadside radiation. This gives the travelling wave array a wider input impedance bandwidth but its main beam will change angle as frequency changes (1% angle for 1% frequency change). Consequently, for an instantaneous wide band signal, a beam broadening effect will occur. Again, both in-line and out-of-line arrays can be designed as the travelling wave type.

Some arrays resemble a series fed array except there are no special radiation elements. Figure 2-13 illustrates some circularly polarised examples of discontinuity wave arrays.

(a)

(b)

(c)

(d)
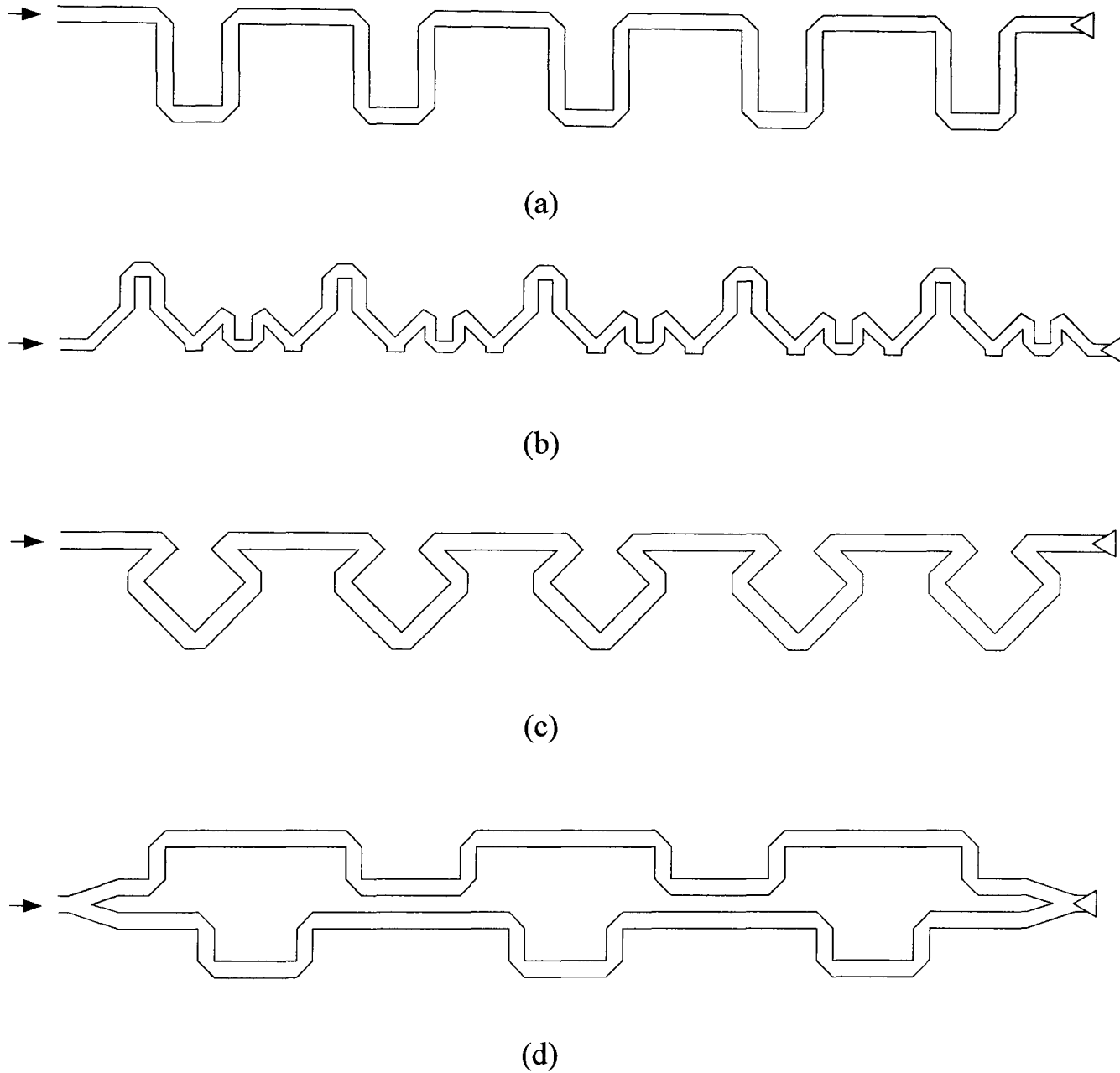
Figure 2-13: (a) Rampart line antenna [77,78], (b) Chain antenna [79], (c) Square loop antenna [80], (d) Crank-type antenna [81].

These antennas consists of long microstrip lines that radiate because they have bends. It has been shown that radiation is produced from such discontinuities [82]. The radiation from each bend is small but when the antenna is properly designed the radiation from all the discontinuities combines to produce a well formed beam, the polarisation of which is controllable by the end which is being fed. The antennas in Figure 2-13 are RHCP as they are being fed from the left hand end, the right hand

here being terminated with a matched load. For LHCP the left hand end should be terminated and the antenna fed from the right.

2.8.1.2 Corporate feed

A corporate or parallel feed network supplies excitation individually to each array element. The majority of corporate feed networks use equal line lengths and power splitters for each element so amplitude and phase drifting with frequency is usually minimal. The input impedance bandwidth of a corporate fed array will be approximately limited by that of the radiating element. If losses are significant the bandwidth may appear larger but at the expense of efficiency. Parallel feed networks with equal path lengths offer wider instantaneous bandwidth than series feeds, but they also incur higher losses and this contributes to a limitation on the realisable gain achievable by microstrip arrays using this feed geometry [83,84].

A typical corporate feed network with linear polarised radiating elements can be seen in Figure 2-14.
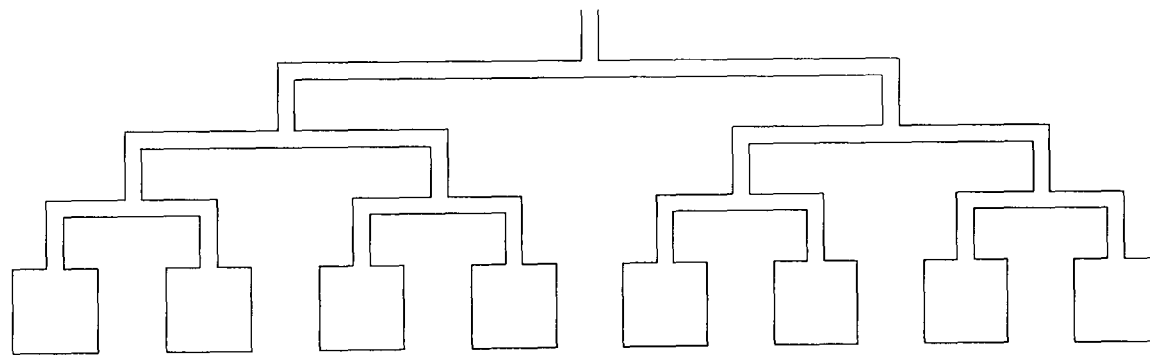
Figure 2-14: Corporate feed network.

The patch elements are fed in parallel by the power division transmission lines. The transmission lines split into two branches, each branch dividing again until it reaches the radiating element. In a series feed arrangement, the remaining power from the first element is used to feed the second element, and so on, with the first element having the shortest transmission line. Most of the insertion loss occurs in the transmission line at the first few elements, as most of the power has radiated by the time the end elements are reached. As a consequence, the insertion loss for a serial feed is less than that of a corporate feed [85].

One of the difficulties encountered when designing planar microstrip arrays is the limitation of available space to maintain sufficient clearance between the radiating elements and the feed network, especially in the corporate feed network. The series feed offers a more compact feed geometry.

However the corporate feed does have one distinct advantage over the series feed. Relative amplitude and phases between radiating elements will remain the same when the frequency changes, as all elements are fed by equal length transmissions lines so no beam squint occurs. The bandwidth of a corporate feed is limited by the bandwidth of the radiating elements and that of the impedance matching circuitry at the power splitting transmission lines.

2.8.1.3 Hybrid feed

A combination of series and corporate feeding network can be combined to form a hybrid feed network as seen in Figure 2-15.
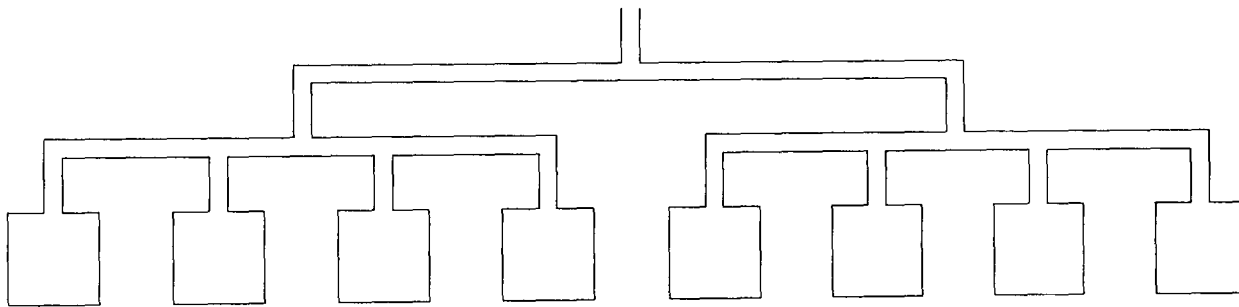
Figure 2-15: Hybrid series/parallel feed.

In a hybrid array, the smaller series fed sub-array will yield a broader beam width, which has smaller gain degradation due to beam squint caused by frequency change. The insertion loss is higher than that of a serial feed because of the corporate feed section; therefore the hybrid makes a compromise between insertion loss and bandwidth.

2.8.2 Array configuration

2.8.2.1 Sequential rotation

In the traditional corporate fed array, seen in Figure 2-14, circular polarised radiating elements share orientation and are fed simultaneously with the same phase. As a consequence, the axial ratio of the array is restricted to the axial ratio of the radiating elements that make up the array. Also, reflections from mismatched elements away from design frequency add at the input terminal degrading the array's input impedance bandwidth. Furthermore, a proportion of this scattered power is then re-radiated leading to degradation in the radiation pattern.

Sequential rotation has been shown to improve the polarisation purity, radiation pattern symmetry and the input impedance bandwidth of circularly polarised microstrip antenna arrays. Each radiating element in the array is physically rotated with respect to its immediate neighbor. This physical rotation is compensated by an appropriate phase delay in each element's excitation. The phase delay is usually achieved by adjusting the line length of that element's feed.

The principle of this technique is that the cross polarised components of elliptically polarised radiating elements are cancelled in the far field because the feeding phase changes are appropriate for the wanted hand of polarisation only. An additional benefit is that of design frequency, due to the phase delays in the feed network, reflections from mismatched radiating elements tend to cancel at the feed point. As a result, sequential rotation increases the axial ratio and input impedance bandwidth of patch antenna arrays without the need for increasing the bandwidth of the radiating elements.

The simplest sequential arrangement is the paired elements seen in Figure 2-16 [86].
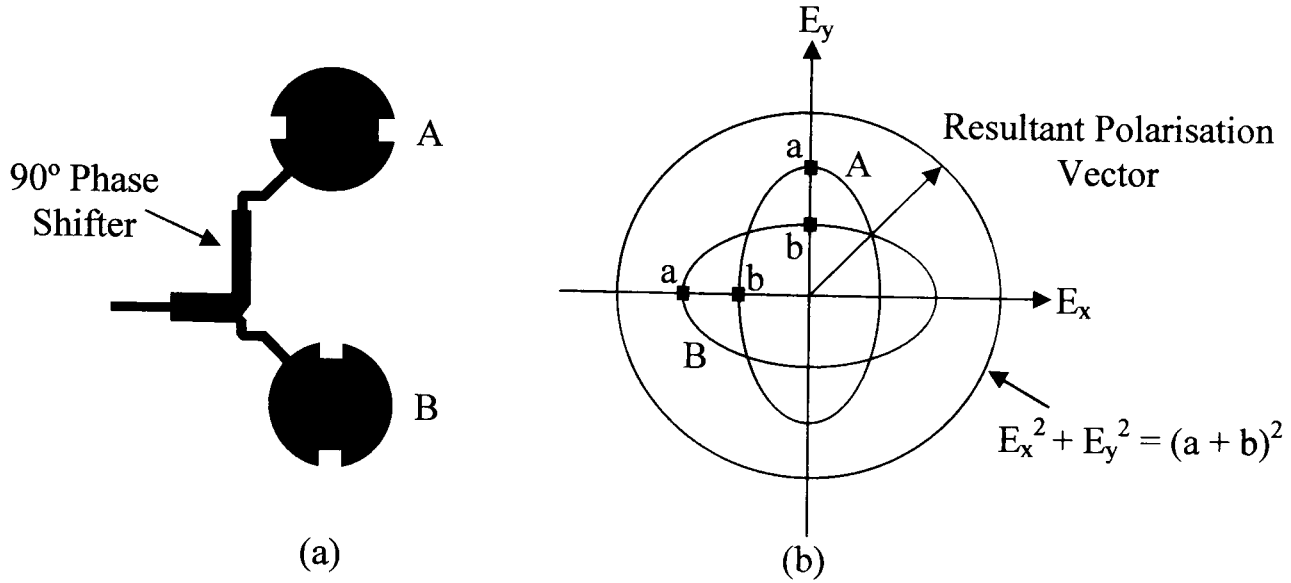
Figure 2-16: (a) Fundamental arrangement of a microstrip paired element unit (b) Polarisation pattern.

The radiating elements are rotated orthogonally on the coplanar plane as seen in Figure 2-16 (a) and are fed with uniform amplitude (at design frequency). There is a $90°$ phase difference between each element's excitation to compensate for this physical rotation. The resulting electric field vector is shown in Figure 2-16 (b) where it is seen that the individual elements of the pair demonstrate elliptical polarisation. The polarisation ellipses marked A and B correspond to those of each element, while the E_x and E_y axes correspond to the horizontal and vertical components of the radiated electric field. The polarisation purity of the individual elements will degrade with frequency. However, if the radiating elements are arranged orthogonally with a 90 degree phase difference in the feed, the resulting polarisation pattern due to the pair is seen to be of perfect circular polarisation. Indeed it has been shown that circular polarisation can be achieved from a sequentially rotated array composed entirely from linearly polarised radiating elements [87], although this can lead to large cross polarised lobes in the diagonal plane unless very small element spacing is used.

The first analysis of sequentially rotated arrays was presented by Teshirogi [11] in which a comparison was made between a conventional and sequentially rotated 4 x 2 array of probe fed notched patches with a non-isolated splitter operating at 2.3GHz. The 1.5:1 VSWR bandwidth was shown to double and the 3 dB axial ratio bandwidth improved by a factor of 15. Several examples followed using dual feed [88], single fed circular notched patches, both probe [89] and microstrip line [90] fed. All of these

39

examples used a corporate feeding system. It was not until 1989 that a comparison between various configurations of sequentially rotated arrays was made [12,67] which showed that due to internal reflections within the feed, a three element array out performed the geometrically more desirable four element 2x2 array, in both input impedance and axial ratio bandwidth. This was shown to be the case with notched patches fed both by a corporate feed and a non-isolated reactive splitter. This choice of radiating element and feed methods was also adopted in following studies of array gain [91], side lobe reduction [92,93]. In [49] an isolated corporate feed using Wilkinson power dividers achieves cross polarisation levels of better than 30 dBs.

More complex structures with alternative radiating elements have also been presented, such as probe fed triangular [94] and truncated corner patches [95]. In the later an isolated triplate layer corporate feeding system was used. Also in [96] a large flat-plate array consisting of circular slot radiating elements and a smaller four element array using shorted quarter wave patches were both fed by a non-isolating corporate feed. In [97] wideband traveling wave radiating elements with a 66% bandwidth were sequentially rotated to form a 2x2 array, although feed phase was continuously maintained across the bandwidth by continual adjustment in the length of the feed cables. This required a multilayer structure.

More recently, attention has been paid to the use of sequential rotation in the design of 4x4 antenna for road tolling applications [98]. In this reference microstrip fed truncated corner patches are excited by a corporate feeding system.

2.8.3 Array summary

Series fed arrays have the advantage of being less complex, more compact, and have lower insertion and line losses when compared to corporate feeds. However, due to the reliance on an excitation phase difference of one wavelength being maintained between the radiating elements, both amplitude and phase errors are greater than in a traditional corporate feed. However, in a sequentially rotated array, various excitation delays are required by all feeding methods, hence the inherent advantage of corporate feed is not realised in such antennas. No research to date has considered the use of a series feed in a sequentially rotated array. This thesis investigates this with a view to combining the benefits of both.

CHAPTER 3

DUAL FEED RADIATING ELEMENT OPTIMISATION

3.1 Introduction

Single microstrip patch antennas are used in a variety of communication systems especially when the receiver needs to be compact and have a low profile. The use of circular polarisation allows the receiver to be placed in any orientation and helps discriminate between reflected signals. Circular polarisation can be achieved using either a single or a dual feed (as discussed in the previous chapter).

Circular polarised antenna that use a dual feed networks have many advantages over single feed antenna such as simplicity of design, less stringent fabrication tolerances and they are less sensitive to mutual coupling when used in arrays [49]. Consequently, in many applications, a dual feed arrangement is preferred.

The microstrip line is an attractive choice of feed medium as it maintains the attractive features associated with the radiating patch (low profile, durability and ease of manufacture). However, step discontinuities between the microstrip feed sections can lead to spurious radiation from the fringing fields at the feed line junctions. Minimising any discontinuity between the widths of the feed line sections will reduce this problem.

In this chapter an optimised design of a dual feed microstrip antenna is presented. This antenna is used as a radiating element within the antenna arrays presented in the following chapter.

Dimensions for the radiating patch are determined and the traditional design of a dual feed network is presented. An equivalent circuit for the radiating patch and feed network are presented with expressions to model the sections of feed line that make up the feed network. Investigation into traditional dual feed design highlights flexibilities and constraints inherent within the traditional design. This is followed by

a new and unconventional approach to the optimised design of the dual feed network using a multi objective genetic algorithm. The aim of the optimisation algorithm is to increase the input impedance at the dual feed point and reduce the step discontinuities traditionally found between the dual feed line sections. Experimental measurement is used to confirm the performance of this design and integrity of this approach.

3.2 Design

3.2.1 Radiating Patch Design

The radiating patch can be any shape but regular shapes such as rectangular or circular patches are most commonly used. Alternative shapes have been considered but these more complex shapes offer no operational improvements, are more difficult to design and manufacture and are more complex to analyse theoretically. Therefore a rectangular patch was chosen.

3.2.1.1 Patch length

The fringing fields, which appear at the radiating edges, cause a slight change in the electrical length compared to the physical length of the patch. This can be described as a line extension of ΔL, as demonstrated in Figure 3-1.
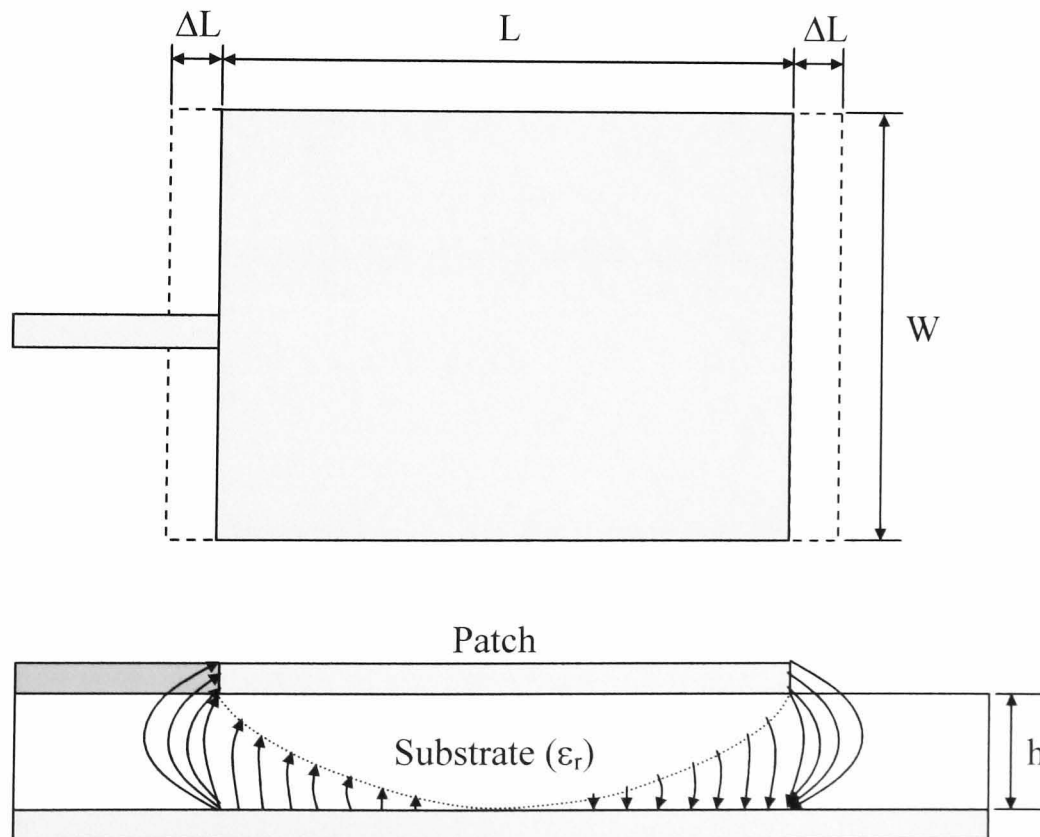
Figure 3-1: Extended length at the edges of the patch antenna.

A practical approximation for the normalised extension of length is given by [99]

$$\frac{\Delta L}{h} = 0.412 \frac{\left(\varepsilon_{eff} + 0.3\right)\left(\dfrac{W}{h} + 0.264\right)}{\left(\varepsilon_{eff} - 0.258\right)\left(\dfrac{W}{h} - 0.8\right)} \tag{3.1}$$

As the fringing fields at the edge of the patch pass through both air and the substrate material an effective permittivity of the substrate has to be obtained. The effective permittivity (ε_{eff}) is the permittivity a substrate would have to be so that a microstrip line completely enclosed within this uniform substrate would share the same electrical characteristics as the microstrip line seen in Figure 3-3.

As air has a relatively low permittivity of 1, effective permittivity usually falls between the permittivity of air and the higher permittivity of the antenna dielectric substrate ($\varepsilon_0 < \varepsilon_{eff} < \varepsilon_r$). As $W/h > 1$, an accurate value for effective permittivity in this application is given by [52]

$$\varepsilon_{eff} = \frac{\varepsilon_r + 1}{2} + \frac{\varepsilon_r - 1}{2}\left[1 + 12\frac{h}{W}\right]^{-\frac{1}{2}} \tag{3.2}$$

as the fringing occurs at each side, the effective length of the patch is now

$$L_{efff} = L + 2\Delta L \tag{3.3}$$

The actual length of the antenna can therefore be found by determining the effective length of the antenna using

$$L_{eff} = \frac{c}{2f_r\sqrt{\varepsilon_{eff}}} \tag{3.4}$$

13

For circular polarisation with a dual feed network, a square patch is required where L is equal to W as each orthogonal mode must be equal in amplitude. In the first iteration, L_{eff} can be determined using (3.4) and this value used for W to determine ΔL using (3.1). The effective length can then be determined using (3.3) and this value substituted back into equation (3.1) as W then ε_{eff} and ΔL re-calculated. The accuracy of the result does not effectively increases with successive iterations beyond this point.

3.2.2 Feed network design

3.2.2.1 Basic structure

A square radiating patch with a dual feed network can be seen in Figure 3-2.
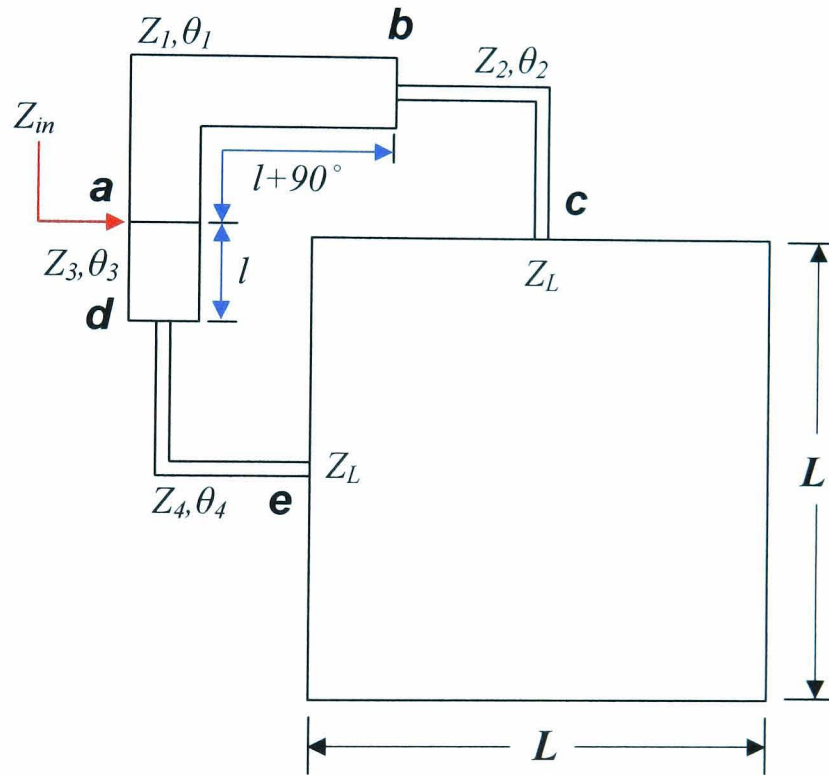
Figure 3-2: Dual feed LHCP radiating element.

The radiating patch is fed by a dual microstrip feed network. For circular polarisation the two orthogonal modes TM_{010} and TM_{001} must be equal in amplitude and 90 degrees out of phase. Equal amplitude is achieved with an equal power splitter at junction **a** and the 90 degree phase difference is realised by extending the length of one of the microstrip feed line sections by a quarter wave length. In Figure 3-2, if the phase delay between node **a** and node **c** is 90 degrees more than the phase delay

between node **a** and node **e** the radiated field will be LHCP. If this line length relationship were reversed, the result would be RHCP radiation.

L is the dimensions of the radiating patch and $Z_1, \theta_1, Z_2, \theta_2, Z_3, \theta_3, Z_4, \theta_4$ represent the characteristic impedance and line length of each feed line section.

3.2.2.2 Microstrip feed line design

The characteristic impedance of a microstrip feed line is a function of the substrate height, specific permittivity and the width of the line. These parameters can be seen in Figure 3-3.
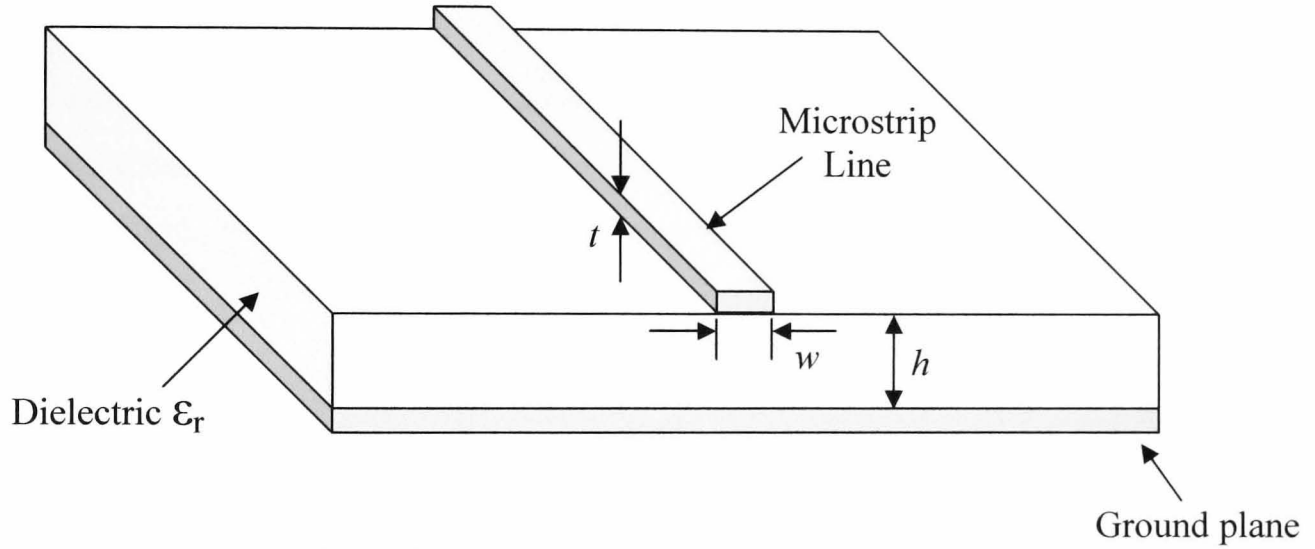
Figure 3-3: Microstrip feed line structure and design parameters.

The width of track w required to implement a feed line with characteristical impedance Z_o on a substrate of height h and specific permittivity ε_r is given by equation (3.5) [100].

$$\frac{w}{h} = \left(\frac{e^H}{8} - \frac{1}{4e^H} \right)^{-1} \tag{3.5}$$

where

$$H = \frac{Z_o \sqrt{2(\varepsilon_r + 1)}}{119.9} + \frac{1}{2} \frac{\varepsilon_r - 1}{\varepsilon_r + 1} \left(\ln \frac{\pi}{2} + \frac{1}{\varepsilon_r} \ln \frac{4}{\pi} \right) \tag{3.6}$$

equation (3.5) is valid when $Z_o > (44 - 2\varepsilon_r)$. This assumes the microstrip is treated as a statically charged capacitor where both electric and magnetic fields are in the transverse plane only. Once a substrate has been selected for antenna realisation, the characteristic impedance becomes a function of microstrip line width.

3.2.2.3 Impedance matching

The input impedance at the edge of the radiating patch Z_L is approximately 300Ω (determined using equation (3.8)). 300Ω can not be realised using a microstrip feed line as the resulting track would be too thin to fabricate using traditional PCB techniques.

Z_L is traditionally matched to nodes **b** and **d**, using sections of feed line a quarter of the effective wavelength long. This feed section, often termed a quarter wave transformers, is commonly used to match one impedance to another using the relationship

$$Z_0 = \sqrt{Z_x \times Z_y} \tag{3.7}$$

where Z_0 is the characteristic impedance of the quarter wave section, Z_x and Z_y are the source and load impedances respectively.

The minimum width of a realisable microstrip line is constrained to 10 mill by the fabrication process. Using equation (3.5), this translates to a characteristic impedance of 145 Ω, hence the highest impedance realisable by traditional PCB techniques.

As the load impedance Z_L is 300Ω and the highest obtainable characteristic impedance for a quarter wave transformers is 145Ω the impedance seen at nodes **b** and **d** is constrained to a maximum of 66Ω as seen in Figure 3-4.
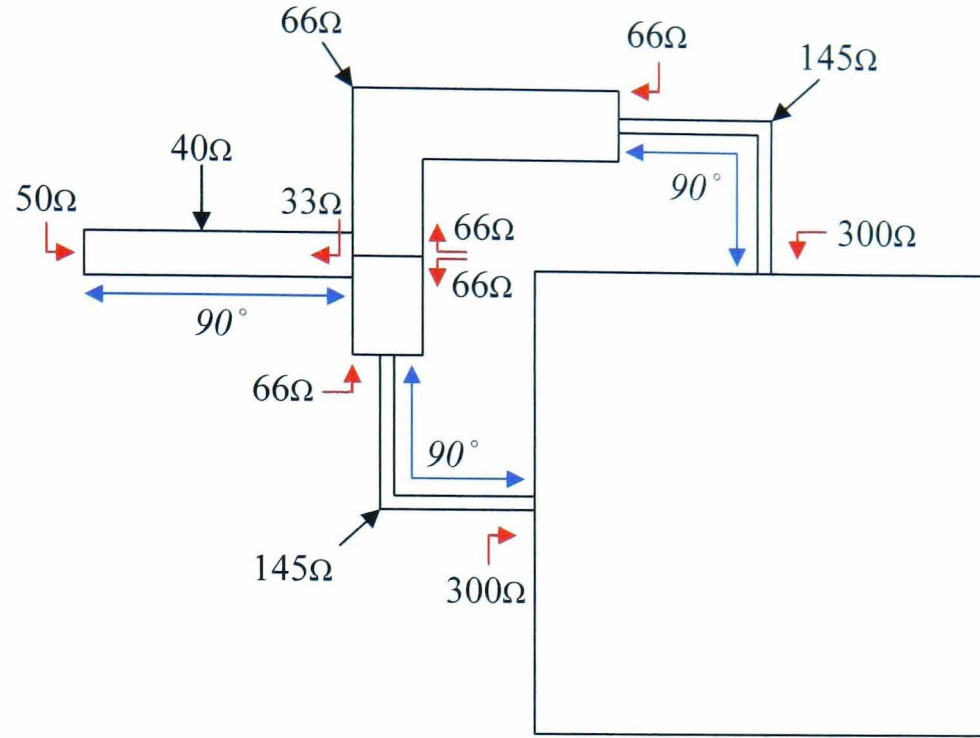
Figure 3-4: Impedance matching in a traditional dual feed network.

To maintain flexibility in length (as one has to be 90 degrees longer that the other) the remaining feed line sections must be matched at the design frequency ($Z_x = Z_0 = Z_y$). Therefore the characteristic impedance and the impedance looking into these feed sections from node **a** are also constrained to 66 Ω. Consequently the input impedance looking into the power splitter, for equal power division, can be no larger than 33 Ω when this traditional design approach is adopted. This highlights one of the limitations inherent within the traditional design process as an additional quarter wave transformer is required to match the input impedance at the power splitter to an input impedance of 50Ω at the input feed point of the antenna.

3.2.3 Analysis

Both radiating patch and microstrip feed lines were modelled using a transmission line model.

3.2.3.1 Radiating patch analysis

The input impedance Z_L of each orthogonal TM mode can be determined using the transmission line model. It treats the patch as two radiating slots perpendicular to the feed line, separated by a transmission line length $L/2$. The slots are represented by a conductance G and a susceptance B as shown in Figure 3-5.
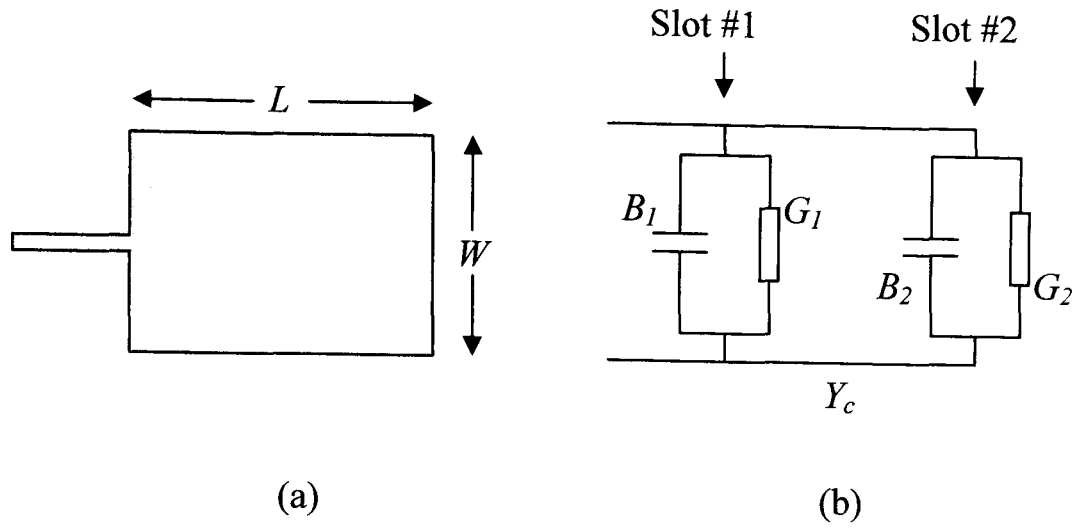
Figure 3-5: (a) Microstrip patch antenna (b) Equivalent circuit.

The admittance of each slot and hence input impedance at the feed point can be determined using [101]

$$Y = G + jB \tag{3.8}$$

where

$$G = \frac{W}{120\lambda_{eff}} \left[1 - \frac{1}{24}(\beta h)^2 \right] \qquad \frac{h}{\lambda_0} < \frac{1}{10} \tag{3.9}$$

and

$$B = \frac{W}{120\lambda_{eff}} \left[1 - 0.636 \ln(\beta h) \right] \qquad \frac{h}{\lambda_0} < \frac{1}{10} \tag{3.10}$$

Where W the finite width of the patch (and equal to L) and h is the substrate height. β is the phase constant in the substrate and can be determined using

$$\beta = \left(\frac{2\pi}{\lambda_{eff}} \right) \qquad \text{and} \qquad \lambda_{eff} = \frac{c}{f_r \sqrt{\varepsilon_{eff}}} \tag{3.11}$$

The input admittance at Slot #1 is obtained by transferring the admittance of Slot #2 using equation (3.12).

3.2.3.2 Feed analysis

The equivalent circuit of the dual feed antenna can be seen in Figure 3-6 where the feed lengths are represented sections of transmission line and each radiating TM mode by load impedance Z_L (as determined in the previous section). The optimisation aims to minimise discontinuity between the feed line sections so discontinuity reactances are not included in the model.
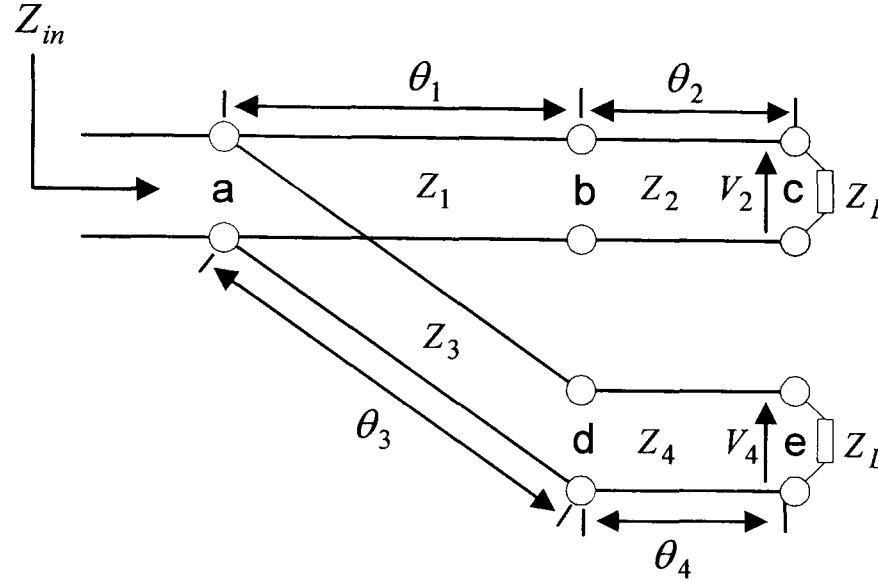
Figure 3-6: Equivalent circuit of dual feed network.

3.2.3.3 Input impedance

Using the equivalent circuit shown in Figure 3-6, the total input impedance at the feed point of the dual feed radiating element Z_{in} can be determined. This is achieved by transforming Z_L back through all of the feed line sections to node **a** using the relationship [102]

$$Z_x = Z_0 \left[\frac{Z_y + jZ_o \tan(\theta)}{Z_o + jZ_y \tan(\theta)} \right] \tag{3.12}$$

Where Z_x is the impedance looking into each feed line section, Z_o is the characteristic impedance and Z_y is the load impedance of each feed section. $\theta = \beta l$ where l is the fractional length of each feed line section. Equation (3.12) reduced to (3.7) when the feed section is a quarter wave in length.

As the dual feed lines act in parallel the total impedance at junction **a** is determined using

$$Z_{in} = \frac{Z_1 in Z_3 in}{Z_1 in + Z_3 in} \tag{3.13}$$

where $Z_1 in$ and $Z_3 in$ are the impedance looking into feed sections Z_1 and Z_3 from node **a**.

3.2.3.4 Axial ratio

The axial ratio of the dual feed radiating element can be determined by finding the relative magnitude and phase of V_2 and V_4 as seen in Figure 3-6. The relationship between these voltages can be found by assuming a constant voltage source of one volt is applied at the feed point which is then transformed through the feed network. using the relationship

$$\frac{V_2}{V_4} = \prod_{n=1}^{N} \frac{e^{(-j\theta_n)}(1 + \Gamma_n)}{1 + e^{(-j2\theta_n)}\Gamma_n} \tag{3.14}$$

where N is the total number of feed line sections between V_2 and V_4, Γ_n and θ_n are the reflection coefficient and length of the nth length of feed line. A full derivation of equation (3.14) can be found in Appendix B.

Once the relative phase and magnitude of V_2 and V_4 have been determined, the axial ratio can be calculated using equation (2.8) where the magnitude of each orthogonal mode, E_y and E_x, have the relationship

$$\frac{E_x}{E_y} = \frac{|V_2|}{|V_4|} \tag{3.15}$$

The phase between the two orthogonal mode voltages

$$\theta = \arg\left(\frac{V_2}{V_4}\right) \tag{3.16}$$

3.2.4 Feed optimisation

With a traditional dual feed patch design manufacturing capabilities restrict the input impedance at the dual feed point to 33Ω as identified in section 3.2.2.3. It is also noted that the step discontinuities between the matched feed line section and matching transformers are relatively large.

The aim of this section is to increase the input impedance at the dual feed point from 33Ω to 50Ω and remove step discontinuities between the various feed line sections by adopting an alternative design procedure based on resistive and reactive complex impedance matching.

Using the transmission line model, it is possible to match a complex load to a complex source impedance [103]. This complex matching will introduce both real and imaginary parts (resistive and reactance elements) at the feed line junctions. Instead of maintaining a 90 degree phase difference between the two orthogonal modes using a quarter wave difference in path length, the phase difference will be obtained by summing the reactance at each junction within the feed network. Moreover, by varying the characteristic impedance and length of the transmission lines that make up the feed network, both impedance matching and the desired relationship between the amplitude and phase of the orthogonal mode voltages can be realised simultaneously.

This approach cannot be implemented by direct analysis and would traditionally rely on a time consuming trial and error approach. Therefore, as there is no direct analytical approach, a Multi-objective Genetic Algorithm (MGA) program has been developed to optimise the size and length of the feed line sections while maintaining the conditions for circular polarisation and impedance matching at the dual feed point [17].

Two additional constraints are placed on the design parameters, one to ensure that the widths of the feed lines are as narrow as possible yet realisable. The other constraint is to ensure that the lengths of the feed lines are sufficient to fit the feed network around the radiating patch.

3.2.4.1 Objective functions

For the structure shown in Figure 3-7 the design variables $Z_1, \theta_1, Z_2, \theta_2, Z_3, \theta_3, Z_4, \theta_4$ constitute the parameter set in the MGA.
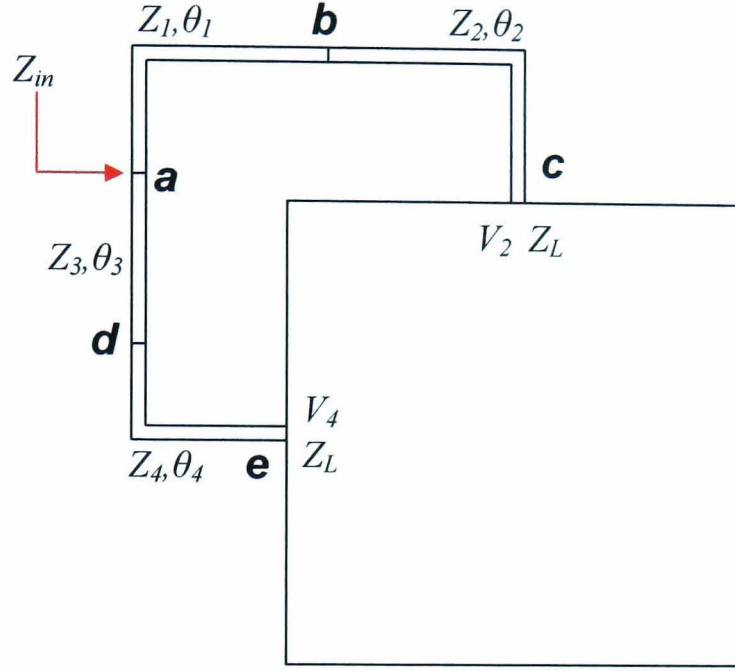
Figure 3-7: Design variables for dual feed network.

The problem involves two objective functions, namely good circular polarisation and impedance matching conditions, therefore this can be characterised as a multi-objective optimisation problem. These two objective functions are given by equations (3.17) and (3.18).

Equation (3.17) describes the condition required for good circular polarisation where the amplitude of V_2 and V_4 are equal in magnitude and the phase of V_2 and V_4 differ by 90°. For the structure shown in Figure 3-7, Equation (3.14) can be rewritten as

$$\frac{V_2}{V_4} = \frac{e^{-j(\theta_1+\theta_2)}[1+\Gamma_1][1+\Gamma_2]}{[1+\Gamma_1 e^{-2j\theta_1}][1+\Gamma_2 e^{-2j\theta_2}]} \times \frac{[1+\Gamma_3 e^{-2j\theta_3}][1+\Gamma_4 e^{-2j\theta_4}]}{e^{-j(\theta_3+\theta_4)}[1+\Gamma_3][1+\Gamma_4]} = \mp j, \qquad (3.17)$$

where $\Gamma_1, \Gamma_2, \Gamma_3$ and Γ_4 are the reflection coefficients at junctions **b**, **c**, **d**, and **e** respectively.

Equation (3.18) describes the condition required for good impedance matching.

$$\Gamma_{in} = \frac{Z_{in} - 50}{Z_{in} + 50} = 0 \qquad\qquad (3.18)$$

Where Γ_{in} is the input reflection coefficient at junction **a** and 50Ω is the desired input impedance at the dual feed point.

3.2.4.2 Constraints

For microstrip realisation values for the impedance parameters Z_1, Z_2, Z_3, Z_4 were restricted to a relatively high search interval of between 120Ω and 145Ω to help reduce the coupling between the feed lines and the radiating patch (by making the tracks thin). 145Ω represents the maximum impedance that can be practically realised. Lengths $\theta_1, \theta_2, \theta_3, \theta_4$ were constrained to an interval between $\pi/4$ and π to ensure the resulting feed can physically fit around the radiating patch.

The tolerance for $|V_2/V_4|$ was 1 ± 0.1 and the $\arg(V_2/V_4)$ was $90° \pm 4°$, so as to ensure good circular polarisation (no worse than 0.6 dB at design frequency), while the tolerance for Γ_{in} was ± 0.02 in order to produce a good impedance match (no worse than a VSWR 1.04:1 at design frequency) at the feed point.

3.2.4.3 The algorithm

Genetic algorithms are structured to solve real-world problems by imitating the processes occurring in natural evolution. Each possible solution is mapped to a unique binary string. A set of strings constitutes a population which evolves from generation to generation through the application of genetic operations such as reproduction, crossover, and mutation. Reproduction is based on the principle of survival of the fittest where each string or chromosome is associated with a fitness value (from a predetermined fitness function) that reflects its fitness relative to other members of the population. The fittest chromosomes tend to reproduce more often. In the crossover mechanism genetic material from each parent is combined, exchanging portions of their chromosome strings. Mutation helps to regenerate the lost genetic material, it is

53

performed by randomly changing one bit of the chromosome. Mutation can be considered as the random search part of the algorithm.

The MGA approach, based on non-dominating sorting genetic algorithm [104], has been developed to produce sets of feasible solutions. A multi-objective optimisation approach has been adopted based on a non-sorting genetic algorithm procedure, a modification of a basic genetic algorithm which involves only the fitness evaluation.

3.2.4.4 Optimisation solutions

The genetic algorithm produced the sets of solutions seen in Table 3-1 for the feed network as seen in Figure 3-7.

	θ_1	Z_1	θ_2	Z_2	θ_3	Z_3	θ_4	Z_4	Z_{in}	$|V_2/V_4|$	$\arg(V_2/V_4)$	CP
1	2.31	135.0	1.96	132.4	0.8	135.2	1.16	134.3	50-0.5i	0.97	86	RHCP
2	1.16	133.5	0.81	127.7	2.32	138.7	2.05	132.9	49.6+0.8i	0.95	88.2	RHCP
3	1.9	134.8	2.3	138	1.16	135.48	1.0	136.1	51.05+0.06i	1.07	86.3	LHCP
4	1.01	139.3	1.01	143.3	0.67	141.7	2.28	140.1	52-0.28I	0.98	90.2	LHCP
5	1.2	137.4	0.74	137.1	2.3	135.7	1.97	138.6	49.5+0.5i	1.08	89.7	LHCP

Table 3-1: Solutions.

Selection was made from the solutions using the pre-assigned conditions and additional factors such as a requirement of similar values of characteristic impedances of the feed lines network. It can be seen that the set of LHCP solutions in row 5 are so similar it is possible to use an average value of 137.2Ω for all four feed line impedances. This makes the design particularly attractive as this removes any step discontinuity between the feed line sections minimising spurious radiation. It is also noted that the algorithm has also successfully achieved an input impedance of 50Ω at the power splitter. This is higher than the traditional dual feed network using resistive matching with quarter wave transformers which was constrained to a maximum of 33Ω by manufacturing capabilities. As a consequence, the structure is more desirable for use in arrays as the higher input impedance leads to thinner feed lines in the arrays feed network. As a single radiating element the structure is more compact as there is no longer the requirement for a matching transformer at the dual feed point.

3.3 Practical Results

The optimised dual feed antenna was fabricated using Rodgers RT 5870 Duroid. This low loss antenna substrate had a specific permittivity of ε_r of 2.33, a substrate height of 0.79 mm and was coated on both sides with ½oz copper. The dual feed structure was etched from the top copper layer using traditional printed circuit board techniques, the lower copper layer was retained for the antennas ground plane.

The integrity of the design has been confirmed over a frequency range of 5.4 – 6.2 GHz. Measurements of input impedance were made using an Anritsu 37347C vector network analyser. A measured VSWR 2:1 bandwidth of 3.3% from 5.7 to 5.893 GHz is confirmed in Figure 3-8 (a). The 90 degree cusp in the Smith chart locus seen in Figure 3-8 (b) indicates good circular polarisation, this impedance locus is typical for this type of circularly polarised radiating element.

Frequency (Hz)

(a)
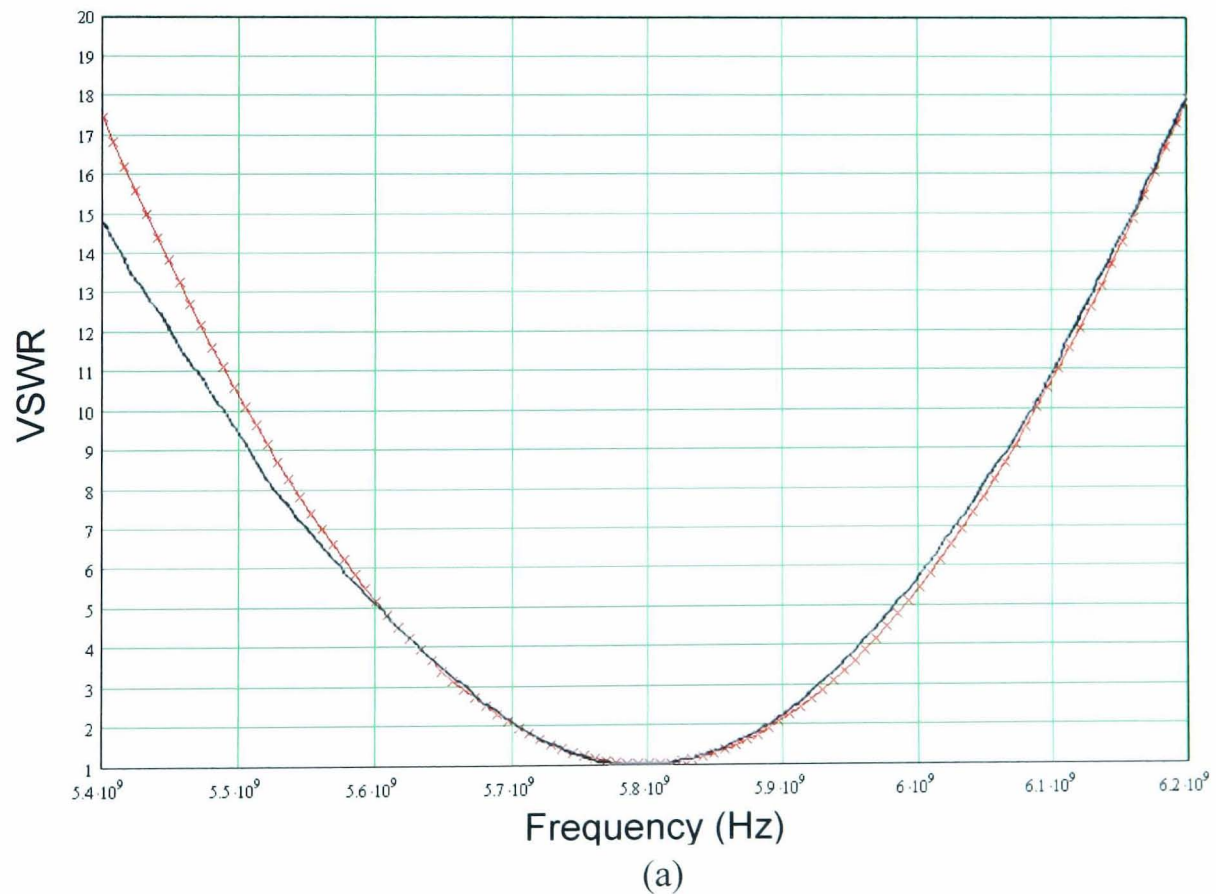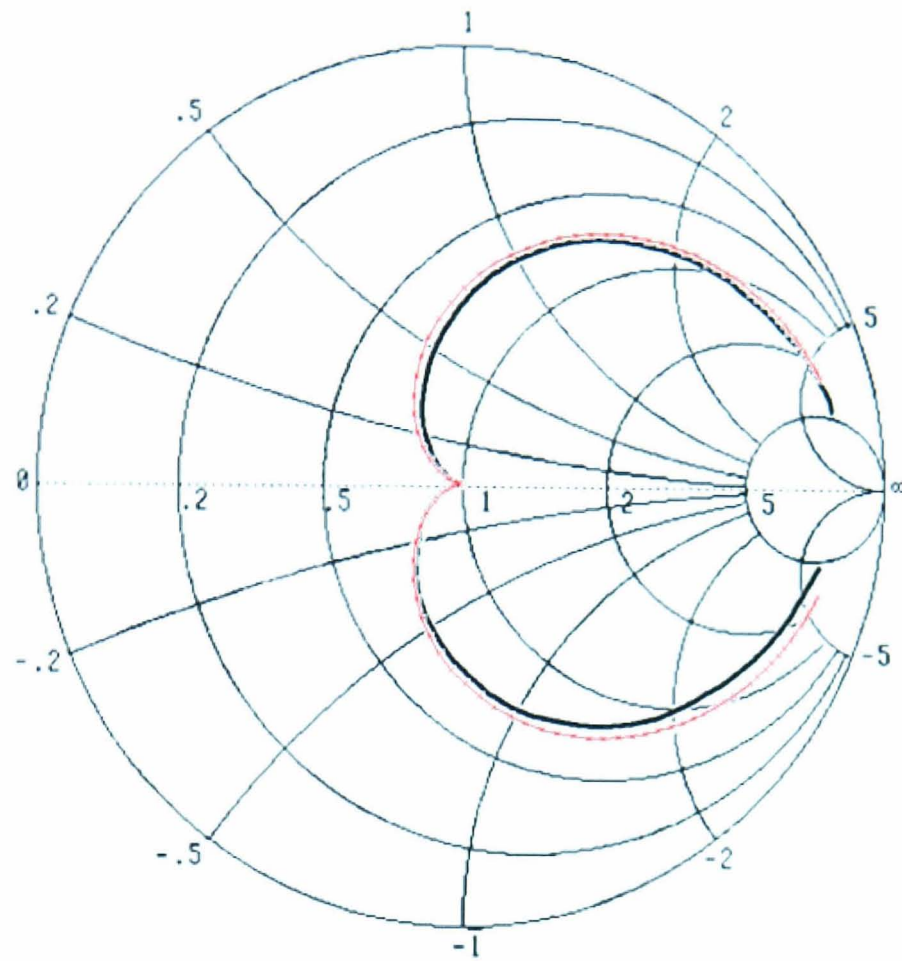
(b)

✖✖✖✖✖   Analysis presented in 3.2.3

———————   Measured

Figure 3-8: Practical measurements of input impedance for optimised dual feed antenna ($Z_1 = Z_2 = Z_3 = Z_4 = 137\Omega$, $\theta_1 = 1.2°$, $\theta_2 = 0.74°$, $\theta_3 = 2.3°$, $\theta_4 = 1.97°$ as defined in Figure 3-7).

Measurements of boresight axial ratio were made over a frequency range of 5.4 to 6.2 GHz in an anechoic chamber. As the angle of the azimuth with respect to the antenna structure cannot be guaranteed, measurements were made at all angles of phi. This method and apparatus is described further in Appendix C. The measurements of axial ratio confirm circular polarisation as shown in Figure 3-9. A 3 dB axial ratio bandwidth of 0.7% is confirmed between 5.780 and 5.820GHz which is less than the VSWR 2:1 bandwidth seen in Figure 3-9. This relationship is expected for this type of radiating element (as previously discussed in section 2.5.2).
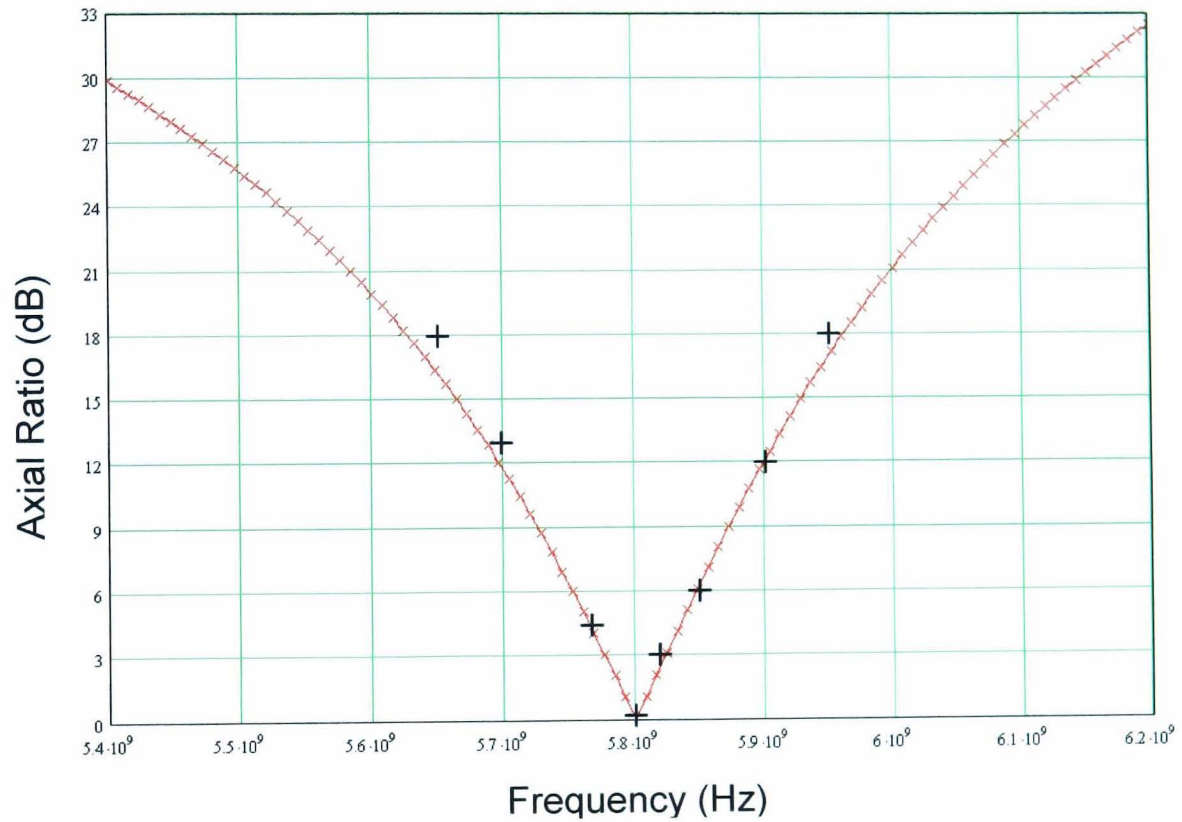
XXXXX   Analysis presented in 3.2.3

+   Measured

Figure 3-9: Practical results of boresight axial ratio for optimised dual feed microstrip patch antenna ($Z_1 = Z_2 = Z_3 = Z_4 = 137\Omega$, $\theta_1 = 1.2°$, $\theta_2 = 0.74°$, $\theta_3 = 2.3°$, $\theta_4 = 1.97°$ as defined in Figure 3-7).

Good agreement is seen between measured results and the analysis presented in section 3.2.3 for input impedance and axial ratio performance, confirming the integrity of the analysis and the validity of this design approach. In both cases characteristical dual feed performance is demonstrated but a higher input impedance of 50Ω has been obtained at the dual feed point.

3.4 Conclusion

The dual feed radiating element has been successfully modelled using the equivalent circuit derived in section 3.2.3. Although this model neglects feed radiation and surface waves it performs with good accuracy when a thin low loss substrate is used for practical realisation.

Manufacturing capabilities constrain the input impedance seen at the power splitter to 33Ω when a traditional resistive matching design approach is adopted. Applying a complex matching technique involves eight unknown variables; therefore a closed form solution can not be obtained with ease. Using the MGA, with specified constraints, it was possible to increase the input impedance at the power splitter to 50Ω. As a consequence, when the antenna is used in isolation, there is no longer the need for a quarter wave matching transformer between the feed point of the antenna the dual feed point. This not only reduces design complexity, but also reduces the size of the structure requiring less board space in which to realise the design. The increase in input impedance makes the antenna more desirable for use within the antenna arrays presented in the following chapter as it allows the use of higher impedances within the arrays feed network. As a direct result the width of the tracks within the arrays feed network is less and unwanted coupling between the arrays feed network and the radiating elements reduced.

An additional benefit of using the MGA within the design process was the ability to make the impedances that make up the feed line the same value removing physical step discontinuities between the feed line sections, hence reducing spurious feed radiation.

Practical measurement of input impedance and axial ratio bandwidth are in good agreement and confirm the validity of this approach.

CHAPTER 4

SEQUENTIALLY ROTATED ARRAYS

4.1 Introduction

Sequential rotation of radiating elements has been shown to increase the input impedance bandwidth, polarization purity and the radiation pattern symmetry of microstrip patch antenna arrays without the need to increase the bandwidth of the radiating elements. Much work has been undertaken on the design and application of sequential rotation to microstrip arrays using a corporate feed network. In this chapter the optimised dual feed radiating element, which was presented in the previous chapter, is sequentially rotated to form two, three and four element arrays that use an out-of-line series feeding system.

Input impedance and axial ratio frequency performance are determined for both series and corporate feeding techniques. The transmission line analysis presented in the previous chapter is expanded to incorporate the unique geometry of each arrays feed network. Using an equivalent circuit, the relative performance of both feeding techniques is evaluated.

The performance of the two, three and four series fed arrays using an alternative single fed planar radiating elements is also presented.

The performance of the new series fed arrays is confirmed by practical measurement.

4.2 Sequential rotation

Two typical examples of four element corporate fed sequentially rotated arrays can be
seen in Figure 4-1.
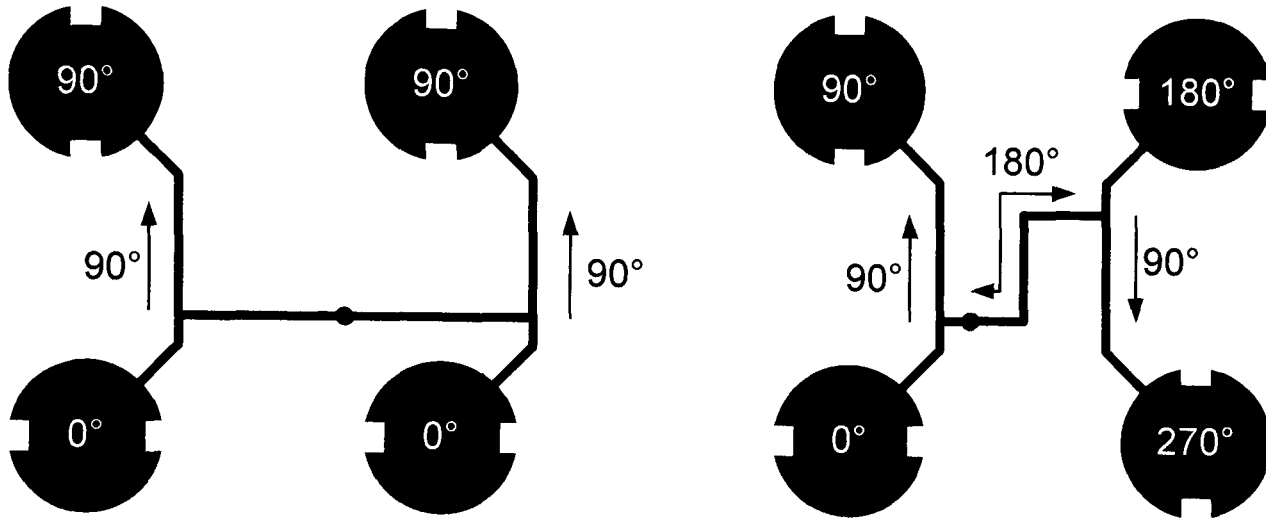
Figure 4-1: (a) Two orthogonal patch pairs arranged at 0°, 90° and 0°, 90° (b) Four
individually rotated patches arranged at 0°, 90°, 180°, 270°.

Figure 4-1 (a) consists of two orthogonal pairs of circularly polarised radiating
elements. The elements within each pair are rotated 90 degrees with respect to each
other. This physical rotation is compensated for by an excitation phase delay of 90
degrees within each pair. The patch pairs share orientation and feed phase. This array
has a sequential rotation factor of one (see equation (4.1)). In Figure 4-1 (b) all four
elements have individual rotation and are fed with individual phase therefore this
example has a sequential rotation factor of two.

A more generalised use of sequential rotation was originally proposed by Teshirogi [11], using a schematic arrangement of an M-element array of circularly polarised radiating elements.
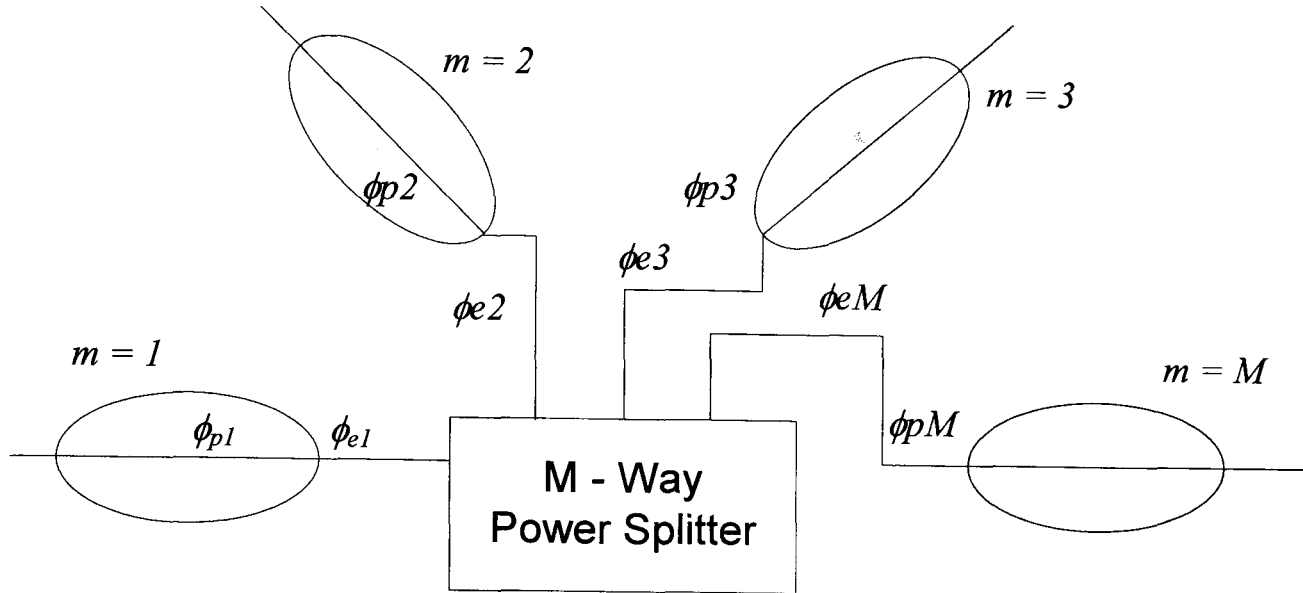
Figure 4-2: Configuration of a sequentially rotated array.

Figure 4-2 shows an array of M patches, the Mth patch has a physical rotation ϕ_{pm} from a fixed reference angle and an excitation phase delay of ϕ_{em}. These rotation angles and feeding phases are determined by the following equations

$$\phi_{em} = \frac{(m-1)p\pi}{M} \qquad \phi_{pm} = \frac{(m-1)p\pi}{nM} \qquad 1 \le m \le M \qquad (4.1)$$

Where the sequential rotation factor p is an integer, M is the total number of radiating elements and n represents the azimuthal number of the array which is 1 for the fundamental mode.

Therefore for each element pair in Figure 4-1 (a) $M = 2$ as there are two elements and $p = 1$. $\phi_{p1} = 0°$ and $\phi_{p2} = 90°$ as the elements are positioned orthogonally in space. $\phi_{e1} = 0°$ and $\phi_{e2} = 90°$, this delay in excitation being achieved by an offset between the feed point and each radiating element. In Figure 4-1 (b) $M = 4$, $p = 2$ and ϕ_{pm}, and ϕ_{em} are 0°, 90°, 180° and 270° respectively.

4.2.1 Input Impedance

If each radiating element in Figure 4-2 is fed with equal power, the excitation voltage at each radiating element V_o is also equal. If the electrical distance between the M way power splitter and each radiating element is ϕ_{em} then reflections from mismatched elements travel another ϕ_{em} back to the feed. The total voltage reflected back to the power splitter from mismatched elements V_r can therefore be determined using [11]

$$V_r = V_o \Gamma \sum_{m=1}^{M} e^{(j2\phi_{em})} \tag{4.2}$$

where Γ is the reflection coefficient of each radiating element.

Substituting (4.1) into (4.2) and using a geometric progression equation (4.2) can be reduced to [12]:

$$V_r = V_o \Gamma \frac{\sin p\pi}{\sin \dfrac{p\pi}{M}} e^{j\frac{(M-1)p\pi}{M}} \tag{4.3}$$

Vr is equal to zero, providing that $0 < p < M$ is satisfied, and perfect input return loss will result.

4.2.2 Axial ratio

If the radiated field from the first element E_l is assumed to be elliptically polarised then

$$E_1(\theta,\phi) = a(\theta,\phi)\hat{\theta} + jb(\theta,\phi)\hat{\phi} \tag{4.4}$$

Where $\hat{\theta}$ and $\hat{\phi}$ are orthogonal unit vectors and a, b are the amplitude of the components.

The total field of the array is given by summing the Mth element fields. The total field on boresight ($\theta = 0$, $\phi = 0$) is therefore given by [12]

$$Et(0,0) = \sum_{m=1}^{M} E_m = \frac{M}{2}(a+b)(\hat{\theta}+j\hat{\phi}) + \frac{1}{2}(a-b)(\hat{\theta}-j\hat{\phi})\frac{\sin p\pi}{\sin\frac{p\pi}{M}}e^{j\frac{(M-1)p\pi}{M}} \qquad (4.5)$$

The first term represents the desired hand of polarisation and the second term the unwanted or cross polarisation. The second term disappears if $a = b$ as all elements are perfectly circularly polarised and no cross polarisation is radiated. The second term also disappears if $0 < p < M$ as the components of the elliptically polarised radiating elements are phased to cancel.

Equation (4.5) assumes that a fully isolated power splitter is used and only the first reflections from mismatched radiating elements back to the feed point are considered. In reality, multiple reflections will scatter within the feed network. This will usually degrade array input impedance. As these additional reflections will contribute to each radiating elements excitation and be re-radiated, there is also degradation in array axial ratio. Taking only the first dominant additional reflection into account equation (4.5) becomes [12]

$$Et(0,0) = \sum_{m=1}^{M} Em = \frac{M}{2}(a+b)(\hat{\theta}+j\hat{\phi}) + \frac{1}{2}(a-b)(\hat{\theta}-j\hat{\phi})\frac{\sin p\pi}{\sin\frac{p\pi}{M}}e^{j\frac{(M-1)p\pi}{M}}$$

$$-\Gamma\frac{M-1}{M}(a+b)(\hat{\theta}+j\hat{\phi})\frac{\sin p\pi}{\sin\frac{p\pi}{M}}\sin^{\frac{(M-1)p\pi}{M}} \qquad (4.6)$$

$$+\frac{\Gamma}{2}(a+b)(\hat{\theta}+j\hat{\phi})\left[\frac{1}{M}\frac{\sin\frac{(M-1)p\pi}{M}}{\sin\frac{p\pi}{M}}\frac{\sin p\pi}{\sin\frac{p\pi}{M}}e^{-j(2M-1)\frac{p\pi}{M}} - \frac{2\sin 2p\pi}{\sin\frac{2p\pi}{M}}e^{-j(2M-1)\frac{p\pi}{M}}\right]$$

All of the additional terms in (4.6) are zero when Γ is zero as no power is reflected back into the feed network by the radiating elements. The first additional term is reference circular polarisation and is zero when $0 < p < M$. The second term is cross polarisation and zero when the radiating elements radiate perfect circular polarisation

as $a = b$. This cross polarisation is also zero for all values of p and M except when $p = M/2$.

The conclusion of [12] was that internal reflections within the feed network dominate array performance. Both feed phase errors and higher order modes were also evaluated however the internal reflections were identified as the predominant problem, particularly when single layer narrow band radiating elements realised on relatively thin substrates are used, this problem being worst in arrays where $p = M/2$ (as demonstrated by equation 4.6).

As only one non-isolating power splitter has been accounted for, this is an unlikely choice of feed design; not easily realised using common feeding methods such as microstrip lines. Due to the importance of internal reflections, accurate expressions for array performance are difficult to make without the inclusion of a specific feed geometries' design parameters as these affect both the amplitude and the phase of the internal reflections. This is partially identified in [67] where Hall took a more rigorous approach to modelling an actual corporate feed network using a transmission line model.

The four element array is an attractive choice for many applications, the rectangular lattice making it a good building block in larger arrays. Both purely analytical approaches [12] and experimental measurement [67] confirmed that the four element array, where $M = 4$ and $p = 2$, performed less well due to the internal reflections within the corporate feeding geometry.

4.3 Feed Geometry

The corporate feed configuration used by Hall in [67] for two (where $M = 2$, $p = 1$), three (where $M = 3$, $p = 2$) and four (where $M = 4$, $p = 2$) element arrays are shown in Figure 4-3 (a). Each element's physical rotation and feed phase delay are shown in degrees. In a conventional corporate feed the distance between the feed point of the array and each radiating element is equal. As a consequence, away from design frequency, excitation phase remains constant across the array. Equal excitation amplitude is also maintained as the power splitting at each feed junction also remains equal. From Figure 4-3 (a) it can be seen that this is no longer the case when a

corporate feed is used in a sequentially rotated array as the delays in excitation that are necessary to compensate for the physical rotation of each radiating element are implemented by change in feed line length. As a direct consequence, the attractive features traditionally associated with a corporate feed are lost as uniform power splitting and excitation phase no longer remain away from design frequency.

(a)   (b)
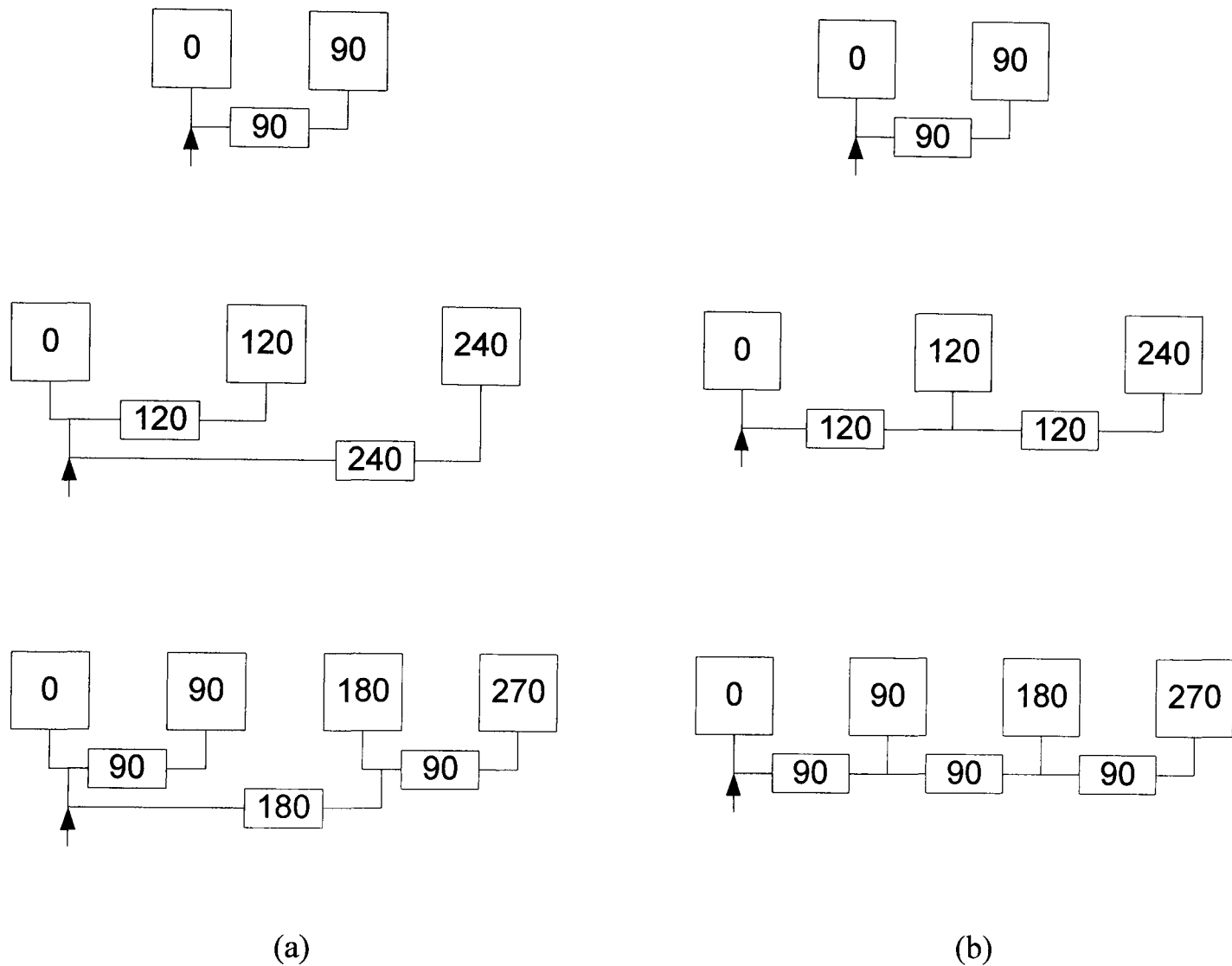
Figure 4-3: Element rotation and feed phase delays (in degrees) within the feed network of a 2, 3 and 4 element sequentially rotated antenna array with (a) a corporate feed [67] (b) a series feed.

Instead of a traditional corporate feed, it is proposed to use an out-of-line series feed network with excitation delays as seen in Figure 4-3 (b). In a conventional series fed array, the radiating elements are generally arranged physically in line. Equal excitation phase is accomplished by spacing each element by an integer of a

wavelength. A drawback to this feeding method is scan skew away from design frequency as relative feed phase uniformity deteriorates.

When the series feed is adapted for use in a sequentially rotated array, where the radiating elements are physical rotated with respect to each other, the excitation phase delays necessary to compensate for this physical rotation are implemented by changing the distance between each element from a multiple of one wave length to the appropriate feed phase delay (ϕ_{em} in Figure 4-3). However, reflected signals will no longer be re-radiated in correct phase; consequently a non-resonant traveling wave array, where the feed is impedance matched to the radiating elements, is required. Equal power distribution across the array is accomplished by diverting an Mth amount of power to each radiating element at each feed junction.

4.4 Transmission line model

In the following section, the transmission line model derived to analyse the dual feed radiating element in Chapter 3 is expanded further to model an entire array of two, three and four radiating elements. This allows an insight into the comparative performance between the corporate feed network presented in [67] and the same arrays using a series feed network.

4.5 Series feed equivalent circuit

In the following section equivalent circuits for the series fed arrays seen in Figure 4-3 (b) are presented. The sections of feed line are represented by transmission lines and the dual feed radiating elements by a load impedance Z_L (as derived in the previous chapter).

The series feed must ensure that equal power is diverted to each radiating element and the radiating elements are matched to an input impedance at the feed point of the array.

4.5.1 Two element array

The equivalent circuit of the two element array can be seen in Figure 4-4. Power is fed into the feed network at node **a**. Half of this power is diverted to the first radiating element attached to node **b**, and the remaining power fed to the second radiating element attached to node **d**.
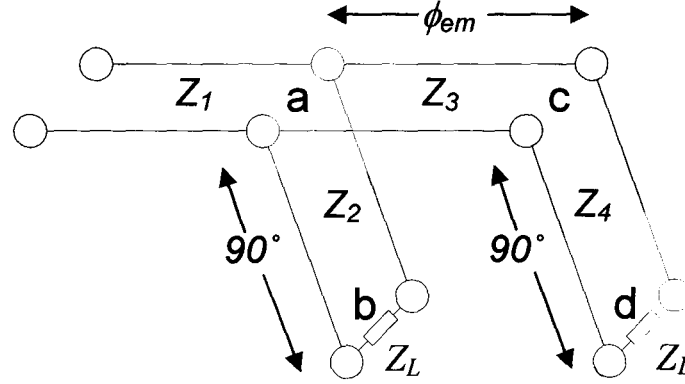
Figure 4-4: Equivalent circuit for a series fed two element array.

At node **a**, for equal power splitting, the impedance looking into Z_2 must equal the impedance looking into Z_3. Therefore

$$Z_2 in = Z_3 in \tag{4.7}$$

and for correct impedance matching to an array input impedance of 50Ω

$$Z_1 out = \frac{Z_2 in \cdot Z_3 in}{Z_2 in + Z_3 in} = 50 \tag{4.8}$$

where $Z_1 out$ is the input impedance to the array. The impedance looking into Z_2 and Z_3 can therefore be determined by substituting (4.7) into (4.8)

$$Z_2 in = 2Z_1 out \text{ and } Z_3 in = 2Z_1 out \tag{4.9}$$

At node **c**, for correct impedance matching

$$Z_3 out = Z_4 in \tag{4.10}$$

4.5.2 Three element array

The equivalent circuit of the three element array can be seen in Figure 4-5. Power is fed into the feed network at node **a**. The radiating elements are attached to nodes **b**, **d**, and **f**.
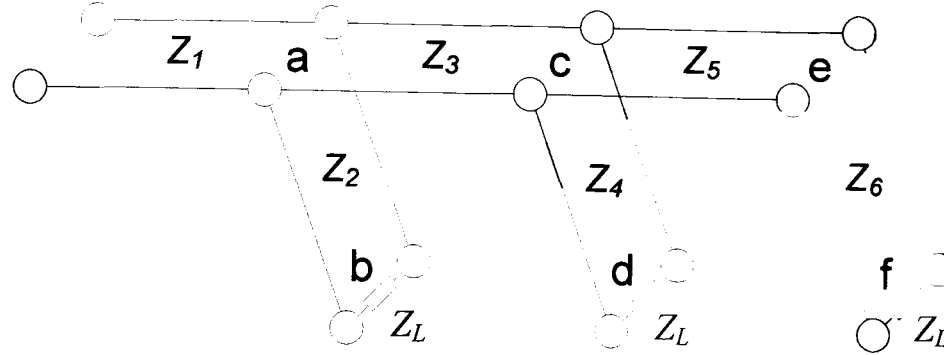
Figure 4-5: Equivalent circuit for a series fed three element array.

At node **a**, for correct power splitting a third of the power must go to first radiating element hence

$$Z_2 in = 2Z_3 in \qquad (4.11)$$

and for impedance matching

$$Z_1 out = \frac{Z_2 in \cdot Z_3 in}{Z_2 in + Z_3 in} = 50 \qquad (4.12)$$

The value looking into Z_2 and Z_3 can therefore be determined by substituting (4.11) into (4.12)

$$Z_2 in = 3Z_1 out \quad \text{and} \quad Z_3 in = \frac{3}{2} Z_1 out \qquad (4.13)$$

At node **c**, for equal power splitting, as the remaining power needs to be equally distributed between the remaining two radiating elements.

$$Z_4 in = Z_5 in \qquad (4.14)$$

and for correct impedance matching

$$Z_3out = \frac{Z_4in \cdot Z_5in}{Z_4in + Z_5in}$$ (4.15)

therefore

$$Z_4in = 2Z_3out \quad \text{and} \quad Z_5in = 2Z_3out$$ (4.16)

At node **e**, for correct impedance matching

$$Z_5in = Z_6in$$ (4.17)

4.5.3 Four element array

The equivalent circuit of the four element array can be seen in Figure 4-6. Power is fed into the feed network at node **a**. The radiating elements are attached to nodes **b, d, f** and **h**.
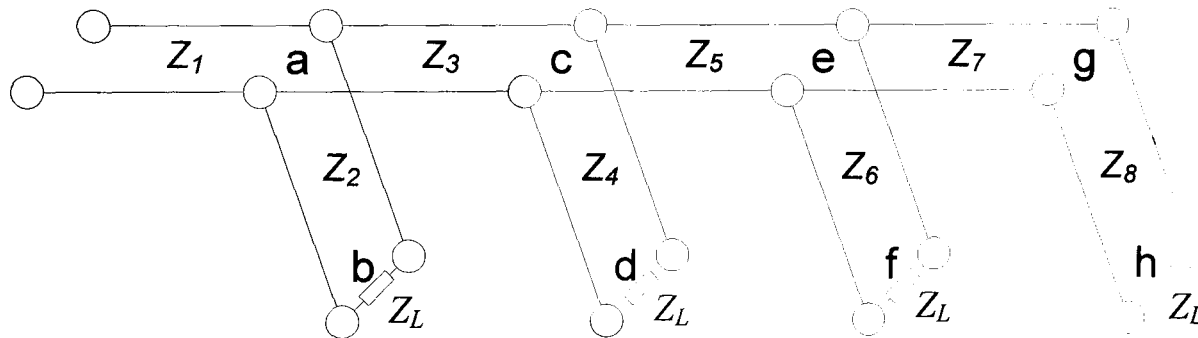
Figure 4-6: Equivalent circuit for a series fed four element array.

At node **a**, for correct power splitting (quarter of the power going to first radiating element)

$$Z_2in = 3Z_3in$$ (4.18)

and for correct impedance matching

69

$$Z_1 out = \frac{Z_2 in \cdot Z_3 in}{Z_2 in + Z_3 in} = 50 \qquad (4.19)$$

The impedance looking into Z_2 and Z_3 can therefore be determined using

$$Z_2 in = 4Z_1 out \quad \text{and} \quad Z_3 in = \frac{4}{3} Z_1 out \qquad (4.20)$$

At node **c**, for correct power splitting (as a third of the remaining power needs to be diverted to the next radiating element).

$$Z_4 in = 2Z_5 in \qquad (4.21)$$

and for correct impedance matching

$$Z_3 out = \frac{Z_4 in \cdot Z_5 in}{Z_4 in + Z_5 in} \qquad (4.22)$$

therefore

$$Z_4 in = 3Z_3 out \quad \text{and} \quad Z_5 in = \frac{3}{2} Z_3 out \qquad (4.23)$$

At node **e**, for equal power splitting (as the remaining power needs to be equally distributed between the remaining two radiating elements).

$$Z_6 in = Z_7 in \qquad (4.24)$$

and for correct impedance matching

$$Z_5 out = \frac{Z_6 in \cdot Z_7 in}{Z_6 in + Z_7 in} \qquad (4.25)$$

70

therefore

$$Z_6in = 2Z_5out \text{ and } Z_7in = 2Z_5out \qquad (4.26)$$

At node **g**, for correct impedance matching

$$Z_7out = Z_8in \qquad (4.27)$$

4.6 Series feed impedance determination

The feed phase delay required to compensate for the physical rotation of the radiating elements is implemented with the odd lengths of feed section ($\theta_{odd} = \phi_{em}$) and determined using (4.1). The dual feed point of each radiating element is matched to the main feed network using quarter feed sections, therefore all even lengths of feed section are a quarter wave in length ($\theta_{even} = 90°$). This is illustrated in Figure 4-4.

In the three element array, the phase delay implemented by the odd feed sections (θ_3 and θ_5) is 120 degrees so matched feed sections are required (the impedance looking into each end of this feed line section must be the same as its characteristic impedance). In the two and four element array, the feed phase delay is 90 degrees allowing the use of quarter wave matching transformers for the sections, thus allowing the source and load impedance of these odd feed sections to differ.

In all cases, Z_2 is a function of both the input impedance into the array (Z_1out) and the input impedance to the dual feed point of the first radiating element (Z_L). Z_2 is therefore constrained to a specific value that satisfies both of these conditions; for the same reason Z_3in is also constrained to a specific value. Z_3 and Z_3out in the three element array are also constrained to the value of Z_3in as a matched line is required (due to 120 degree length). However, if they satisfy conditions for correct power splitting and impedance matching, the characteristic impedance of the remaining feed sections are only constrained by the limits imposed by microstrip line realisation and the load impedance of the radiating elements.

Solutions for the two and three element array have been generated manually; however, due to the large number of unknown variables, manual generation of the variables within the 4 element array is too complex to find efficient solutions. The feed values were therefore generated and optimised for minimum track width using the optimisation algorithm presented in the following chapter.

The design parameters for the three series feed networks can be found in Table 4-1 where the input impedance at the feed point of the array was set to 50Ω and the input impedance to the radiating elements set to 50Ω.

Design Parameter	Two element array	Three element array	Four element array
Z_1	50Ω	50 Ω	50 Ω
θ_1	0°	0°	0°
Z_2	70.7 Ω	86 Ω	100 Ω
θ_2	90°	90°	90°
Z_3	100 Ω	75 Ω	80 Ω
θ_3	90°	120°	90°
Z_4	70.7 Ω	86 Ω	120 Ω
θ_4	90°	90°	90°
Z_5		150 Ω	96 Ω
θ_5		120°	90°
Z_6		86 Ω	80 Ω
θ_6		90°	90°
Z_7			128 Ω
θ_7			90°
Z_8			80 Ω
θ_8			90°

Table 4-1: Design parameters for series fed arrays.

4.7 Array performance

Array performance can be obtained by expanding the analysis derived to model the dual feed radiating element presented in Chapter 3.

4.7.1 Input impedance

Array input impedance, as a function of frequency, can be determined by transforming each radiating element's input impedance through the feed network, back to the input terminal.

The input impedance of each radiating element (Z_L), derived in Chapter 3, is transformed through the even numbered series feed sections using

$$Z_{in} = Z_0 \left[\frac{Z_L + jZ_0 \tan\left(\frac{\pi}{2}\right)}{Z_o + jZ_L \tan\left(\frac{\pi}{2}\right)} \right] \qquad (4.28)$$

where Z_{in} is the input impedance and Z_0 is the characteristic impedance of each even feed line section. The length of these feed sections is set to $\pi/2$ as the resulting quarter wave transformer allows the radiating elements to be easily matched to the main feed section.

Impedances are transformed through the odd numbered feed sections using

$$Z_{in} = Z_0 \left[\frac{Z_{out} + jZ_o \tan(\phi_{pm})}{Z_0 + jZ_{out} \tan(\phi_{pm})} \right] \qquad (4.29)$$

where Z_{out} is the impedance looking into each odd feed section back to the array feed point and ϕ_{pm} is the feed phase delay for that array.

The impedance at each node is resolved using

$$Z_{odd}out = \frac{Z_{odd}in \times Z_{even}in}{Z_{odd}in + Z_{even}in}$$ (4.30)

as detailed in the previous section.

Array input impedance of the four element array is therefore determined by transforming Z_L (the input impedance of the last patch) up Z_8 and then Z_7 using (4.28) and (4.29). The input impedance of the next patch is transformed up Z_6. The resulting impedance looking into node **e** is found by adding the resulting transformed impedances using

$$Z5out = \frac{Z6in \times Z7in}{Z6in + Z7in}$$ (4.31)

In the same way, this impedance is then transformed back to node **c** through Z_5 and summed with the next radiating elements input impedance, once it has been transformed up Z_4. This continues until the input impedance of all radiating elements have been transformed back to the arrays feed point.

4.7.2 Axial ratio

The axial ratio of a single radiating element can be found by determining the relative phase and magnitude of the orthogonal mode voltages as described in Chapter 3. The array's axial ratio can be determined by summing the relative magnitude, phase and physical orientation of the fields from all of the patches that make up that array.

As with the dual feed radiating element, the reflection coefficients at all the junctions within the feed network must first be determined. Both magnitude and phase of each patches orthogonal mode voltage relative to the feed signal can then be obtained by multiplying the voltage ratio of each feed section back to the arrays input terminal. A relative comparison can then be made between the magnitude and phase of each patch's orthogonal mode voltages.

The relative amplitude and phased of each orthogonal patch mode voltage was determined by transforming all orthogonal patch mode voltages back through the array to the arrays feed point using equation (3.14). These voltages were then resolved

into X and Y components. If the first dual feed patch in the array has relative orthogonal mode voltages V_a and V_b, the contribution from V_a to the X and Y components (V_{ax} and V_{ay} respectively) of the resulting far field radiation pattern is given by

$$V_{ax} = V_a \cos \phi_p \text{ and } V_{ay} = V_a \sin \phi_p \qquad (4.32)$$

Where ϕ_{pm} is the physical rotation of that element.

The contribution from V_b can be found in the same way, however as the two modes on the patch are orthogonal in space (for circular polarisation), $\pi/4$ must be added to the rotation angle as V_b is physically rotated 90 degrees with respect to V_a. Therefore

$$V_{bx} = V_b \cos \left(\phi_p + \frac{\pi}{4} \right) \text{ and } V_{by} = V_b \sin \left(\phi_p + \frac{\pi}{4} \right) \qquad (4.33)$$

The total contribution from each patch orthogonal mode voltage to the X component of the far field radiation pattern is therefore given by

$$X_{total} = \sum_{m=1}^{M} V_{axm} \cos \phi_{pm} + V_{bxm} \cos \left(\phi_{pm} + \frac{\pi}{4} \right) \qquad (4.34)$$

and the total resulting Y component is given by

$$Y_{total} = \sum_{m=1}^{M} V_{axm} \sin \phi_{pm} + V_{bxm} \sin \left(\phi_{pm} + \frac{\pi}{4} \right) \qquad (4.35)$$

It should be noted that in an array where the sides of the patches are in geometric alignment (as in the two and four element array), each orthogonal mode voltage will contribute wholly to only the X or Y component. Therefore in equation (4.32) and (4.33) either the first or second term will always be zero. However provision as to be made for cases where the patches orthogonal modes are not in relative alignment with each other as in a three element array.

4.7.3 Series feed performance

Using analysis presented in the previous section both VSWR and axial ratio frequency performance were determined for the two, three and four element arrays.
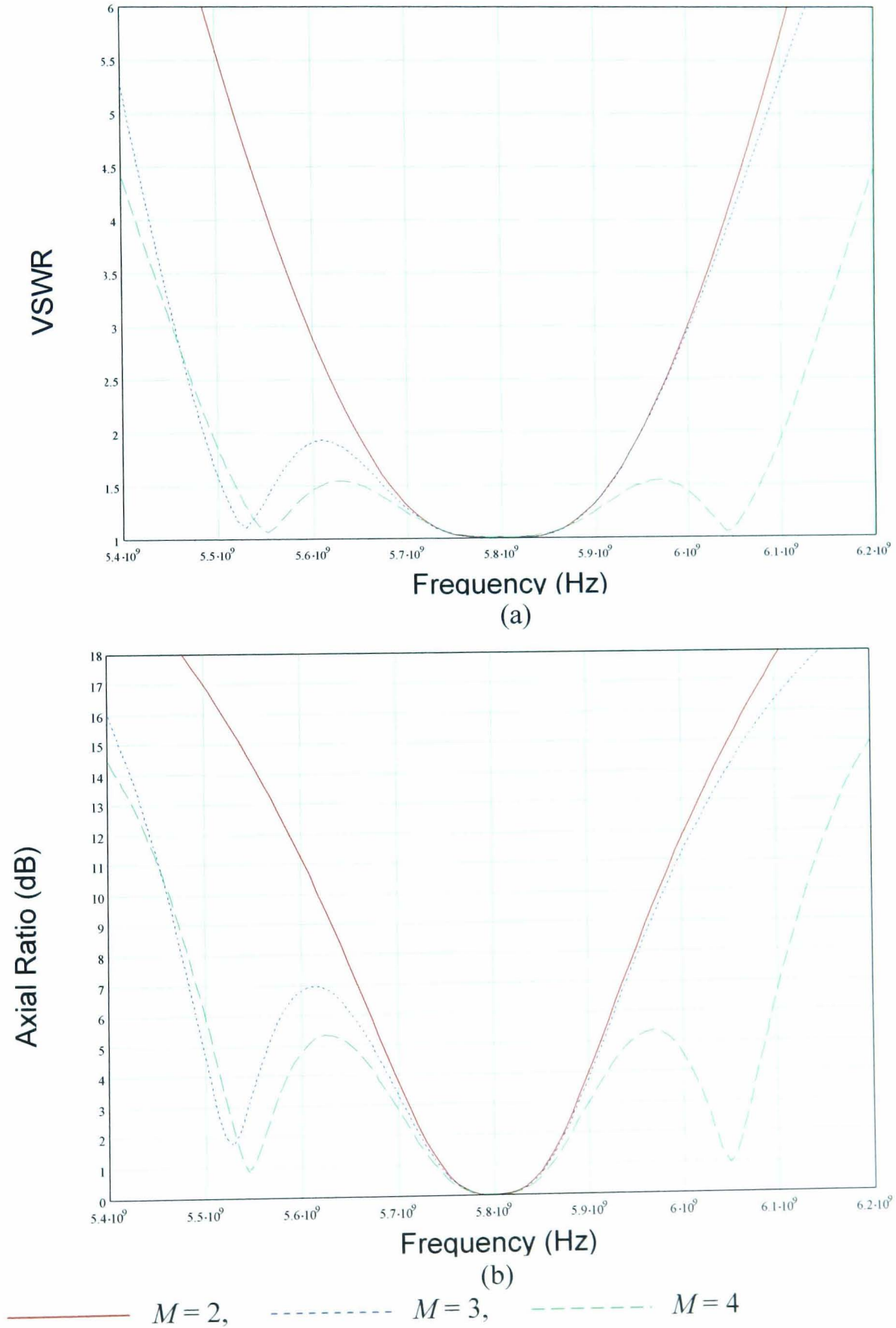
Figure 4-7: (a) VSWR (b) Axial ratio performance of a two, three and four element array using a series feed network ($\varepsilon_r = 2.33$, $h = 0.79$ mm).

Although an improvement is seen over the single radiating element, the two element array displays the least VSWR and axial ratio bandwidth improvement of the three series fed arrays presented here. The three element array has a wider VSWR bandwidth than the two element array this improvement is not symmetrical around the design frequency, as seen in Figure 4-7 (a), and the VSWR 2:1 bandwidth is very sensitive due to the amount of ripple in the pass band. The four element array has the widest bandwidth, with a VSWR 2:1 bandwidth that is almost twice as wide as that demonstrated by the other series fed configurations presented here.

The 4 element array also has the widest axial ratio bandwidth although only marginally wider than the 3 element array which in turn is marginally wider than the two element array as seen in Figure 4-7 (b). Although axial ratio bandwidth does increase over that of the single radiating element, the improvement is not as large as seen with the VSWR bandwidth.

4.7.4 Corporate feed performance

The characteristic impedance and length of the feed line sections of the arrays seen in Figure 4-3 (a) (where $d_2 = 0$ in reference [67]) can be found in Figure 4-8.
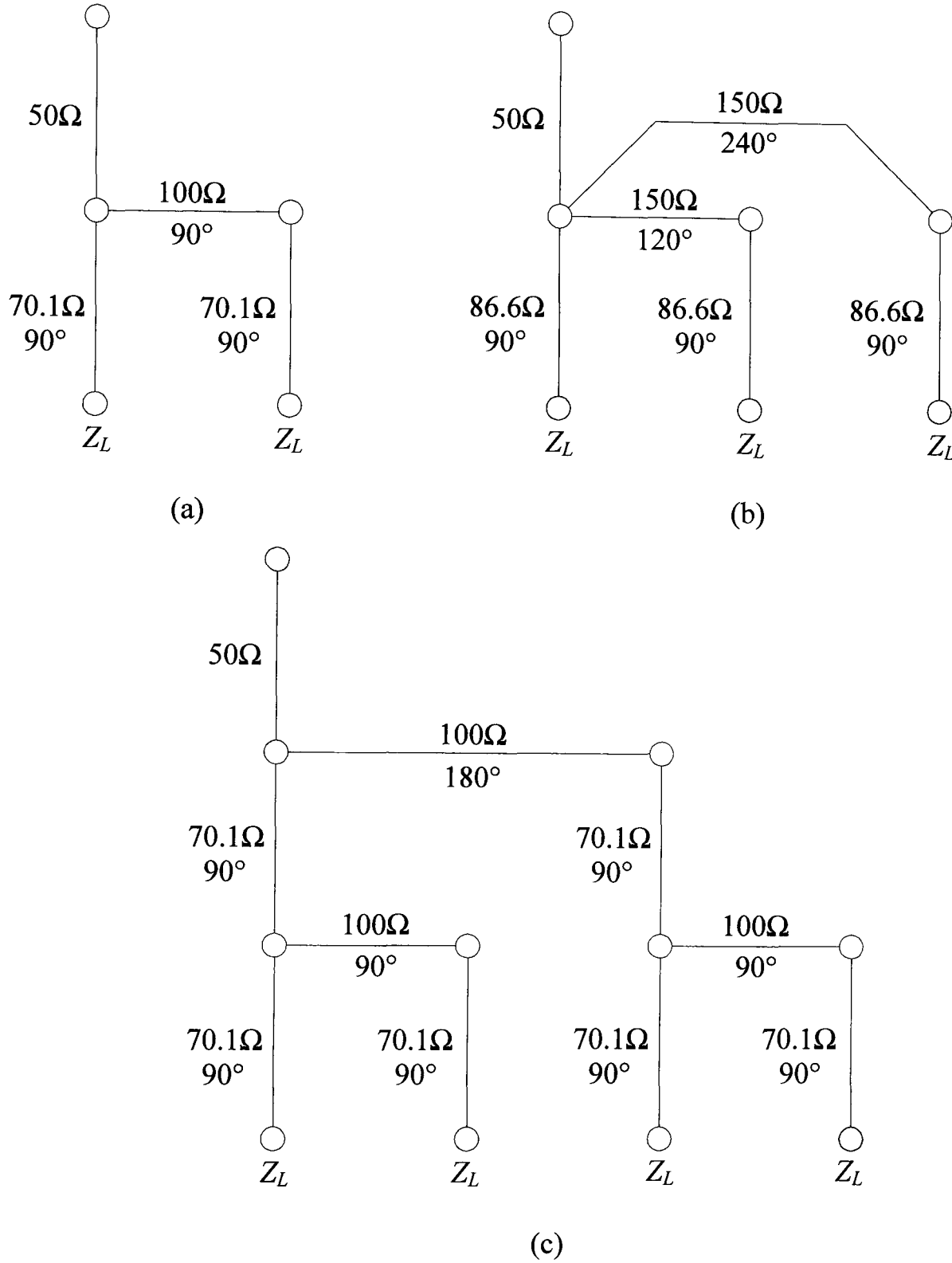
Figure 4-8: Design parameters for (a) two, (b) three and (c) four element corporate fed array.

The analysis presented in Section 4.7.1 and 4.7.2 is used to evaluate the performance of the corporate fed arrays seen in Figure 4-8. Both input impedance and axial ratio

performance can be seen in Figure 4-9. The results are in good agreement with [67] which predicts the three element array to have superior performance over the two and four element arrays.
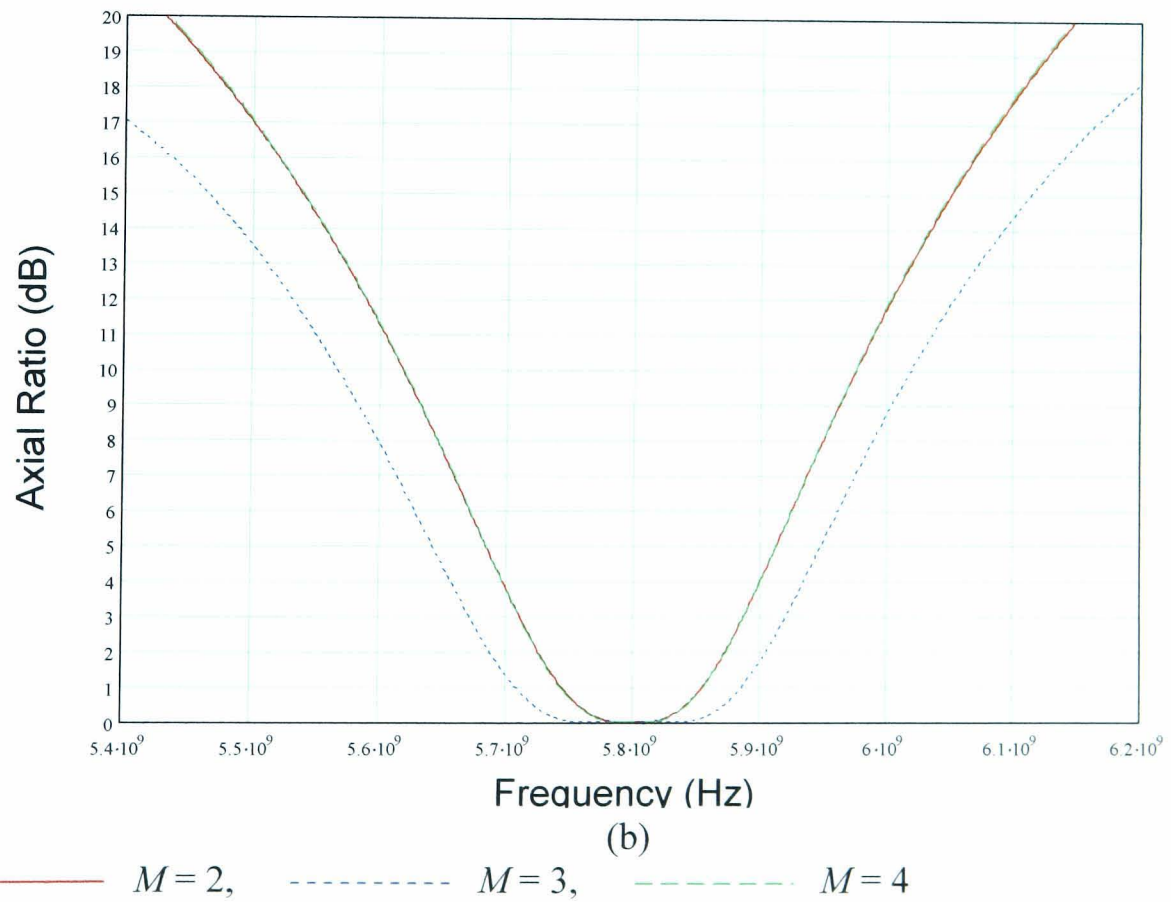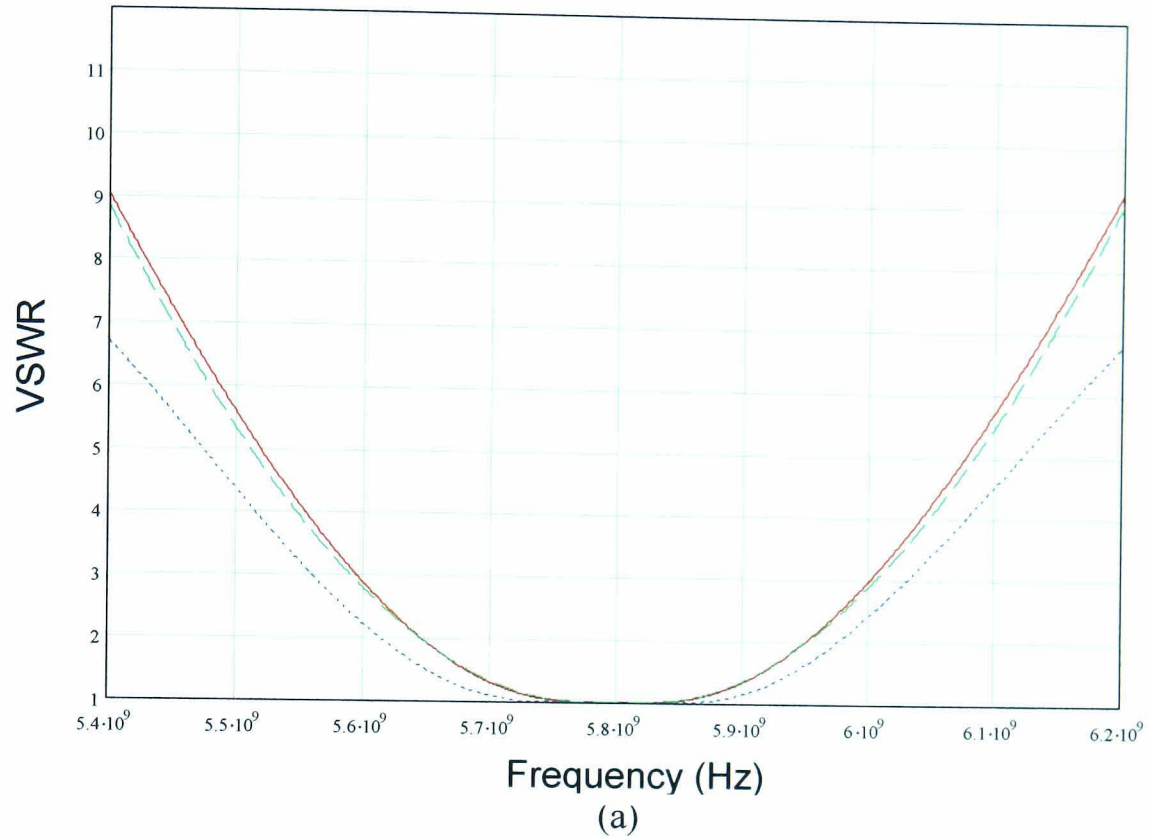
Figure 4-9: Performance of a two, three and four element array using a corporate feed network ($\varepsilon_r = 2.33$, $h = 0.79$ mm) (a) Input impedance and (b) Axial ratio.

The performance of the two element array (where $M = 2$ and $p = 1$) is the same as the performance of the four element array (where $M = 4$ and $p = 2$). This is expected as the four element array is composed of two 2x1 element pairs. The patch pairs require a 180 degree difference in feed phase, so are separated by a half wave section of feed line which acts as an impedance transformer with no cancellation effect. These configurations have the narrowest input impedance and axial ratio bandwidths. This is expected as both two and four element array configuration satisfy $p = M/2$; shown in Section 4.2 to be least sympathetic to multiple internal reflections within the corporate feed network. The three element array has the broadest bandwidth when a corporate feed is used.

4.7.5 Series and Corporate feed comparison

The performance of the two element array is the same for both corporate and series fed arrays. This is because when the 90 degree feed delay is introduced into the corporate feed it adopts the same geometry as the series feed (as seen in Figure 4-3). The performance of the corporate fed 3 element array is not only more symmetrical around design frequency than the series fed example, but also has the widest axial ratio bandwidth of all arrays considered in this section. However, from a geometrical perspective, this array is not as attractive as the 4 element array. The four element array using a series feed not only out performs the four element corporate fed array but also demonstrates the widest VSWR 2:1 bandwidth of all arrays considered in this section. A summary of all array performance can be found in Table 4-2.

Feed	Bandwidth	2 patch array	3 patch array	4 patch array
Series	VSWR 2:1	5.2%	7.9%	10.4%
	3 dB Axial Ratio	3%	3.1%	3.5%
Corporate	VSWR 2:1	5.2%	6.1%	5.2%
	3 dB Axial Ratio	3%	4.2%	3%

Table 4-2: Bandwidth of series and corporate fed two, three and four element arrays.

4.8 Alternative radiating elements

The optimised dual feed radiating element developed in chapter 3 have so far been used in the arrays. In the following section evaluation is made into array performance when a single feed nearly square radiating element is used as an alternative monolithic radiating element. Later, in Chapter 7, array the performance of the four element serial fed arrays using a multi layer aperture coupled radiating element is also evaluated.

4.8.1 Single feed radiating element design

The design parameters for a single feed nearly square patch antenna can be found in Figure 4-10.
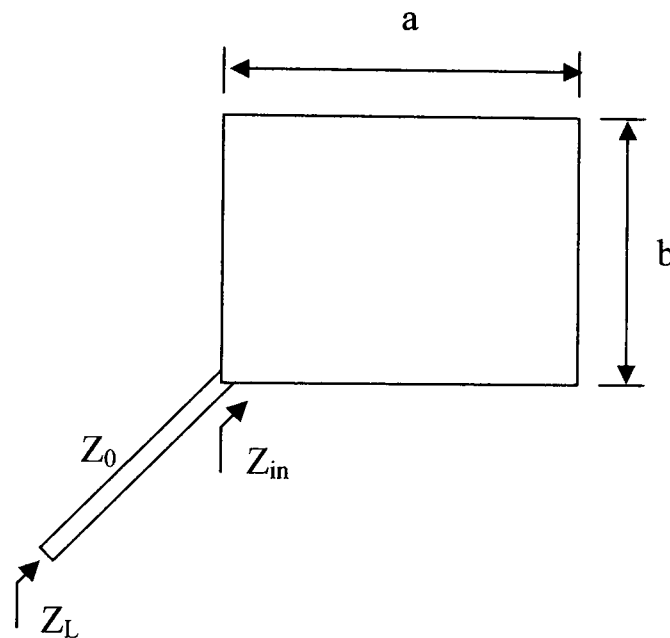
Figure 4-10: Nearly square patch design parameters (a = 16.495 mm, b = 16.135 mm, Z_{in} = 305Ω, Z_0 = 123Ω, Z_L = 50Ω, h = 0.79 mm and ε_r = 2.33).

The dimensions of the patch **a** and **b** were determined using a method based on the Green function approach as detailed in [105]. Z_{in} is the input impedance seen at the corner of the nearly square patch and was determined using [106].

Three array configurations of single feed radiating elements can be seen in Figure 4-11 they share physical rotation and the feed phase with the arrays of dual feed radiating elements seen in Figure 4-3 (b).
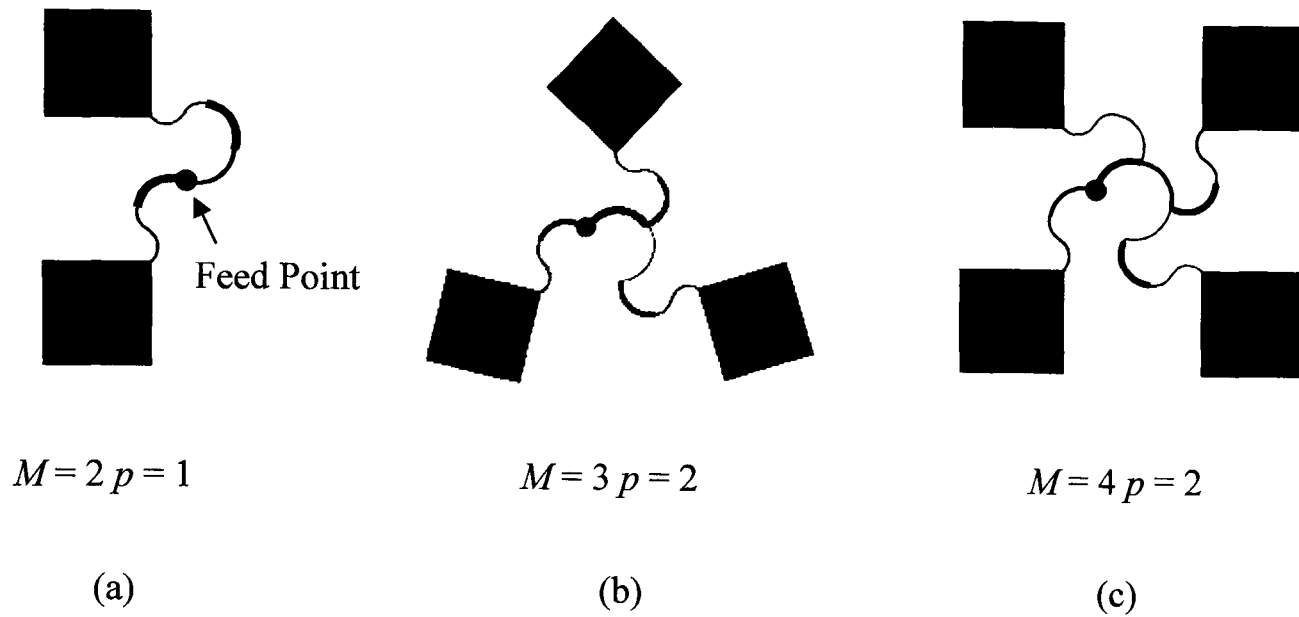
Figure 4-11: Two, three and four element arrays using single feed nearly square radiating elements.

The quarter wave matching transformer between the corner of the nearly square patch and the series feed network ensures an input impedance Z_L of 50 ohms, allowing the use of the series feed design parameters presented in Table 4-1.

Single feed radiating elements have far less dimensional tolerance than dual feed radiating elements. As a consequence, due to the detuning effect of adjacent elements, they are far more sensitive to mutual coupling. For this reason, VSWR and axial ratio performance has been evaluated using full wave simulation and are presented in Figure 4-12.
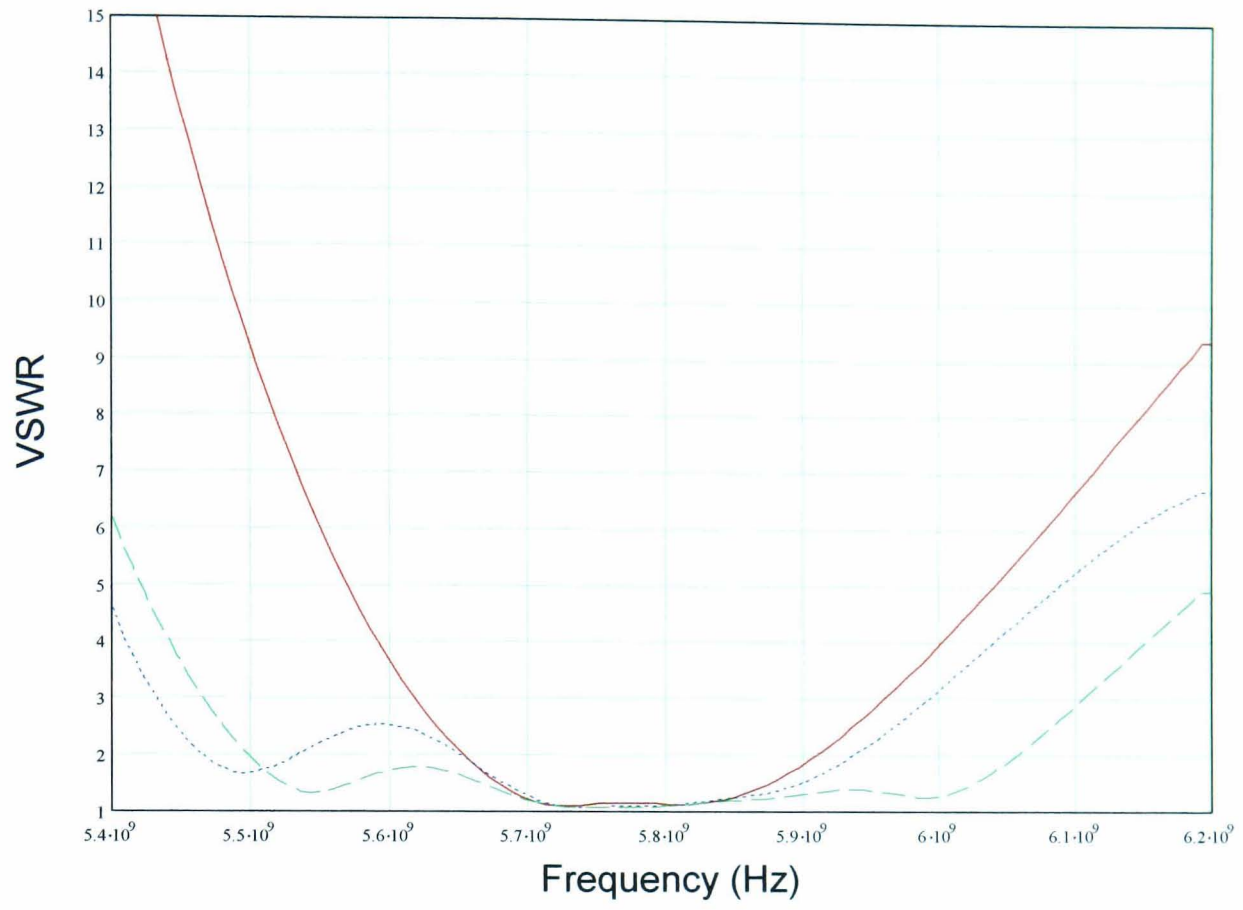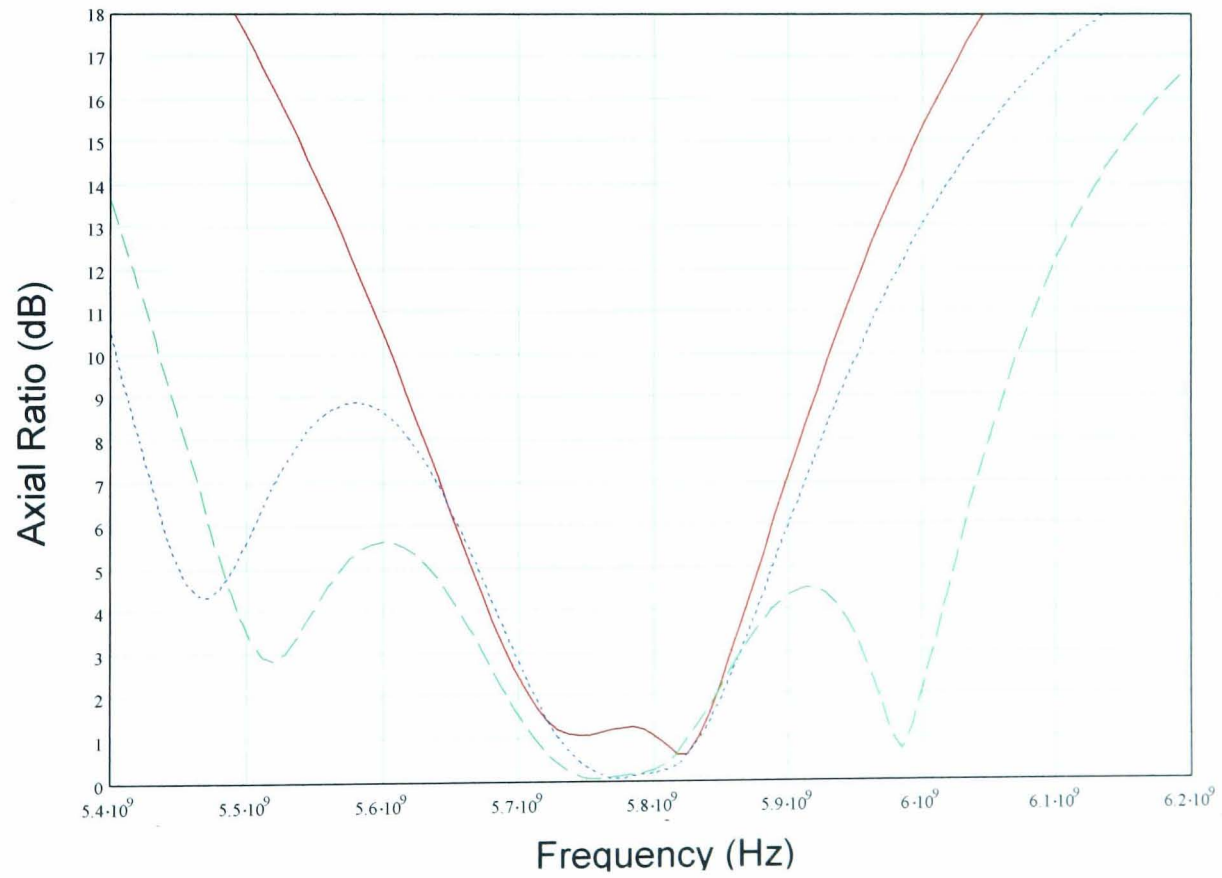
Figure 4-12: (a) VSWR (b) Axial Ratio of arrays containing single fed elements (ε_r = 2.33, h = 0.79 mm).

From Figure 4-12 it can be seen that the performance of the arrays using single feed radiating elements is characteristically similar to the performance of the same arrays using the optimised dual feed radiating elements. This information is summarised in Table 4-3. The arrays with single feed radiating elements demonstrate less VSWR and axial ratio bandwidth when compared to the arrays using dual feed radiating elements. Although the input impedance of the three element array demonstrates the same characteristical frequency performance, the VSWR 2:1 bandwidth is substantially less due to increased ripple in the pass band.

		2 patch array	3 patch array	4 patch array
Dual feed	VSWR 2:1	5.2%	7.9%	10.4%
	3 dB Axial Ratio	3%	3.1%	3.4%
Single feed	VSWR 2:1	4.4%	5%	9.6%
	3 dB Axial Ratio	2.98%	2.9%	3.3%

Table 4-3: Summary of bandwidth of monolithic Dual and Single feed radiating elements.

4.9 Practical realisation

4.9.1 Array layout design

The series fed arrays described in Figure 4-3 (b) can be seen in Figure 4-13. The radiating elements form small clusters as this helps radiation pattern symmetry [67]. The series feed line sections were wrapped around to fit within the radiating elements and, where possible, smooth bends were used as it has been shown that this can reduce spurious feed radiation [107]. It is noted that the series feed offers a particularly elegant and compact structure. Indeed at this patch spacing, when dual feed radiating elements are used, there is insufficient room for a corporate feeding system without the feed line sections becoming over crowded.

$$M = 2\ p = 1 \qquad\qquad M = 3\ p = 2 \qquad\qquad M = 4\ p = 2$$

(a)   (b)   (c)
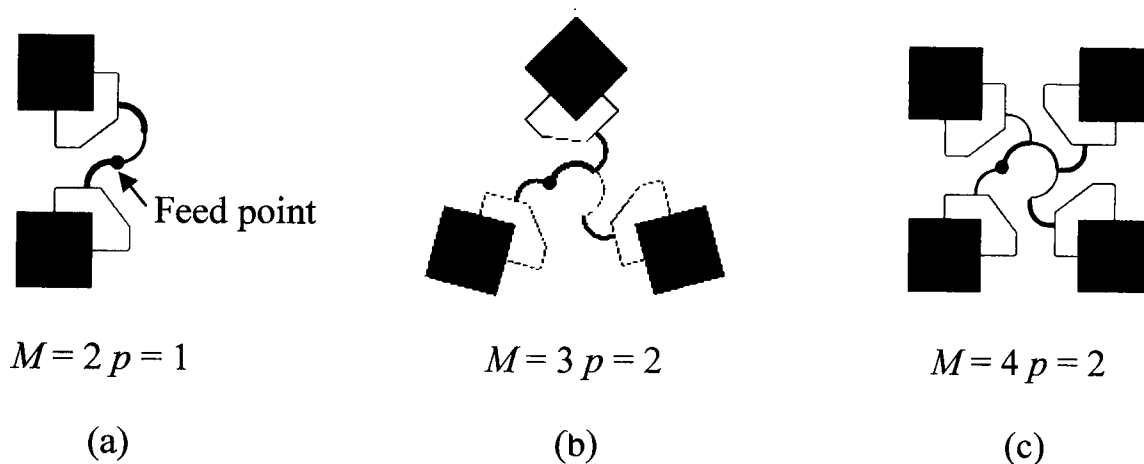
Figure 4-13: Sequentially rotated series fed arrays composed of two, three and four dual feed radiating elements.

4.9.2 Fabrication

The series fed arrays were fabricated using 0.79 mm 1/2oz RT 5870 Duroid (ε_r of 2.33) using traditional printed circuit board techniques. In all cases the arrays are probe fed from behind the ground plane using an SMA connector.

4.10 Practical Results

Measurements of input impedance and axial ratio were made between 5.4 and 6.2 GHz. Practical measurement of input impedance were made using an Anritsu 37347C vector network analyser and measurements of axial ratio made within an anechoic chamber as described in Appendix C.

From Figure 4-14 it can be seen that the two patch array has a measured VSWR 2:1 bandwidth of 5.4% between 5.6346GHz and 5.9463GHz. The axial ratio has was measured at less than 3 dB between 5.711 and 5.885GHz resulting in a 3 dB bandwidth of 3%.

From Figure 4-15 it can be seen that the three patch array has a VSWR 2:1 bandwidth of 7.6% between 5.505GHz and 5.95GHz. The 3 dB axial ratio bandwidth was measured at 2.6% between 5.76 and 5.9GHz.

From Figure 4-16 it can be seen that the four patch array has a VSWR 2:1 bandwidth of 10.4% between 5.48GHz and 6.085GHz. The 3 dB axial ratio bandwidth was measured at 3.1% between 5.705 and 5.885GHz.

These results are in close agreement with the results generated from the analysis presented in 4.7.3 as seen in Table 4-4.

		2 patch array	3 patch array	4 patch array
VSWR	Modelled	5.2%	7.9%	10.4%
	Measured	5.4%	7.6%	10.4%
3 dB Axial Ratio	Modelled	3%	3.1%	3.4%
	Measured	3%	2.6%	3.1%

Table 4-4: Summary of predicted and measured results.
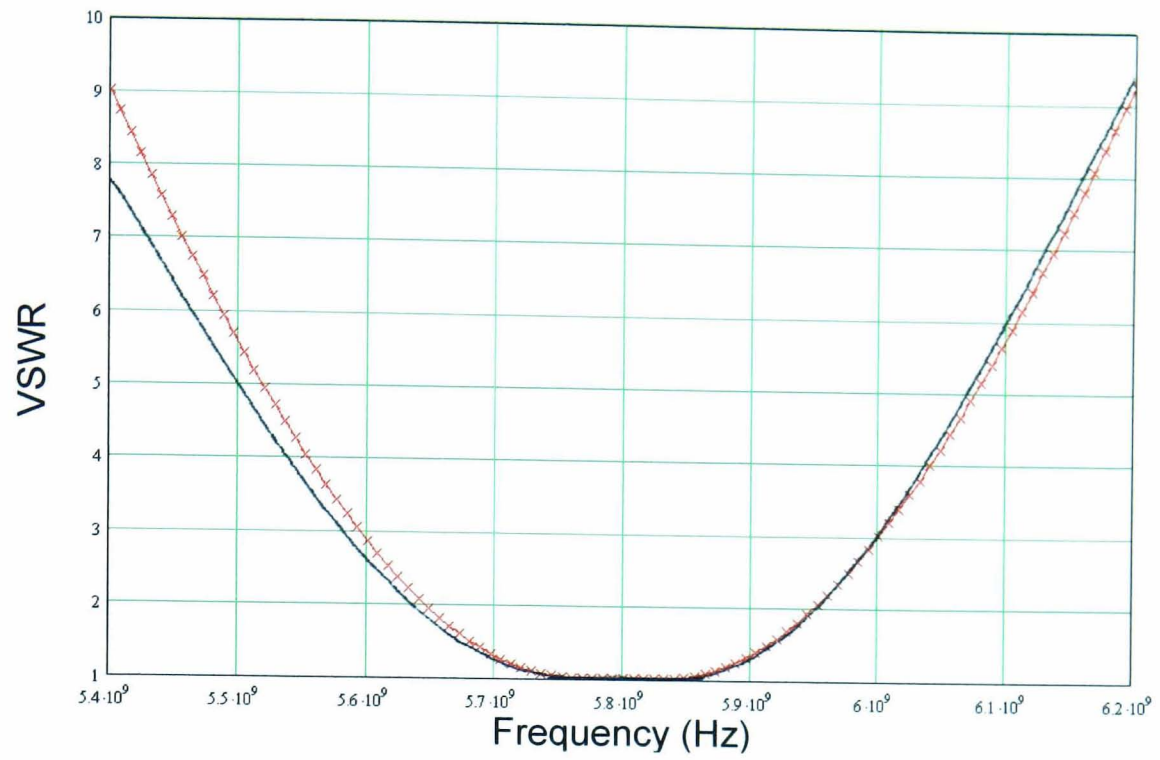
****** Analysis from section **4.7.3**, ———— Measured

(a)
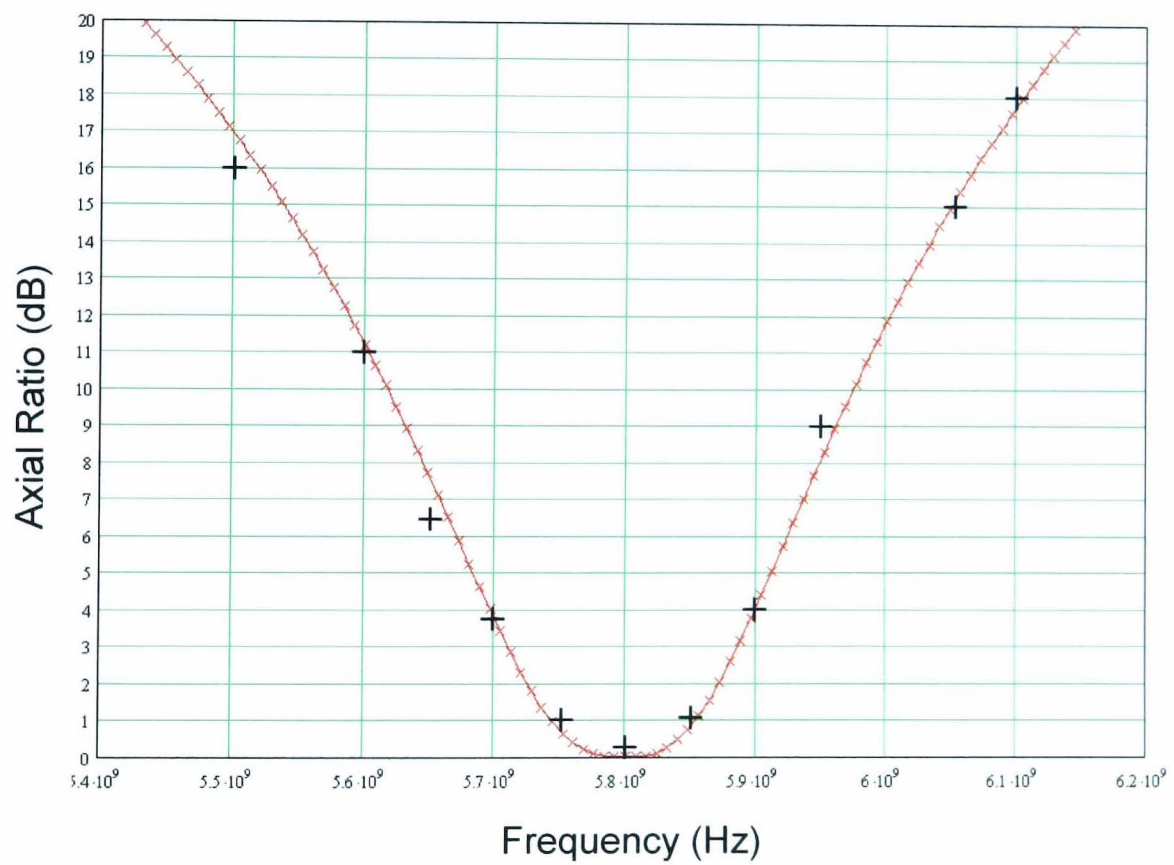
****** Analysis from section **4.7.3**, ✛ Measured

(b)

Figure 4-14: Measured performance of two element array (a) VSWR (b) Axial Ratio.
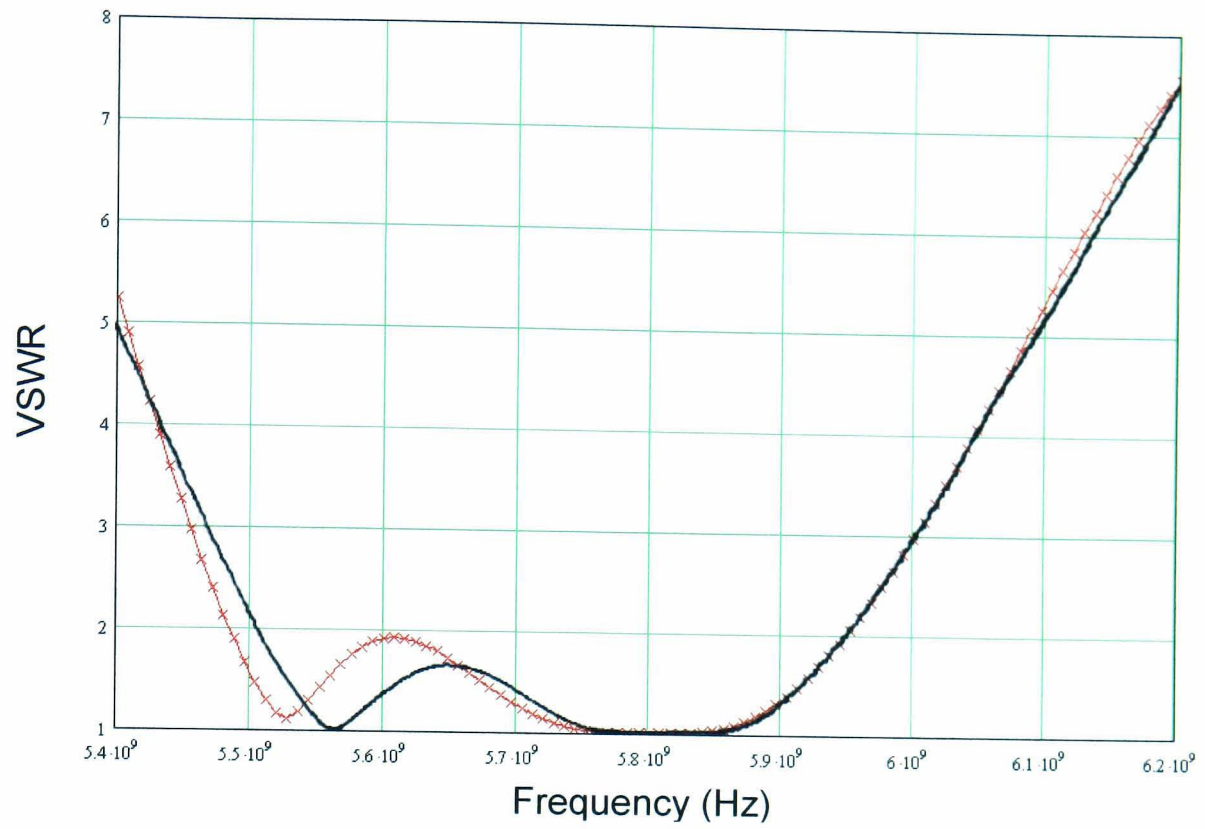
XXXXXX Analysis from section 4.7.3, ———— Measured

(a)
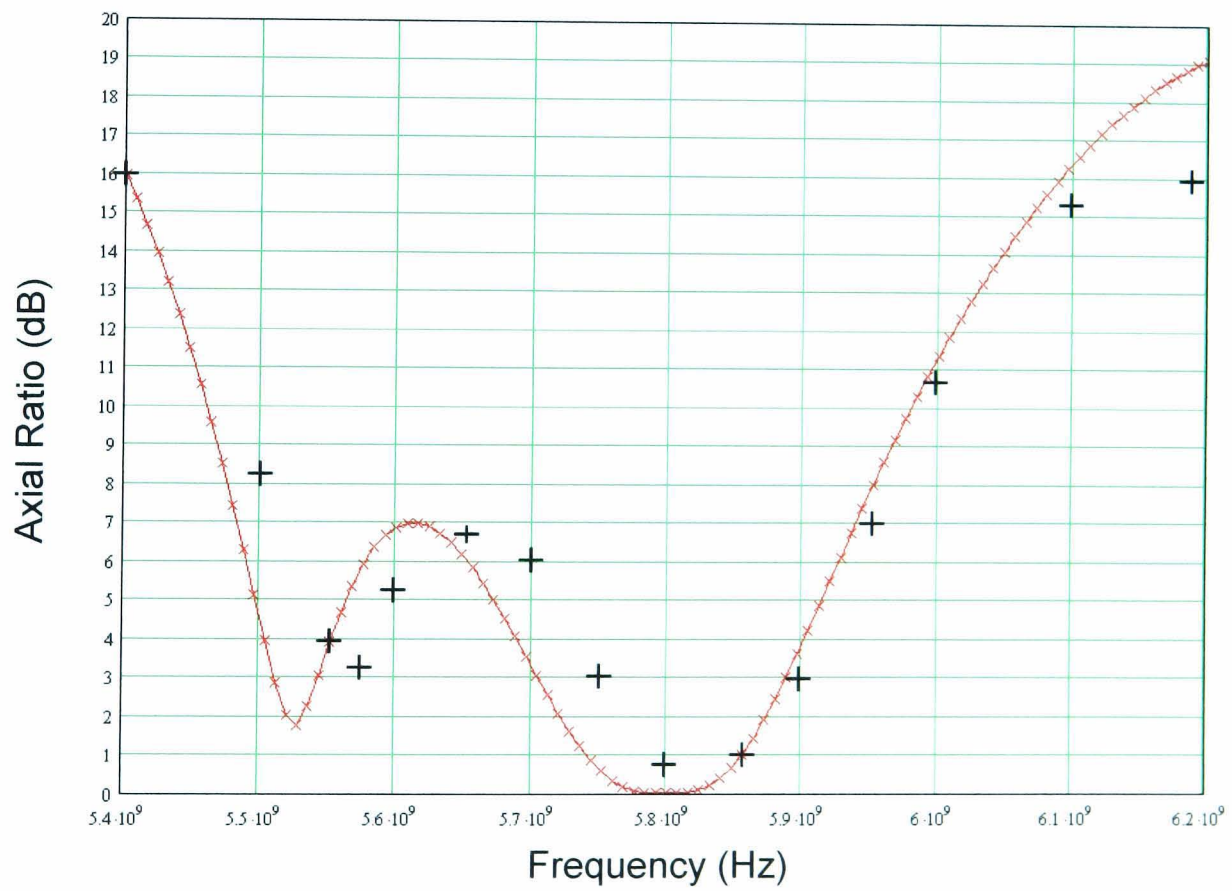
XXXXXX Analysis from section 4.7.3, + Measured

(b)

Figure 4-15: Measured performance of three element array (a) VSWR (b) Axial Ratio.
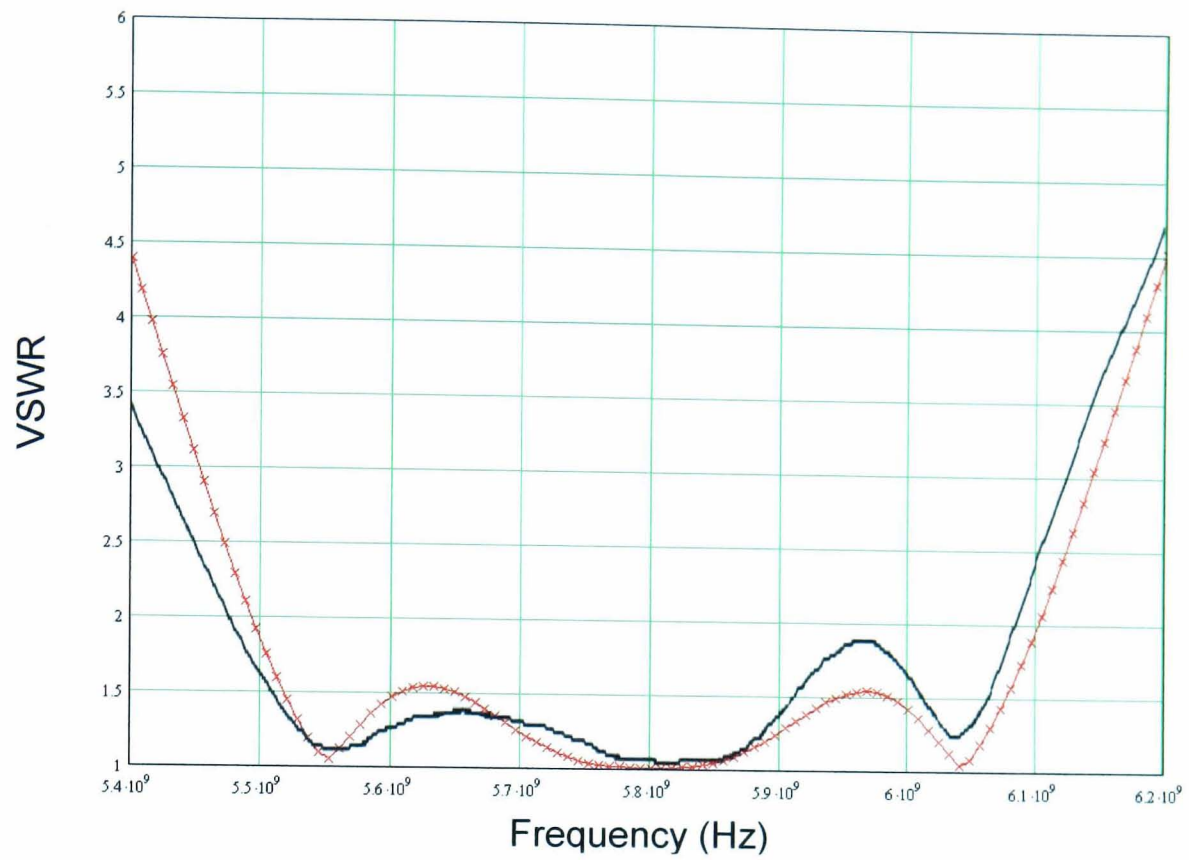
XXXXXX Analysis from section 4.7.3, ———— Measured

(a)
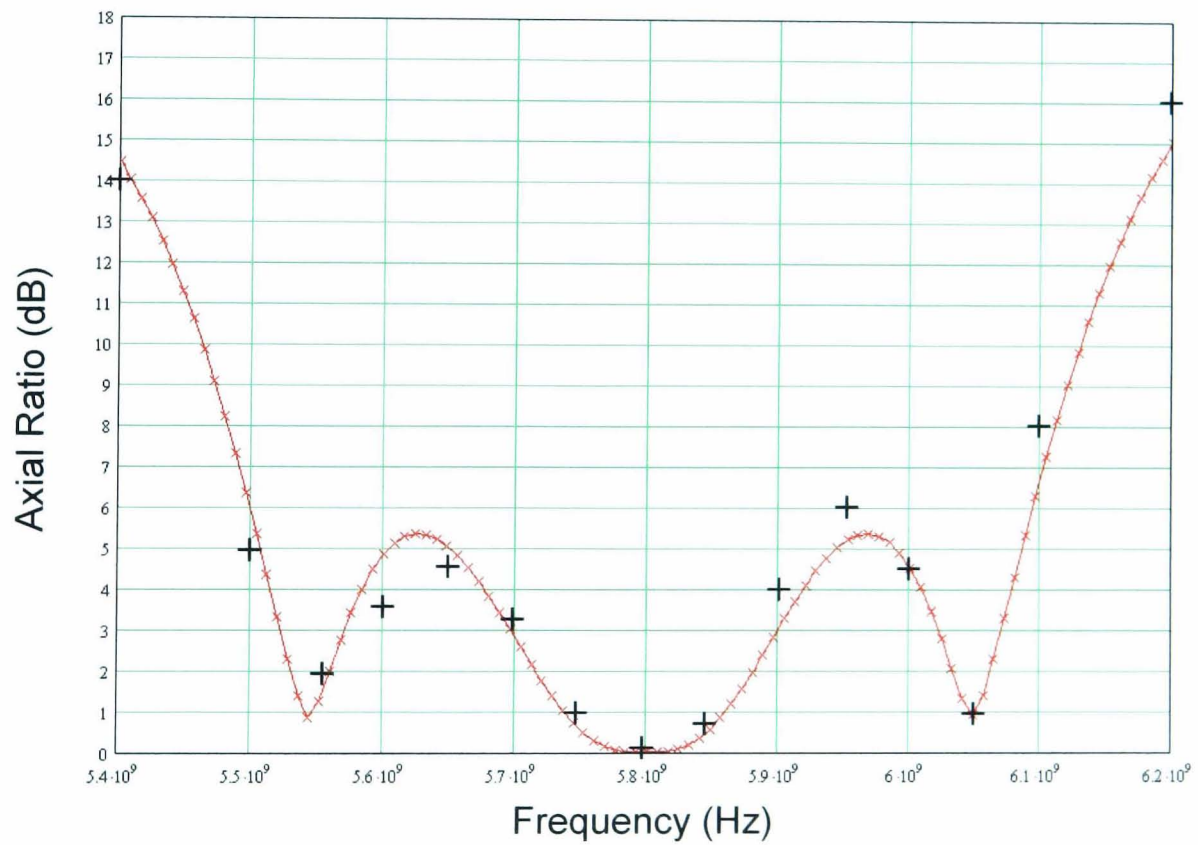
XXXXXX Analysis from section 4.7.3, ✛ Measured

(b)

Figure 4-16: Measured performance of four element array (a) VSWR (b) Axial Ratio.

89

4.11 Conclusion

Sequential rotating radiating elements leads to an improvement in VSWR and Axial ratio bandwidth. The amount of improvement is dependant upon both the choice of feed geometry and number of radiating elements in each array.

Both series and corporate fed two element arrays demonstrate the same bandwidth performance. This is because in a two element array the feed geometries are equivalent.

In the three element arrays, the VSWR 2:1 bandwidth is wider when a series feed is used but the pass band is very sensitive and not symmetrical around design frequency. The corporate fed three element array demonstrates widest 3 dB axial ratio frequency bandwidth of all arrays considered in this chapter.

While the four element corporate fed array has the same bandwidth as the two element arrays, the four element series fed array has the widest Axial Ratio bandwidth of all series fed arrays and the widest VSWR 2:1 bandwidth of all arrays considered in this chapter.

The optimum array configuration will depend upon the real estate resource, gain and bandwidth requirements of a specific application.

It is also noted that the compact nature of the series feed allows the use of dual feed radiating elements. Although the arrays of single fed radiating elements have a less congested feed network, the dual feed radiating elements are more robust to manufacturing tolerances and less susceptible to mutual coupling.

In all cases both modelled and measured results were in close agreement.

CHAPTER 5

OPTIMISED DESIGN OF 2X2 ARRAY

5.1 Introduction

The logistics of an access control application scenario require the range between the OBU and the RSU to be restricted to the length of one vehicle as an unauthorised vehicle refused at a barrier should not be granted access by an authorised vehicle approaching from behind. Furthermore, a broad communication zone is advantageous as lane discipline cannot always be guaranteed at a barrier entry. These requirements are quantified in Table 1-1 and can be satisfied by a four element 2x2 microstrip antenna array. This configuration is particularly attractive as the resulting rectangular lattice is well suited to act as a building block in larger arrays, as seen in the following chapter. This chapter presents the optimum design of a 2x2 array for use within the RSU of an access control system. Both optimisation of the feed network and optimum choice of dual feed radiating element are investigated.

In the previous chapter, it became apparent that manual generation of the feed impedance values for the four element series fed array was problematic as there is no closed form expression to represent all eight feed impedance values. As a consequence, the values must be generated using a time consuming process of trial and error that is very inefficient when performed manually. The series feed network needs to ensure equal distribution of power to each patch antenna while maintaining impedance matching at the design frequency. These constraints do not uniquely define values for the feed impedance elements allowing investigation of optimum solutions which have other desirable features.

In this chapter an adaptation of SA is used to optimise the series feed network. A brief historical introduction into SA is presented; the algorithm is then described and implemented using a computer program. The program is used to generate feed impedance values which are then optimised to a high target value resulting in thin PCB tracks. Various alternative objective functions are also considered. As a direct

result of this research an IEE Electronic Letter has been published titled "Application of simulated annealing to design of serial feed sequentially rotated 2x2 antenna array" [18]. Furthermore, this array has successfully been used within the RSU of a commercial traffic management system.

In Chapter 3 two designs of dual feed radiating elements were presented. Both a traditional design, where the radiating patch was matched to the dual feed using quarter wave transformers, and an optimised design that used complex impedance matching were studied. This chapter also investigates the performance of the 2x2 array when the traditional dual feed radiating elements is used. Both the effect upon array bandwidth and practical implications are highlighted. It was shown in chapter 3 that when a traditional design approach is adopted, the designer has the freedom to change the length of the dual feed lines while maintaining the conditions necessary for circular polarisation. The effect altering the traditional dual feed line length has upon array performance is also investigated.

Experimental measurement confirms array performance, full wave simulation is also used to further validate the integrity of the optimised design approach.

5.2 Series feed optimisation

5.2.1 Simulated annealing

SA exploits an analogy between the natural annealing process (the way in which a metal cools and freezes into a minimum energy crystalline structure) and the search for a minimum in a more general system. The technique is based upon an algorithm originally presented by Metropolis et al. [108] as a means of finding the equilibrium configuration of a collection of atoms at a given temperature. The connection between this algorithm and mathematical minimisation was first noted by Pincus [109], but it was Kirkpatrick et al. [110] who proposed that it form the basis of an iterative improvement optimization technique for combinatorial problems.

In a traditional iterative improvement algorithm, a small change is made to a systems configuration and the resulting fitness of this candidate solution is measured using an objective function. If improvement is seen the candidate configuration is accepted as a

new configuration and the process is repeated until no improvement is seen. The fundamental problem with this approach is that it will become trapped in local but not global minima as it cannot cater for any up hill movement. This is not the case with SA as the Metropolis algorithm allows the possibility of accepting worse solutions.

SA is an optimisation algorithm suitable for optimising very complex or poorly defined systems [110]. As a consequence there has been much recent interest in the use of SA to aid the design of microstrip patch antennas [111,112,113,114]. In this application its virtue is simplicity, well understood behaviour and its ability to determine a single solution.

5.2.2 Network model

The algorithm requires a model of the feed network to act upon. This model can be seen in Figure 5-1 and represents the equivalent transmission line circuit seen in Chapter 4.
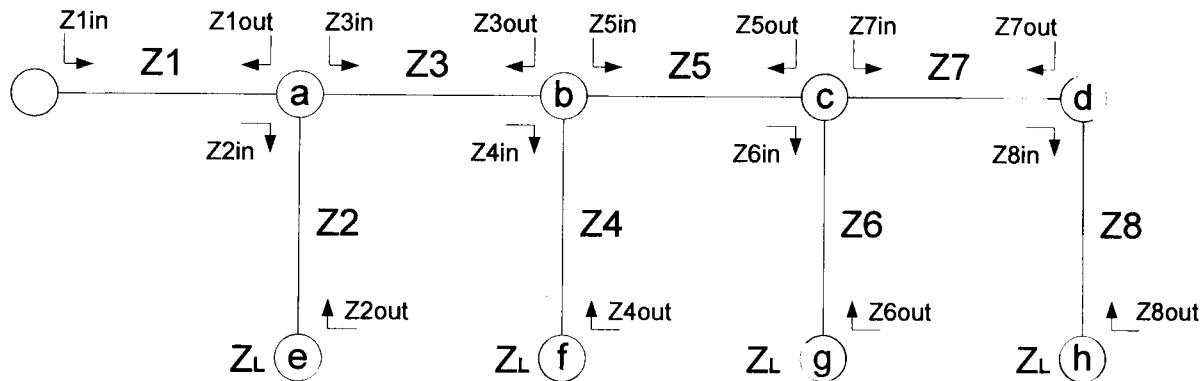
Figure 5-1: Impedance model of series feed network for the four element array.

As the feed phase delays ϕ_p for this four element array are 90 degrees, all feed sections in Figure 5-1 are a quarter wave in length. Therefore the relationship between each feed sections characteristic impedance and the impedance looking into each end of that feed section can be determined using equation (3.7).

Nodes **a** to **h** represent the feed junctions, where power is fed into the array at node **a** and the radiation elements are attached to nodes **e, f, g** and **h**.

During an optimisation run, when the value of a feed elements characteristic impedance is perturbed, this change must be translated to an appropriate change in load and source impedance of that feed section. When both ends of the feed element are free to move, the change in input and output impedances are scaled equally and can be determined using

$$Zin' = k\ Zin \quad \text{and} \quad Zout' = k\ Zout \tag{5.1}$$

Where Zin' and $Zout'$ are the new input and output impedance values and

$$k = Z_0'/Z_0 \tag{5.2}$$

Where Z_0 and Z_0' are the original and the new characteristic impedance of that feed section.

The impedance looking into some of the feed sections is fixed. The impedance looking into node **a** is constrained to the desired input impedance at the feed point of the array. The input impedance at nodes **e**, **f**, **g** and **h** are constrained to the input impedance of the radiating elements. Therefore if one end of a feed section is fixed to a value, its change in characteristic impedance has to be translated to a change in its remaining 'free' end using

$$Zin' = k^2\ Zin \tag{5.3}$$

Where Zin' is the new impedance looking into the free end of that feed section.

Appropriate change must also be made to all other impedances that connect to that node. As correct power splitting and impedance matching are required simultaneously at each node equations (4.18) to (4.27) must be satisfied. Therefore, the appropriate change to connecting feed elements impedance can be determined using

Node **a**: If Z1 changes then Z2in = 4Z1out, Z3in = (4Z1out)/3

If Z2 changes then Z3in = Z2in/3, Z1out = Z2in/4

If Z3 changes then Z1out = (3Z3in)/4, Z2in = 3Z3in

Node **b**:   If Z3 changes then Z5in = (3Z3out)/2, Z4in = 3Z3out

If Z4 changes then Z3out = Z4in/3, Z5in = Z4in/2

If Z5 changes then Z3out = (2Z5in)/3, Z4in = 2Z5in

Node **c**:   If Z5 changes then Z6in = 2Z5out, Z7in = 2Z5out

If Z6 changes then Z5out = Z6in/2, Z7in = Z6in

If Z7 changes then Z5out = Z7in/2, Z6in = Z7in

Node **d**:   If Z7 changes then Z8in = Z7out

If Z8 changes then Z7out = Z8in

5.2.3 The algorithm

In an annealing process a melt is initially at high temperature and disordered. As cooling proceeds and the temperature T reduces, the system becomes more ordered and approaches a ground state (when T = 0) where order is at a maximum and energy is at a minimum. When annealing is simulated during the optimisation of the feed network, the current state of the thermodynamic system is analogous to the current feed solution, the energy equation for the thermodynamic system is analogous to the objective function, and ground state is analogous to the global minimum or optimum configuration.

The algorithm has to perturb a randomly selected feed elements' value, the network must then be resolved and the resulting fitness evaluated. The magnitude of perturbation is proportional to a temperature variable which reduces as the optimisation run progresses. This is analogous to the loss in an atoms thermal mobility in a natural annealing process. If the new solution is fitter than the last it is accepted unconditionally. If it is worse, then there is a probability it may still be accepted. This process is repeated for a set number of iterations at each temperature as shown in the flow chart in Figure 5-2.
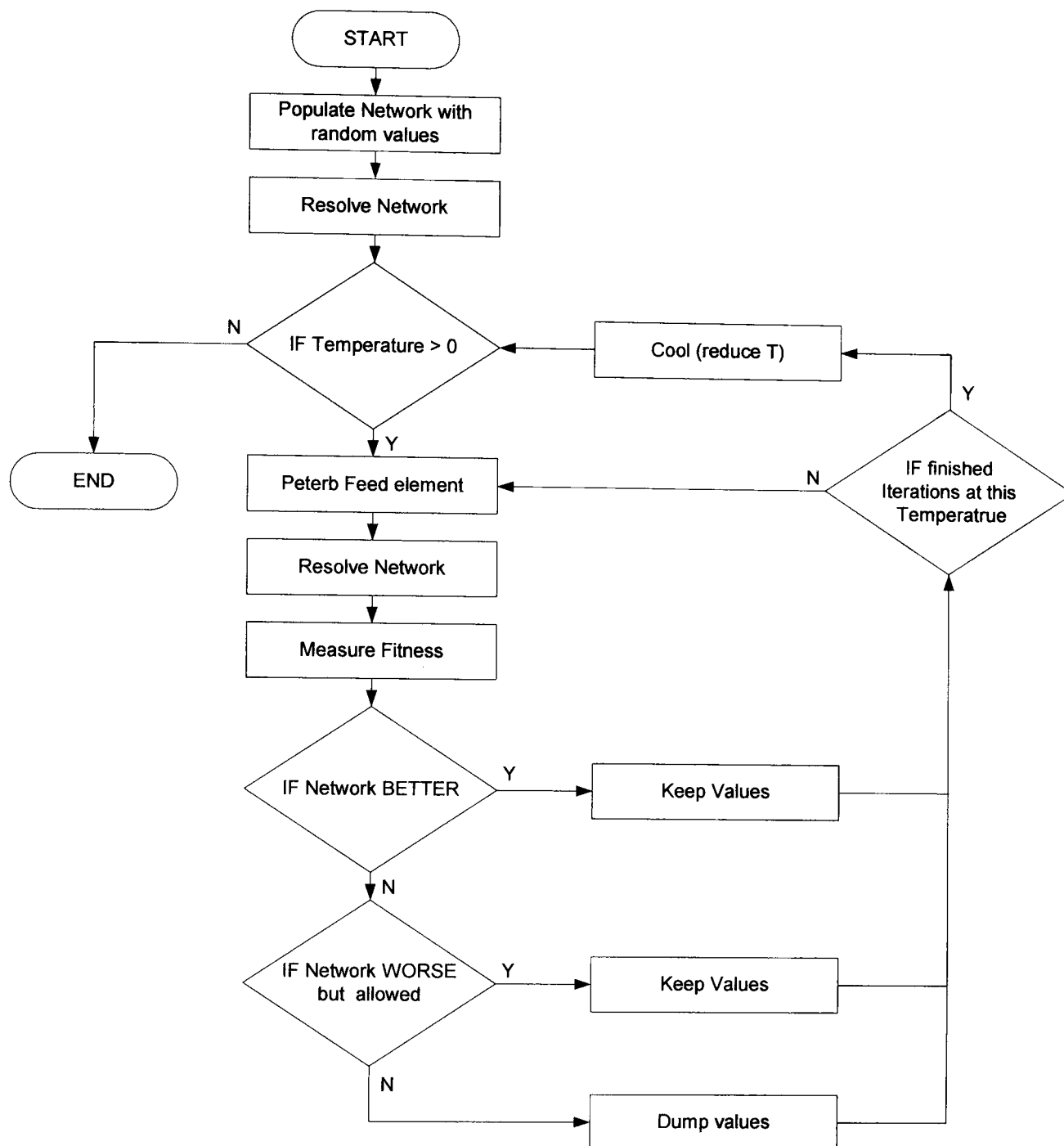
Figure 5-2: Flow chart of the SA algorithm.

The algorithm is run several times and the best solutions saved, as with a traditional iterative improvement algorithm, multiple runs from random starting position reduces further the possibility of the final solution being a local rather than global minima.

5.2.3.1 Network Initialisation

The model must first be initialised to some initial values that are valid. The SA algorithm is relatively insensitive to starting position [110], so random values are entered at unknown nodes, resolving after each entry until all feed elements are correctly defined.

5.2.3.2 Random perturbation

Perturbation is applied at random to the characteristic impedance of any feed element in any direction. These perturbations reflect the current optimisation temperature, so the magnitude of perturbation reduces as an optimisation run progresses.

5.2.3.3 Network resolution

When a feed element is perturbed, this change in characteristic impedance must be translated to an appropriate change in load and source impedance. To maintain correct power splitting and impedance matching at each junction of the feed network, the source or load impedance of all feed sections that connect to that node must also be scaled accordingly. The resulting change in characteristic impedance of these feed sections must then be determined to ensure they remain within an acceptable range. This always ensures a correct network to full mathematical precision.

5.2.3.4 Objective function

The fitness of a candidate network is quantified using an objective function that generates a scalar fitness value. Modifying the fitness function is trivial for any particular application as it is logically separate from the rest of the algorithm, it may even be a weighted sum of multiple factors without any penalty in the rest of the optimisation system.

5.2.3.5 Candidate acceptance

Once the fitness of the candidate solution has been determined the algorithm has to decide whether to accept this new configuration. If the candidate solution is fitter than the current network it is accepted unconditionally. If the candidate solution is less fit than the current solution then its acceptance is determined using the Boltzman probability factor (as used in original metropolis algorithm).

$$\exp{-(\Delta f / K_B T)} \tag{5.4}$$

where Δf is the change in fitness, T is optimisation temperature and K_B is Boltzman's constant.

5.2.3.6 Cooling

The magnitude of random perturbation and the probability of accepting worse solutions are both functions of optimisation temperature T. Therefore, the behavior of the algorithm changes dramatically as an optimisation run progresses and the temperature decreases. When the temperature is high, the magnitude of feed section perturbation is large and the possibility of accepting worse solutions is high. Therefore, in the early stages of an optimisation run the algorithm jumps wildly around the solution space finding areas of possible interest. As the temperature lowers the algorithm focuses in a specific area successively approximating an optimum solution until T reaches zero.

The annealing or cooling schedule defines the starting temperature, how this temperature is lowered as the optimisation run progresses and how many iterations the algorithm remains at each temperature. Traditionally the rate of cooling was chosen to be similar to a physical cooling system, where the temperature is reduced exponentially in annealing time. This is the Metropolis cooling schedule [108] and entirely arbitrary. Quicker cooling schedules may be chosen, though they may not be guaranteed to find the global minimum as the original does [115]. This adaptation of SA is known as simulated quenching [116], the effect of the modified algorithm is to trade off coverage of the solution space for speed of convergence.

Popular alternative cooling schedules include the linear cooling schedule where

$$T_{new} = T_{old} - \Delta T \tag{5.5}$$

and the proportional cooling schedule where

$$T_{new} = C \times T_{old} \text{ where } C < 1.0 \tag{5.6}$$

5.2.4 Implementation

The algorithm has been implemented using C++ running on a standard PC.
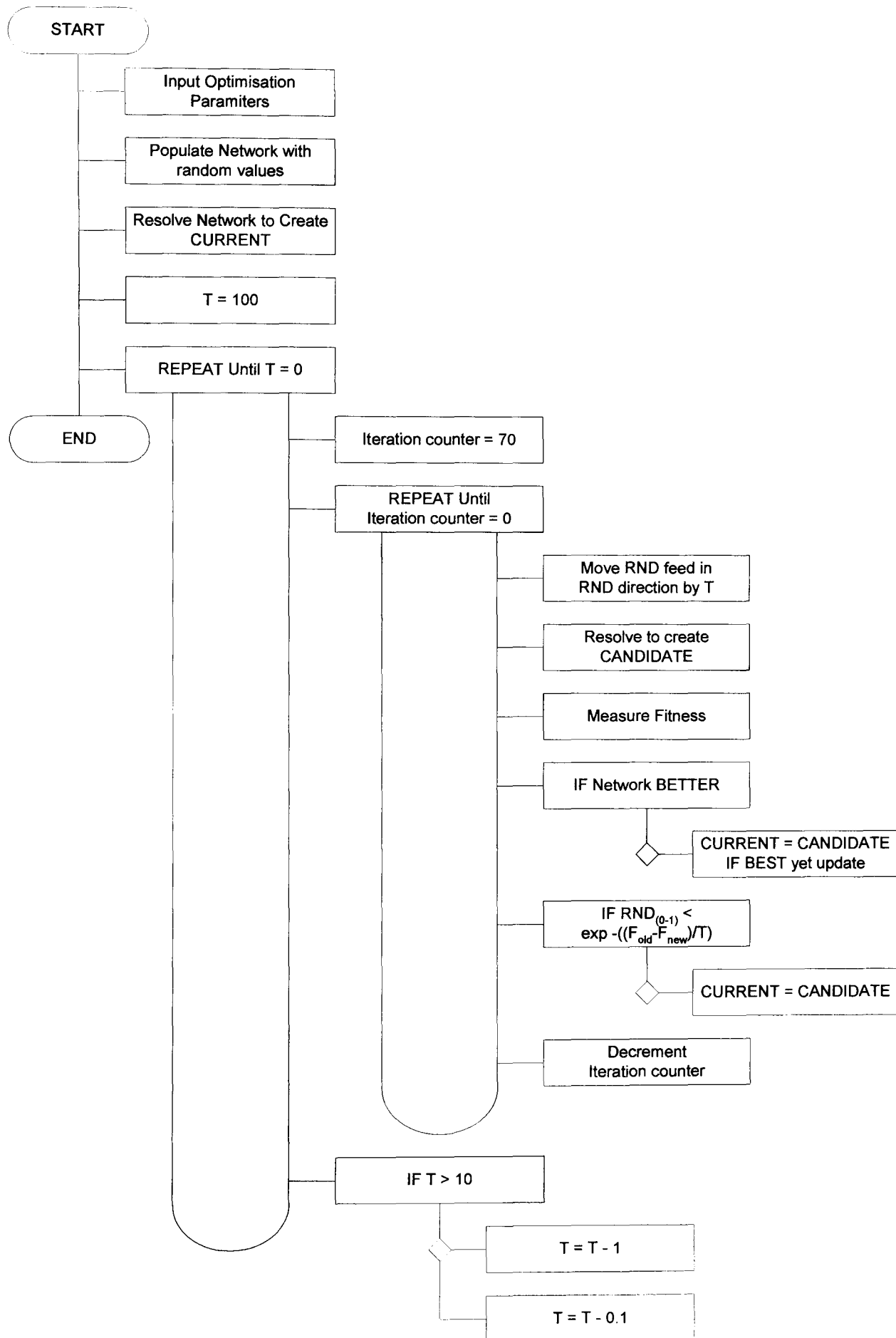
Figure 5-3: Design structure diagram of SA optimisation program.

99

The structure of the program is illustrated by the design structure diagram shown in Figure 5-3.

The input impedance to the feed network and the input impedance of the radiating elements are entered into the program. The choice of objective function and allowable range of feed impedances are also defined. The network is populated with random values until it can be successfully resolved generating a current network.

The algorithm is composed of a pair of nested loops. The outer loop controls the reduction in temperature (which is proportional to the reduction in the magnitude of random perturbation and probability of accepting a less fit network). A starting temperature of 100 was selected, initially this value is too high to produce good networks but un-resolvable solutions are successively discarded until the temperature reduces to a point at which good networks are generated. Two cooling gradients are implemented by decrementing the temperature variable T by 1 each cycle until the temperature is less than 10 from which point the temperature is only reduced by 0.1. This second cooling gradient increases the accuracy of the final solution as all feed sections are in relative proportion and the majority of random perturbations result in networks that can be successfully resolved.

The inner loop runs the optimisation iterations at each temperature. A randomly selected feed element within the current network is perturbed in a random direction by T. The network is resolved creating a candidate network. The fitness of the candidate is assessed using the pre-defined objective function. The simplest objective function uses a target impedance method. The difference between each feed sections characteristic impedance and the target is summed to produce a single fitness value. Various alternative approaches were also investigated including maximizing the minimum impedance, maximizing the average impedance, and a local smoothness function to avoid large physical step discontinuities between connecting impedance elements. If the candidate is fitter than the current, the candidate network becomes the current network for the next iteration. If the candidate is less fit, the probability of accepting it as the current network is computed. If the result from equation (5.6) is greater than a random number between 0.0 and 1.0, the candidate solution is accepted and becomes the current solution for the next iteration. Conversely, if the probability

is less than the random number, the candidate solution is rejected, the current solution remains unchanged and is used in the next iteration. As a consequence the algorithm can go uphill as well as downhill; but the larger the error or the lower the temperature the less likely any significant uphill excursion becomes.

The iteration count was set to 400 to allow the probability of each feed element being perturbed approximately fifty times at each temperature. Once all iterations at a given temperature have been performed, the flow of the program drops back to the outer loop and T is reduced.

5.2.5 Solutions

The following section presents solutions for traditional and optimised dual feed radiating elements and for an alternative impedance range (defined by manufacturing constraints); these solution sets were generated using a target impedance objective function. These solutions are followed by solutions generated using three alternative objective functions. Only the characteristic impedance for each feed section is presented here. A more comprehensive set of results, including the input and output impedance of each feed line section, can be found in Appendix D.

The first set of solutions, seen in Table 5-1, are for feed networks where radiating elements with an input impedance of 33Ω and 50Ω are used. These figures represent the input impedance to a traditionally designed dual feed radiating element and the complex matched radiating element respectively. In all solutions the input impedance at the arrays feed point was set to 50Ω.

The range of allowable impedance values is defined by the resulting track thickness of the microstrip lines that will make up the feed network. Low impedance values are undesirable as they result in thick tracks, the minimum impedance was therefore constrained to 70Ω. The maximum impedance is set to 137Ω as this is approaching maximum impedance that can be consistently fabricated.

As a feed sections characteristic impedance decreases in size, the resulting track width thickens increasing coupling between other feed lines and the radiating patches. To maintain thin tracks, the target impedance was set to the maximum impedance value of 137Ω.

Z_L / Ω	Z1 / Ω	Z2 / Ω	Z3 / Ω	Z4 / Ω	Z5 / Ω	Z6 / Ω	Z7 / Ω	Z8 / Ω
33	50.00	81.24	80.53	98.13	99.75	67.09	136.90	67.34
50	50.00	100.00	87.44	131.16	108.36	82.62	136.95	82.88

Table 5-1: Feed impedance values for radiating elements with an input impedance of 33 and 50Ω.

Table 5-2 presents solutions where the maximum characteristic impedance in the allowable impedance range is set to 137Ω and 145Ω. 145Ω is widely regarded as the absolute maximum impedance that can reasonably be realised as a microstrip line (on the proposed low loss substrate). Any higher the resulting track width becomes too thin to reliably fabricate using traditional PCB techniques. Again the target impedance is set to the maximum impedance; the input impedance of the radiating elements is set to 50Ω.

Z_{max} / Ω	Z1 / Ω	Z2 / Ω	Z3 / Ω	Z4 / Ω	Z5 / Ω	Z6 / Ω	Z7 / Ω	Z8 / Ω
137	50.00	100.00	87.44	131.16	108.36	82.62	136.95	82.88
145	50.00	100.00	87.48	131.23	111.60	85.04	144.95	85.22

Table 5-2: Feed impedance values with the maximum impedance constrained to 137Ω and 145Ω.

In Table 5-1 and Table 5-2 a target impedance was used as an objective function. Solutions generated using three alternative objective functions are presented in Table 5-3. For these solutions 50Ω radiating elements are used. The target impedances in these examples are defined by the algorithm itself. The 'total error' minimises the total error of all impedances from a target value. The 'maximum error' minimises the largest error between any one feed impedance and the target value. 'local smoothness' minimises the relative difference between the resulting feed impedances.

Fitness Function	Z2 / Ω	Z3 / Ω	Z4 / Ω	Z5 / Ω	Z6 / Ω	Z7 / Ω	Z8 / Ω
Total Error	100.00	50.75	76.12	50.11	57.87	58.91	50.90
Max Error	100.00	50.00	75.66	52.07	68.82	74.79	54.34
L Smoothness	100.00	50.00	75.00	50.11	66.82	66.87	50.04

Table 5-3: Feed impedance values using three alternative fitness functions.

In all solution sets Z1 is constrained to 50Ω (the input impedance to the array). Z2 has to match this source impedance to the first patch while maintaining appropriate power splitting at the first feed junction (node **a**). As a consequence, the value of Z2 is a

function of the array and patch input impedance only. Therefore when a radiating element with an input impedance of 50Ω is used Z2 it is always constrained to 100Ω. When a radiating element with an input of impedance of 33Ω is used Z2 is always constrained to 81Ω as demonstrated in Table 5-1.

From Table 5-1 it can be seen that the use of a radiating element with a higher input impedance leads to higher impedances within the feed network. In both sets of solutions Z7 has been pushed to the maximum impedance. This was found to be the case when manually generating solutions as this impedance is pushed up by impedances Z6 and Z8 (the lowest). This is confirmed in Table 5-2 where Z7 is pushed up from 137Ω to the maximum impedance value 145Ω allowing Z6 and Z8 to lift to just over 85Ω.

The algorithm enabled the evaluation of a number of different fitness functions. Table 5-3 presents the results of three alternatives. Due to the relatively low characteristic impedance of the resulting feed line sections, these solutions are less well suited to microstrip line realisation as the resulting tracks would be too thick.

The optimum choice of feed solutions for use in the RSU is considered to be where 50Ω radiating elements are used with a maximum feed impedance of 137Ω. These solutions are detailed in the second row of Table 5-1 and the first row of Table 5-2. This solution set is well suited to microstrip realisation as the impedances are relatively high leading to a narrow track width. The maximum impedance of 137Ω provides a relatively thin feed line while maintaining a small amount of headroom below the absolute maximum impedance of 145Ω. This helps to reduce coupling within the feed network while relaxing manufacturing tolerances.

5.2.6 Discussion

At the beginning of an optimisation run the temperature is high and the algorithms behavior is quite erratic. Large changes are made to the network as the amount of perturbation is large. The chance of a worse solution ending up better in the long run is far greater hence Boltzman's probability is maintained. More iterations are required when the temperature is high as the probability of finding valid (realisable) candidate network is small. However when improvement is seen it is usually buy quite a lot. The

relatively steep cooling gradient results in a reduction in run time. Although the resulting solution sets lack precision, a lack of precision at this stage in the optimisation run is not a problem as the feed sections are still finding relative proportion.

Later, to increase the precision of the final result, the temperature is lowered more slowly. The success rate of network perturbation is far greater with far more candidate networks being successfully resolved and demonstrating a small improvement in fitness. At this stage, the chance of a worse solution being a step in the right direction is far less so equation (5.6) ensures the probability of accepting worse solutions is low. Although less iterations are required to generate a good sample of valid candidate solutions, as T reduces progress slows hence the same iteration count is maintained thought the optimisation run.

The dual gradient cooling schedule proved much quicker than the slower Metropolis system but was less thorough as a result. Running the algorithm over many iterations maintaining a global 'BEST' helped coverage. However, a lack of ergodicity is not necessarily a bad thing, particularly as solutions that are missed will be poor solutions due to their implicit sensitivity in at least one dimension. This sensitivity translates directly to manufacturing tolerances, which need to be quite insensitive to small variations in the element values. Thus it is argued that an accelerated cooling schedule can be used to get high quality results.

5.3 Alternative dual feed radiating element

Two types of dual feed radiating element were presented in Chapter 3, a traditional design that used quarter wave transformers to match the radiating patch to the dual feed network and an optimised design that used complex matching. The complex matched antenna allowed an increase in input impedance and the removal of step discontinuities within the feed network. The performance of a 2x2 array containing these optimised dual feed radiating elements was presented in the previous chapter. In the following section the performance of the 4 element 2x2 array is explored using traditional dual feed radiating elements.

5.3.1 Array performance

It was shown in Chapter 3 that the traditional dual feed design is not constrained to a specific overall length. The length of this feed section has a direct effect upon the relationship between internal reflections within the arrays feed network. Using the extended transmission line model presented in chapter 4 it is possible to alter this length and assess the resulting change in array VSWR and axial ratio bandwidth. The length of each dual feed line is changed from 0 to 1 wavelength. A quarter wave length of matched feed line is always added to one of the feeds to provide the 90 degree phase delay required for circular polarisation.

5.3.1.1 Input impedance

The variation of VSWR as a function of frequency and dual feed line length is illustrated in Figure 5-4. The total length of dual feed for the shortest length is 0.25λ increasing to a maximum length of 2.25λ.
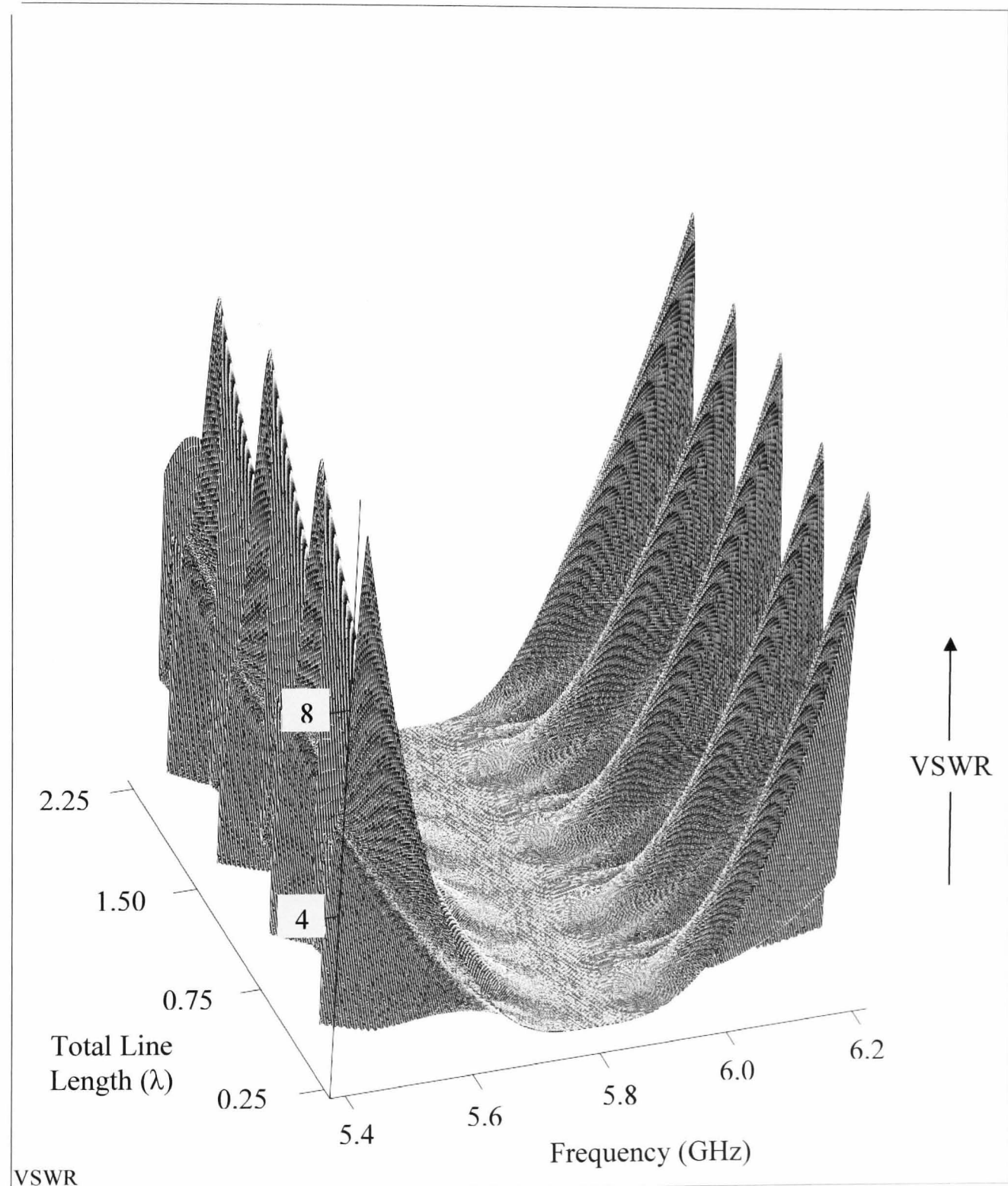
VSWR

Figure 5-4: Variation in VSWR frequency performance with dual feed line length (ε_r = 2.33, h = 0.79 mm).

A plot of VSWR 2:1 and 1.5:1 bandwidths against feed line length quantifies this effect and is shown in Figure 5-5. It can be seen that the arrays VSWR 2:1 bandwidth varies from 6.5% to almost 12%. Array VSWR 1.5:1 bandwidth varies from just below 5% to just above 8%.
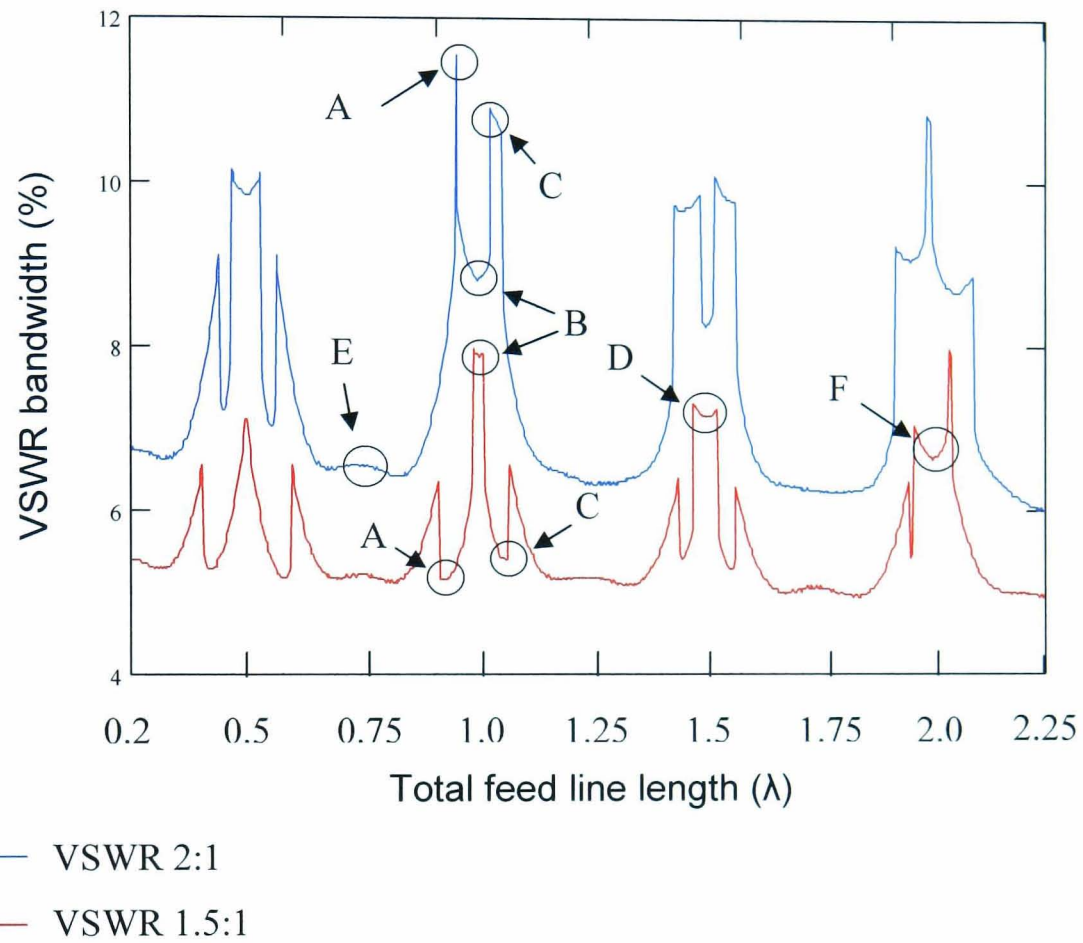
Figure 5-5: Array VSWR bandwidth variation with dual feed line length.

The variation of VSWR as a function of frequency for feed lengths labelled A, B and C in Figure 5-5 can be seen in Figure 5-6.
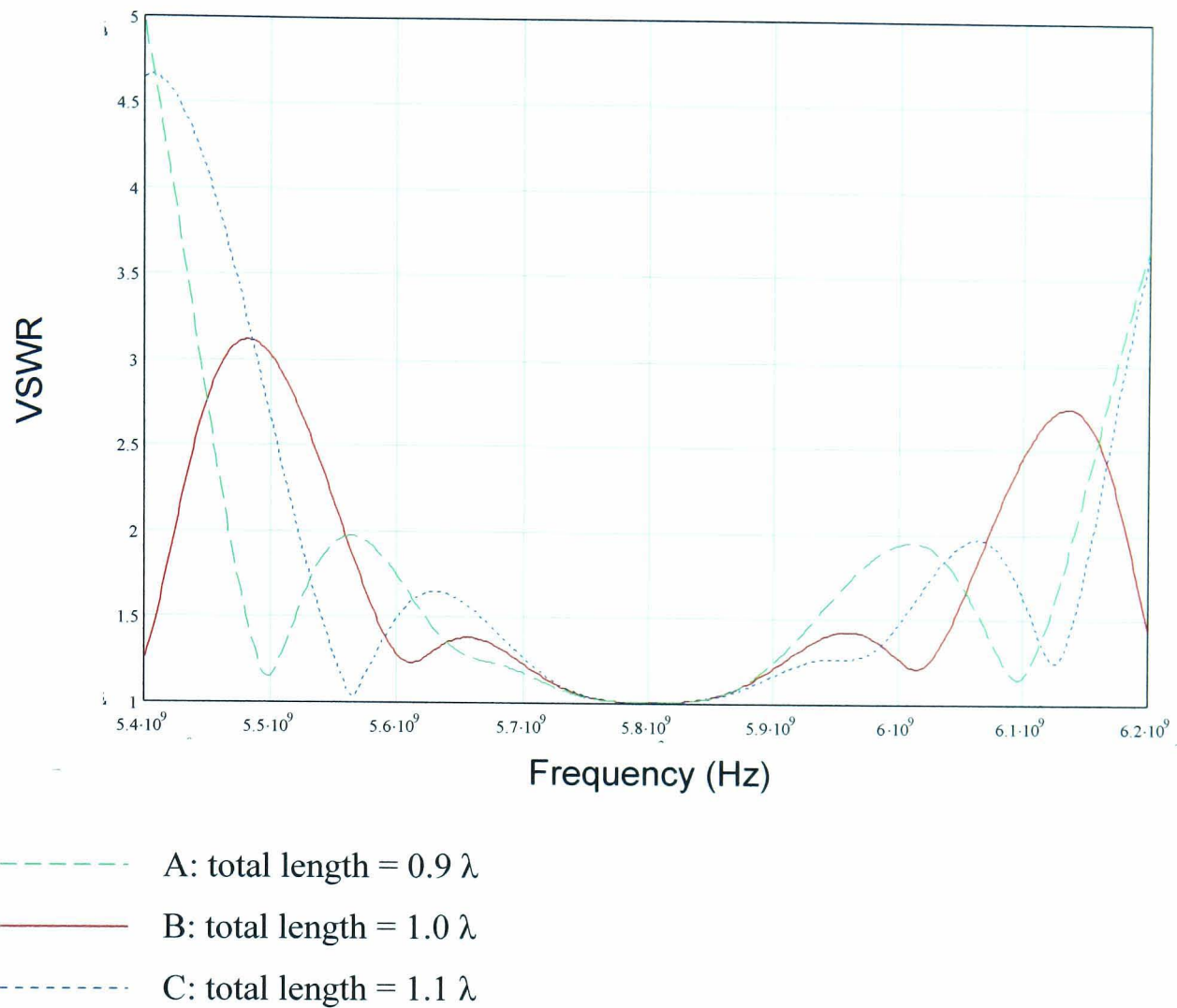
Figure 5-6: VSWR as a function of frequency for feed line lengths A, B and C.

Although lengths A and C demonstrate wider VSWR 2:1 bandwidths than length B, they are not symmetrical around design frequency and are a lot more sensitive due to the large amount of ripple in the pass-band. Although length B has a narrower VSWR 2:1 bandwidth, the performance is far more robust. As expected, due to the pass-band ripple, the VSWR 1.5:1 bandwidth for examples A and C are far narrower than that of example B. Similar frequency performance to length B is seen at lengths D and F.

The three lengths that maximise VSWR 1.5:1 bandwidth (labeled B, D and F in Figure 5-5) represent total feed lengths of 1λ, 1.5λ and 2λ respectively. These are considered in more detail in Figure 5-7.
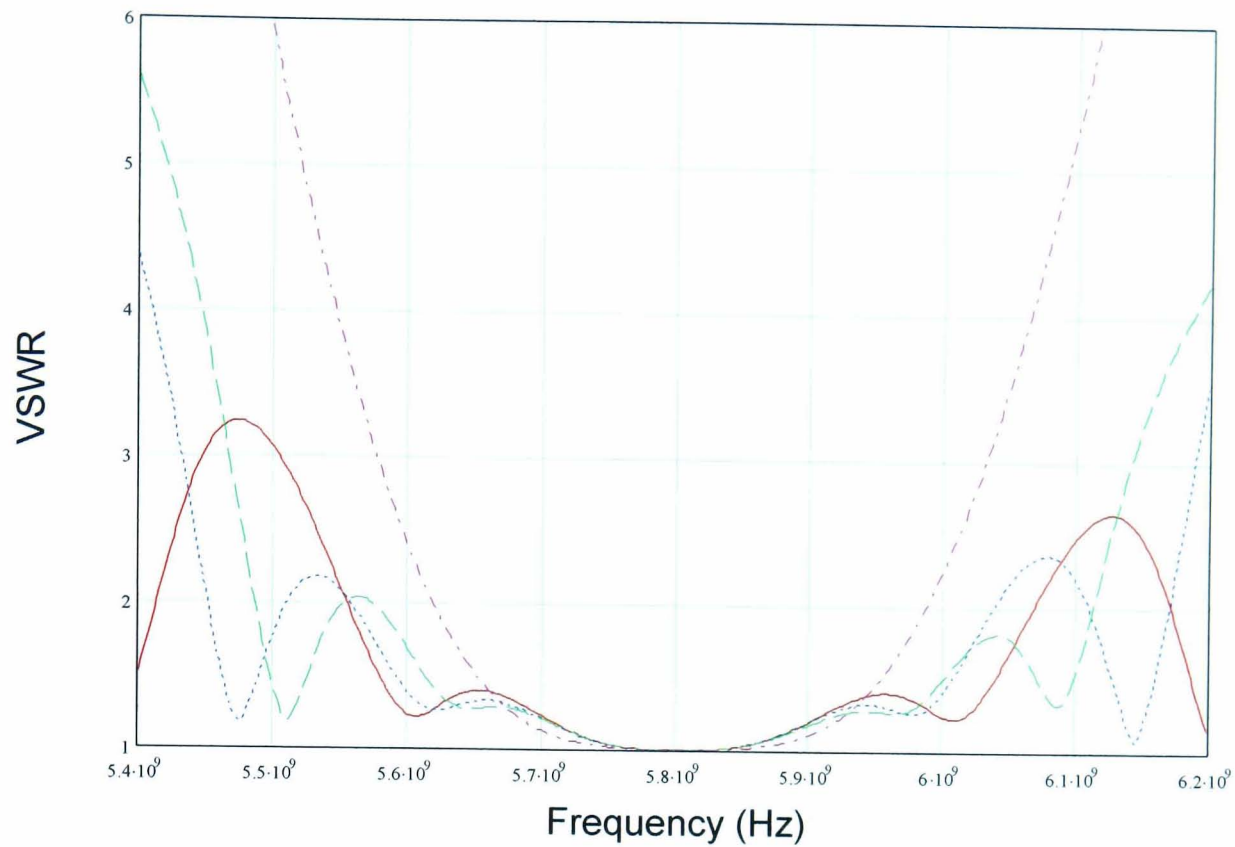
Figure 5-7: VSWR as a function of frequency for feed lengths B, D, F and E.

Minimum VSWR 1.5_1 bandwidths are seen at 0.75 λ, 1.25 λ and 1.75 λ. The 1.75 λ length, labelled E in Figure 5-5, can also be seen in Figure 5-7.

Length B, where the total length of dual feed line is one wavelength, has the widest 1.5:1 bandwidth although lengths D and F have similar performance and may be preferable lengths depending upon desired patch spacing and real estate resource within a specific array geometry. Length E has the narrowest VSWR 1.5:1 bandwidth but has no ripple in the pass band. Length E may therefore be more desirable if a narrower bandwidth is permissible and lower VSWR is required throughout the pass-band.

5.3.1.2 Axial ratio

The variation of array boresight axial ratio, as a function of frequency and feed line length, can be seen in Figure 5-8.
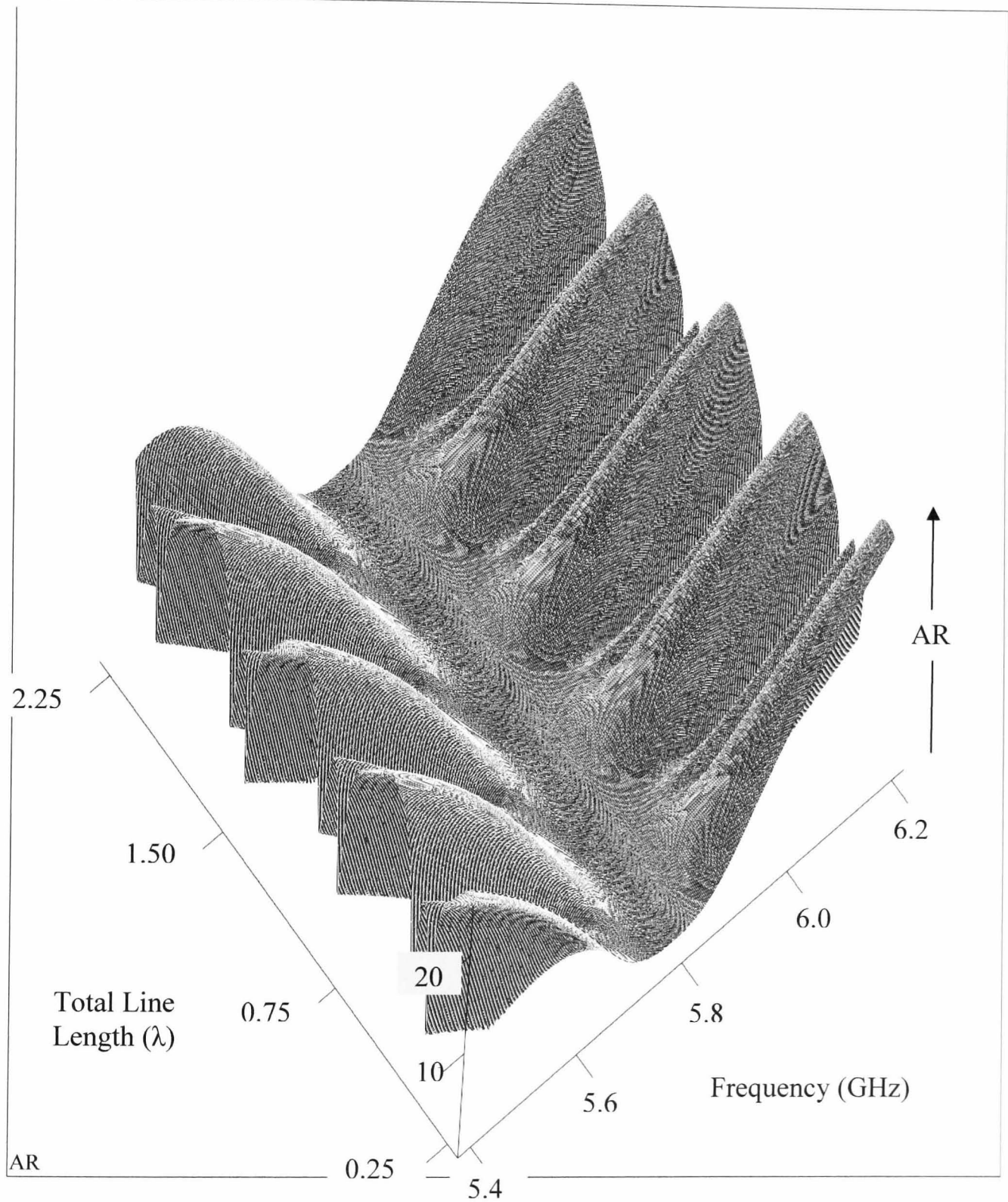
Figure 5-8: Variation in Axial Ratio frequency performance with dual feed line length ($\varepsilon_r = 2.33$, $h = 0.79$ mm).

It can be seen that, as with input impedance, array axial ratio performance changes drastically with dual feed line length. This change in bandwidth is quantified in Figure

5-9 where the arrays 3 dB and 4.5 dB bandwidths can be seen. The arrays 4.5 dB bandwidth, like the VSWR 1.5:1 bandwidth, varies from just under 5% to almost 8%. Indeed it is noted that this response is almost identical. The 3 dB bandwidth, like the VSWR 2:1 bandwidth, is slightly misleading in that the peaks correspond to sensitive results that are not symmetrical around design frequency.
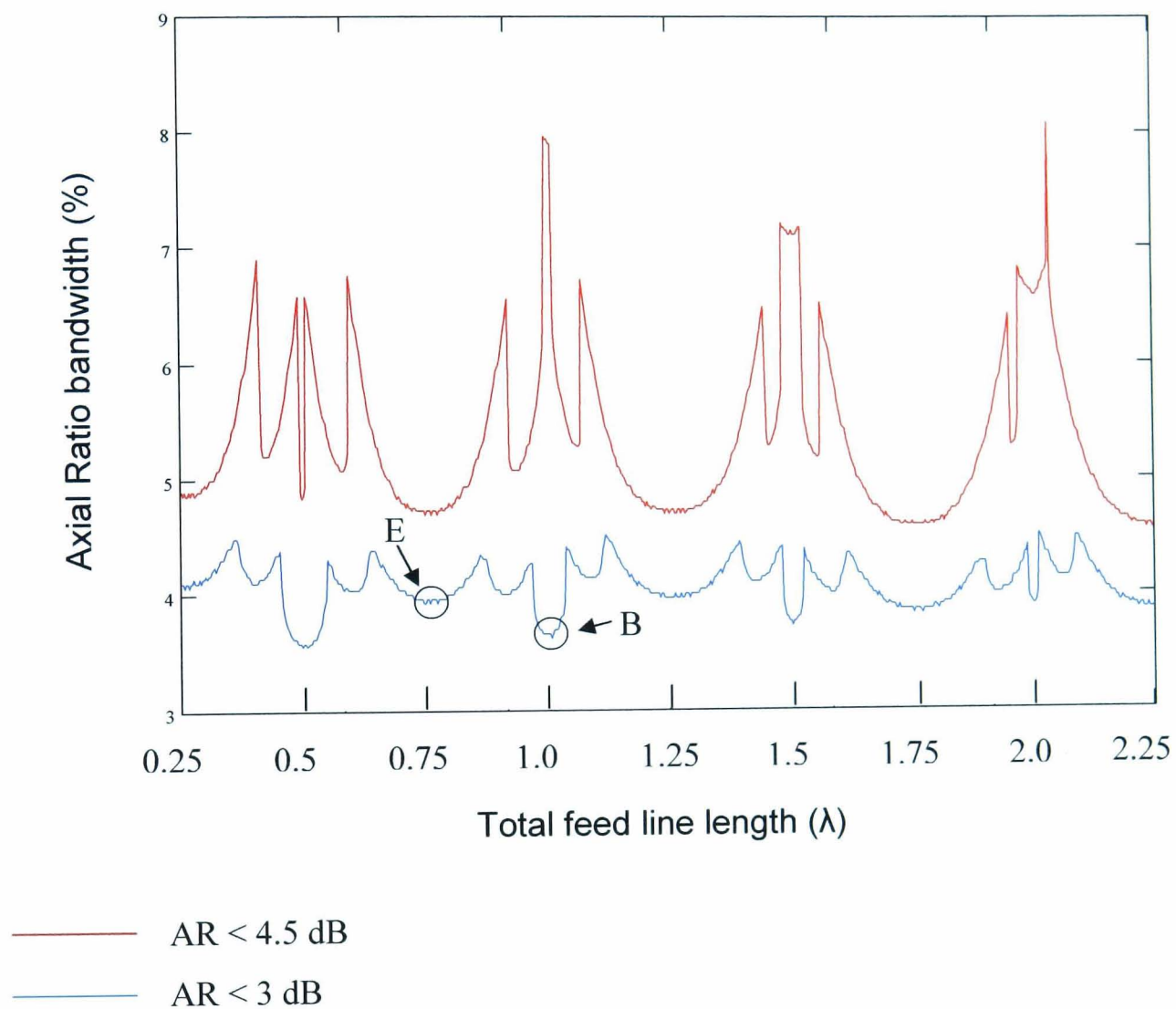
Figure 5-9 : Array axial ratio bandwidth variation with dual feed line length.

Axial ratio performance of dual feed lengths B and E as a function of frequency are shown in more detail in Figure 5-10.
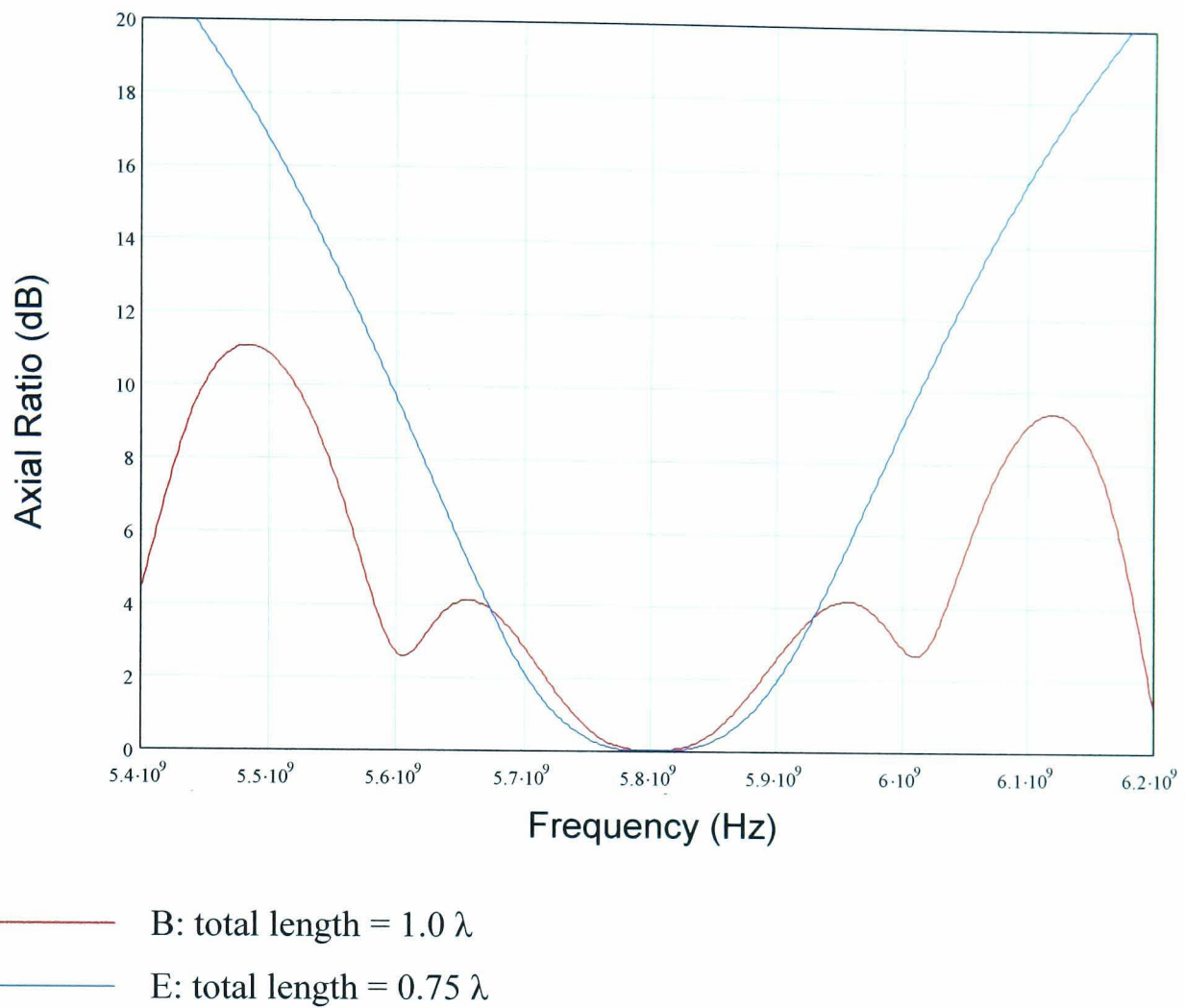
Figure 5-10: Axial Ratio as a function of frequency for lengths B and E.

As with VSWR, length B has the widest 4.5 dB axial ratio bandwidth of just over 8% but has a similar amount of ripple in its pass band as seen with the 1.5:1 VSWR performance of length B. Therefore, as with VSWR, if an application demands higher axial ratio performance and can tolerate a reduction in bandwidth then length E is likely to be optimal. It is also noted that the 3 dB axial ratio bandwidth of E is almost as wide as the 3 dB axial ratio bandwidth demonstrated by the corporate fed three element array presented in Chapter 4.

A relative comparison between VSWR and Axial Ratio bandwidth is made in Figure 5-11.
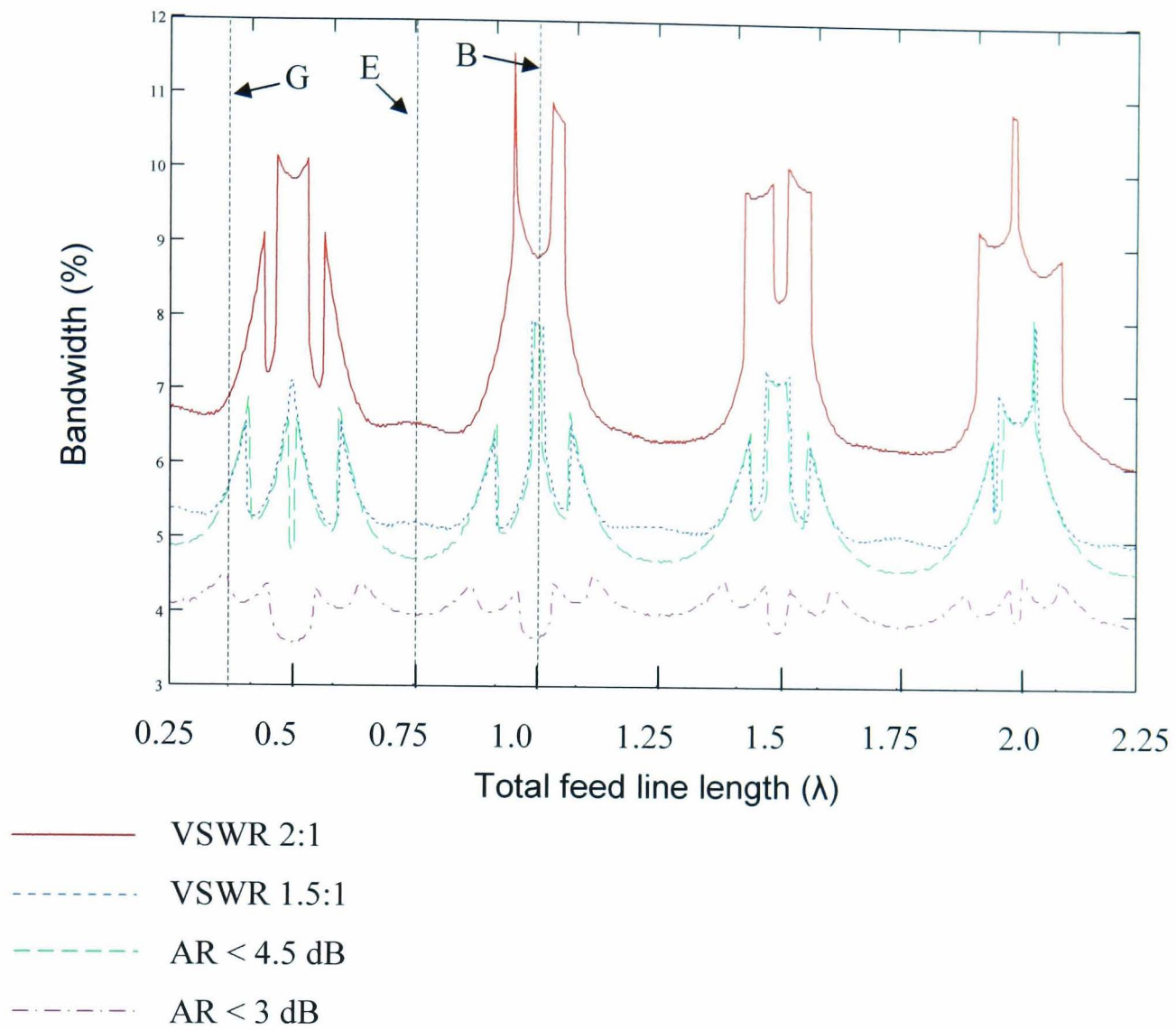
Figure 5-11: VSWR and axial ratio bandwidths as a function of dual feed line length.

From Figure 5-11 it can be seen that the VSWR 1.5:1 bandwidth "matches" the 4.5 dB axial ratio bandwidth regardless of line length. This relationship is due to the relatively narrow band radiating elements, the same relationship being seen by Hall [67] in these arrays where radiating patches with a similar Q were used.

For widest bandwidth but most ripple in the pass band then example B would be the most desirable choice, almost doubling the VSWR 1.5:1 and 4.5 dB axial ratio bandwidths. For highest performance but narrowest bandwidth example E may be more appropriate however the reduction in bandwidth is substantial for a nominal increase in performance.

It is also interesting to note that the resistively matched dual feed radiating element with feed length B and the complex matched dual feed radiating element optimised in

Chapter 3, both have a total feed length of one wavelength. Although the axial ratio bandwidths are comparable, the optimised dual feed radiating element from Chapter 3 demonstrates a wider VSWR 2:1 bandwidth.

Ultimately, the optimum dual feed line length will depend on the bandwidth requirement of a specific application. Allowable feed line lengths are also dependant upon patch spacing within the array, array feed geometry and the resulting real estate availability.

5.4 Practical realisation

5.4.1 Array layout design

2x2 arrays containing traditional and optimised dual feed radiating elements can be seen in Figure 5-12. In both cases the radiating elements are spaced at 0.74λ as it has been shown that this patch spacing helps minimise mutual coupling without substantial degradation of the radiation pattern by side lobes when dual feed radiating elements are used [9].

(a)   (b)

(c)
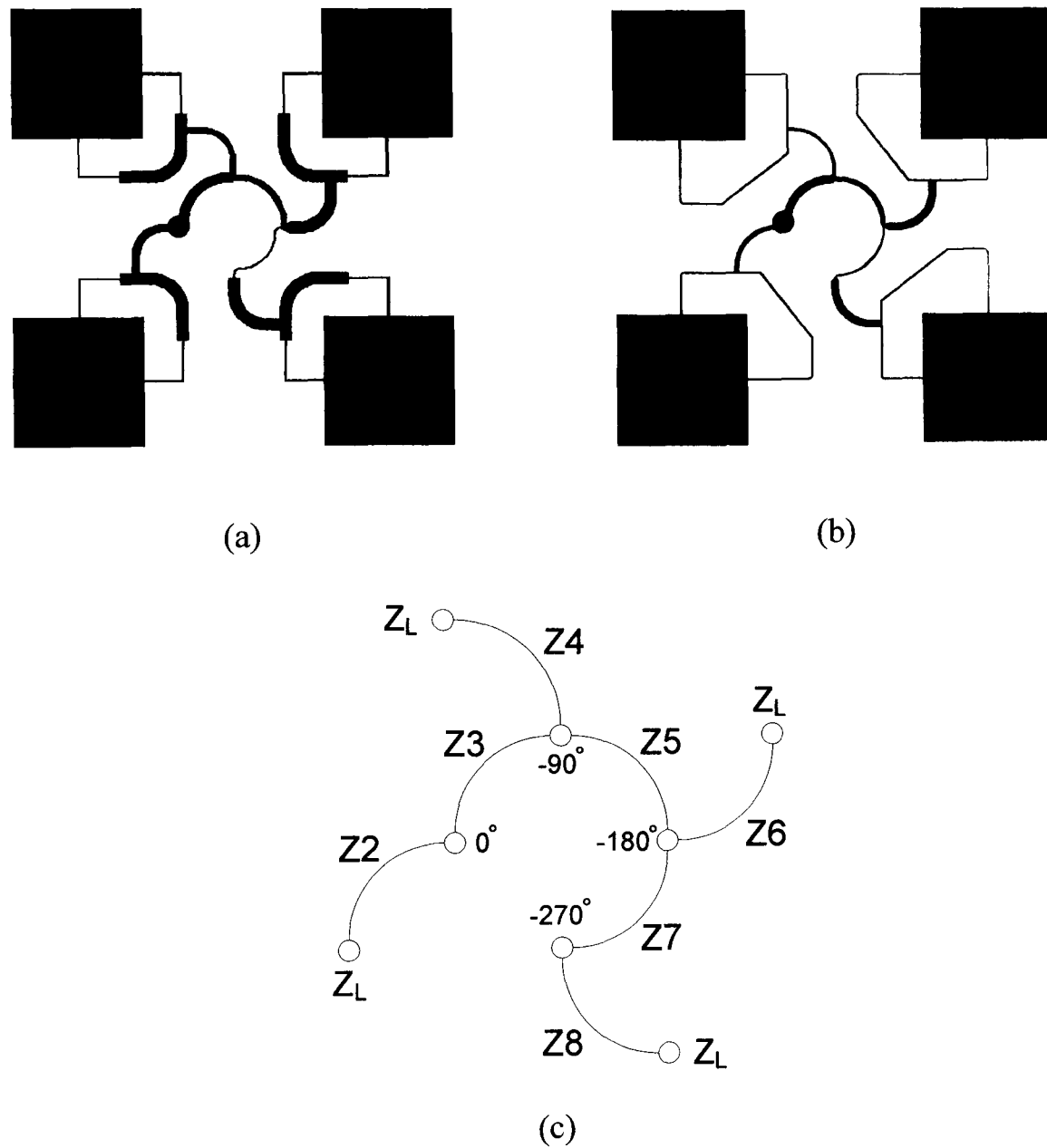
Figure 5-12: 2x2 sequentially rotated array with (a) Traditional dual feed radiating elements (b) Optimised dual radiating elements (c) Feed impedance definition.

Considering the thickness of the 66Ω feed line and this patch spacing, there is little flexibility in the length of the traditional dual feed line. Figure 5-12 (a) shows a 2x2 array composed from traditional dual feed radiating elements with a total dual feed length of 0.376 λ (0.063 + 0.063 + 0.25). This is length is labelled G in Figure 5-11.

The traditional dual feed radiating element has an input impedance value of 33Ω as defined in Chapter 3. The series feed impedance values for this array are as defined in Figure 5-12 (c) and can be found in the first row of Table 5-1. The resulting track widths within the series feed network are noticeably wider than within the network feeding the optimised radiating elements with a higher input impedance of 50Ω as seen in Figure 5-12 (b). Furthermore, the quarter wave transformers used to match the radiating patch to the traditional dual feed network result in undesirably thin tracks.

5.4.2 Fabrication

Both antennas were fabricated using 0.79 mm 1/2oz RT 5870 Duroid (ε_r of 2.33) using traditional printed circuit board techniques. Both arrays are probe fed from behind the ground plane using an SMA connector.

5.5 Practical results

5.5.1 Traditional dual feed elements

The frequency performance of the array containing traditional dual feed radiating elements has been confirmed by experimental measurement. Both input impedance and boresight axial ratio performance have been measured over a frequency range of 5.2 – 6.4GHz. Measurement of input impedance, made using an Anritsu 37347C vector network analyser, confirm a VSWR 2:1 bandwidth of 7% from 5.55 to 5.96GHz as seen in Figure 5-13. This compares very well with the models prediction (example G, Figure 5-11).

XXXXXX Modeled
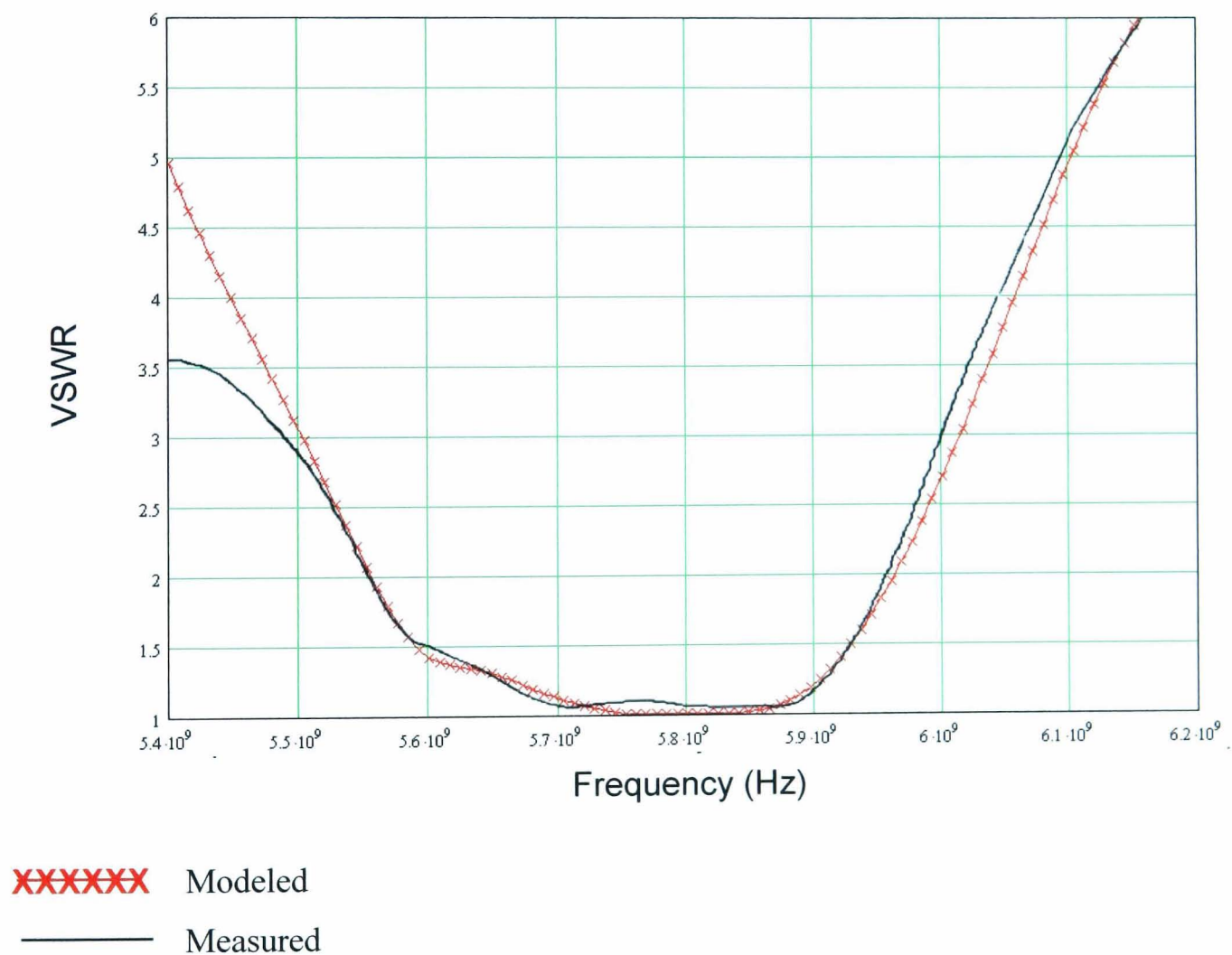
———— Measured

Figure 5-13: VSWR performance of 2x2 array containing traditional dual feed radiating elements.

Measurement of boresight axial ratio (as described in Appendix C) confirm a 3 dB axial ratio bandwidth of 4.2% from 5.65 to 5.895GHz as seen in Figure 5-14. It is

noted that this bandwidth is asymmetrical around design frequency. Again this compares very favorably with the models prediction.
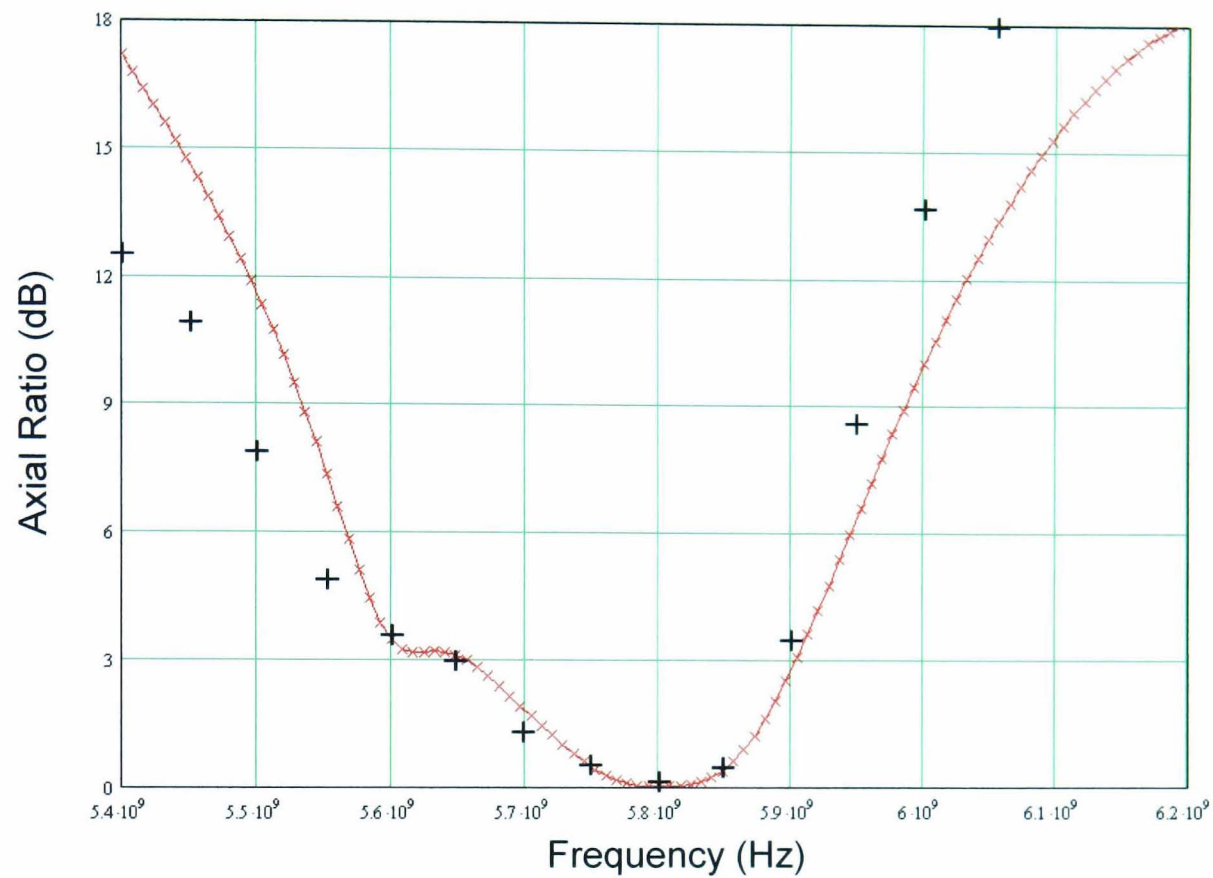
XXXXXX   Modeled.

+   Measured.

Figure 5-14: Boresight axial ratio performance of 2x2 array containing traditional dual feed radiating elements.

5.5.2 GA optimised dual feed radiating elements

5.5.2.1 Frequency performance

The frequency performance, as first presented in the previous chapter, of the 2x2 array containing optimised dual feed radiating elements (as seen in Figure 5-12 (b)), has been further confirmed using full wave simulation [117] as seen in Figure 5-15.

119

(a)

(b)
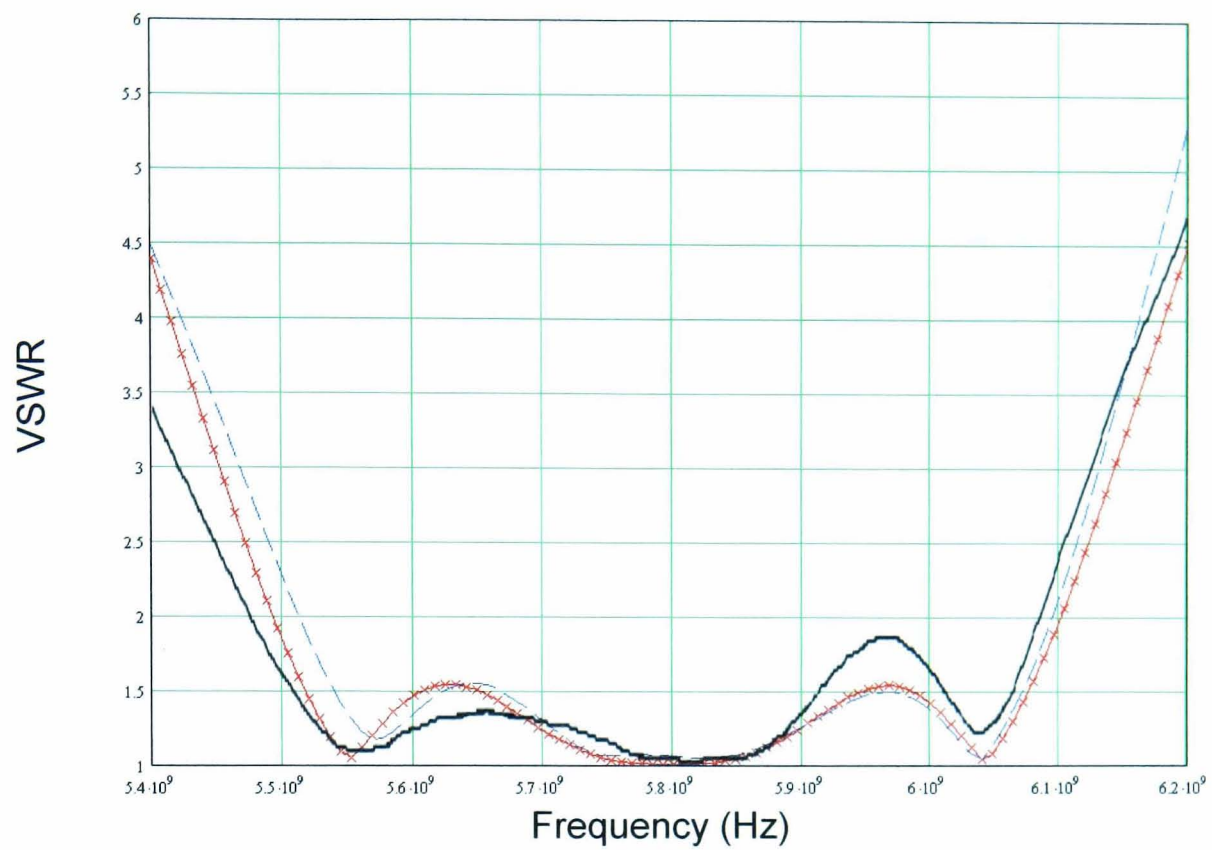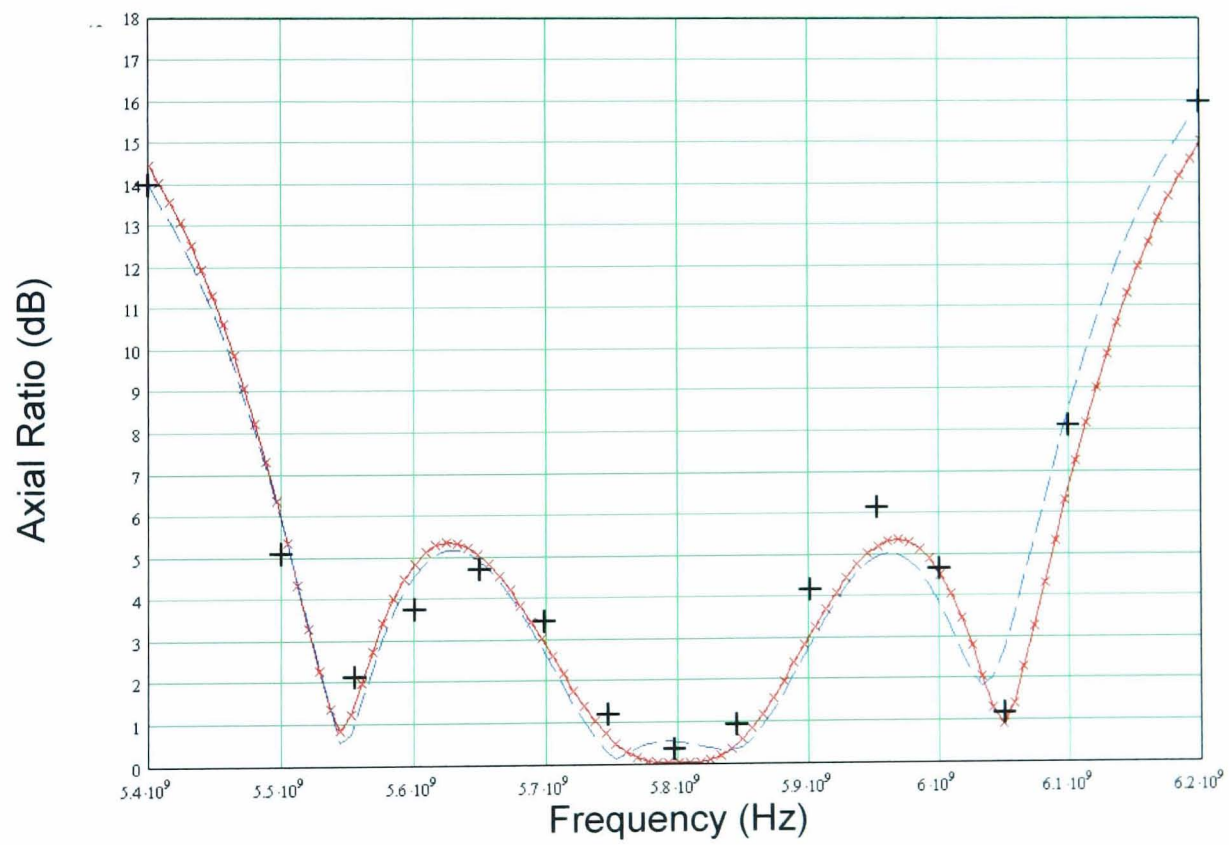
✗✗✗✗✗✗	Modeled
- - - - - -	Full Wave Simulation
——— , ✛	Measured

Figure 5-15: Performance of 2x2 array containing optimised dual feed radiating elements.

The array containing optimised radiating elements demonstrates a much wider VSWR 2:1 bandwidth of 10.4%. This array also demonstrates a slightly narrower but far more symmetrical 3 dB axial ratio bandwidth.

5.5.2.2 Radiation pattern

The radiation pattern of the 2x2 array containing optimised dual feed radiating elements, as seen in Figure 5-16, was determined within an anechoic chamber using the method and equipment described in Appendix C. The gain of the main lobe was measured at 12.4 dBi with a 3 dB beam width of 45°. There is 11 dB difference between the main beam and side lobes seen at +/- 60° with nulls at 39° from boresight.

XXXXX   Full wave simulation.

————   Measured.
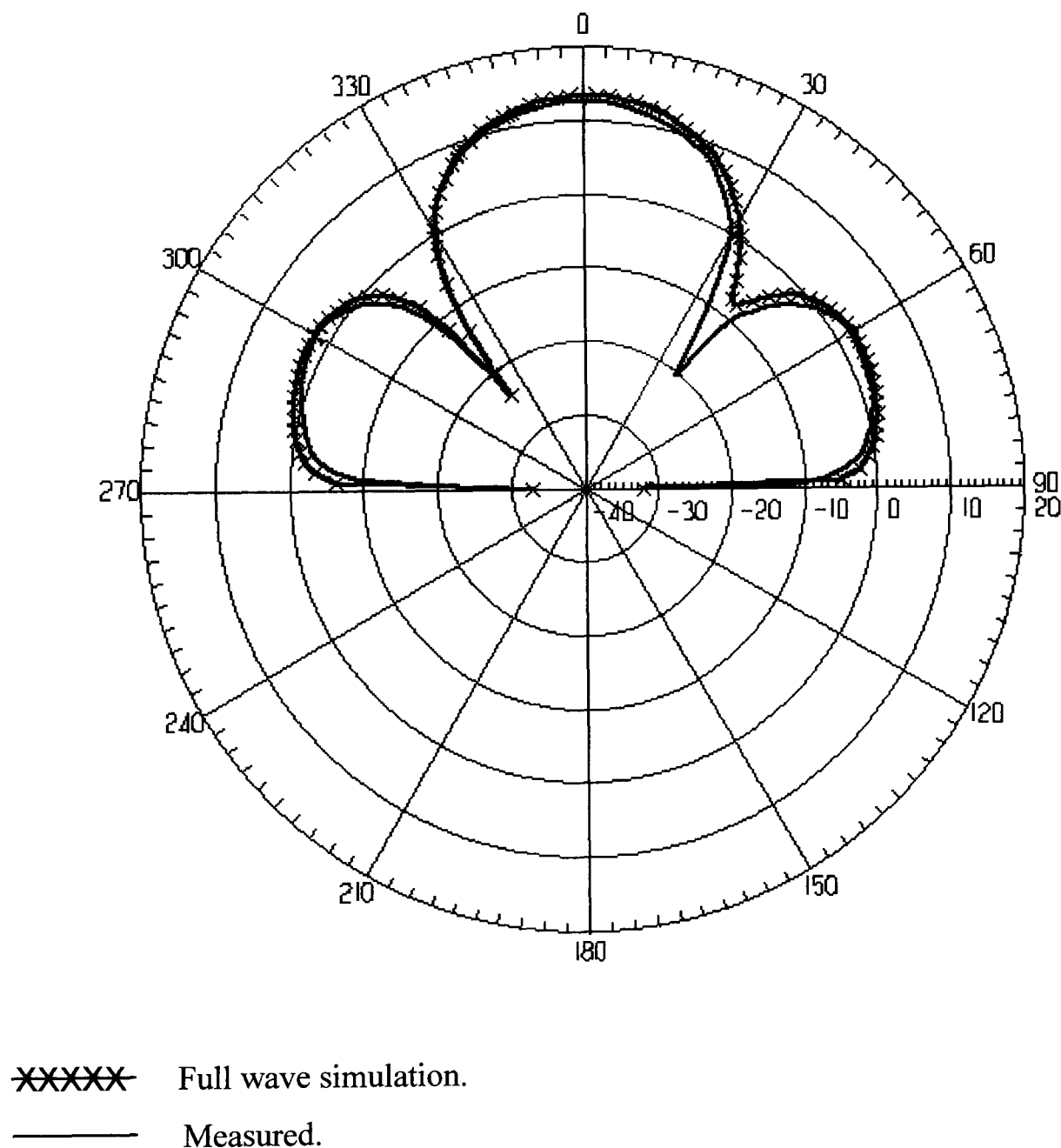
Figure 5-16: Radiation pattern of 2x2 at 5.8 GHz (gain in dBi against θ where $\phi = 0$).

5.6 Conclusion

An algorithm based on an adaptation of SA has successfully been used to generate and optimise the series feed sections within the four element array presented in Chapter 4 for which no closed form expression exists. The accuracy of the result is high with low resources and computer run time. An accelerated cooling schedule reduces run time while avoiding sensitive solutions. This proves beneficial in this application as these map directly to tight manufacturing tolerances.

When traditional dual feed radiating elements are used in a four element array, the total dual feed line length has a significant effect upon array performance, doubling VSWR 2:1 bandwidth. The increase in axial ratio is less significant due to the narrow band radiating elements. This further reinforces the theory that the effect of internal reflections can have a dramatic effect on array performance. However, allowable line lengths are ultimately constrained by desired patch spacing and real estate resource.

The performance of the 2x2 antenna array has been confirmed by full wave simulation and experimental measurement.

CHAPTER 6

4X4 ARRAY FOR MOTORWAY APPLICATIONS

6.1 Introduction

There is a requirement for the RSU to be mounted to an overhead gantry that spans across motorway carriageways. This mounting position ensures good relative alignment between the OBU (when centrally mounted behind the windscreen) and the overhead RSU. Indeed, this may be the only mounting position available in many multi lane environments. There is therefore the need for a light weight compact array that is mechanically robust, as access for maintenance is restricted. For motorway use, a higher gain is required to provide additional range and reduce the width of the communication zone to a single lane. For the latter, side lobe reduction is also desirable.

In response to these requirements, there has been much recent interest in using 4x4 patch antenna arrays for road tolling applications [118,119] but again these arrays use a corporate feeding system. This chapter presents a new compact 4x4 array using a series feed that has the necessary gain and side lobe control required by a motorway tolling application.

In has already been shown in chapter 4 that a sequential rotated microstrip array with a series feed, can have a wider frequency bandwidth than the same array using a corporate feed; particularly when used in a 2x2 arrangement due to the favourable relationship between internal reflections within the series feed network. In this chapter the same series feeding technique is adopted within a sixteen element 4x4 array constructed by sequentially rotating four of the 2x2 sub-arrays optimised in Chapter 5. The layout is presented and its performance evaluated using an extension of the transmission line model presented in chapter 4, enabling comparison with the performance of the same array using a corporate feed. As a direct result of this research a letter has been published in IEE electronic letters [19]. Furthermore, this

array has successfully been used within the RSU of a commercial traffic management system.

Side lobe reduction is achieved by varying excitation power distribution across the array; results are presented for two modified arrays. Full wave simulation and experimental measurements assess the validity of this approach and confirm the integrity of this design.

6.2 Array Design

6.2.1 Array layout

The basic sixteen element 4x4 array is composed of four sequentially rotated 2x2 sub-arrays as seen in Figure 6-1.
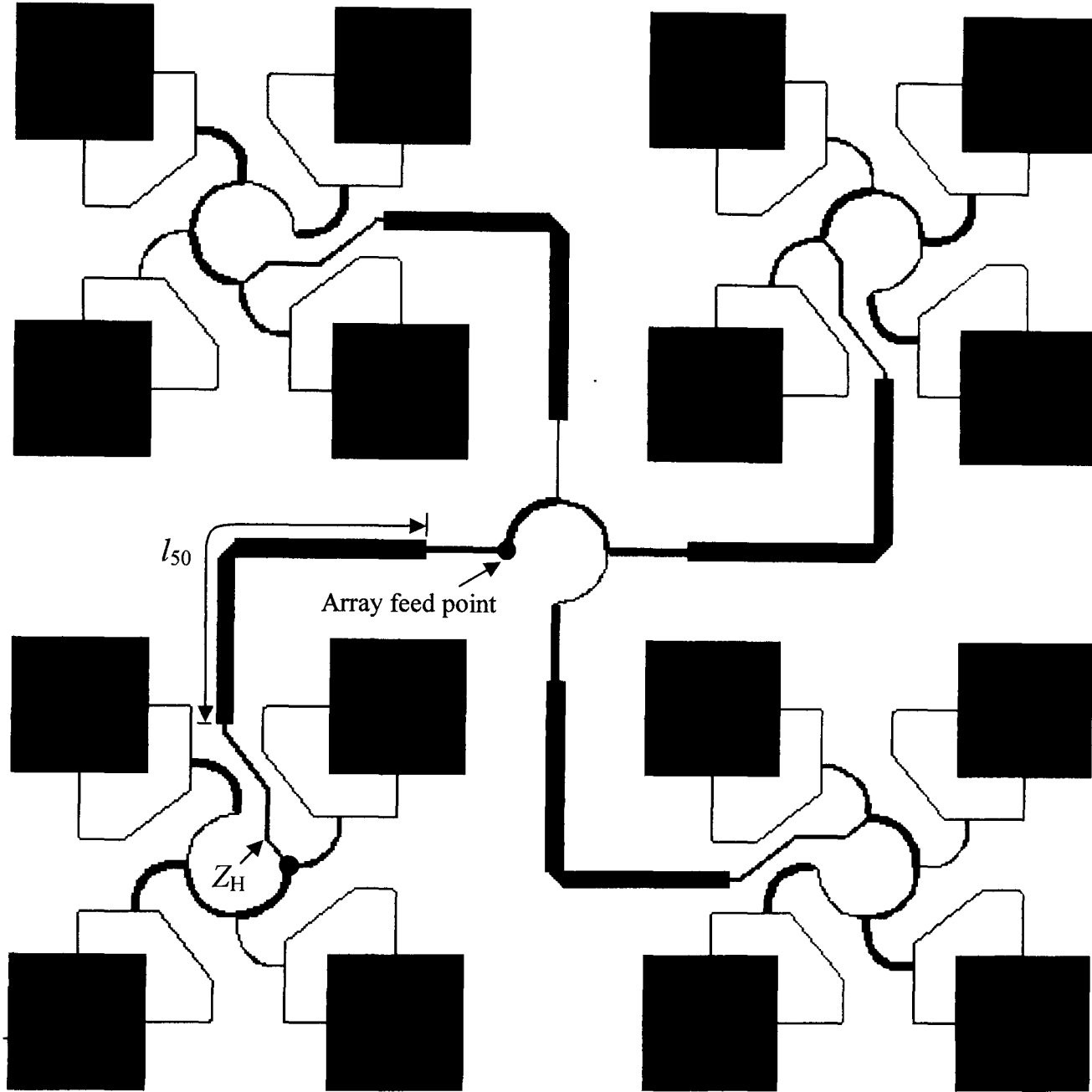
Figure 6-1: Layout design 16 element 4x4 array composed from four 2x2 sub-arrays.

For each 2x2 sub-array $M = 4$, $p = 2$ and $\phi_f = 90°$ as defined in chapter 4. M of these sub-arrays are themselves sequentially rotated by ϕ_f to make the larger array which in turn adopts the same series feeding technique. The clustering of the sub-arrays helps reduce beam squint. Furthermore, as the sub-arrays are themselves sequentially

rotated to make the larger array, spurious radiation from each sub-arrays will tend to cancel in the far field.

In the basic array, seen in Figure 6-1, the values of the series feed sections used to make up the main array feed are identical to the values of the feed sections within the sub-arrays as they share power splitting and excitation phase requirements. Impedance matching requirements are also identical as the input impedance at the feed point of the dual feed radiating elements and the input impedance at the feed point of the sub-arrays are both 50Ω.

The sub-arrays are connected to the central feed using a matched length of 50Ω microstrip feed line of length l_{50}. As this microstrip line is of relatively low characteristical impedance, the resulting PCB track is relatively wide making routing to the sub-arrays feed point problematic. Therefore, the impedance at the feed point of the sub-array is transformed to the periphery of the sub-array using a section of feed line a half wavelength long (Z_H in Figure 6-1). From equation (3.12) it can be seen that if $l = \lambda/2$ then $Z_{in} = Z_{out}$ regardless of the microstrip lines characteristic impedance Z_0, allowing a favorable characteristic impedance value for Z_H to be chosen. The higher the value of Z_H the higher the voltage midway along Z_H will be, increasing interference with the surrounding feed lines. The wider this line the greater the coupling to surrounding feed lines as the physical distance between them decreases. In this array, 120Ω is considered to be a good compromise.

6.2.2 Frequency performance of basic array

Array frequency performance is determined by expanding the model used in Chapter 4 to the 4x4 array seen in Figure 6-1. Both VSWR and axial ratio frequency performance were evaluated, allowing a comparison to the performance of the same array using a corporate feeding system.

———— Series feed,   ·············· Corporate feed
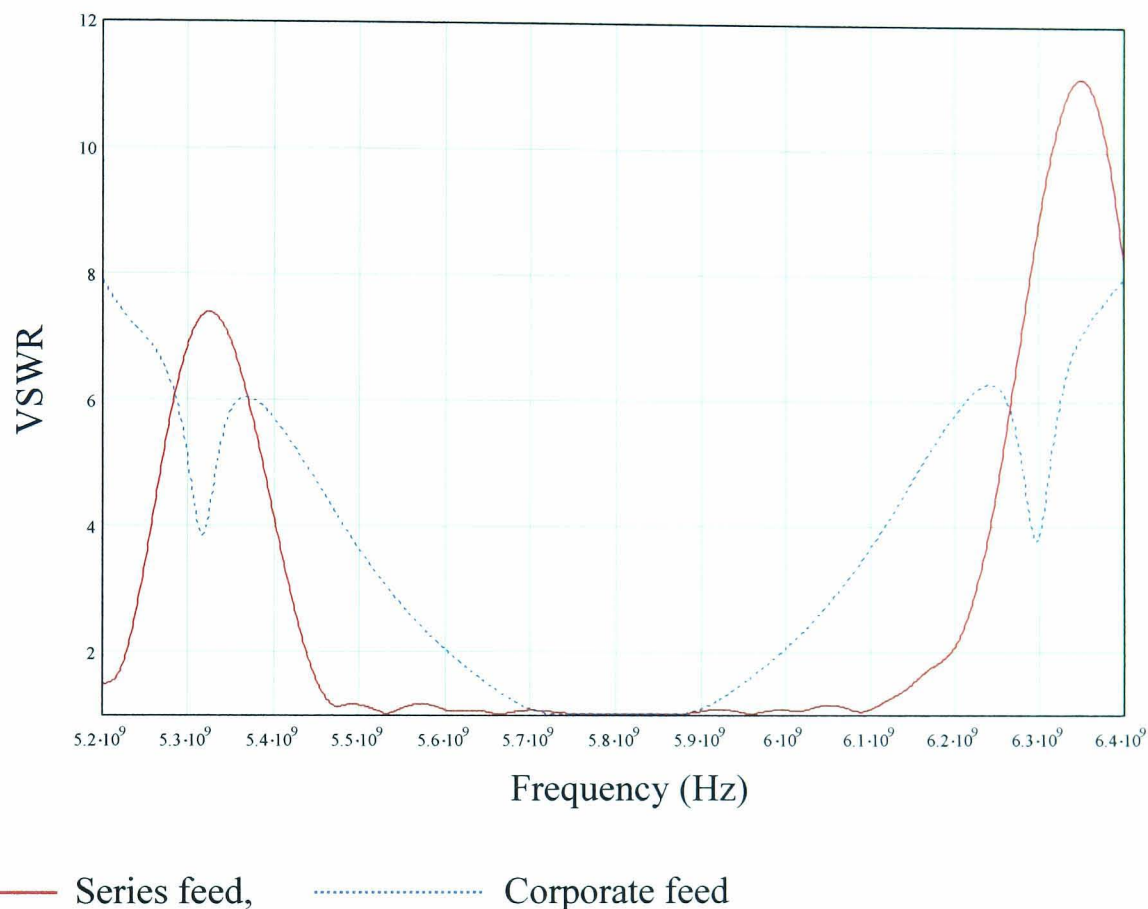
Figure 6-2: VSWR of 4x4 array using both feeding techniques ($\varepsilon_r = 2.33$, $h = 0.79$ mm).

Figure 6-2 shows array VSWR against frequency for a series and corporate fed 4x4 array. It can be seen that the 4x4 array using a series feed has a VSWR 2:1 bandwidth of 13.3% between 5.431 and 6.204 GHz, which is 6.3% wider than when a corporate feed is used in the same array (corporate feed bandwidth 7% between 5.6 - 6.0 GHz). The VSWR 1.5:1 bandwidth of the series fed array shows further improvement over the VSWR 1.5:1 bandwidth of the corporate fed array.

Figure 6-3 shows array boresight axial ratio against frequency for a series and corporate fed 4x4 array.
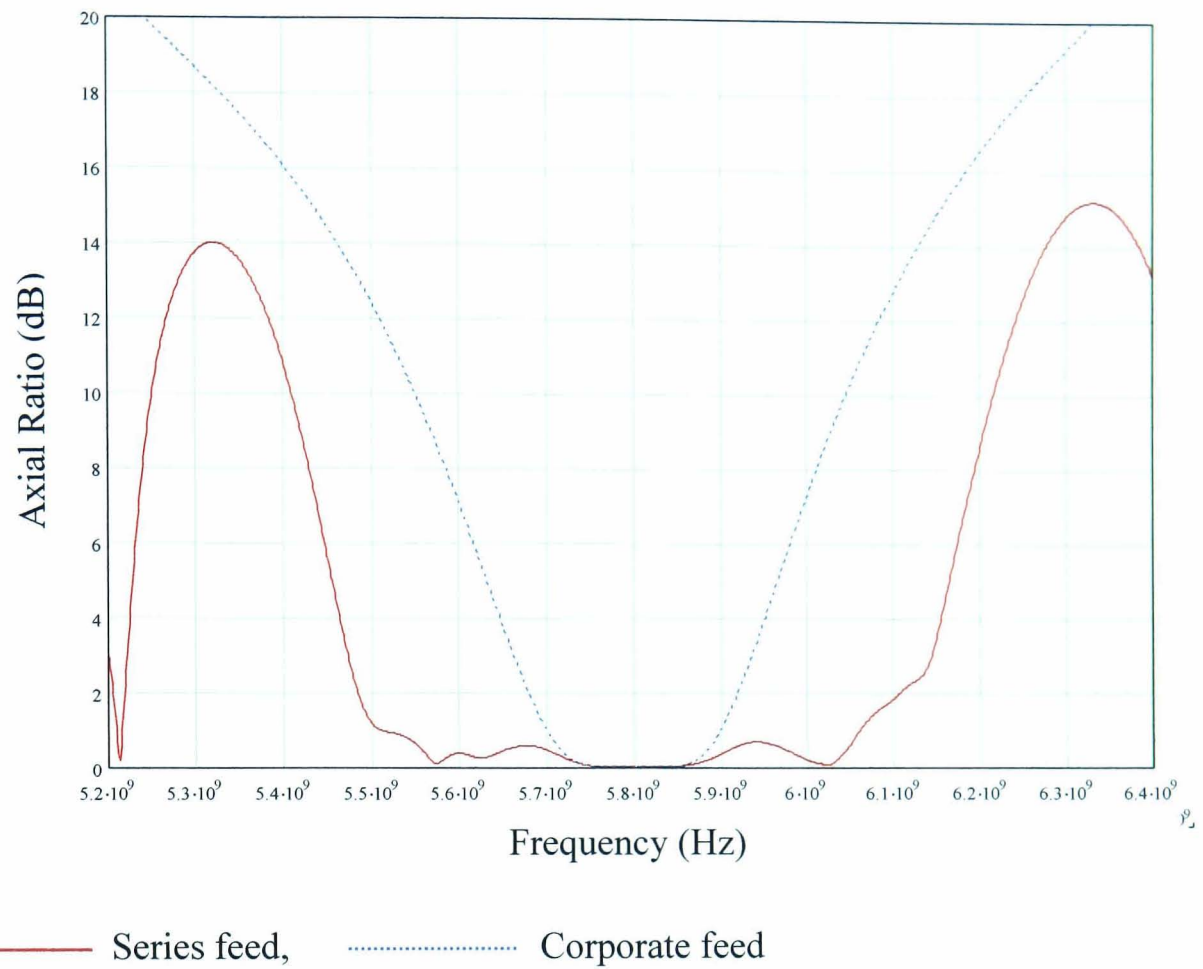
Figure 6-3: Axial ratio of 4x4 array using both feeding techniques ($\varepsilon_r = 2.33$, $h = 0.79$ mm).

Figure 6-3 shows the 3 dB axial ratio of the series fed array is 10.3% (between 5.5 and 6.1 GHz) which is more than twice as wide as the corporate fed array at 4.6% (5.66 – 5.93 GHz).

Unlike the series fed 2x2 array, the series fed 4x4 array has a comparable VSWR 2:1 and 1.5:1 bandwidth as there is less ripple in the pass band. Furthermore, the VSWR 2:1 and 3 dB axial ratio bandwidths are more comparable with each other in the 4x4 array.

6.3 Side lobe reduction.

At boresight, the electric fields from the radiating elements add in phase, as the distance between each radiating element and the measuring reference point in the far field is approximately equal. Away from boresight the fields encounter a small phase delay as the path length is no longer equal (see Figure 6-5). When the path length difference is in the region of half a wavelength the fields destructively interfere creating nulls in the radiation pattern. At wider angles the fields begin to add constructively once again, resulting in side lobes.

Reduction in side lobe levels can be achieved by altering either the excitation phase [92,93, 120] or the excitation amplitude [26] of the individual radiating elements that make up that array. In this microstrip array, altering the phase of excitation would require a change in feed line length which is not suited to this feed geometry. Despite the compact nature of the series feed network, there is limited real estate to further extend any of the feed sections. Furthermore, all of the series feed sections being a quarter wave in length aids impedance matching. Altering the distribution of power across the array was therefore the chosen method of side lobe reduction.

6.3.1 Radiation pattern calculation

The relative size of the side lobes and the angle with respect to the main beam at which they occur can be calculated as follows.
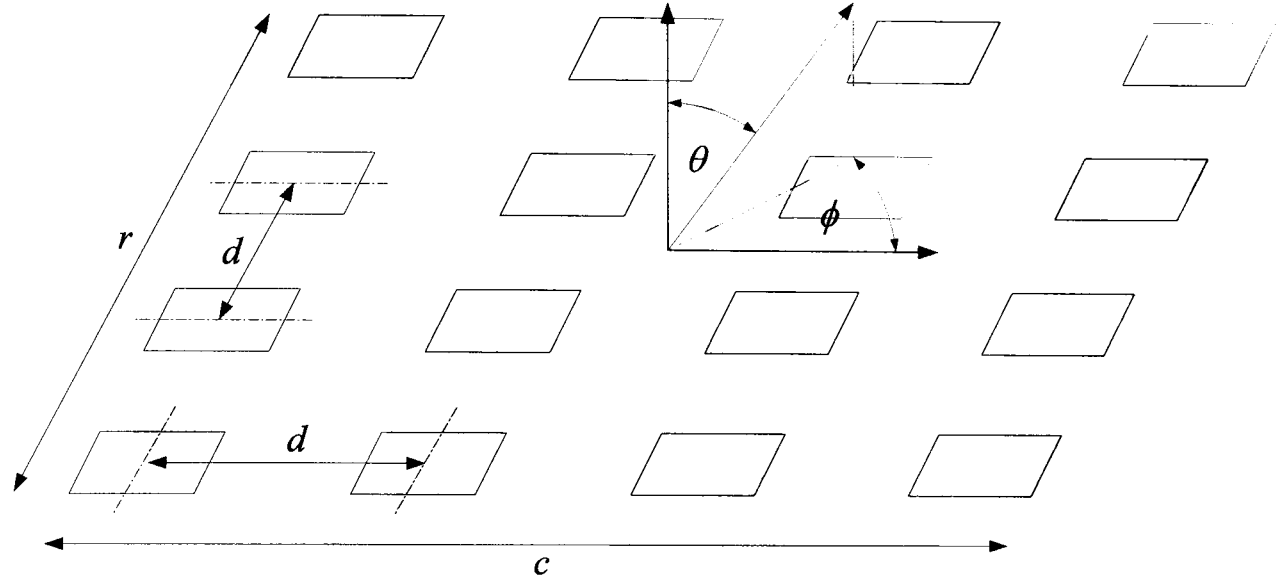
Figure 6-4: Array geometry with rows r, columns c and patch spacing d.

A 4x4 array of patch antennas can be seen in Figure 6-4. Each column of patches has a column number c and each row has a row number r. Each patch is spaced at d, fed with phase $\phi_{r,c}$ and with power $P_{r,c}$.

The total field as a function of θ is found by summing the contribution from each patches X and Y components and finding the resultant. A cos relationship is assumed for the radiation pattern of a single patch as it can be considered as two radiating slots with approximately half a wavelength separation, therefore.

$$E_{(\theta,0)} = \cos\theta \times \sqrt{\sum E_x^{\,2} + \sum E_y^{\,2}} \tag{6.1}$$

Each component of the resulting field from each patch with feed power $P_{r,c}$ and feed phase $\phi_{r,c}$ can be determined using (6.2). The value used for feed phase is the relative difference in excitation phase once the physical rotation has been subtracted from the actual excitation phase (hence always zero in this array).

$$E_x = \sqrt{P_{r,c}} \times \cos(\phi_{r,c} + \alpha x) \text{ and } E_y = \sqrt{P_{r,c}} \times \sin(\phi_{r,c} + \alpha x) \tag{6.2}$$

where path delay $\alpha x = cd \sin \theta$ with patch a spacing of d and column number c (for $\phi = 0$, $\alpha x = rd \sin \theta$ when $\phi = 90$) as shown in Figure 6-5.
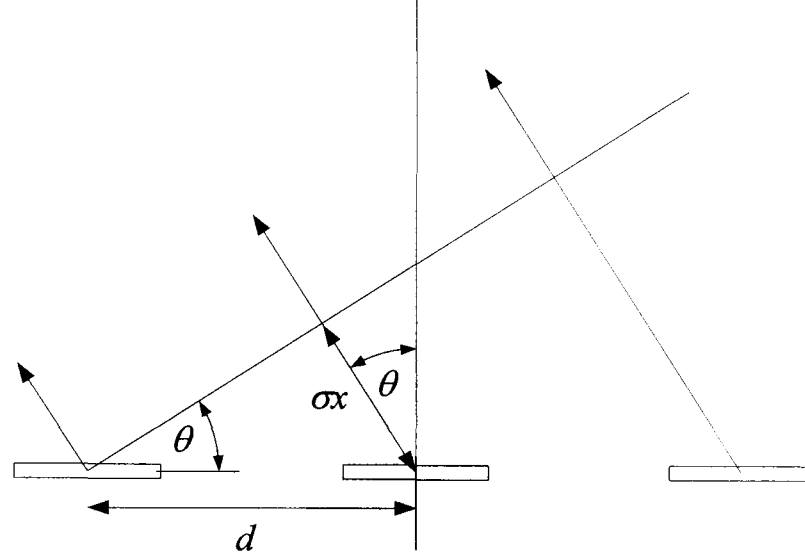
Figure 6-5 : Path delay.

6.3.2 Array power distribution

Three arrays with alternative power distribution can be seen in Figure 6-6. In Array A, power is equally distributed across the array. In Array B 64% of total array power is distributed to the center of the array. Therefore, 16% of total array power is fed to each of the four center patches and 3% of array power is fed to the outer patches. In Array C, almost 80% of total array power is fed to the center patches.

6.25	6.25	6.25	6.25
6.25	6.25	6.25	6.25
6.25	6.25	6.25	6.25
6.25	6.25	6.25	6.25

(a)

3	3	3	3
3	16	16	3
3	16	16	3
3	3	3	3

(b)

1.8	1.8	1.8	1.8
1.8	19.6	19.6	1.8
1.8	19.6	19.6	1.8
1.8	1.8	1.8	1.8

(c)
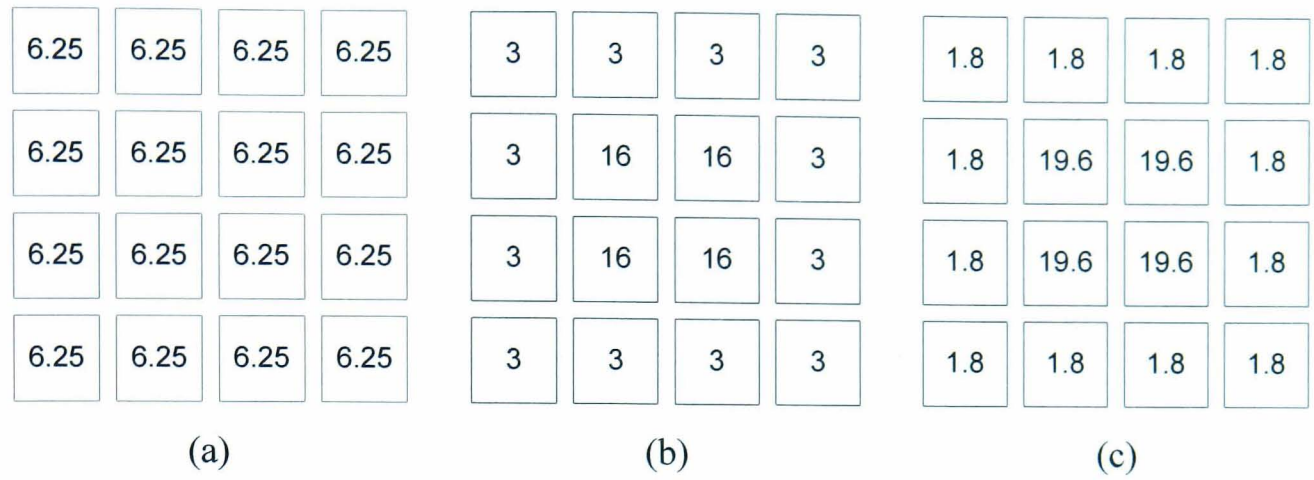
Figure 6-6: Power distribution to each radiating element in percent of total 4x4 array power (a) Array A (b) Array B (c) Array C.

The resulting radiation pattern for these arrays can be determined using equation (6.1) and can be seen in Figure 6-7.

—————— Array A
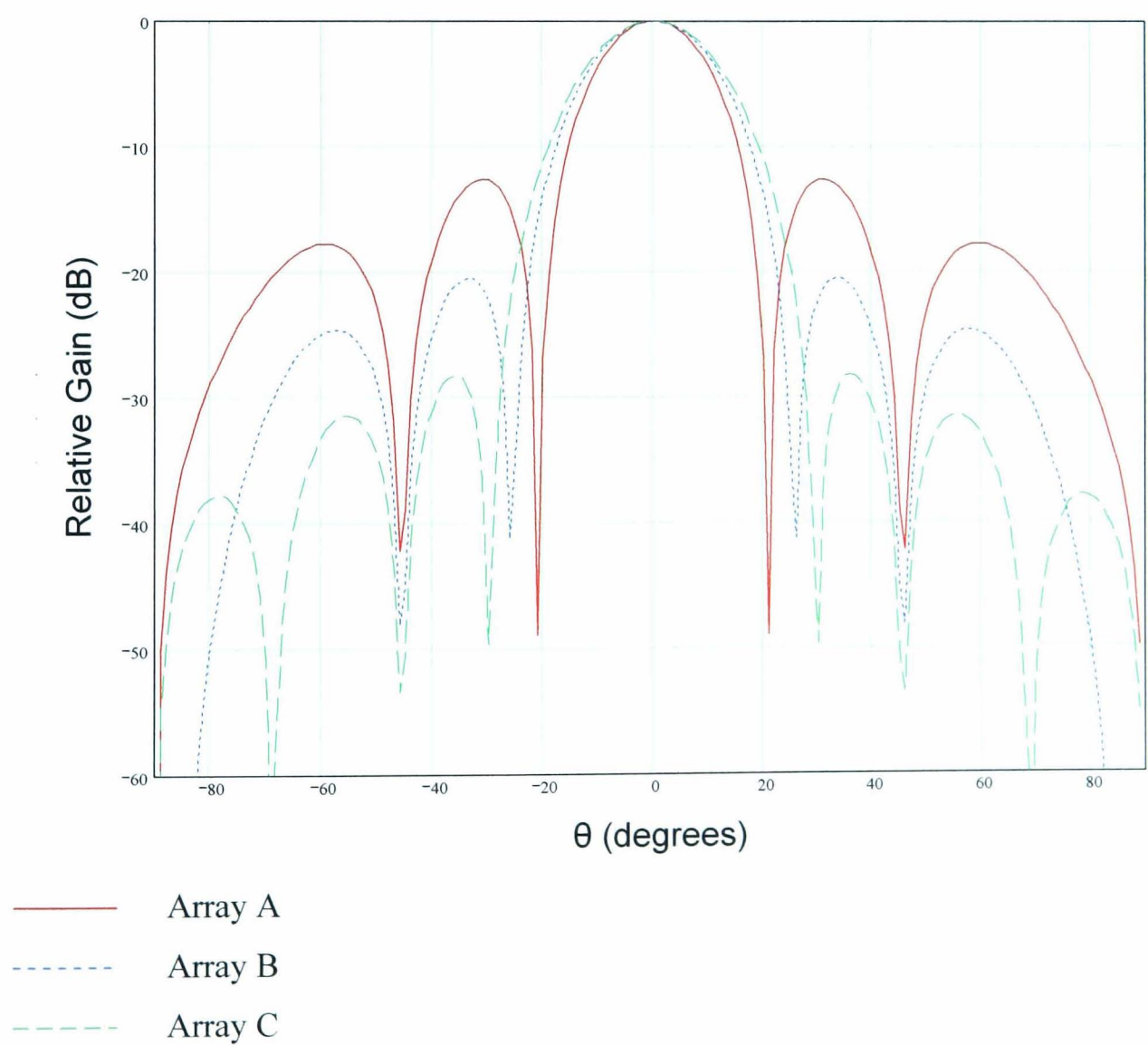
- - - - - - Array B

— — — — Array C

Figure 6-7: Resulting radiation pattern for the three arrays.

132

From Figure 6-7 it can be seen that as more power is diverted to the center of the array, the magnitude of the side lobes reduces while the main beam becomes slightly broader. This effect is quantified in Table 6-1.

Array	10 dB gain angle	1st side lobe relative gain	1st side lobe relative angle	2nd side lobe relative gain	2nd side lobe relative angle
A	+/- 15	-12.5	+/- 30	-18	+/- 59
B	+/- 17.5	-20.5	+/- 33	-24.5	+/- 57
C	+/- 19	-28	+/- 35	-31.5	+/- 56

Table 6-1: Radiation pattern summary.

6.3.3 Implementation

Diverting more power to the center patches of the 4x4 array is achieved by altering the percentage of power that is fed to the first patch within each of the 2x2 sub-arrays that make up the 4x4 array. This is achieved by modifying the power division at the first junction of the sub-arrays feed network (node **a** in figure 4-6).

The modified feed values for the 2x2 sub-arrays were generated using the optimisation algorithm presented in Chapter 5. Additional inputs were added to the program allowing user defined power splitting at each junction of the series feed. The required power distribution within the 2x2 sub-array is defined in Table 6-2.

Array	4x4 array power fed to :		2x2 array power fed to :	
	Center patches	Outside patches	First patch	Remaining patches
A	6.25%	6.25%	25%	25%
B	16%	3%	64%	12%
C	19.6%	1.8%	78%	7.2%

Table 6-2: Required power distribution within the 2x2 sub-array.

The minimum feed impedance was again constrained to 70Ω to reduce coupling and spurious radiation. Solutions were found with a maximum impedance of 140Ω, a target impedance of 128Ω and a patch input impedance of 50Ω.

The following values for the sub-array series feed sections were generated and can be found in Table 6-3. The feed impedances are as defined in Figure 5-12 (c). The length of all feed line sections remain a quarter wave in length.

Sub –Array	Z_1	Z_2	Z_3	Z_4	Z_5	Z_6	Z_7	Z_8
B	64	80	128	103	83	80	128	80
C	64.6	73	140	87.2	76.3	87.5	140	80

Table 6-3: 2x2 sub-array series feed impedance values.

From Table 3 it can be seen that, due to the modified power division at node **a**, the value of Z_3 is lifted to the maximum impedance value hence Z_1 can no longer remain at 50Ω. Z_1 is positioned between the extremities of the main 50Ω matched feed line (Z_{50}) and the half wavelength feed section (Z_H).

As the value of Z_1 ensures the input impedance to the sub-arrays is 50 Ω, the central series feed of the 4x4 array retains the original feed values produced in chapter 5 ensuring that, at design frequency, equal power is distributed to each of the 2x2 sub-arrays.

6.3.4 Frequency performance of array with reduced side lobes

The frequency performance of the modified arrays can be evaluated using the extended model that was used to assess the performance of Array A (the basic 4x4 array).

The VSWR frequency performance of all three arrays can be seen in Figure 6-8.
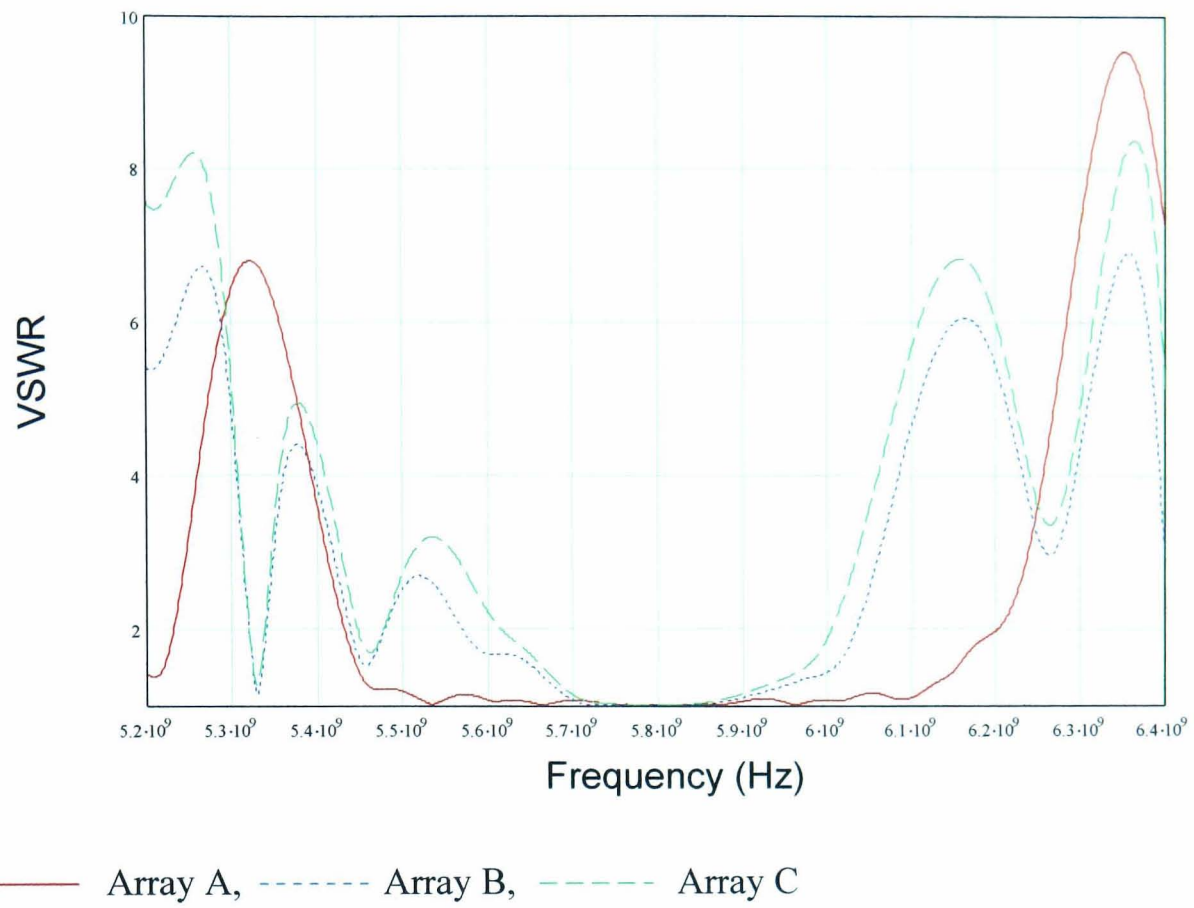
Figure 6-8: VSWR frequency performance of Array A, B and C ($\varepsilon_r = 2.33$, $h = 0.79$ mm).

The VSWR 2:1 bandwidth of Array B is 8% between 5.57 and 6.03GHz and of array C is 6.8% between 5.61 and 6.01 GHz as seen in Figure 6-8.

The boresight axial ratio, as a function of frequency, for all three arrays can be seen in Figure 6-9.
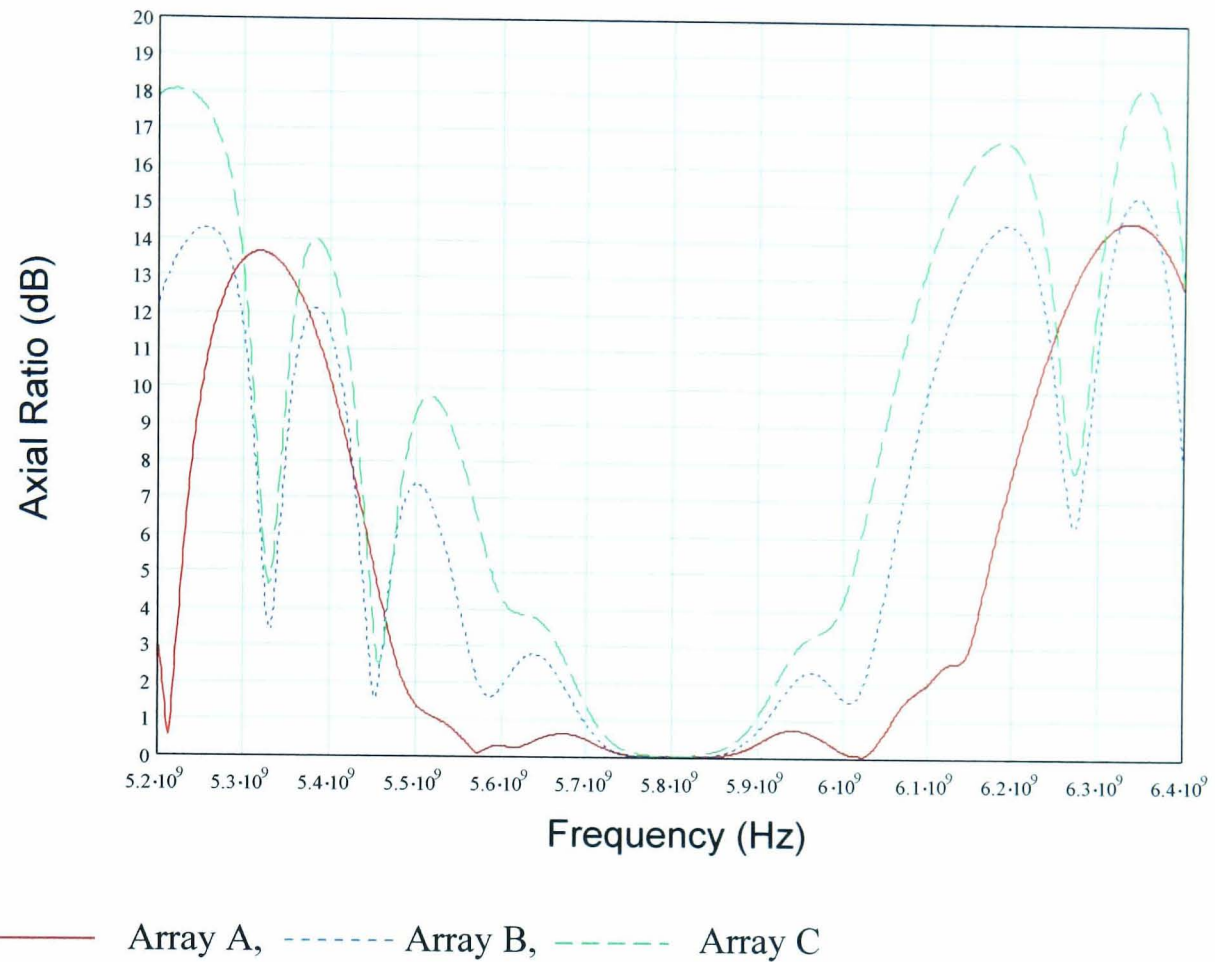
Figure 6-9: Axial Ratio frequency performance of array A, B and C ($\varepsilon_r = 2.33$, $h = 0.79$ mm).

The 3 dB axial ratio of array B is 8.1% between 5.56 and 6.03 GHz and of array C is 5% between 5.66 and 5.95 GHz.

It can be seen that Arrays B and C demonstrate a large reduction in both VSWR and axial ratio bandwidth when compared to the basic Array A. This reduction in performance is due to a less favorable relationship between the internal reflections within the modified sub arrays.

In the basic 2x2 sub-array, where equal power is fed to each element, reflections from mismatched radiating elements were equivalent in magnitude; as each radiating element is separated by a quarter wave length line, these reflections tend to cancel out. In the modified 2x2 sub-array, more power is fed to the first patch and less power is fed to the remaining three patches. As a consequence, the magnitudes of the reflections are longer equivalent reducing the efficiency of this cancellation

mechanism. The bandwidth of Arrays B and C is comparable to the corporate fed 4x4 array, as the corporate feed does not benefit from the series feeds unique cancellation properties (when used in a four element array).

6.4 Practical realisation

The three 4x4 antenna arrays were fabricated using 0.79 mm 1/2oz RT 5870 ($\varepsilon_r =$ 2.33) and traditional PCB techniques. All arrays are probe fed from behind the ground plane using an SMA connector.

6.5 *Practical results*

The integrity of the designs were confirmed using both full wave simulation [117] and experimental measurement.

6.5.1 Frequency performance

Both input impedance and boresight axial ratio performance of the basic Array A with equal power distribution (as seen in Figure 6-1) have been confirmed over a frequency range of 5.2GHz – 6.4GHz. Practical measurements were made of input impedance were made using an Anritsu 37347C vector network analyser. Boresight axial ratio was determined across this frequency range within an anechoic chamber using the method and apparatus as described in Appendix C.

XXXXXXX   Modeled

‐ ‐ ‐ ‐ ‐ ‐   Full Wave Simulation
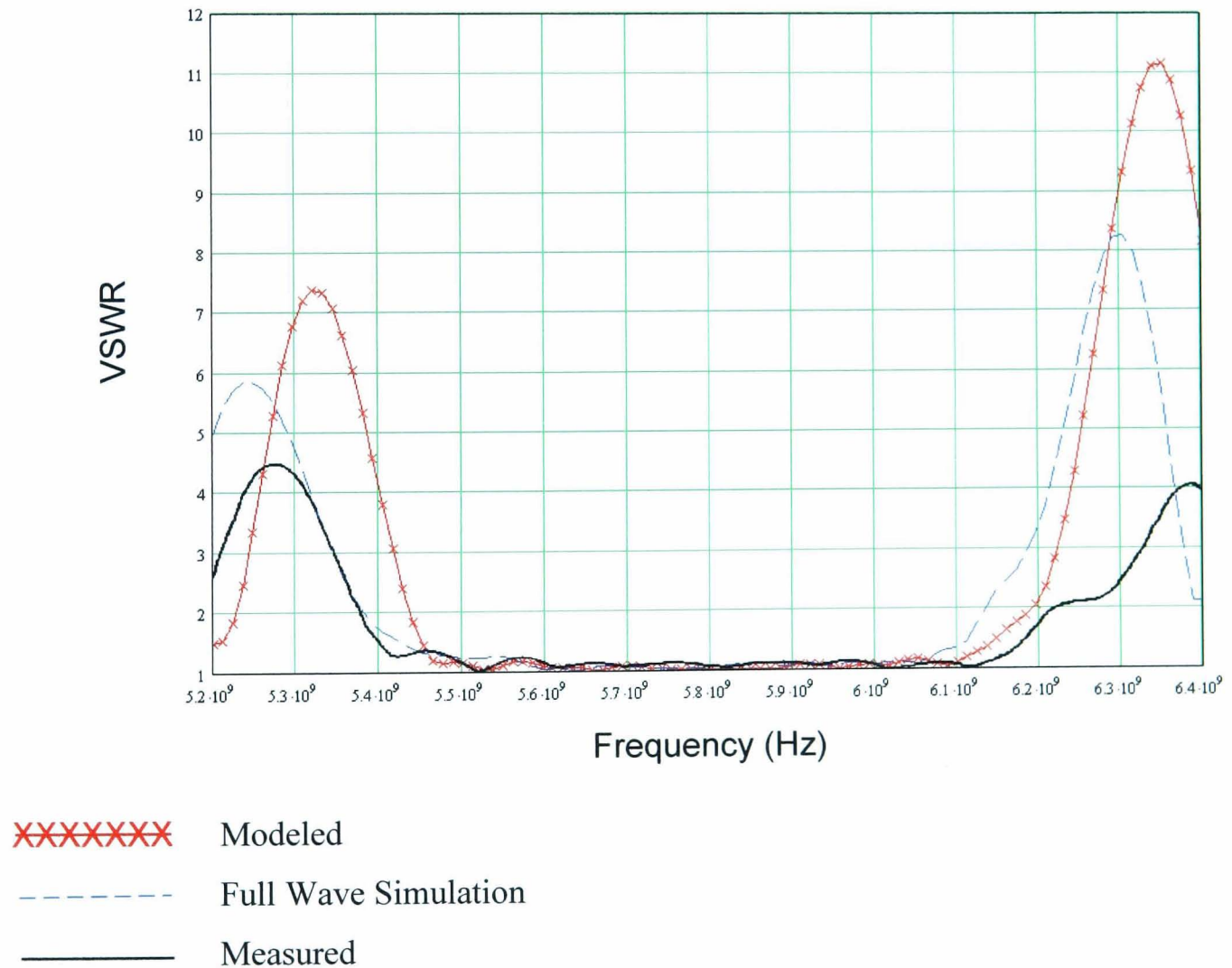
────────   Measured

Figure 6-10: VSWR of Array A.

A VSWR 2:1 bandwidth of 14.7% was measured between 5.38 GHz and 6.23 GHz as shown in Figure 6-11.

138

Figure 6-11: Boresight axial ratio of Array A.

A 3 dB axial ratio bandwidth of 12.4% was measured between 5.44 GHz and 6.16 GHz as seen in Figure 6-11.

Measured results of both VSWR and Axial ratio bandwidth are in good agreement with that predicted by the analysis and full wave simulation.

6.5.2 Radiation pattern

The radiation pattern of Array A, Array B and Array C were determined within an anechoic chamber using the methods and equipment described in Appendix C.

The normalised radiation pattern of Array A can be seen in Figure 6-12. The gain of the main lobe was measured at 18 dBi with a 10 dB beamwidth of 30°. The peak of the first side lobe occurred 29° from the main lobe. Isolation between the main lobe and the first side lobe was measured at 14.5 dB. This is in close agreement with the performance predicted in Table 6-1.

XXXXXX   Full wave simulation
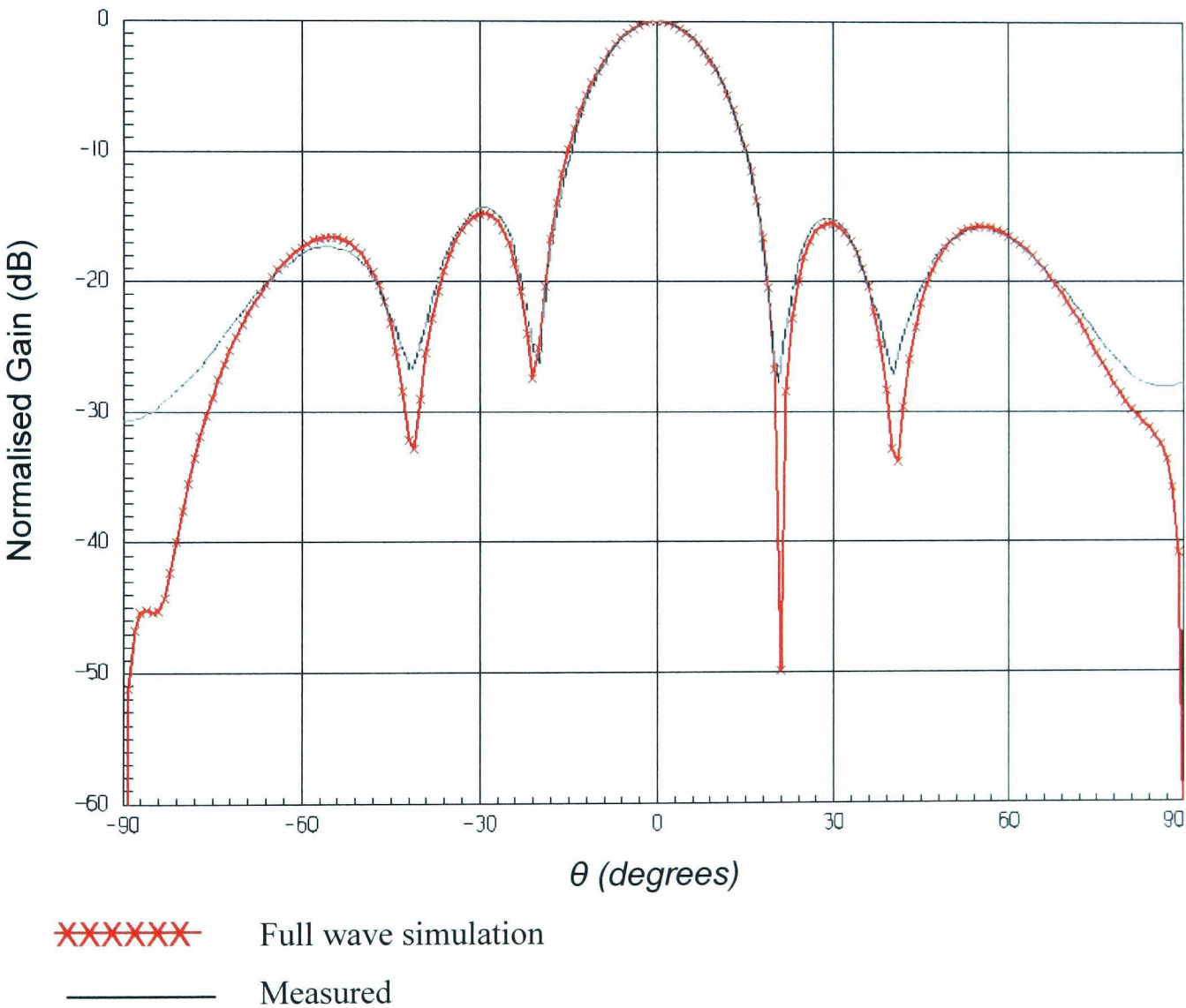
————   Measured

Figure 6-12: Measured and simulated radiation pattern of Array A ($\phi = 0$).
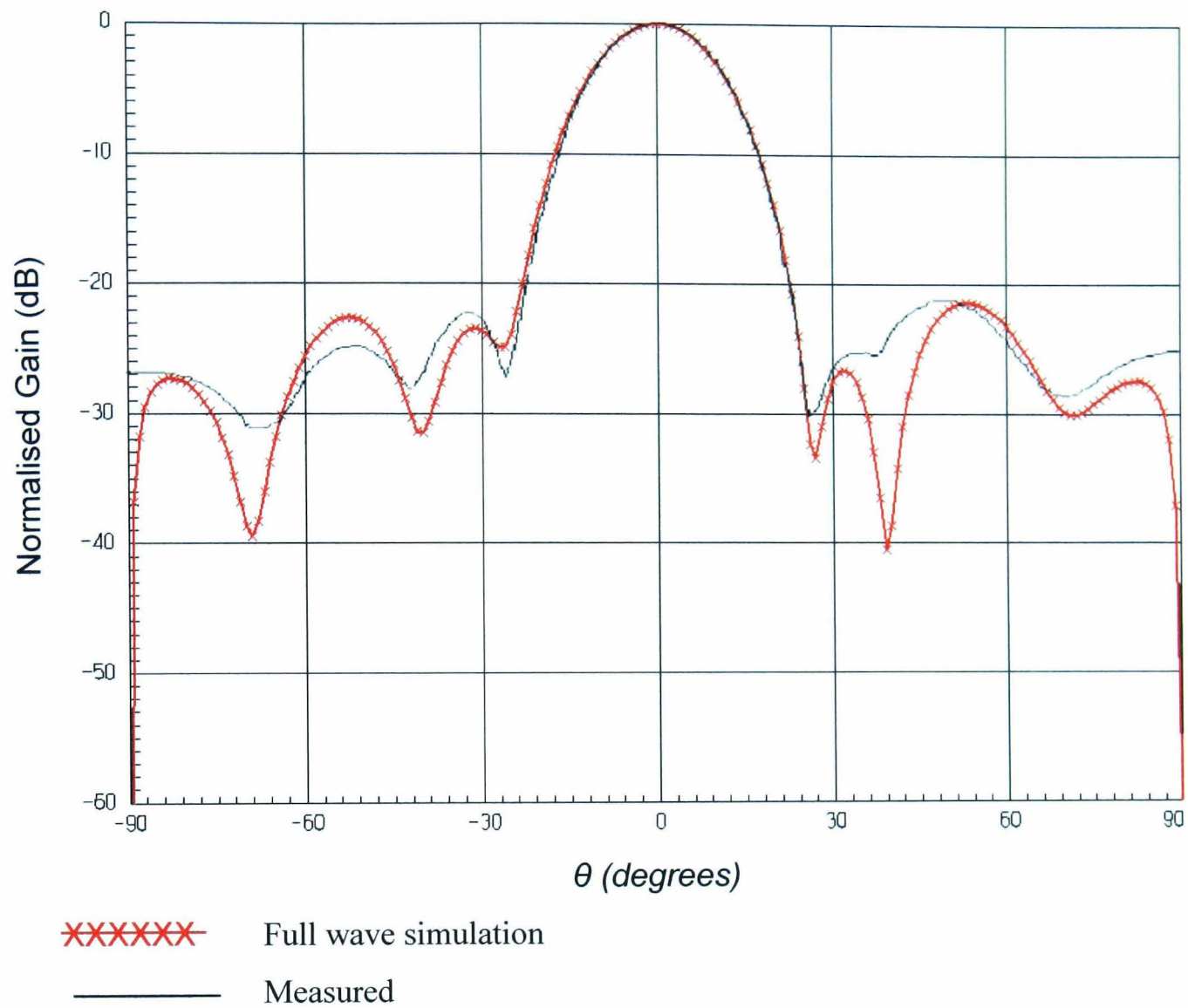
Figure 6-13: Measured and simulated radiation pattern of Array B ($\phi = 0$).

The radiation pattern of Array B can be seen in Figure 6-13. The gain of the main lobe was measured at 16.9 dBi. The 10 dB beamwidth of the main lobe was measured at 35°. There is a minimum of 21 dB isolation between the main lobe and the side lobes, this is sufficient isolation to satisfy the requirements of the DSRC traffic management system seen in Table 1-1. These results are in close agreement with Table 6-1 although the relative positioning of the side lobes differs.
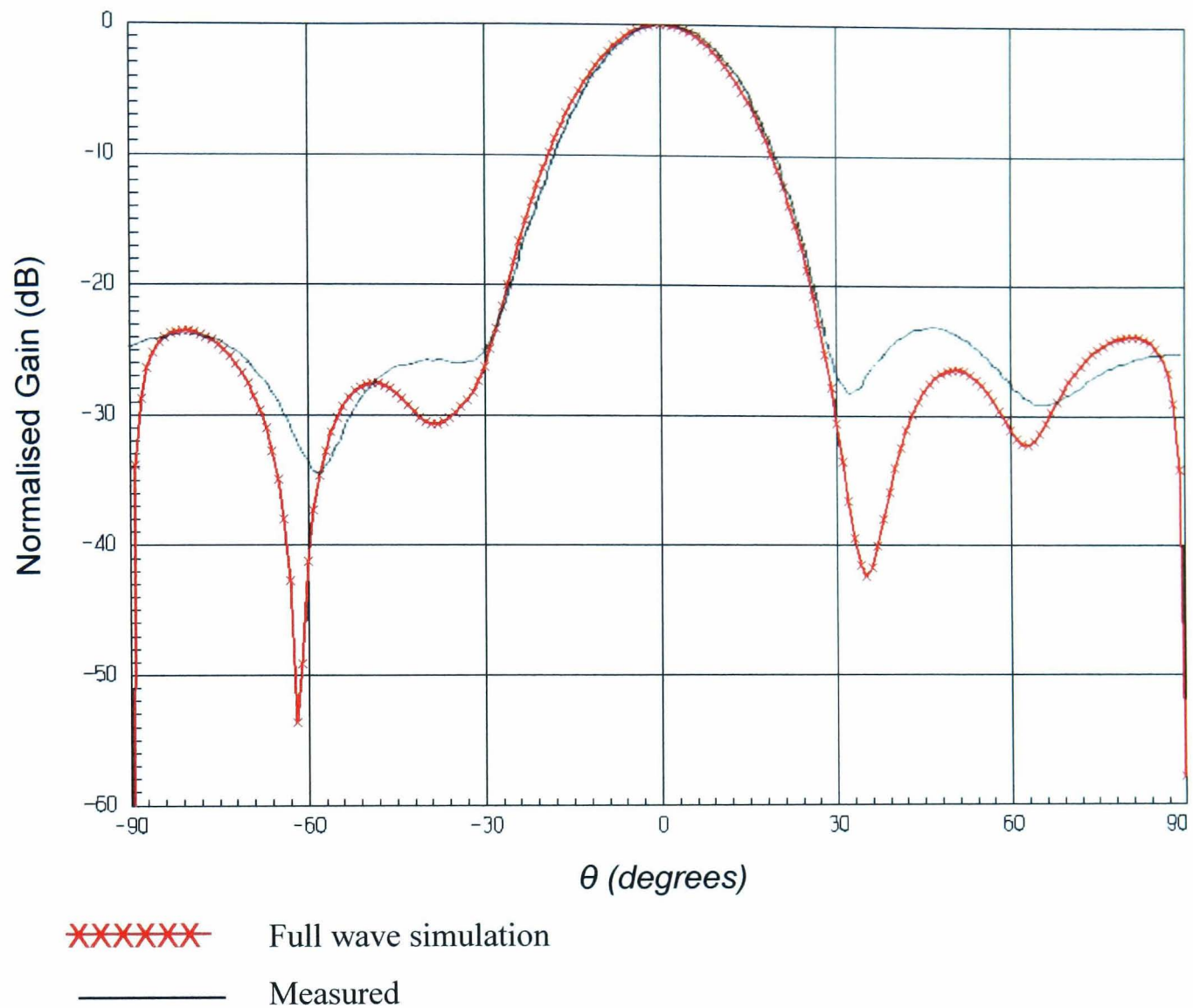
Figure 6-14: Measured and simulated radiation pattern of Array C ($\phi = 0$).

The radiation pattern of Array C can be seen in Figure 6-14. The gain of the main lobe was measured at 16.25 dBi. The 10 dB beamwidth of the main lobe was measured at 38°. There is a minimum of 23 dB isolation between the main lobe and the side lobes.

In all arrays, the analysis of Section 6.3.1 predicts the behaviour of the main lobe with a high degree of accuracy, this is not the case predictions of the side lobe behaviour in the arrays with unequal power distribution is not as accurately expressed. Although in Array C increased isolation between the main beam and the side lobes is demonstrated, it is not as great as that predicted in Table 6-1. This is possibly due to small errors in the array's power distribution which becomes far more apparent when only a small amount of power is fed to the outer patches and as theta increases. The lack of symmetry is due to the contribution of spurious radiation from the asymmetrical central feed network to the radiation pattern.

In all three examples, good agreement is seen between the full wave simulation and experimental measurement confirming the integrity of the anechoic chamber.

6.6 Conclusion

A 5.8GHz circular polarized 4x4 antenna array composed of sequentially rotated 2x2 sub-arrays with a series feed network has been realised. The use of an out-of-line series feed allows a more compact structure with enhanced frequency bandwidth over a corporate feed when used in this array. A further advantage of sequentially rotating the sub-arrays is that any spurious feed radiation will tend to cancel in the far field.

In the basic Array A, the measured VSWR and Axial ratio frequency bandwidth were almost twice that of the same array using a corporate feed as described in [67]. This improvement in performance was due to a more favorable relationship between internal reflections within the series feed network. Unlike the 2x2 sub-array the VSWR 2:1 and the VSWR 1.5:1 bandwidth are more comparable as there is less ripple in the pass band. Furthermore, the 3 dB axial ratio bandwidth is more comparable to the VSWR 2:1 bandwidth.

Side lobe reduction has been successfully achieved demonstrating 20 dB isolation between the main lobe and the side lobes. Although the gain of the main lobe has been reduced, it has also broadened hence off bore sight the gain is greater. The broadening effect is advantageous as, due to the difference in windscreen rakes, the OBU and RSU will not always be in optimal alignment. The arrays with reduced side lobes did not benefit from frequency bandwidth enhancement to the same extent as that shown by the basic Array A.

CHAPTER 7

INCREASING THE BANDWIDTH OF THE 2X2 ARRAY

7.1 Introduction

The OBU of the DSRC traffic management system needs to have a low profile, use inexpensive materials, be cheap to manufacture and be mechanically robust. A compact structure is preferred as the intended mounting position for the OBU is behind the windscreen of the vehicle and it is important not to obscure the drivers view. Further, to ensure that the OBU can be placed in any orientation, circular polarisation is required.

The antenna within the OBU also has to have robust frequency performance for the following reasons. Firstly, due to the OBU's close proximity with various types of windscreen there is a varied detuning effect. Secondly, the OBU's single antenna is not part of an array, therefore does not benefit from the bandwidth enhancement offered by sequential rotation as seen in the RSU arrays. The bandwidth of the single antenna can be increased using aperture coupling where the radiating patch and feed network are implemented on separate substrates, allowing a patch with a lower Q.

In this chapter a wide band single feed aperture coupled patch antenna suitable for use within the OBU is developed. This work required the development of a cavity model of a cross aperture coupled antenna. Such a model can provide not only a good physical understanding of the complex operation of the antenna but also allow the use of a computer aided design approach to readily examine the trade off between the different design parameters. This work has contributed to a paper published in the IEE transactions on antennas and propagation [20].

The antenna is then used as a broad band radiating element in the series fed four element array presented in Chapter 4. As a direct result of this research a letter has been published in Microwave and Optic Technology letters titled "Increasing the

bandwidth of a 2x2 sequentially rotated patch array" [21]. Both full wave simulation and experimental measurement confirm the integrity of this design.

7.2 Aperture coupled patch antennas

Microstrip feed lines are the most common choice of feed method however the use of striplines have also been demonstrated [121]; the microstrip feed line is etched onto the bottom of the feed substrate. The radiating patch is etched onto the top of the antenna substrate. The thickness and dielectric constants of these two substrates can therefore be chosen independently to optimise the distinct electrical functions of radiation and circuitry hence cater for the conflicting requirements. As a result, a wide band patch is possible without incurring additional feed losses. The aperture is etched into the separating ground plane which minimises the contribution of spurious feed radiation to the main radiation pattern. Although a rectangular slot is the most common shape of aperture, several other shapes have been published such as the 'dog bone' [122] and the 'bow tie' or 'butterfly' [123]. These can allow greater coupling from a smaller aperture resulting in less back radiation and ease of positioning in dual or circular polarised configurations where two orthogonal coupling apertures are required.

While single layer direct fed patch antennas are limited to an input impedance bandwidth of between 2% - 5%, aperture coupled elements have been demonstrated with bandwidths of 10 – 15% [124,125,126], and up to 30-50% with stacked patch configurations [127,128].

7.3 Circularly polarised aperture coupled patch antennas

The first dual feed circular polarised aperture coupled patch antenna was presented by Adrian and Schaubert [129], two orthogonal non-overlapping slots were used to feed a square patch. Dual linear polarisation was achieved with 18 dB isolation and circular polarisation obtained using a 90 hybrid as an external polariser. This configuration can be seen in Figure 7-1 (a).

(a) (b)

(c) (d)
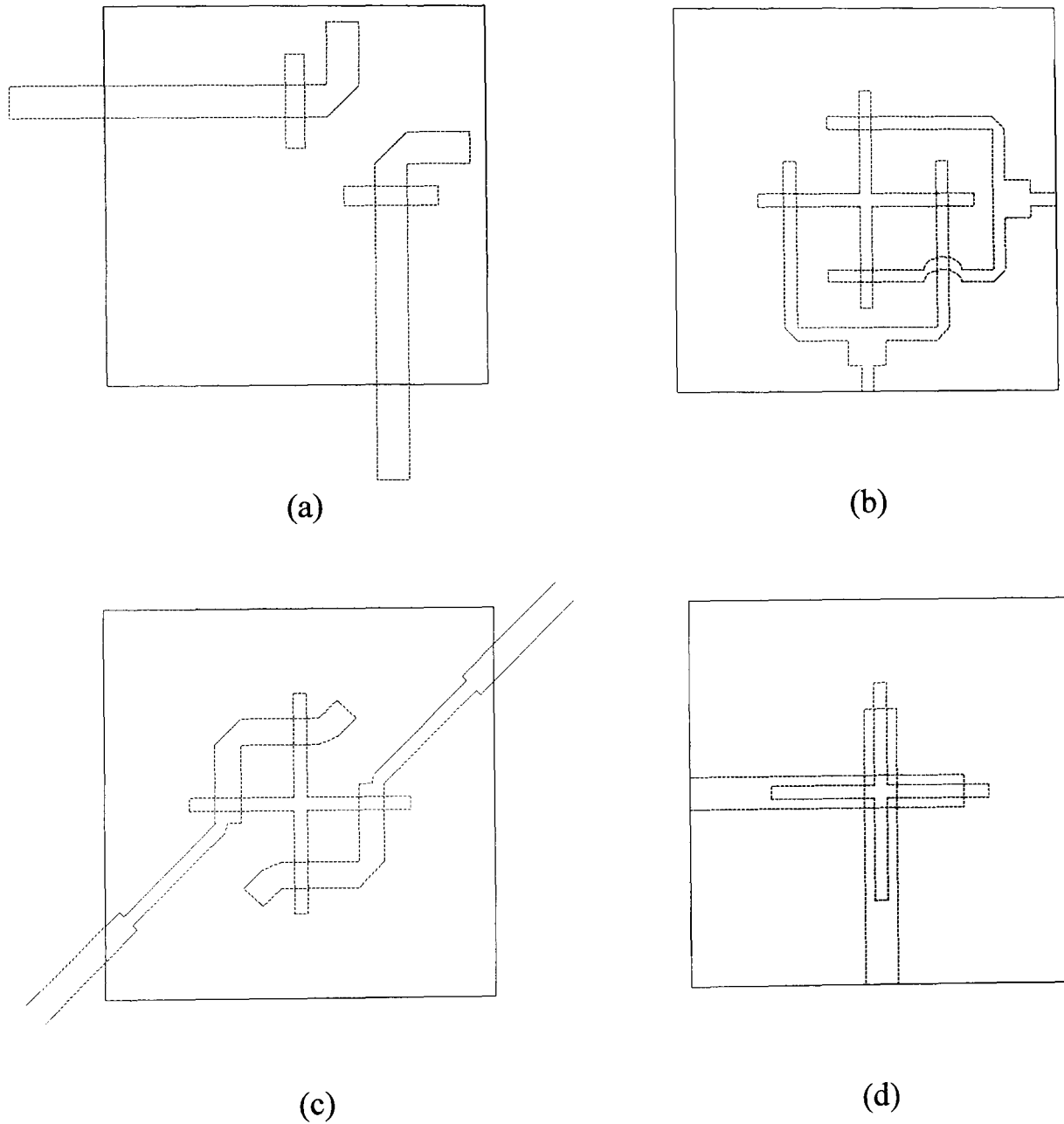
Figure 7-1: Dual feed circularly polarised patch antenna.

A drawback to this structure was that the coupling level was constrained by the slot size due to their asymmetry, this also limited isolation and polarisation purity. An alternative method can be seen in Figure 7-1 (b) in which a cross slot to feed the patch

146

achieving 27 dB isolation and good bandwidth [130]. However the balanced feed lines required an air gap to bridge one of the feed arms. Targonski and Pozar, using the alternative feed and slot arrangement seen in Figure 7-1 (c), overcame this problem achieving input impedance and 3 dB axial ratio bandwidths of up to 50% [131]. An alternative solution using a cross slot and two feed lines located on two separate feed substrates as shown in Figure 7-1 (d) has also been proposed [132].

Circular polarisation has also been demonstrated using a single feed line. One approach is to use a linearly polarised aperture coupled patch antenna and external feed lines that couple the aperture-excited mode to the orthogonal mode [133]. This structure can be seen in Figure 7-2 (a).

(a)   (b)
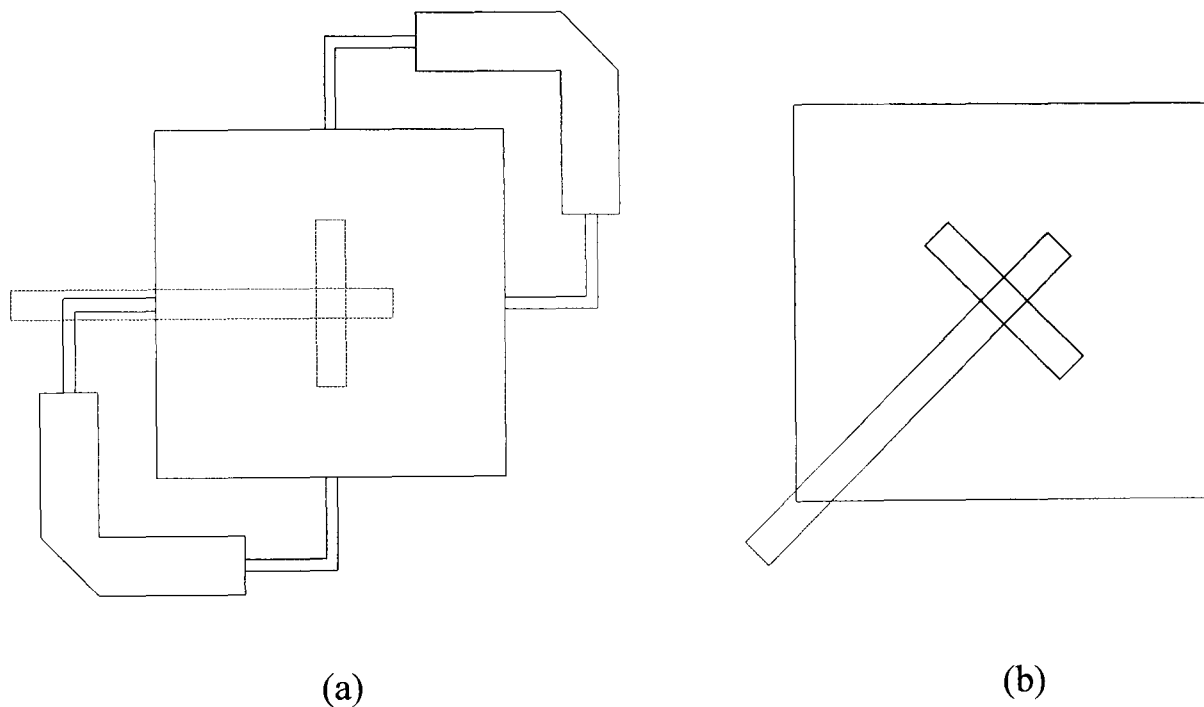
Figure 7-2: Single feed aperture coupled patch antennas.

For circular polarisation, the length of this feed must be an odd multiple of 90 degrees. A drawback of this technique is that correct impedance matching must be maintained to ensure the orthogonal modes are of equal amplitude.

A single slot perpendicular to the feed line with the patch rotated at an angle to the linear polarised position has been demonstrated [134,135] and can be seen in Figure 7-2 (b). Phase quadrature, between the two orthogonal modes developed on the patch,

is achieved using a nearly square patch working on the principle of a corner fed degenerate mode patch antenna. This arrangement is simple and compact but, as with the original nearly square patch, is very sensitive to manufacturing tolerances. Further, the resulting axial ratio and input impedance bandwidth are very narrow.

Vlasits proposed a solution to this problem using a cross slot fed by a single microstrip line [136] as seen in Figure 7-3. In this arrangement the cross is constructed from two orthogonal apertures. The single feed line excites both apertures equally in both magnitude and phase. Circular polarisation is achieved using a nearly square radiating patch. The cross aperture is positioned below the centre of each patch as this excitation symmetry helps to maintain good polarisation purity.
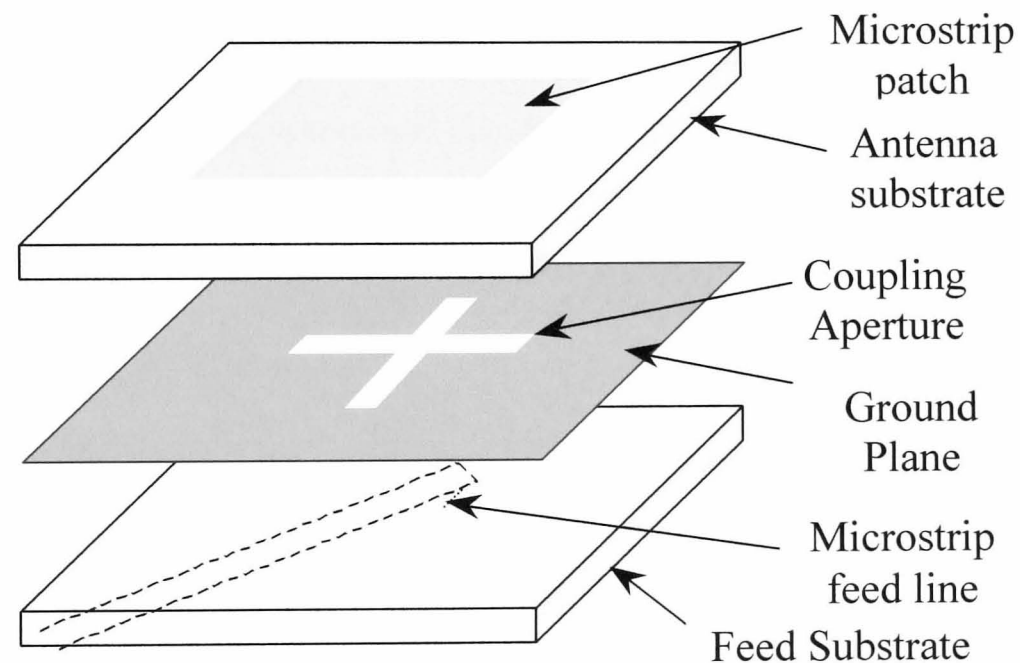
Figure 7-3: Single feed cross aperture coupled patch antennas as proposed by Vlasits.

7.4 Cavity model

Antenna analysis can aid the design process considerably by reducing the costly and time consuming trial and error cycles. This benefit is far more apparent when the design has to be optimised over a number of design parameters as in an aperture coupled antenna.

The presence of two dielectric layers and the microstrip to slot transition complicate analysis of the aperture coupled patch antenna. The original analysis of the aperture coupled element presented a simplified cavity-type model [31], the structure first

receiving rigorous analysis by Sullivan and Schaubert [16] who used a full wave MoM solution. This work presented data showing the effects of various design parameters such as slot position and size on the input impedance locus of the antenna. Pozar [137] then introduced a method of treating the feed line to slot transition using the reciprocity theorem which eliminated the need for brute force modeling of the microstrip feed line and stub.

Full wave analysis is very useful, rigorous, highly accurate and versatile enough to handle practical variations such as stacked patches, patches with radome layers and patches fed with stripline. However, these methods require large scale computational software with the added expense of relatively long computer run times, due to the slow convergence of the reaction integrals or tabulation of the Green's functions. Furthermore, model accuracy is increased by model complexity and with simplicity comes ease of use, implementation and physical insight. In addition these complex methods of analysis do not generate equivalent circuit models of the antenna, thus making it difficult to use the computer aided design approach preferred by many engineers.

A popular simple model is the cavity model. The cavity model uses magnetic wall boundary condition approximation for the periphery of the patch. This model generates a general equivalent circuit where the patch is represented by a number of tuned circuits all connected in parallel. A cavity model has been developed for the analysis of linear polarised aperture coupled patch antennas [138,139], with good results for the input impedance of antennas on thin substrates. This first reference was later modified to account for thick ground planes [140]. A further generalisation of this model breaks the periphery of the patch into a set of ports, each with an effective load admittance modeling edge of the patch as well as the feed point. This multi port network model [141] has the advantage of being capable of handling fairly arbitrary patch shapes and port elements.

In order to design a cross aperture coupled single feed radiating element, the cavity model has to be adapted to this particular structure. This adaptation can then be used to generate the required design parameters required for practical realisation.

7.5 Cross aperture cavity model

A cavity model of the cross aperture coupled patch antenna has been developed [20] that allows investigation into input impedance and axial ratio frequency performance. Using the analytical expressions for the patch admittances at the apertures found in [20], an equivalent circuit has been derived and can be seen in Figure 7-4.
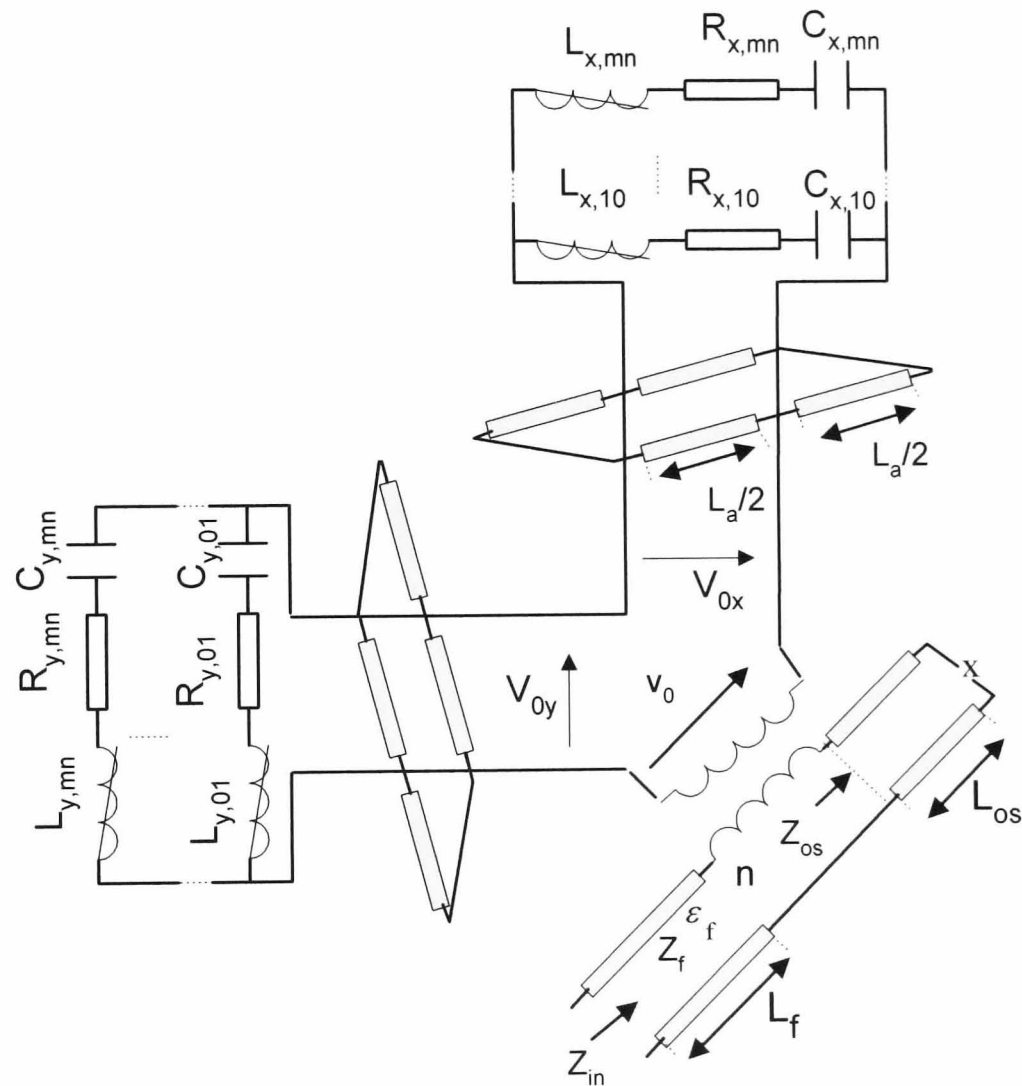
Figure 7-4: Equivalent circuit.

The input impedance of the antenna is given by

$$Z_{in} = \frac{n^2}{Y_{x,ant} + Y_{ap}} + \frac{n^2}{Y_{y,ant} + Y_{ap}} - jZ_{os} \qquad (7.1)$$

Assuming two orthogonal apertures make up the cross aperture, n is the turns ratio of the microstrip feed line to aperture impedance transform. Y_{ap} is the self admittance of

the aperture and $Y_{x,ant}$ and $Y_{y,ant}$ are the radiating patch admittances at the apertures. Z_{os} is the impedance looking into the tuning stub and can be expressed as

$$Z_{os} = Z_f \cot(k_f L_{os})$$

(7.2)

$Y_{x,ant}$ and $Y_{y,ant}$ are expressed using a string of $m \times n$ series RCL circuits all connected in parallel and can be found in [20]. The values of these circuit elements can be determined using

$$L_{x,mn} = \frac{d_a}{16\varepsilon c^2 A_{mn}^2} \cdot \left\{ \frac{\text{sinc}\left(k_n \frac{W_a}{2}\right)\sin\left(\frac{n\pi}{2}\right)\cos\left(\frac{m\pi}{2}\right)}{\sin\left(k_a \frac{L_a}{2}\right)} \cdot \frac{k_a\left[\cos\left(k_m \frac{L_a}{2}\right)-\cos\left(k_a \frac{L_a}{2}\right)\right]}{k_a^2-k_m^2} \right\}^{-2}$$

$$C_{x,mn} = L_{x,mn}^{-1}\frac{\varepsilon_{ra}\,k_{mn}^2}{c^2}, \qquad\qquad R_{x,mn} = L_{x,mn}\,k_{mn}\,c\,\delta_{eff}$$

(7.3)

and

$$L_{y,mn} = \frac{d_a}{16\varepsilon c^2 A_{mn}^2} \cdot \left\{ \frac{\text{sinc}\left(k_m \frac{W_a}{2}\right)\sin\left(\frac{m\pi}{2}\right)\cos\left(\frac{n\pi}{2}\right)}{\sin\left(k_a \frac{L_a}{2}\right)} \cdot \frac{k_a\left[\cos\left(k_n \frac{L_a}{2}\right)-\cos\left(k_a \frac{L_a}{2}\right)\right]}{k_a^2-k_n^2} \right\}^{-2}$$

$$C_{y,mn} = L_{y,mn}^{-1}\frac{\varepsilon_{ra}\,k_{mn}^2}{c^2}, \qquad\qquad R_{y,mn} = L_{y,mn}\,k_{mn}\,c\,\delta_{eff}$$

(7.4)

respectively. m or n is equal to 1 for each fundamental mode, as defined in Figure 2-9. A_{mn} is the magnitude of the Eigen function and ε_c is the cavity permittivity. L_a is the length and K_a is the wave number of each aperture. K_m and K_n are the wave number of each orthogonal mode of the patch. d_a, ε_{ra} and δ_{eff} are the thickness, permittivity and effective loss tangent of the antenna substrate.

151

The axial ratio of the antenna is determined by finding the orthogonal voltages V_{0x} and V_{0y} as seen in Figure 7-4 where

$$V_{0x} = V_0 \cdot \frac{\left(Y_{x,ant} + Y_{ap}\right)^{-1}}{\left(Y_{x,ant} + Y_{ap}\right)^{-1} + \left(Y_{y,ant} + Y_{ap}\right)^{-1}}$$ (7.5)

and

$$V_{0y} = V_0 \cdot \frac{\left(Y_{y,ant} + Y_{ap}\right)^{-1}}{\left(Y_{x,ant} + Y_{ap}\right)^{-1} + \left(Y_{y,ant} + Y_{ap}\right)^{-1}}$$ (7.6)

far field components E_x and E_y can then be expressed using

$$E_x = \frac{d_a k_0 e^{-jk_0 r}}{2\pi\omega\varepsilon r} \cdot V_{0x} \cdot \sum A_{m0} B_{y,m0}$$ (7.7)

and

$$E_y = \frac{d_a k_0 e^{-jk_0 r}}{2\pi\omega\varepsilon r} \cdot V_{0y} \cdot \sum A_{0n} B_{x,0n}$$ (7.8)

The mode coefficients $B_{x,mn}$ and $B_{y,mn}$ are defined in [20] and r is the distance between the magnetic current and the observation point.

7.6 Design of cross slot aperture coupled patch antenna

Bandwidth increases with antenna substrate thickness [142]. Antenna substrate thickness is limited when probe or microstrip line feeding methods are adopted as the impedance locus of the element becomes increasingly inductive [143]. Also spurious radiation from the feed line at bends and other discontinuities is unacceptably high for substrates thicker than a few hundredths of a wavelength. Aperture coupling can be used in response to these problems as the radiating patch and feed line are fabricated on separate substrates, allowing a think antenna and thin feed substrate.

Bandwidth decreases with an increase in dielectric constant, as the element size decreases raising the Q of the resonator. Using thick substrates with high dielectric constants increases surface wave generation and may lead to spurious radiation and radiation pattern degradation. Therefore a thick antenna substrate with a low dielectric constant is preferred for good bandwidth. Therefore a thick air substrate for the antenna was used with a height of 2.4 mm. Air has a low permittivity ε_r of 1 and does not suffer from the traditional problems related to thick antenna substrates, namely greater weight and increased cost. An additional benefit of using a low permittivity substrate is the resulting increase in nearly square patch size translates directly to a relaxation in manufacturing tolerances.

For the feed line and matching stub a much thinner low loss substrate with a higher permittivity of 2.33 and a height of 0.79 mm.

The following design parameters were generated using the adapted cavity model, as seen in Figure 7-5.
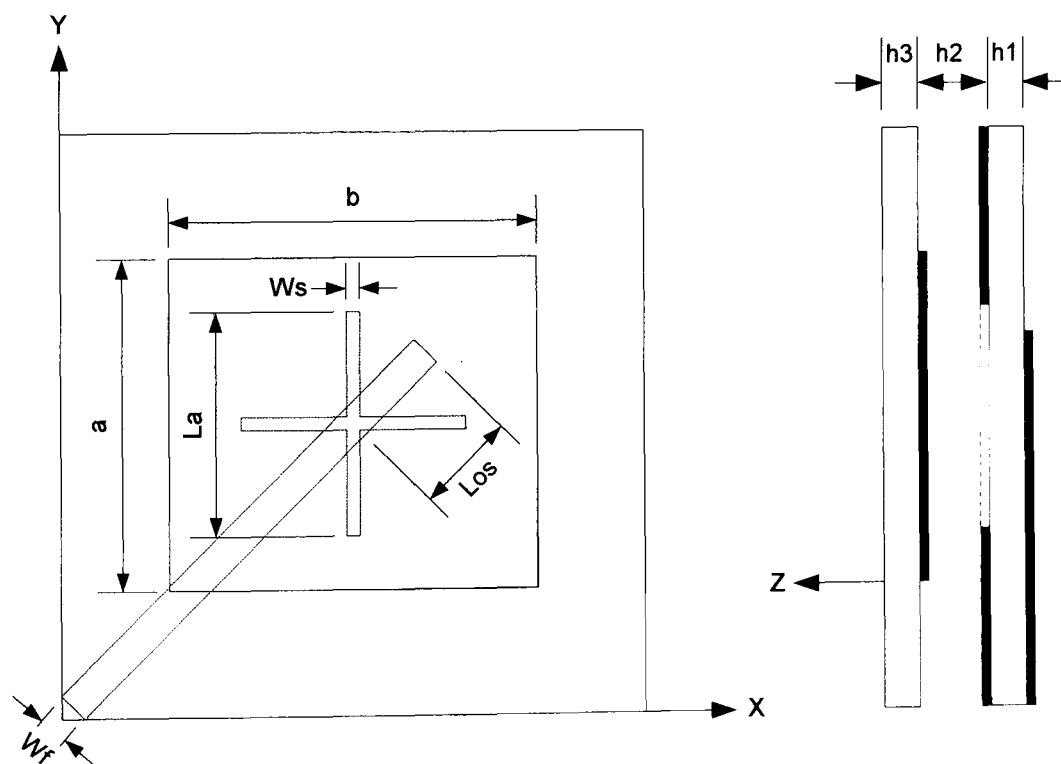
Figure 7-5: Radiating element design parameters a = 15.3, b = 17.1, La = 12.5, Ws = 1, Los = 4.8, Wf = 0.5, h1 = 0.79, h2 = 2.6, h3 = 0.8 (all dimensions in mm).

The design of this antenna differs from the structure presented in [136] and [20]. This structure operates at a higher frequency (5.8GHz not 2.4GHz) and uses a lower permittivity antenna substrate ($\varepsilon_r = 1$ not 2.33). The width of the single feed line has also been reduced as this has been shown to increase coupling through the aperture [131]. The resulting mismatch at the antenna feed point is removed using a quarter wave transformer.

7.7 Wideband array

As with traditional patch antenna arrays, aperture coupled elements can be used in arrays fed by both corporate [144,145] and serial [146] feed networks and offer the following advantages. There is more room for the feed network as it is fabricated on a separate substrate to the radiating elements. Furthermore, the problem of spurious feed radiation contribution to the main beam is eliminated by the ground plane that isolates the feed from the radiating elements. There is however a higher level of back radiation from the coupling apertures. This unwanted radiation can be shielded by another ground plane below the aperture [147], or by placing a patch antenna behind the aperture as a reflector that is intentionally operated well above its first resonance [131].

In the following section the cross aperture coupled patch antenna is used as a radiating element in a four element series fed sequentially rotated array.

7.7.1 Array layout

The configuration of the antenna array is shown in Figure 7-6.
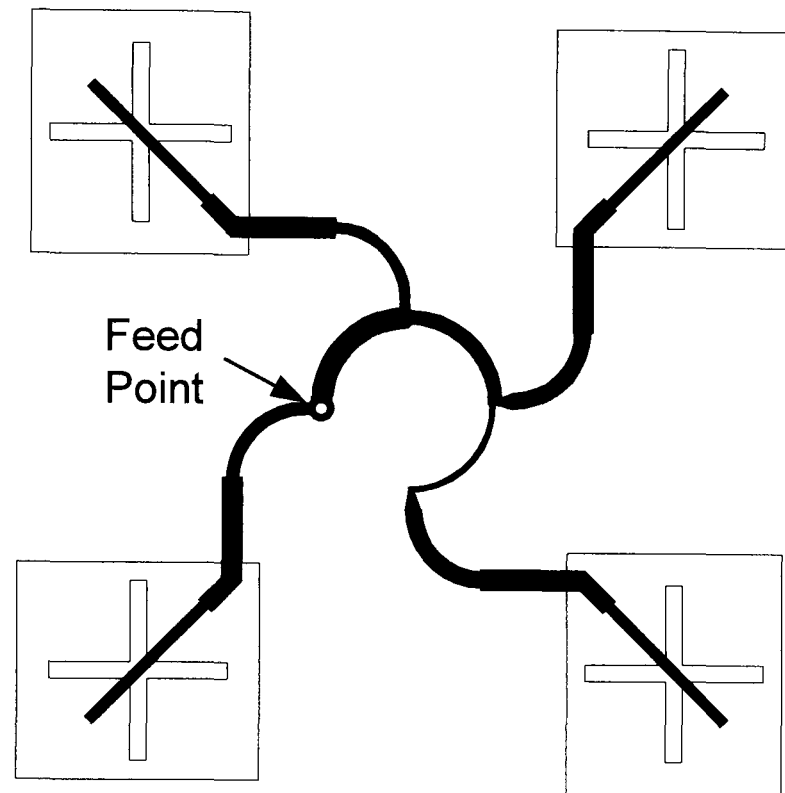
Figure 7-6: Configuration of aperture coupled patch array for LHCP.

Each cross aperture coupled radiating element is sequentially rotated by 90 degrees with respect to each element's immediate neighbor at a patch spacing of 0.74λ. The series feed compensates for this physical rotation by shifting the phase of each element's excitation by 90 degrees while distributing the power equally to each element and maintaining an input impedance of 50Ω at the feed point at the design frequency. As the input impedance to each radiating element is 50Ω, the feed is constructed using the design parameters presented in chapter 5. Radiating element design parameters and layer spacing are as defined in the previous section.

7.8 Fabrication

The feed network was fabricated using 0.79 mm 1/2oz RT 5870 Duroid ($\varepsilon_r = 2.33$). The nearly square patches were etched onto a standard 0.8 mm 1/2oz FR4 PCB radome. Using M2 nylon bolts, the radome is supported 2.4 mm above the apertures which are etched into the ground plane of the feed substrate.

7.9 Practical Results

The integrity of this structure and the validity of this design was confirmed using full wave simulation [117] and practical measurement.

7.9.1 Frequency performance

Results were obtained over a frequency range of 4.5GHz – 7.5GHz using both full wave simulation and practical measurement. Measurements of input impedance were made using an Anritsu 37347C vector network analyser confirming a VSWR 2:1 bandwidth of at least 22.8% from 5.28 to 6.6GHz as seen in Figure 7-7 (a). Array input impedance bandwidth can could be increased further using an aperture closer to resonance [131] however this leads to more unwanted back radiation.

Measurement of boresight axial ratio confirms LHCP with a 3 dB axial ratio bandwidth of 17.5% between 5.44GHz and 6.45GHz as seen in Figure 7-7 (b).

Frequency (GHz)
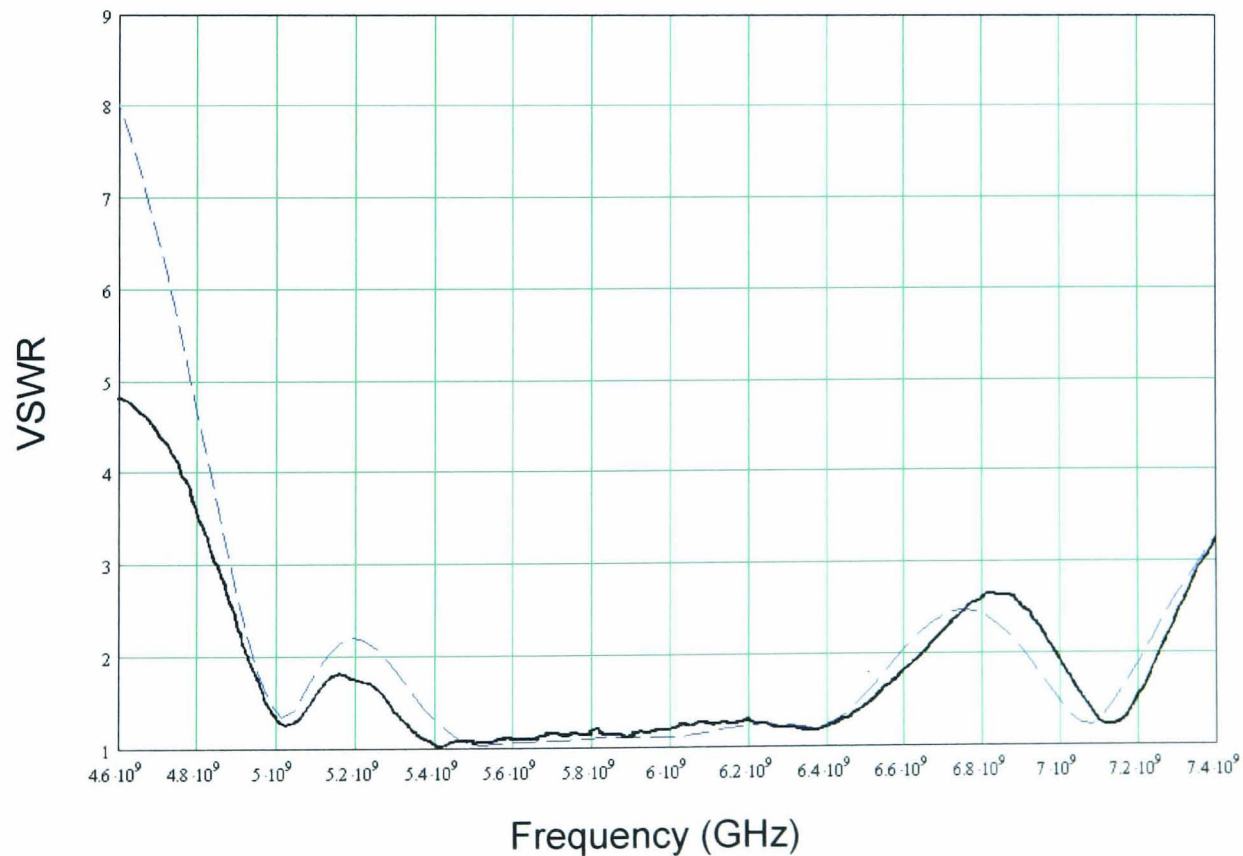
(a)
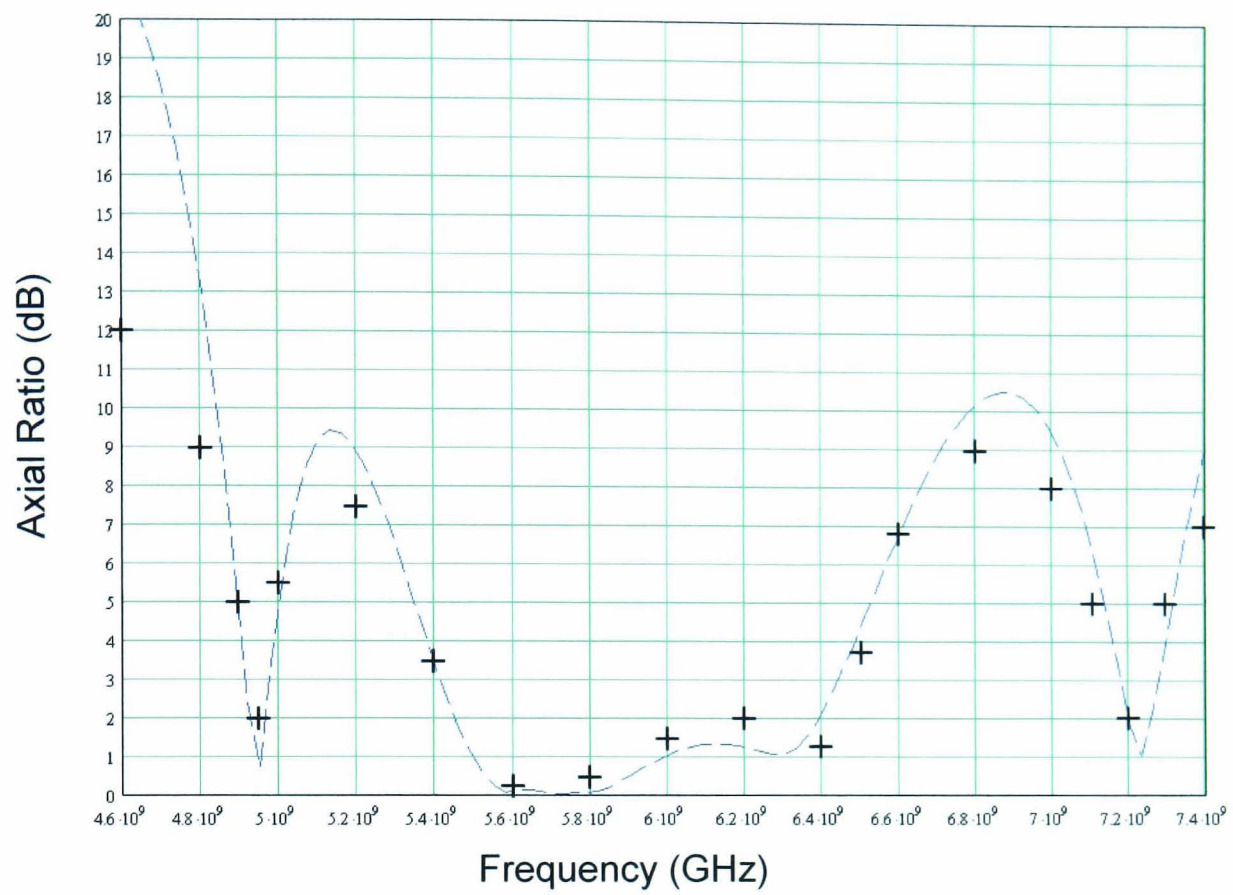
(b)

— — — — — —   Full wave simulation

   +   Measured

Figure 7-7: (a) Input impedance (b) Boresight axial ratio.

7.9.2 Radiation pattern

The radiation pattern of the array was determined within the anechoic chamber, using the methods and equipment described in Appendix C.

The radiation pattern at 5.8GHz can be seen in Figure 7-8, the gain of the main lobe has been measured at 14.25 dBi with a 3 dB beam width of 30°. There is 14.5 dB difference between the main beam and side lobes seen at +/- 60° with nulls at 42° from boresight.
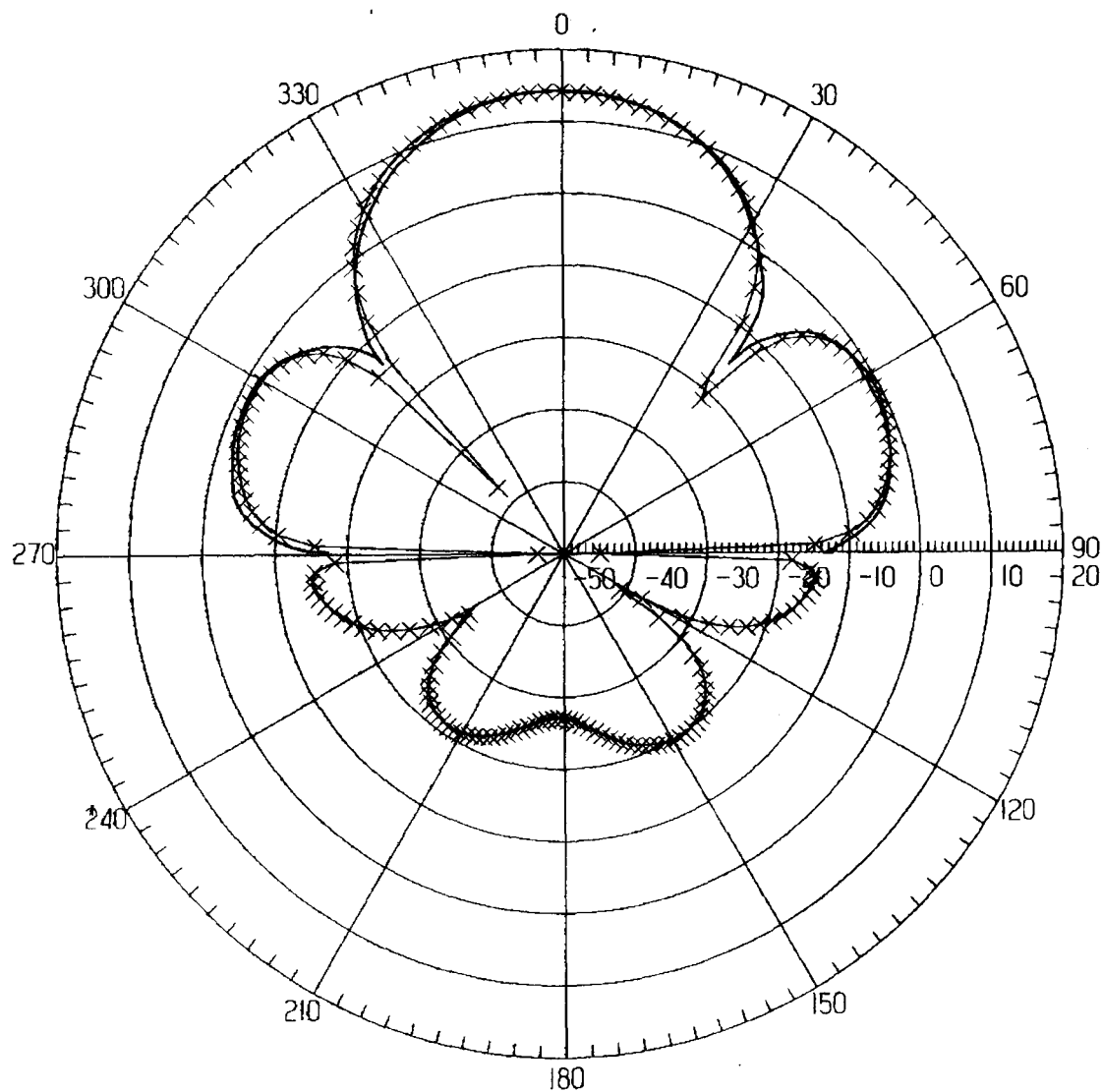
Figure 7-8: Radiation pattern of wideband array at 5.8 GHz (gain in dBi against θ where $\phi = 0$).

Conclusion

A single wide band radiating element suitable for use in the OBU of a traffic management system has been presented. As a consequence of utilising both aperture coupling and a single feed arrangement, the requirement for space is reduced considerably as a single fed antenna does not require an external polariser. The use of an antenna substrate with a low permittivity increases the difference between the dimension of each orthogonal mode on the nearly square patch relaxing manufacturing tolerances. The use of air allows the patch to be supported using the OBU's plastic enclosure as a radome, hence fabrication complexity is also reduced. The relaxing of fabrication tolerances and reduction of fabrication complexity translates to a reduction in manufacturing costs; cost being an important consideration if large quantities of OBU's are required in large scale motorway tolling applications. The result is a compact structure that is less expensive to produce with a significant improvement in frequency bandwidth.

A new wide-band sequentially rotated 2x2 antenna array with a series feed and cross aperture coupled radiating elements has also been presented. Using the single feed aperture coupled radiating elements within an array excited by the series feed network leads to a particularly compact array design. This maximises the space available when incorporating microwave circuitry on the low loss feed substrate.

The performance of the array has been confirmed by full wave simulation and experimental measurement verifying a VSWR 2:1 bandwidth of at least 22.8% and 3 dB axial ratio bandwidth of 17.5%, a significant improvement over the monolithic four element array presented in chapter 4. Due to the increased resonant bandwidth of each radiating element, array VSWR 2:1 is now more comparable to 3 dB axial ratio bandwidth.

CHAPTER 8

CONCLUSIONS AND FURTHER WORK

8.1 Summary of research

A single layer dual feed circularly polarised microstrip patch antenna was successfully optimised for use within a series fed sequentially rotated array. Using a genetic algorithm and a complex impedance matching design approach it was possible to increase the input impedance at the dual feed point from 33 to 50 ohms; this results in a reduction of track width within the array's feed network. Step discontinuities between the dual feed sections were removed, reducing spurious feed radiation and internal reflections within the dual feed network away from design frequency.

A series feed was used in two, three and four element sequentially rotated arrays. This feed geometry is particularly compact allowing the use of the optimised dual feed radiating elements. The performance of the three arrays with series and corporate feeding systems was evaluated. The performance of the two element arrays is comparable when either feeding system is adopted as, due the excitation phase delay, both feed network geometries are equivalent. The series fed three element array has a wider VSWR 2:1 bandwidth when compared to the same array using a corporate feed, although the pass-band is not symmetrical around the design frequency. The corporate fed three element array has the widest 3 dB axial ratio bandwidth of the monolithic arrays considered here.

The four element series fed array demonstrates a considerable increase in VSWR 2:1 bandwidth when compared to the four element corporate fed array, although the 3 dB axial ratio bandwidth is not as wide band with either feed. The benefit in VSWR bandwidth is due to a favorable relationship between internal reflections within the series feed network; the trade off being increased complexity of series feed design. As a consequence, an adaptation of simulated annealing was developed to generate the values of the series feed sections for which no closed form expression exists. Using this technique it was also possible to minimise the width of the tracks in the series

feed network. An accelerated cooling schedule within the algorithm resulted in less thorough coverage of the solution space in exchange for a reduction in run time. This lack of coverage is justified, as sensitive solutions translate directly to tight manufacturing tolerances.

The frequency bandwidth of the four element array with traditional dual feed radiating elements was shown to be heavily dependant upon the radiating element's dual feed length. However, array VSWR bandwidth did not exceed that of the same array containing the optimised dual feed radiating elements.

The performance of all three monolithic series fed arrays using single feed nearly square radiating elements have less bandwidth performance than the same arrays using the optimised dual feed radiating elements.

The ideal choice between series or corporate fed arrays is ultimately dependant upon the choice of radiating elements, the patch spacing, the real estate availability within the array, the bandwidth and the gain requirements of a specific application.

The gain and radiation pattern characteristics of the four element 2x2 array satisfy the range and communication zone requirements of a vehicle access control application, whereas the characteristics of a sixteen element 4x4 array are required to satisfy the requirements of a motorway tolling application. A 4x4 antenna array was constructed from sequentially rotated 2x2 arrays, fed with the same series feed. This array demonstrated comparable VSWR 2:1 and 3 dB bandwidth; which is twice as wide as the same array using a corporate feed. Side lobe reduction was demonstrated by altering the power division within the series feed. The input impedance and axial ratio performance of these modified arrays is comparable to the corporate fed array as the desirable relationship between internal reflections within the series feed network no longer remained.

A single feed cross aperture coupled patch antenna results in a compact wide band radiating element ideal for use within the OBU of a traffic management system. Using air for the antenna substrate leads to both a relaxation in the nearly square radiating patch's dimensional tolerance and allows the use of the OBU's plastic case to support

161

the antenna. The result is a reduction in fabrication precision and complexity which leads to a reduction in manufacturing cost. An adaptation of the cavity model proved a useful design tool for the development of this antenna, reducing time consuming trial and error attempts when altering the many interrelated design parameters.

Using the cross aperture coupled antenna as a broadband radiating element within the four element series fed array resulted in an improvement of both input impedance and axial ratio bandwidth. Using the cross aperture coupled radiating elements increased the VSWR 2:1 bandwidth by a factor of 2.5 and the 3 dB axial ratio bandwidth by a factor of 6 compared with the monolithic four element array presented in Chapter 5. This four element array's VSWR 2:1 bandwidth is now comparable to its 3 dB axial ratio bandwidth, this is due to the increased resonant bandwidth of the radiating elements. The use of a compact feeding geometry maximises available real estate on the low loss feed substrate for the inclusion of microwave circuitry.

A good measure of the success of this research is that as a consequence of a joint venture between the University of Northumbria, Resero Technology Systems Ltd, a local SME, and Racal, a large traffic management system has been implemented at Bluewater®, a large shopping centre located south of the Dartford Tunnel. At the time of installation, this was the largest 5.8Ghz traffic management system in operation within the United Kingdom [148].

8.2 Suggestions for further work

8.2.1 Cross polarised radiating elements

The input impedance and axial ratio bandwidth of a single circularly polarised radiating elements can be increase by intentionally cross polarising the radiating element; the trade off is in performance at design frequency. As a consequence this radiating element may be of little benefit in isolation. However, due to the canceling effect shown in arrays of sequentially rotated radiating elements, good performance at design frequency can be achieved while increasing array bandwidth further. Using sequential rotation to allow the use of cross polarised radiating elements has been demonstrated in the past. In [149] travelling wave elements are sequentially rotated to form an array compensating for a lack of boresight from the single elements. In [49]

cross polarised notched disc radiators are used in a sequentially rotated array to slacken manufacturing tolerances. Indeed, in [87] linear polarised radiating elements are sequentially rotated to form a circularly polarised array. However, to the author's knowledge, intentional cross polarisation has never been used directly as a bandwidth enhancing technique.

In a LHCP array composed of dual feed radiating elements, an increase in array performance is seen when the dimension of the patch mode fed with the 90 degree phase delay is reduced with a corresponding increase in the dimension of the orthogonal mode. In a LHCP array of single feed nearly square patches the benefit is seen when the patch is made 'even less' square. Reversing the dimensional variation has the opposite effect reducing the individual radiating elements frequency bandwidth and that of arrays composed from these elements. In [49] elliptical polarisation was achieved by decreasing the depth of the notch in a notched disc, however the significance of the cross polarised being in this direction (i.e. increasing the depth of the notch) is not addressed.

Using full wave simulation, a preliminary investigation into using this technique been conducted. In Table 9-1 a comparison is made between the performance of 2x2 arrays using perfectly circularly polarised radiating elements and the performance of the same arrays where the radiating elements are elliptically polarised.

		-/+ 3 mill	Original	+/- 3 mill	+/- 6 mill
Dual feed	VSWR 2:1	8.5%	8.9%	9.1%	9.46%
	-3 dB AR	2%	3.2%	4.1%	4.8%
Single feed	VSWR 2:1	9.4%	9.68%	10.03%	10.5%
	-3 dB AR	2.4%	3.325%	4.25%	5%

Table 9-1: Four element array performance containing radiating elements with varying degrees of cross polarisation (patch Q = 47).

This increase in frequency bandwidth performance has been shown to be at the expense of main lobe gain [91], where the power is redistributed to cross polarisation

in the diagonal plane. As a consequence, the benefit of using this technique will depend on the specific bandwidth and gain requirements of an application.

References

1 HILLS, P.J. and BLYTHE, P.T.:'The Future for Road User Charging in the UK'. Ingenia, Journal of the Royal Academy of Engineering, No. 14, December, 2002.

2 WALKER, J.:'Advances in mobile information systems' Artech House, London. 1999

3 BLYTHE, P.T.:'Road User Charging: Technology and Options'. Proc. IEE Seminar on Road User Charging, London, UK, March. 2003

4 BLYTHE, P.T. A review of road pricing and smartcard research in Europe. Proc. Special Executive Session on Asia-Europe Strategic Research, 10th World Congress on Intelligent Transport Systems and Services, Madrid, November. 2003.

5 VAN EWIJK, L. J. and VAN DER SPEK, G. A.:'Simulation of reflection effects for a dedicated short range microwave communication system'. IEE Proc.-Commun., Vol. 147, No. 3, June 2000. pp. 195-199.

6 KOSSEL, M.:'An active tagging system using circular polarisation modulation'. IEEE Trans. On Microwave theory and techniques. 47(12) December 1999. pp.2242-2248.

7 YOON, J., KWAK, K.:'Fabrication and measurement of a microstrip-array antenna for the electronic toll collection system (ETCS)'. Microwave-and-Optical-Technology-Letters, 36(2). Jan. 2003. pp. 77-79

8 KURAMOTO, A., KITANO, S.:'Beam forming antenna for electronic toll collection system'. NEC-Technical-Journal. 54(7), July 2001. pp. 15-18

9 CHAN, T.K, "Development of a two-way microwave communication system for traffic applications". Ph.D. Thesis, UNN, June 1994.

10 VALASIT, T, "Modelling and Application of a cross-aperture coupled single feed circularly polarised patch antenna", Ph.D. Thesis, UNN, Feb 1997.

11 TESHIROGI, T., TANAKA, M., and CHUJO, W.:'Wideband circularly polarised array antenna with sequential rotations and phase shifts of elements'. Int. Symp. on Ant. and Prop., ISAP 85, Tokyo. Pp. 117-120, 1985.

12 HALL, P. S., DAHELE, J. S., and JAMES, J. R.:'Design principles of sequentially fed, wide bandwidth, circularly polarised microstrip antennas'. IEE Proc. Vol. 136, Pt. H, No. 5 October 1989. pp. 381-389.

13 BHARTIA, P., RAO, K. V. S., and TOMAR, R. S.:'Millimeter-wave microstrip and printed circuit antennas'. Artech House, Canton, MA, 1991.

14 HUANG, C.Y, "Designs for a aperture coupled compact circularly polarised microstrip antenna", IEE Proc, Microwave propagation, Vol. 146, No 1, Feb 1999.

15 DUFFY, S.M. POZAR, D.M, "Circularly polarised aperture coupled microstrip antenna", electronic letters, May, 1995.

16 SULLIVAN, P.L, SCHAUBERT D.H, "Analysis of an aperture coupled microstrip antenna", IEEE Trans, Antennas and Propagation, Vol. 34, August, 1986.

17 ALJIBOURI B., LIM E.G., EVANS H, and SAMBELL A. `Multiobjective genetic algorithm approach for a dual feed circular polarised patch antenna design', Electron. Lett. vol 36, No 12, pp.1005-1006, 2000.

18 EVANS H., GALE P., ALJIBOURI B., LIM E.G., KOROLKEIWICZ E and SAMBELL A.:'Application of SA to design of serial feed sequentially rotated 2x2 antenna array', Electron. Lett. 2000, vol 36, No 24, pp.1987-1988, November 2000.

19 EVANS H., GALE, P., and SAMBELL, A.:'Performance of a 4x4 Sequentially Rotated Patch Antenna Array Using a Series Feed.', Electron. Lett, vol 39, No 6, pp.493 – 494, March 2003.

20 ALJIBOURI, B., EVANS H., LIM E. G., KOROLKIEWICZ, E.K., and VLASITS, T.:'Cavity Model of circularly polarised cross-aperture-coupled microstrip antenna', IEE Proc. Antennas Propag. vol 148, No 3, pp.147-152, June 2001.

21 EVANS H., and SAMBELL, A.:'Wideband 2x2 sequentially rotated patch antenna array with a series feed'. Microwave and Optic Technology Lett. vol 40, No 4, pp.293 – 294, February 2004

22 DESCHAMPS, G.A.:'Microsrtip Microwave Antennas'. 3rd USAF Symp. On antennas, 1953.

23 GUTTON, H., BAISSINOT, G.:'Flat aerial for ultra high frequencies '. French Patent No. 703 113, 1955.

24 MUNSON, R. E.:'Conformal Microstrip Antennas and Phased Arrays', IEEE Trans. Antennas Propagat., vol. 22, pp. 74-78, 1974.

25 CARVER, K. R. and MINK J. W.,:' Microstrip antenna technology', IEEE Trans. Antennas Propagat., vol. 29, no. 1, pp. 2-24, Jan. 1981.

26 JAMES, J.R. and HALL, P.S.:'Handbook of Microstrip Antennas'. London UK, Peter Peregrinus, 1989

27 LEE, K. F.:'Microstrip Patch Antennas – Basic Properties and Some Recent Advances'. Journal of Atmospheric and Terrestrial Physics, Vol.51, 1989.

28 BAHL, I. J., BHARTIA, P.:" Microstrip Antennas ", Artech House, 1982.

29 POZAR, D.M.:'Microstrip Antennas'. Proc IEEE, Vol. 80, No. 1, pp 79-81, Jan 1992.

30 SCHAUBERT, D. H., POZAR, D. M., ADRIAN, A.:'Effect of microstrip antenna substrate thickness and permittivity: 'Comparison of theories and experiment'. IEEE Trans. Antennas Propagat., vol. 37, pp. 677-682, June 1989.

31 POZAR, D. M.:'A microstrip antenna aperture coupled to a microstrip line'. Electronic Letters., Vol 21, pp.49-50, Jan. 1995.

32 OLTMAN, H. G., HUEBNER, D. A.:'Electromagneticaly coupled microstrip dipoles', IEEE Trans. Antennas Propagat., vol. AP-29, pp.151-157, Jan. 1981.

33 ZHANG, Q., FUKUOKA, Y. and ITOH, T.:'Analysis of a suspended patch antenna excited by an electromagnetically coupled inverted microstrip feed'. IEEE Trans. Antennas Propagat., vol. AP-33, pp.895-899, Jan. 1985.

34 POZAR, D. M. and KAUFMAN, B.:'Increasing the bandwidth of a microstrip antenna by proximity coupling'. Electronic Letters., Vol 23, pp.368-369, Apr. 1987.

35 POZAR, D., VODA, S. M.:'A rigorous analysis of a microstripline fed patch antenna'. IEEE Trans. Antennas Propagat., vol. AP-35, pp.1343-1349, Dev. 1988.

36 PARRIKAR, R. P., GUPTA, K. C.:'Multiport network model for CAD of electromagnetically coupled microstrip patch antennas'. IEEE Trans. Antennas Propagat., vol. 46, No. 4, pp.475-483, April. 1998.

37 BELENTEPE, B.:'Modelling and Design of Electromagnetically Coupled Microstrip-patch antenna and antenna arrays'. IEEE Ant Prop Mag, Vol. 37, No 1, Feb 1995.

38 PAREKH, S. V.:'Simple Formula for circular-Polarisation Axial Ratio Calculations'. IEEE Antennas Propagat. Magazine, vol. 33, pp.30-32, Feb. 1991.

39 JAMES, J.R., HALL, P.S. and WOOD, C.:'Microstrip Antenna Theory and Design'. IEE, Peter Peregrinus, pp. 194-224, 1981

40 BRIAN, D. J., MARK, J. R.:'The disc antenna – a possible L Band Aircraft Antenna '. IEE Conference publication 95. pp. 14-16, 1973

41 HOWELL, J.Q.'Microstrip antennas'. IEEE Trans. Antennas Propagat., vol. AP-23, pp.90-93, 1975.

42 MILLIGAN, T. A.:'Modern Antenna Design'. Mc Graw-Hill book Co, 1985.

43 SANFORD, G. G. and MUNSON, R. E.:'conformal VHF antenna for the Apollo-Soyuz test project'. IEE Int. Conf. On Antennas for Aircraft and Spacecraft, London, pp. 130-135. (Munson told Kerr about NS in 1975).

44 CRAVER, K. R., COFFEY, E. L.:'Theoretical investigation of the microstrip antenna'. Physic. And Sci. Lab., New Mexico State Univ., Las Cruces, Tech. Rep. PT-00929, Jan. 23, 1979.

45 SHARMA, P. C., GUPTA, K. C.:'Analysis and optimised design of single feed circularly polarised microstrip antennas'. IEEE Trans. AP-31 (6), 1983.

46 KERR, J. L.:'Microstrip polarization techniques'. in Proc. 1978 Antenna Applications Symp., Allerton Park, IL, Sept. 1978.

47 'IEEE Standard Definitions of Terms for Antennas'. IEEE Trans. Antennas Propagat., vol. AP-17, pp. 222, 1969.

48 'Advances in Microstrip and printed antennas' John Wiley & Sons, Inc. 1997

49 KRAFT, U. R.:'An experimental study of 2x2 sequential-Rotation arrays with circularly polarized microstrip radiators'. IEEE Trans. Antennas and Propagation, Vol. 45, No. 10, pp. 1459-1466, October 1997.

50 BALANIS, C. A.:'Antenna Theory analysis and design'. John Whitley & Sons, New York, 1997, pp. 740.

51 POZAR, D. M.:'Microwave Engineering second edition'. John Wiley & Sons, 1998.

52 BALANIS, C. A.:'Advanced Engineering Electromagnetics'. John Whitley & Sons, New York, 1989.

53 KUMAR, G., and RAY, K.P.'Broadband Microstrip Antennas', Artech House, 2003, pp. 311.

54 HALL, P. S.:'Application of sequential feeding to wide bandwidth, circular polarised microstrip patch antenna arrays'. IEE Proc. Vol. 136, Pt. H, No. 5 October 1989. pp. 393

55 COLLIER, R. J., and WHITE, P. D.:'Surface waves in microstrip circuits'. Proc. 6th European microwave conference, pp.632-636, 1976.

56 MUNSON, R. E.:'Conformal Microstrip Antennas and Phased Arrays', IEEE Trans. Antennas Propagat., vol. 22, pp. 74-78, 1974.

57 DERNEYD, A. G.:'Linearly polarized microstrip antennas'. IEEE Trans. Antennas Propagat., Vol 23, 1975.

58 CARVER, K. R., and MINK, J. W.:'Microstrip antenna technology'. IEEE trans. Antennas Propag. Vol AP-29, pp2-24, Jan 1981.

59 PUES, H., VAN de CAPELLE, A.:'Accurate transmission line model for the rectangular microstrip antenna '. Proc. Inst. Elect. Eng., vol. 131, pt H. pp. 334-340, 1984.

60 VAN de CAPELL, A.:'Transmision line model for rectangular microstrip antennas'. Handbook of microstrip antennas, chapter 10, Peter Peregrinus Ltd, 1989

61 DEMUYNCK, F., VAN de CAPELL, A.:'Higher order modes in micristrip antenna design via the transmission line model'. Electronic Letters., Vol 28, No 18 pp.1732-1734, Aug. 1992.

62 RICHARDS, W. F., LO, Y. T., and HARRISON, D.:'An improved theory for microstrip antennas and applications'. IEEE Trans. Antennas Propagat., vol AP-29, pp. 38-46, Jan 1981.

63 CARVER, K. R., and MINK, J. W.:'Microstrip antenna technology'. IEEE trans. Antennas Propag. Vol AP-29, pp2-24, Jan 1981.

64 CHATERJEE, R.:'Elements of Microwave Engineering '. Horward, 1985.

65 LO, Y. T., SOLOMON, D and RICHARDS, W. F.:'Theory and experiment on microstrip antennas'. IEEE Transactions antennas and propagation, Vol. 27, pp. 137-145, 1979.

66 GUPTA, K. C., BENALLA, A.:'Multiport network modelling approach for CAD of microstrip patches'. Electromagnetics, Vol. 9, pt. 4, 1989.

67 HALL, P. S.:'Application of sequential feeding to wide bandwidth, circular polarised microstrip patch antenna arrays'. IEE Proc. Vol. 136, Pt. H, No. 5 October 1989. pp. 390-398.

68 HUANG, J and POZAR, D.M.:'Advances in microstrip and printed antennas', John Wiley & Son, 1997, pp. 123.

69 ENTSCHLADEN, H., NAGEL, U.:'Microstrip patch antenna array'. Electronic Letters., Vol 20, pp.931-933, Oct. 1984.

70 MILLER, P. A., MacKICHAN, J. C., STALKER, M. R., DAHELE, J. S.:'A Wide bandwidth low side lobe low profile microstrip array antenna for communication applications'. Proc. ISAP, pp.525-528, 1989.

71 HALL, P., S, HALL, C., M.:'Coplanar corperate feed effects in microstrip patch array design'. IEE Proc., Vol 135, Pt. H, No 3, pp.180-186, June 1988.

72 DERNEYD, A. G.:'Linear microstrip array antennas'. IEEE Trans. Antennas Propagat., Vol AP-24, pp. 846-851, 1976.

73 METZLER, T.:'Microstrip Series Arrays'. IEEE Trans. Antennas Propagat., Vol AP-29, pp. 174-178, 1981.

74 HAUNG, J.:'A Parallell-series-fed microstrip array with high efficiency and low corss-polarisation'. Microwave Opt. Technol. Lett., Vol. 5, pp 230-233, 1992.

75 JAMES, J. R., HALL, P.S., WOOD, C.:'Microstrip antenna: theory and design'. Peter Peregrinus, London 1981.

76 HUANG, J.:'A Parallel-series-Fed Microstrip Array with High Efficiency and Low Cross-Polarization'. Microwave and Optical Tech. Lett., vol. 5, no 5, pp. 230-233, May 1992.

77 HALL, P.S.:'Rampart microstrip antenna line'. European Parent Application 79301340.0, 1979

78 HALL , P.S.:'Microstrip linear array with polarisation control'. IEE Proc., vol. 103H, pp. 215-224, 1983.

79 HENRIKSSON, J.,MARKUS, K., and TIURI, M.:'A circularly polarised travelling-wave chain antenna'. Proc 9th European Microwave Conference, Brighton, pp. 174-178, 1979.

80 MAKIMOTO, T., and NISHIMURA, S.:'Circular polarised microstrip line antenna'. US Patient 4 398 199, 1983.

81 NISHIMURA, S., SUGIO, Y., and MAKIMOTO, T.:'Crank-type circular polarised microstrip line antenna '. IEEE AP-S Int. Symposium Antennas and Propagat. Digest, pp.215-224, 1983.

82 LEWIN, L.:'Radiation from discontinuities in microstrip-line'. IEE Proc., Vol 107C, pp.163-170, 1960.

83 COLLIER, M.:'Microstrip antenna array for 12GHz TV'. Microwave J., vol. 20. no. 9, pp 67-71, Sept. 1977.

84 JAMES, J. R., HALL, P. S., and WOOD, C.:'Microstrip Antenna Theory and Design'. Stevenage England: Peter Pengrinus, pp 186-189, 1981.

85 BHARTIA, P., RAO, K. V. S., and TOMAR, R. S.:'Millimeter-wave microstrip and printed circuit antennas'. Artech House, Canton, MA, 1991.

86 HANEISHI, M., YOSHIDA, S., and GOTO, N.:'A Broadband microstrip array composed of single-feed type circularly polarised microstrip antennas'. In Int Symp. Dig. Antennas Propagat. Soc., pp. 160-163, May 1982.

87 HAUNG, J.:'Technique for an array to generate circular polarisation with linearly polarised elements'. IEEE Transactions on antennas and propagation, Vol AP-34, No 9, pp. 1113-1124, Sept 1986.

88 OHMANI, K., and MURATA, T.:'Planar array antenna for L band satellite communications'. SBMO Int. Microwave Symp. Proc., Rio de Janeiro, July 1987, pp, 115-120.

89 ALEXANDER, M. J., TRUMPESS, C. J., GRIFFIN, J. M., NEWTON, M. L., and ROEDERER, A.:'A microstrip patch array for L band satellite communications'. Proc. IEE Conf. on Ant. and Prop. ICAP 87, York, UK, March 1987, pp 285-288.

90 HALL, P. S.:'Feed radiation effects in sequentially rotated microstrip patch arrays'. Electronic letters, Vol. 23, No 17, pp. 877-878, Aug 1987.

91 HALL, P. S.:'Gain of circularly polarised arrays composed of linearly polarised elements'. Electronic letters, Vol. 25, No 2, pp. 124-125, Jan 1989.

92 HALL, P. S., and SMITH, M. S.:'Sequentially rotated arrays with reduced sidelobe levels'. Electronic letters, Vol. 28, No 18, pp. 1761-1762, Aug 1992.

93 HALL, P. S., and SMITH, M. S.:'Sequentially rotated arrays with reduced sidelobe levels'. IEE Proc. Microw. Antennas Propag. Vol. 141, No. 4, August 1994. pp.321-325.

94 KAN, H. K., and WATERHOUSE, R. B.:'A small CP-Printed antenna using 120° Sequential rotation'. IEEE Trans. Antennas and Propagation, Vol. 50, No. 3, pp. 398-399, March 2002.

95 OWENS, R. P., and SMITH, A. C.:'Low-profile dual band, dual polarised array antenna module'. Electronic letters, Vol. 26, No 18, pp. 1433-1434, Aug 1990.

96 SMITH, M. S., and HALL, P. S.:'Analysis of radiation pattern effects in sequentially rotated arrays'. IEE Proc. Microw. Antennas Propag. Vol. 141, No. 4, August 1994. pp. 313-320

97 MORROW, I., and JAMES, J. R.:'Sequentialy rotated large bandwidth circularly polarised printed antennas'. Electronic letters, Vol. 31, No 24, pp. 2062-2064, Nov 23, 1995.

98 YOON, J., and KWAK, K.:'Fabrication and Measurement of a microstrip array antenna for the electronic toll collection systems.' Microwave and optical technology letters, Vol. 36, No. 2, January 2003.

99 HAMMERSTAND, E. O.:'Equations for microstrip circuit design'. Proc. Fifth European Microwave Conf., pp. 268-272, September 1975.

100 YIP, P.:'High frequency circuit design and measurement'. Chapman and Hall, pp. 24, 1990.

101 HARRINGTON, R., F.:'Time-Harmonic Electromagnetic fields'. McGraw-Hill Book Co., pp. 183, 1961.

102 POZAR, D. M.:'Microwave engineering second edition'. John Wiley and Sons, Inc. pp.68 ,1998.

103 DAY, P.I.:'Transmision line transformation between arbitrary impedances using the smith chart', Electron. Lett., 1975, pp. 772-773.

104 SRINIVAS, N., and KALYANMOY, D. :' Mutiobjective optimization using nondominating sorting in genetic algorithms' Evolutionary Computation 1995 2(3), pp 221-248

105 LIM, B.W., KOROLKIEWICZ, E., and SCOTT., S.:'Optimised design of corner microstrip fed nearly square patch antenna for circular polarisation'. Electronic Letters, Vol 32, No 7 pp.610-612, March. 1996.

106 LIM, B.W., KOROLKIEWICZ, E., and SCOTT., S.:'Analysis of corner microstrip fed patch antenna'. Electronic Letters, Vol 31, No 9 pp.691-693, April. 1995.

107 HALL, P.S. and HALL C.M.:'Coplanar corporate feed effects on microstrip patch array design', IEE proc. H, 1988, **135**(3), pp.180-186

108 METROPOLIS N., ROSENBLUTH A. W., ROSENBLUTH M. N., TELLER A. H., TELLER E.:'Equation of state calculations by fast computing machines', J. Chem. Phys. 1953, **21**(6), pp.1087-1092.

109 PINCUS, M., A Monte Carlo Method for the Approximate Solution of Certain Types of Constrained Optimization Problems, Oper. Res. 18, 1225-1228, 1970.

110 KIRKPATRICK S., GELATT C. D. & VECCHI, M. P.:'Optimisation by Simulated annealing', 1983, Science, **220**, pp.671-680

111 ARES F., RENGARAJAN E., VILLANUEVA E., SKOCHINSKI E and MORENO E.:'Application of genetic algorithms and Simulated annealing techniques in optimising the aperture distributions of antenna array patterns', Electron. Lett. 1996, **32**(3), pp.148-149.

112 Electromagnetic Optimization by Genetic Algorithms Yahya Rahmat-Samii (Editor), Eric Michielssen (Editor) ISBN: 0-471-29545-0 July 1999

113 RODRIGUEZ, J. A., Ares, F., and E. MORENO, E.:'Linear Array Pattern Synthesis Optimizing Array Element Excitations Using the Simulated annealing Technique', Microwave and Optical Tech. Lett., Vol. 23, pp. 224-226, 1999.

114 REDVIK, J."Simulated annealing optimization applied to antenna arrays with failed elements", IEEE Antennas and propagation society international symposium. Digest. Vol. 1 11-16 july 1999 Orlado.

115 INGBER A.L.:'Very Fast Simulated Re-Annealing'. J Mathl. Comput. Modelling 1989, Vol 12, pp.967-973.

116 INGBER A.L.:'Simulated annealing: Practice versus theory', Mathl. Comput. Modelling 1993, **18**(11), pp.29-57.

117 Ansoft Ensemble® V6.1 - Method of Moments 2.5D EM field solver.

118 YOON, J., KWAK, K.:'Fabrication and measurement of a microstrip-array antenna for the electronic toll collection system (ETCS)', Microwave and Optical Technology letters. Vol 36, No 2, January 2003.

119 KURAMOTO, A., KITANO, S.:'Beam forming antenna for electronic toll collection system'. NEC technical journal, vol 54, No 7, pp. 15 - 18, July 2001.

120 LOPEZ, P., RODRIGUEZ, J. A., ARES, F., and MORENO.:'Low-sidelobe patterns from linear and planar arrays with uniform excitations except for phase of a small number of elements'. Electronic letters, Vol. 37, No 25, December 2001.

121 DAS, N. K., and POZAR, D. M.:'A class of enhanced electromagnetically coupled feed geometries for printed antenna applications'. IEEE Antennas and Propagation Symposium Digest, pp. 1100-1103, 1990.

122 POZAR, D. M., and TARGONSKI, S. D.:'Improved coupling for aperture coupled microstrip antennas'. Electronic letters, Vol. 27, No 13, pp. 1129-1131, June 1991.

123 HALL, R. C.:'Full-wave aperture coupled patch antenna'. Electronic letters, Vol. 29, No 24, pp. 2073-2074, Aug 1993.

124 ZURCHER, J. F.:'The SSFIP: a global concept for high performance broadband planar antennas'. Electronic letters, Vol. 24, pp. 1433-1435, Nov 1988.

125 TARGONSKI, S., POZAR, D. M.,:'Design of wideband circular polarised aperture coupled microstrip antennas'. IEEE trans. Antennas and Propagation, Vol. 41, pp. 214-220, Feb 1993.

126 CROQ, F., PAPIERNIK, A.:'Large bandwidth aperture coupled microstrip antenna'. Electronic letters, Vol. 26, pp. 1293-1294, Aug 1990.

127 CROQ, F and POZAR, D. M.:'Millimeter wave design of wide band aperture coupled stacked microstrip antennas', IEEE Trans. Antennas and Propagation, Vol. 39, pp. 1770-1776, Dec 1991.

128 EDIMO, M., RIGOLAND, P., TERRET, C.:'Wideband dual polarised aperture coupled stacked patch antenna array operating in C-band', Electronic letters, Vol. 30, pp. 1196-1197, July 1994.

129 ADRIAN, A., SCHAUBERT, D. H.:'Dual aperture-coupled microstrip antenna for dual or circular polarisation'. Electronic letters, Vol. 23, pp. 1226-1228, Nov 1987.

130 TSAO, C. H., HWANG, Y. M., KILLBURG, F., DIETRICH,'Aperture coupled patch antennas with wide bandwidth and dual polarisation capabilities'. IEEE Antennas and Propagation Symposium Digest, pp. 936-939, 1988.

131 TARGONSKI, S. D., POZAR, D. M.:'Design of wideband circular ploarised aperture coupled microstrip antennas'. IEEE trans. Antennas and Propagation, Vol. 41, pp. 214-220, Feb 1993.

132 EDIMO, M., SHARAIHA, A., TERRET, C.:'Optimised feeding of dual-polarized broadband aperture coupled printed antenna'. Electronic letters, Vol. 28, pp. 1785-1787, Nov 1992.

133 DUFFY, S. M., and POZAR, D. M.:'Circularly polarised aperture coupled microstrip antenna'. Electronic letters, Vol. 31, No. 16, pp. 1303- 1304, Aug. 1995.

134 AKSUN, M. I., CHUANG, S. L., LO, Y. T.:'Theory and experiment of electromagnetically excited microstrip antennas for circular polarisation operation'. IEEE Symposium on Antennas and Propagation digest, pp. 1142-1145, San Jose, 1989.

135 AKSUN, M. I., et al.:'On slot-coupled mircrostrip and their applications to CP operation – Theory and Experiment'. IEEE Transactions Antenna and Propagation, vol 83, pp. 1224 – 1230, 1990.

136 Valasits, T, Korolkiewicz E, "Performance of a cross-aperture coupled single feed circularly polarised patch antenna", electronics letters, Vol. 32, No. 7, march 1996.

137 POZAR, D. M.:'A reciprocity method of analysis for printed slot and slot–coupled microstrip antennas'. IEEE Transactions Antenna and Propagation, vol ap-34, No. 12, pp. 1439 – 1445, 1986.

138 HIMDI, M., DANIEL, J. P., and TERRET, C.:'Analysis of aperture-coupled microstrip antenna using cavity method'. Electronic letters, Vol 25, No 6, pp.391-392, 1989.

139 ITTIPIBOON, A., OOSTANDER, R., and ANTAR, Y. M. M.:'Modal expansion method of analysis for slot-coupled microstrip antenna'. Electronic letters, Vol 25, pp.1338-1340, Sept 1989.

140 HIMDI, M., LAFOND, O., LAINGNIER, S. and DANIEL, J. P.:'Expansion of cavity method to analyse aperture-coupled microstrip patch antenna with thick ground plane'. Electronic letters, Vol 34, No 16, pp.1534-1536, 1998.

141 GUPTA, K. C.:'Multiport network modeling approach for computer aided design of microstirp patches and arrays'. IEEE Antennas and Propagation Symposium Digest, pp. 786-789, 1987.

142 SCHAUBERT, D. H., POZAR, D. M., and ADRIAN. A.:'Effect of microstrip antenna substrate thickness and permitivity: Comparison of theories and experiment'. IEEE Transactions Antenna and Propagation, vol ap-37, pp. 677 – 682, June 1989.

143 CHANG, E., LONG, S. A., and RICHARDS, W. F.:'Experimental investigation of electricaly thick rectangular microstrop antennas'. IEEE Transactions Antenna and Propagation, vol ap-34, pp. 767-772, June 1986.

144 ZURCHER, J. F.:'The SSFIP: a global concept for high performance broadband planar antennas'. Electronic letters, Vol. 24, pp. 1433-1435, Nov 1988.

145 EDIMO, M., RIGOLAND, P., TERRET, C.:'Wideband dual polarised aperture coupled stacked patch antenna array operating in C-band', Electronic letters, Vol. 30, pp. 1196-1197, July 1994.

146 WU, C., WAND, J., FRALICH, R. and LITVA, J.:'Analysis of a serial-fed aperture coupled patch array antenna'. Microwave and Optical Technology letters, Vol. 4, pp 110-113, February 1991.

147 CHAKRABARTY, S.B., KLEFENZ, F., and DREHER, A.:'Dual-polarised wideband stacked microstrip antenna with aperture coupling for SAR applications'. IEE Antennas Propagation Symp. Dig., USA, 2000, pp. 2216-2219.

148 Personal communication with Don Mackinnon, Project manager, Charging and local transport division, Department Environment Transport Regions (DETR), 2000.

149 MORROW, I,. JAMES, J. R.:'Sequentially rotated large bandwidth circular polarised printed antennas' IEE electronic letters, vol 31 no (24) Nov 1995.

Appendix A: Traffic management system

Specification of system parameters

Frequency of operation

The recommended frequency of operation for traffic applications in Europe s is 5.725 - 5.875GHz as designated by CEPT.

Power

The maximum Effective Isotropic Radiated Power (ERIP) for the 5.8GHz system is +3 dBW or 2 W as recommended by CEPT.

Polarisation

Both the Carrier Wave (CW) transmitted from the RSU and the reflected CW from the OBU use LHCP. If the CW is reflected either by the road or from a vehicle, the polarisation is reversed to RHCP and consequently is ignored.

Communication mode

To reduce the expense of the OBU, the system uses a simplex communication mode.

Transmission mode

It has been decided to use asynchronous transmission mode as it is an efficient and adequate means of transmitting this information.

Data rate

A data rate of 250Kbits/sec is used or the up-link. This is considered the best compromise between requirements for the amount of information to be transmitted, and the compatibility with the OBU's clock frequency.

Bit error rate

The recommended raw Bit Error Rate (BER) for the system is 10^{-6}. From experimental work carried out it has been found that if the vehicle is in a good communication zone no errors have been detected.

Up link sub-carrier frequency

To reduce the interference from flicker noise a sub-carrier is used. The frequency of the sub-carrier must be high enough to minimise the effect of the flicker noise while being readily extracted from the microcontroller's oscillator within the OBU. A convenient frequency of the sub-carrier is therefore 1MHz.

Up link sub-carrier modulation

For reasons of hardware implementation, data recovery and BER performance, the data Difference Phase Shift Key (DPSK) modulates the 1MHz sub carrier. This is achieved using Non Return to Zero (NRZ) encoding producing 180 degree phase shift for a '1' and 0 degree phase shift for a '0'.

Uplink modulation of the 5.8GHz carrier

The DPSK modulated sub-carrier Phase Shift Key (PSK) modulates the 5.8GHz carrier wave as it is efficient and readily realised using a single diode at the OBU. The diode modulator provides a double side-band output signal.

System operation

The RSU transmits a constant 5.8GHz CW. When not in use, the OBU adopts a low power or 'sleep' mode to conserve power. The OBU must automatically detect the constant CW when it enters the communication zone and 'wake up'. The OBU then transmits its individual ID back to the RSU by phase shifting the reflected CW, before re-entering sleep mode.

A schematic diagram of the RSU and the OBU are shown in Figure A-1.
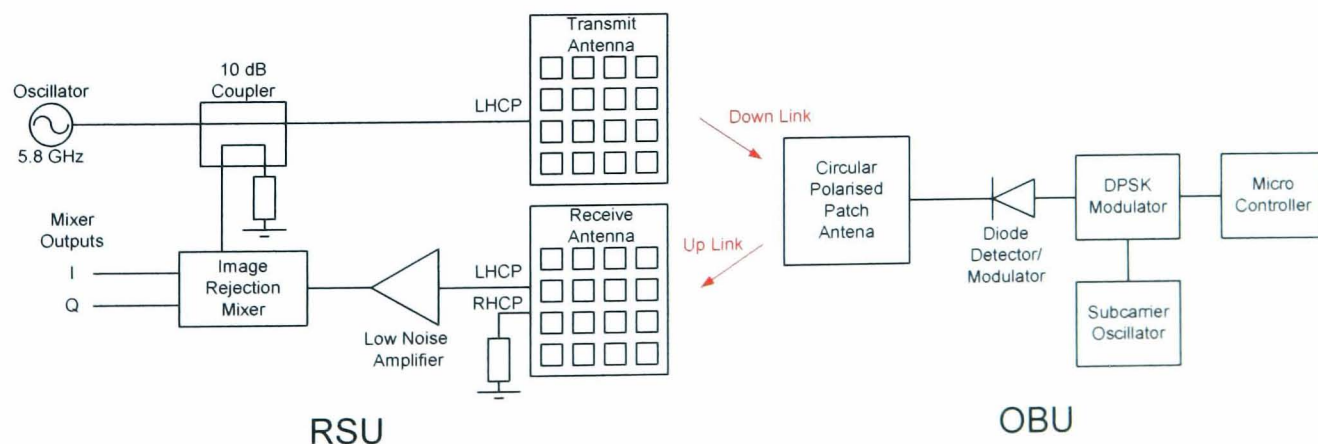
Figure A-1: Schematic diagram of the RSU and OBU.

For downlink transmission, from the roadside to the vehicle, the carrier signal is transmitted using LHCP via the transmit antenna array. In the vehicle a single LHCP microstrip antenna receives the signal. The 8 bit microcontroller detects CW using the simple diode detector. For the up-link transmission, CW transmitted by the RSU is reflected back by the OBU, thus eliminating the requirement for a microwave oscillator within the OBU. PSK modulation of the reflected CW is implemented using the same single diode (by switching it on and off) thus maintaining a compact OBU.

The RSU receives the OBU's 24 bit ID within a 17 byte data stream. Interface circuitry within the RSU performs the necessary error checking before presenting the ID to a host PC as three bytes of data. The host PC is required to validate the ID, through some form of administration data base, and take appropriate action such as granting, denying or logging access, controlling barriers, traffic lights and variable message signs.

RSU and OBU mounting

The RSU is mounted at an angle of 45 degrees with the road, although flexibility in this angle is required. For use on the open road, the RSU can be mounted to a vertical surface such as a motorway gantry or to a horizontal surface such as an RSJ girder beneath a bridge, as seen in Figure A-2.
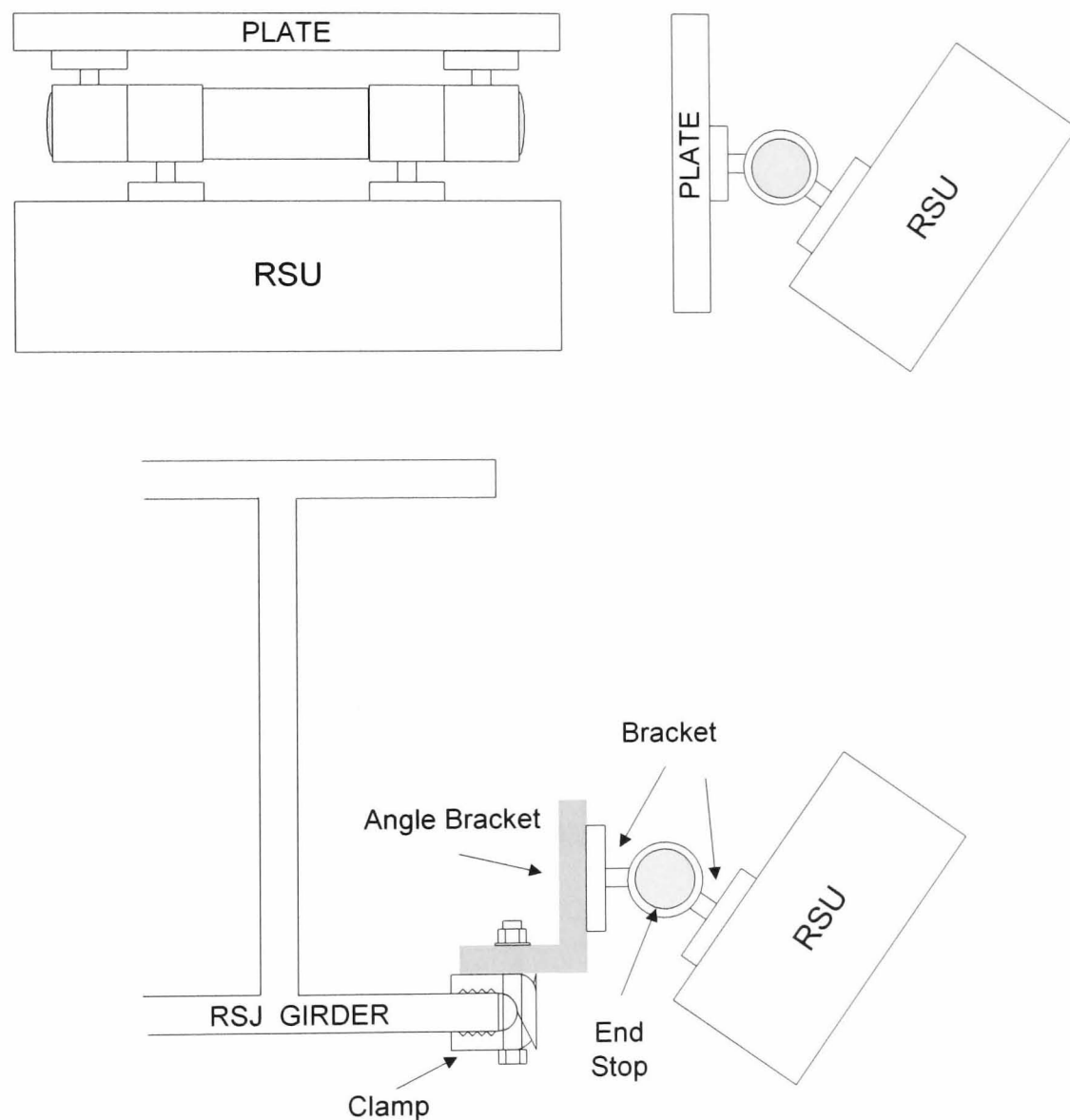
Figure A-2: Overhead RSU fixing.

For use at a barrier entry, the RSU is mounted to the barrier enclosure as seen in Figure A-3. As the RSU is positioned at the side of the road, this fixing has an additional degree of freedom allowing the RSU to tip forward and swing round into the road.
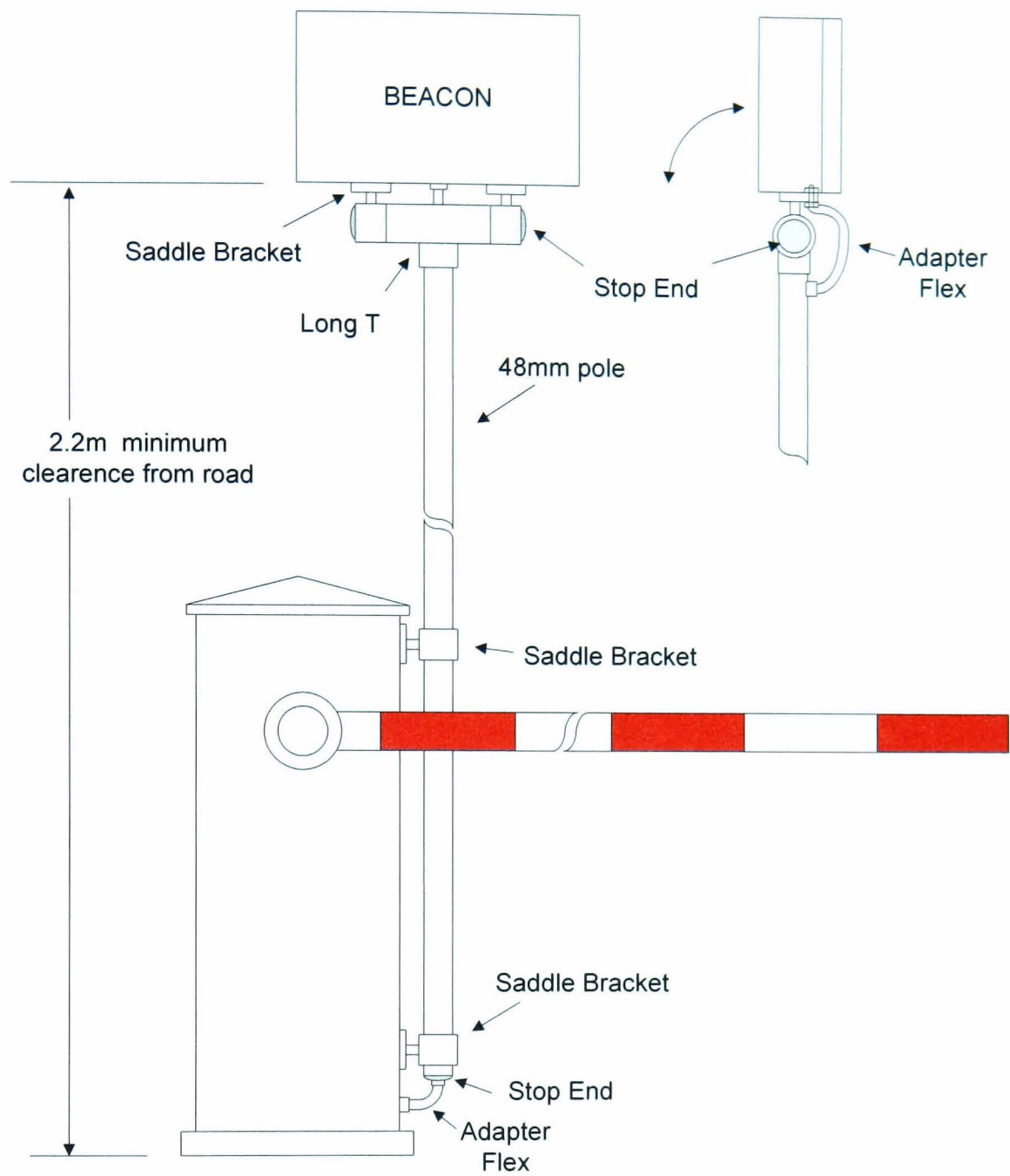
Figure A-3: RSU mounted to barrier cabinet.

The OBU is centrally mounted behind the rear view mirror of the vehicle, allowing optimal alignment between the OBU and an overhead RSU. This also allows a barrier mounted RSU to be on either side of the road.

System testing

System performance and footprint outline can be determined using a test OBU that continuously transmits a test code and a portable interface unit that can identify when this code is being successfully received.

Test OBU

The test OBU continuously sends the test code hex 807F80. This ID or code (binary 10000000, 01111111, 10000000) results in long streams of 0's and 1's, this being particularly difficult for the decoder within the RSU to read as it maximises the risk of losing the bias point. When the test OBU's push button is pressed and released the test OBU begins transmitting a continuous stream of test codes. When the button is pressed and released again it stops. The fact the test OBU can be latched on enables hands free testing (such as driving through the communication zone).

Test interface unit

The test interface unit beeps once every time it identifies a test code, the duration of the tone is the same as the duration of the test code hence results is a continuous tone when the test OBU is in the communication zone. The tone becomes 'gritty' when at the periphery of the communication zone. An additional green LED signifies an ID other than the test ID has been received.

Footprints

The communication zone of the system is dictated by the alignment of the RSU and choice of the antenna arrays within the RSU. To obtain the footprint of the system using 2x2 and 4x4 antenna arrays, the test interface unit was connected to the RSU and the test OBU used to trace out the footprint. In both scenarios, the test OBU was positioned at 45 degrees to the road, always facing directly forward in the direction of travel, at a height of 2cm from the road surface.

The footprint of an access control system, using the 2x2 antenna arrays optimised in Chapter 5, can be seen in Figure A-4. The RSU was tilted at 45 degrees with respect to the road and twisted by 45 degrees into the road. The RSU was mounted in alignment with the side of the road (the thickest vertical line in Figure A-4) at a height of 2.2 meters. The symbols represent the edges of the communication zone that demonstrated a clear tone when using the test OBU and interface unit. Gritty reads were obtained beyond these footprints but were deemed unreliable hence are not marked on this figure.
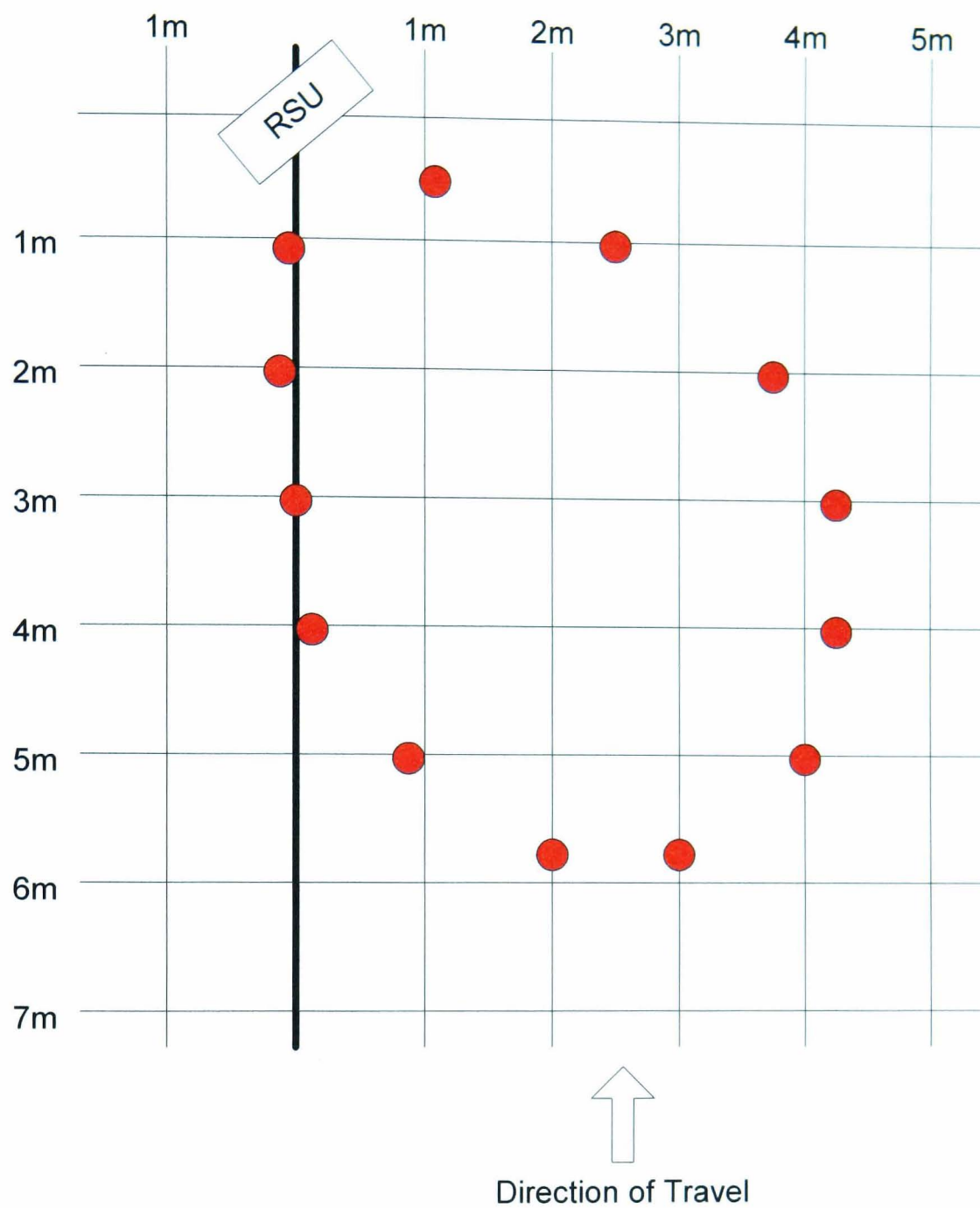
Figure A-4: Footprint of access control RSU using the 2x2 arrays.

Although faint side lobes were detected, these were gritty so are not marked in the figure.

The footprint of a motorway tolling system, using the 4x4 antenna arrays with reduced side lobes presented in Chapter 6 (Array B) can be seen in Figure A-5.
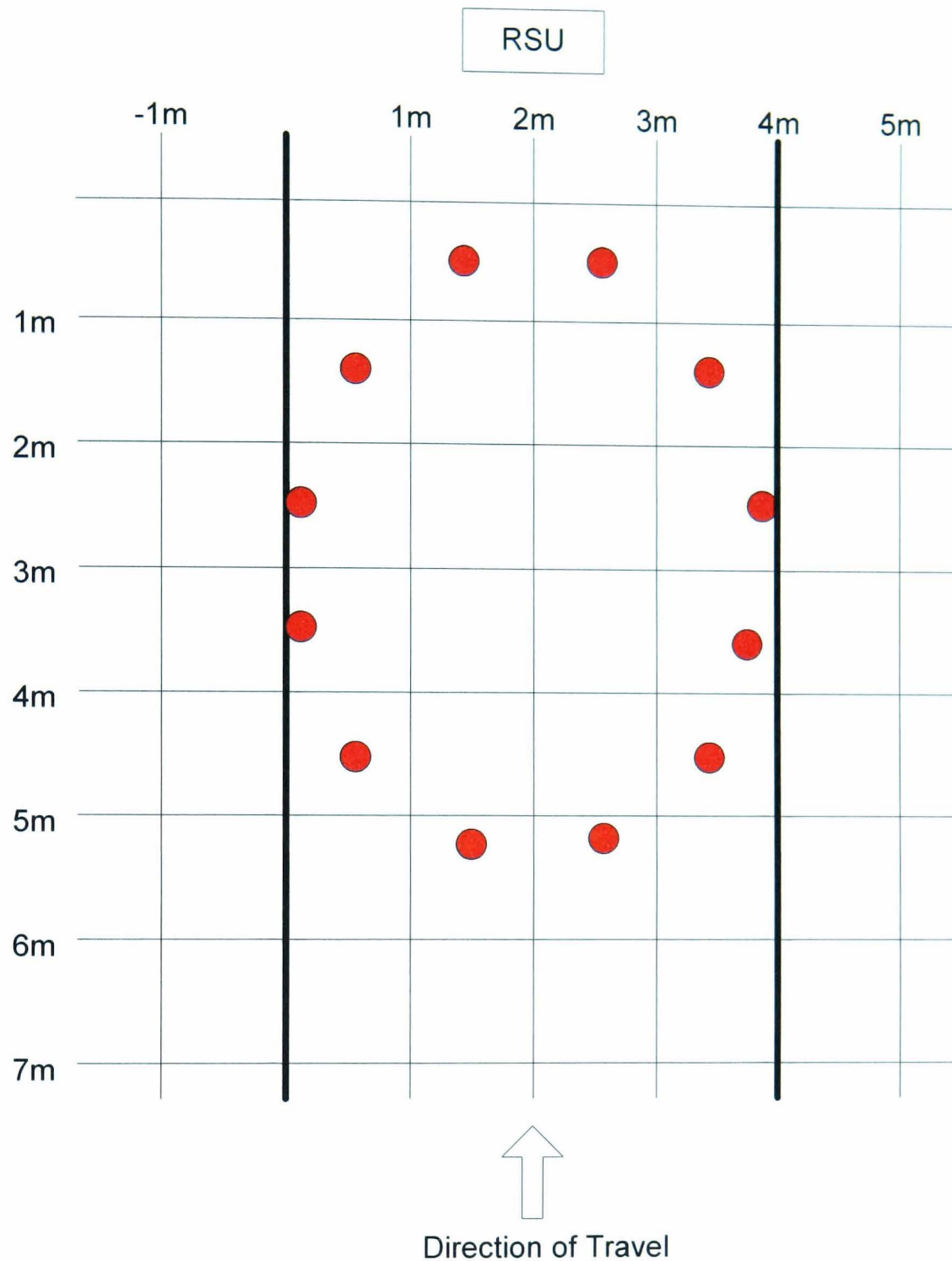
Figure A-5: Footprint of motorway tolling RSU using the 4x4 arrays.

The RSU was centrally mounted at a height of 8 meters perpendicular to the carriageway and tilted down at an angle of 45 degrees. The distance between the RSU and the center of the communication zone was 9 meters. The thick vertical lines in Figure A-5 designate the periphery of the lane.

In both application scenarios measurements were taken at road height so the dimensions of the communication zone of a vehicle mounted OBU can be obtained by projecting lines from the edge of these footprints to the RSU in both side and end

elevations. Raising the RSU further can increase the width and length of the communication zone, however even a car traveling at high speed only requires a small amount of communication zone to successfully transmit the ID; the footprint area is therefore required for coverage only.

Application

The antenna arrays developed in this thesis have been successfully used in a commercial traffic management system installed at Bluewater shopping center in Kent. The system has two distinct tasks. It has to monitor vehicles entering site, both under a motorway gantry and a bridge. RSUs using the 4x4 antenna arrays developed in Chapter 6 were mounted at these locations. The system also has to control access to four designated staff car parks at the periphery of the site. RSUs with the 2x2 antenna arrays optimised in chapter 5 were used at these locations. It is pleasing to note that as a direct consequence of this research, a commercially viable traffic management system employing 3500 OBUs has been developed and installed.

Appendix B: Axial ratio formula derivation

The axial ratio of the radiating element is found by finding the relative magnitude and phase of V_2 and V_4 as seen in Figure B-1. The relationship between these voltages can be found by assuming a constant voltage source of one volt is applied at the feed point which is then transformed through the feed network.

Each section of feed line is treated as a section of transmission line. In general, the ratio between the voltages at each end of a transmission line section can be found by determining V_{in} and V as defined in Figure B-1.
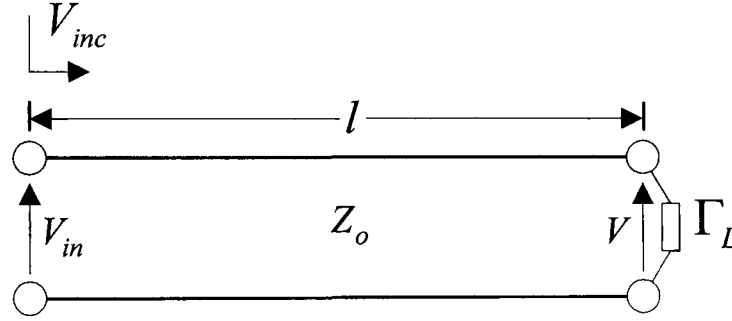
Figure B-1: Feed line section represented as a section of transmission line.

V_{inc} is an incident voltage of 1 volt and Γ_L is the reflection coefficient of the load. V is determined by adding the incident voltage just before it has been reflected, with the incident voltage just after it has been reflected by a mismatched load. This can be expressed as

$$V = V_{inc}e^{(-j\beta l)}(1+\Gamma)$$ (B.1)

V_{in} can be found by adding the original incident voltage with its returning reflection, hence expressed as

$$V_{in} = V_{inc}\left[1+e^{(-j\beta 2l)}\Gamma\right]$$ (B.2)

The voltage ratio V_2/V_4 in Figure 3-6 is determined by finding the product of the ratio V/V_{in} for each feed line section between these two points, hence

$$\frac{V_2}{V_4} = \prod_{n=1}^{N} \frac{e^{(-j\beta l_n)}(1+\Gamma_n)}{1+e^{(-j\beta 2l_n)}\Gamma_n}$$

(B.3)

where N is the number of feed line sections, Γ_n is the reflection coefficient and l_n the length of nth feed.

Appendix C: Far Field Measurement

The axial ratio of an elliptically polarised antenna is the ratio between the signal strengths on the major and minor axis of the ellipse. The major axis of the ellipse, the azimuth, can be at any angle relative to the antenna. Therefore it is necessary to measure the signal strength at all azimuths and select the highest and lowest readings. As a consequence, measurements of axial ratio made using a spinning receiving a antenna.

The antenna under test is mounted at one end of an anechoic chamber and is connected to a plain carrier wave source of the desired frequency. Mounted on a rotary joint at the opposite end of the chamber is a small linearly polarised receiving antenna, this is connected to the input of the spectrum analyser. A small electric motor causes the receiving antenna to turn at about 120rpm, i.e. the antenna's azimuth rotates twice per second. An output from the spectrum analyser is connected to an interface unit which enables instantaneous signal strength to be passed to a PC.

As measured samples are not synchronised with the azimuth of the antenna the PC software detects the turning points in signal strength. If the strength is rising the samples continue until the current sample is less than the previous sample, then a record is made of the previous sample as the maximum. Samples continue as the signal strength falls until the current sample is higher than the previous sample, and a record of the previous sample is made as the lowest value. Each revolution of the receiving antenna gives two maximums, and two minimums, so the data is continuously updated four times a second.

Once 200 samples have been taken, the mean difference between the maximum highest and minimum lowest values is displayed as axial ratio in dBs on the PC's screen. It is necessary to manually set the signal generator and spectrum analyser to the next frequency.

The gain of the antenna under test (the transmitting antenna) was also determined from received signal strength, the transmitted power, the gain of the receiving antenna and the path loss which is given by

$$20\log\frac{4\pi r}{\lambda_0} \qquad\qquad (C.1)$$

where r is the distance between the antenna under test and the receiving antenna. A component of the maximum and minimum signal strength is used as the received signal strength to cater for any cross polarisation.

Measurements were taken as a function of theta or beam heading by mounting the antenna under test onto a rotator driven by a stepper motor controlled by the same PC, which rotates from $\theta = -90°$ to $\theta = 90°$. To perform the test, the PC first sets the beam heading to -90 degrees. The PC software samples the signal strength at 200 samples per second for approximately one second, i.e. about two rotations of the receiving antenna. It was found that sampling for two rotations of the receiving antenna gave more accurate results when the axial ratio was poor. The rotator is then moved clockwise by 0.9° (the resolution of the rotator's stepper motor) to -89.1°, and a new set of 200 samples is taken and plotted for this new beam heading. This process is repeated 200 times until the antenna under test has rotated 180° and the beam heading is +90 degrees.

Appendix D: Feed optimisation solutions

```
C:\DOCUME~1\Huw\Desktop\PH.D\ANNEAL2.EXE                              _ □ ✕

Temperature = -0.1
Z[0] =   50.0000, Zin[0] =   50.0000, Zout[0] =   50.0000, Zpress[0] =      0
Z[1] =   81.2404, Zin[1] =  200.0000, Zout[1] =   33.0000, Zpress[1] =      0
Z[2] =   77.7878, Zin[2] =   66.6667, Zout[2] =   90.7640, Zpress[2] =     59
Z[3] =   94.7926, Zin[3] =  272.2921, Zout[3] =   33.0000, Zpress[3] =     42
Z[4] =   96.7231, Zin[4] =  136.1460, Zout[4] =   68.7156, Zpress[4] =     40
Z[5] =   67.3441, Zin[5] =  137.4312, Zout[5] =   33.0000, Zpress[5] =     70
Z[6] =  137.3947, Zin[6] =  137.4312, Zout[6] =  137.3582, Zpress[6] =    -79
Z[7] =   67.3262, Zin[7] =  137.3582, Zout[7] =   33.0000, Zpress[7] =     70

Best:
Z[0] =   50.0000, Zin[0] =   50.0000, Zout[0] =   50.0000, Zpress[0] =      0
Z[1] =   81.2404, Zin[1] =  200.0000, Zout[1] =   33.0000, Zpress[1] =      0
Z[2] =   80.5296, Zin[2] =   66.6667, Zout[2] =   97.2752, Zpress[2] =     56
Z[3] =   98.1338, Zin[3] =  291.8257, Zout[3] =   33.0000, Zpress[3] =     39
Z[4] =   99.7543, Zin[4] =  145.9129, Zout[4] =   68.1977, Zpress[4] =     37
Z[5] =   67.0899, Zin[5] =  136.3955, Zout[5] =   33.0000, Zpress[5] =     70
Z[6] =  136.9028, Zin[6] =  136.3955, Zout[6] =  137.4120, Zpress[6] =    -81
Z[7] =   67.3394, Zin[7] =  137.4120, Zout[7] =   33.0000, Zpress[7] =     70
Hit a key please_
```

Table 5-1, Row 1, 33Ω patch, 137 max and target.

```
C:\DOCUME~1\Huw\Desktop\PH.D\ANNEAL2.EXE                              _ □ ✕

Temperature = -0.1
Z[0] =   50.0000, Zin[0] =   50.0000, Zout[0] =   50.0000, Zpress[0] =      0
Z[1] =  100.0000, Zin[1] =  200.0000, Zout[1] =   50.0000, Zpress[1] =      0
Z[2] =   87.3703, Zin[2] =   66.6667, Zout[2] =  114.5035, Zpress[2] =     50
Z[3] =  131.0554, Zin[3] =  343.5105, Zout[3] =   50.0000, Zpress[3] =      6
Z[4] =  108.6260, Zin[4] =  171.7552, Zout[4] =   68.7001, Zpress[4] =     28
Z[5] =   82.8855, Zin[5] =  137.4002, Zout[5] =   50.0000, Zpress[5] =     54
Z[6] =  137.3652, Zin[6] =  137.4002, Zout[6] =  137.3303, Zpress[6] =    -73
Z[7] =   82.8644, Zin[7] =  137.3303, Zout[7] =   50.0000, Zpress[7] =     54

Best:
Z[0] =   50.0000, Zin[0] =   50.0000, Zout[0] =   50.0000, Zpress[0] =      0
Z[1] =  100.0000, Zin[1] =  200.0000, Zout[1] =   50.0000, Zpress[1] =      0
Z[2] =   87.4408, Zin[2] =   66.6667, Zout[2] =  114.6883, Zpress[2] =     50
Z[3] =  131.1611, Zin[3] =  344.0649, Zout[3] =   50.0000, Zpress[3] =      6
Z[4] =  108.3616, Zin[4] =  172.0325, Zout[4] =   68.2559, Zpress[4] =     28
Z[5] =   82.6171, Zin[5] =  136.5119, Zout[5] =   50.0000, Zpress[5] =     54
Z[6] =  136.9536, Zin[6] =  136.5119, Zout[6] =  137.3968, Zpress[6] =   -131
Z[7] =   82.8845, Zin[7] =  137.3968, Zout[7] =   50.0000, Zpress[7] =     54
Hit a key please_
```

Table 5-1, Row 2, Table 5-2, Row1, 50Ω patch, 137 max and target.

```
C:\DOCUME~1\Huw\Desktop\PH.D\ANNEAL2.EXE                          _ □ ×

Temperature = -0.1
Z[0] =   50.0000, Zin[0] =   50.0000, Zout[0] =   50.0000, Zpress[0] =        0
Z[1] =  100.0000, Zin[1] =  200.0000, Zout[1] =   50.0000, Zpress[1] =        0
Z[2] =   58.7714, Zin[2] =   66.6667, Zout[2] =   51.8112, Zpress[2] =       86
Z[3] =   88.1571, Zin[3] =  155.4336, Zout[3] =   50.0000, Zpress[3] =       57
Z[4] =   79.3395, Zin[4] =   75.0000, Zout[4] =   83.9302, Zpress[4] =       66
Z[5] =   91.6134, Zin[5] =  167.8604, Zout[5] =   50.0000, Zpress[5] =       53
Z[6] =  145.3337, Zin[6] =  167.8604, Zout[6] =  125.8300, Zpress[6] =      -67
Z[7] =   79.3190, Zin[7] =  125.8300, Zout[7] =   50.0000, Zpress[7] =       66

Best:
Z[0] =   50.0000, Zin[0] =   50.0000, Zout[0] =   50.0000, Zpress[0] =        0
Z[1] =  100.0000, Zin[1] =  200.0000, Zout[1] =   50.0000, Zpress[1] =        0
Z[2] =   87.4847, Zin[2] =   66.6667, Zout[2] =  114.8035, Zpress[2] =       58
Z[3] =  131.2270, Zin[3] =  344.4106, Zout[3] =   50.0000, Zpress[3] =       14
Z[4] =  111.5999, Zin[4] =  172.2053, Zout[4] =   72.3238, Zpress[4] =       33
Z[5] =   85.0434, Zin[5] =  144.6476, Zout[5] =   50.0000, Zpress[5] =       60
Z[6] =  144.9522, Zin[6] =  144.6476, Zout[6] =  145.2574, Zpress[6] =      -70
Z[7] =   85.2225, Zin[7] =  145.2574, Zout[7] =   50.0000, Zpress[7] =       60
Hit a key please
```

Table 5-2, Row 2, 50Ω patch, 145 max and target.

```
C:\DOCUME~1\Huw\Desktop\PH.D\ANNEAL3.EXE                          _ □ ×

 targetZ= 136.1300, minZ=   50.0000, maxZ= 137.0000
Z[0]=   50.0000, Zin[0]=   50.0000, Zout[0]=   50.0000, Zpress[0]=     0.0000
Z[1]=  100.0000, Zin[1]=  200.0000, Zout[1]=   50.0000, Zpress[1]=     0.0000
Z[2]=   57.7426, Zin[2]=   66.6667, Zout[2]=   50.0132, Zpress[2]=    78.3874
Z[3]=   86.6140, Zin[3]=  150.0395, Zout[3]=   50.0000, Zpress[3]=    49.5160
Z[4]=   75.8984, Zin[4]=   75.0198, Zout[4]=   76.7873, Zpress[4]=    60.2260
Z[5]=   87.6284, Zin[5]=  153.5747, Zout[5]=   50.0000, Zpress[5]=    48.4952
Z[6]=  136.9959, Zin[6]=  153.5747, Zout[6]=  122.2068, Zpress[6]=  -300.0000
Z[7]=   78.1687, Zin[7]=  122.2068, Zout[7]=   50.0000, Zpress[7]=    57.9556

Best: targetZ=   54.3500, fitness (total distance from target):   41.1410
Z[0]=   50.0000, Zin[0]=   50.0000, Zout[0]=   50.0000, Zpress[0]=     0.0000
Z[1]=  100.0000, Zin[1]=  200.0000, Zout[1]=   50.0000, Zpress[1]=     0.0000
Z[2]=   50.7498, Zin[2]=   66.6667, Zout[2]=   38.6332, Zpress[2]=     3.6002
Z[3]=   76.1248, Zin[3]=  115.8996, Zout[3]=   50.0000, Zpress[3]=   -21.7748
Z[4]=   50.1176, Zin[4]=   75.0000, Zout[4]=   33.4903, Zpress[4]=     4.2324
Z[5]=   57.8708, Zin[5]=   66.9806, Zout[5]=   50.0000, Zpress[5]=    -3.5208
Z[6]=   58.9149, Zin[6]=   66.9806, Zout[6]=   51.8203, Zpress[6]=    -4.5649
Z[7]=   50.9020, Zin[7]=   51.8203, Zout[7]=   50.0000, Zpress[7]=     3.4480
Hit a key please_
```

Table 5-3, Row 1 50Ω patch, target 'sweep'. Fitness function: Total error.

```
C:\DOCUME~1\Huw\Desktop\PH.D\ANNEAL3.EXE                          _ □ ×

 targetZ= 136.1300, minZ=  50.0000, maxZ= 137.0000
Z[0]=  50.0000, Zin[0]=  50.0000, Zout[0]=  50.0000, Zpress[0]=   0.0000
Z[1]= 100.0000, Zin[1]= 200.0000, Zout[1]=  50.0000, Zpress[1]=   0.0000
Z[2]=  57.7579, Zin[2]=  66.6667, Zout[2]=  50.0397, Zpress[2]=  78.3797
Z[3]=  86.6369, Zin[3]= 150.1191, Zout[3]=  50.0000, Zpress[3]=  49.5045
Z[4]=  75.6066, Zin[4]=  75.0596, Zout[4]=  76.1575, Zpress[4]=  60.5434
Z[5]=  87.2683, Zin[5]= 152.3151, Zout[5]=  50.0000, Zpress[5]=  48.8733
Z[6]= 137.0143, Zin[6]= 152.3151, Zout[6]= 123.2505, Zpress[6]=  -0.8661
Z[7]=  78.5018, Zin[7]= 123.2505, Zout[7]=  50.0000, Zpress[7]=  57.6282

Best: targetZ=  63.0500, fitness (max distance from target):  12.6113
Z[0]=  50.0000, Zin[0]=  50.0000, Zout[0]=  50.0000, Zpress[0]=   0.0000
Z[1]= 100.0000, Zin[1]= 200.0000, Zout[1]=  50.0000, Zpress[1]=   0.0000
Z[2]=  50.4408, Zin[2]=  66.6667, Zout[2]=  38.1642, Zpress[2]=  12.6092
Z[3]=  75.6613, Zin[3]= 114.4925, Zout[3]=  50.0000, Zpress[3]= -12.6113
Z[4]=  52.0694, Zin[4]=  57.2463, Zout[4]=  47.3607, Zpress[4]=  10.9806
Z[5]=  68.8191, Zin[5]=  94.7214, Zout[5]=  50.0000, Zpress[5]=  -5.7691
Z[6]=  74.7921, Zin[6]=  94.7214, Zout[6]=  59.0559, Zpress[6]= -11.7421
Z[7]=  54.3396, Zin[7]=  59.0559, Zout[7]=  50.0000, Zpress[7]=   8.7104
Hit a key please
```

Table 5-3, Row 2 50Ω patch, target 'sweep'. Fitness function: Maximum error.

```
C:\DOCUME~1\Huw\Desktop\PH.D\ANNEAL3.EXE                          _ □ ×

 targetZ= 136.1300, minZ=  50.0000, maxZ= 137.0000
Z[0]=  50.0000, Zin[0]=  50.0000, Zout[0]=  50.0000, Zpress[0]=   0.0000
Z[1]= 100.0000, Zin[1]= 200.0000, Zout[1]=  50.0000, Zpress[1]=   0.0000
Z[2]=  57.7712, Zin[2]=  66.6667, Zout[2]=  50.0627, Zpress[2]=  78.3664
Z[3]=  86.6568, Zin[3]= 150.1881, Zout[3]=  50.0000, Zpress[3]=  49.4846
Z[4]=  75.8180, Zin[4]=  75.0941, Zout[4]=  76.5488, Zpress[4]=  60.3320
Z[5]=  87.4922, Zin[5]= 153.0977, Zout[5]=  50.0000, Zpress[5]=  48.6494
Z[6]= 137.0116, Zin[6]= 153.0977, Zout[6]= 122.6158, Zpress[6]=  -0.8636
Z[7]=  78.2994, Zin[7]= 122.6158, Zout[7]=  50.0000, Zpress[7]=  57.8306

Best: targetZ=  52.6100, fitness (local smoothness):  25.0000
Z[0]=  50.0000, Zin[0]=  50.0000, Zout[0]=  50.0000, Zpress[0]=   0.0000
Z[1]= 100.0000, Zin[1]= 200.0000, Zout[1]=  50.0000, Zpress[1]=   0.0000
Z[2]=  50.0000, Zin[2]=  66.6667, Zout[2]=  37.5000, Zpress[2]=   2.6100
Z[3]=  75.0000, Zin[3]= 112.5000, Zout[3]=  50.0000, Zpress[3]= -22.3900
Z[4]=  50.1122, Zin[4]=  56.2500, Zout[4]=  44.6441, Zpress[4]=   2.4978
Z[5]=  66.8162, Zin[5]=  89.2882, Zout[5]=  50.0000, Zpress[5]= -14.2062
Z[6]=  66.8667, Zin[6]=  89.2882, Zout[6]=  50.0756, Zpress[6]= -14.2567
Z[7]=  50.0378, Zin[7]=  50.0756, Zout[7]=  50.0000, Zpress[7]=   2.5722
Hit a key please
```

Table 5-3, Row 3, 50Ω patch, 137 max target 'sweep'. Fitness function: Local smoothness.

Appendix E: Published Work

Multiobjective genetic algorithm approach for a dual-feed circular polarised patch antenna design

B. Aljibouri, E.G. Lim, H. Evans and A. Sambell

A design procedure for a dual feed network is presented to produce a circular polarised matched antenna involving eight design parameters with associated constraints. Determination of such design parameters has been made possible by utilising a multiobjective genetic algorithm (MGA) approach. The conditions for circular polarisation and impedance matching were the objective functions employed in the MGA. The associated constraints were the lengths and characteristic impedance values of the feed network. The return loss and axial ratio for a 5.8GHz antenna were investigated and good agreement was obtained between simulated and practical measurements.

Introduction: Microstrip patch antennas are used in a variety of communication systems, especially when the receiver needs to be compact and have a low profile. Further, for applications such as radio frequency identification (RFID) systems in which the receiver may be placed in any orientation, circular polarisation is used. Circular polarisation can be realised by using either a single [1] or a dual feed [2, 3]. In many cases, owing to the simplicity of design and manufacture a dual-feed arrangement is preferred.

An MGA programme has been developed to optimise the design of the dual-feed network, involving eight variables, which are required to meet the conditions for circular polarisation and matching at the feed port. Two constraints on the design parameters have also been applied, one to ensure that the widths of the feed lines are as narrow as possible yet realisable, and the other constraint to ensure that the lengths of the feed lines are sufficient to fit the network around the square patch antenna.
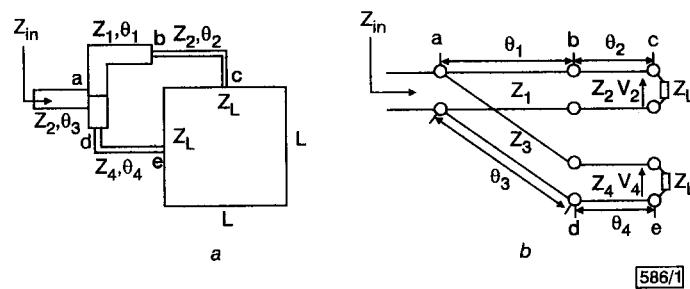
Fig. 1 *Dual-feed LHCP square patch antenna and equivalent circuit*

Design of feed network using multiobjective genetic algorithm approach: A dual feed network based on a power divider to produce circular polarisation is shown in Fig. 1a and its transmission line model in Fig. 1b.

It is possible, using a transmission line approach, to match a complex load impedance to a complex source impedance by relaxing the constraint length of a traditional $\lambda/4$ transformer [4]. Consequently, by varying the impedance and lengths of the transmission lines of the feed network, both matching and circular polarisation conditions can be satisfied. For the structure shown in Fig. 1 the design variables' parameters (characteristic impedances and element lengths of the feed network) are Z_1, θ_1, Z_2, θ_2, Z_3, θ_3, Z_4, θ_4 and constitute the parameter set in the MGA. The two objective functions employed in the MGA are given by eqns. 1 and 2 below and give the conditions required for circular polarisation and impedance matching, respectively. For circular polarisation

$$\frac{V_2}{V_4} = \frac{e^{-j(\theta_1+\theta_2)}[1+\Gamma_1][1+\Gamma_2]}{[1+\Gamma_1 e^{-2j\theta_1}][1+\Gamma_2 e^{-2j\theta_2}]}$$
$$\times \frac{[1+\Gamma_3 e^{-2j\theta_3}][1+\Gamma_4 e^{-2j\theta_4}]}{e^{-j(\theta_3+\theta_4)}[1+\Gamma_3][1+\Gamma_4]} = \mp j \qquad (1)$$

where Γ_1, Γ_2, Γ_3 and Γ_4 are the reflection coefficients at junctions b, c, d, and e, respectively (see Fig. 1).

For the impedance matching

$$\Gamma_{in} = \frac{Z_{in} - Z_0}{Z_{in} + Z_0} = 0 \qquad (2)$$

where Γ_{in} is the input reflection coefficient at junction 'a'.

For microstrip realisation, search intervals between 120Ω and 140Ω

were used for the parameters Z_1, Z_2, Z_3, Z_4. The 120Ω impedance was chosen to reduce the coupling between the feed lines and the antenna and also to minimise the step discontinuities at the feed lines junctions, thereby reducing spurious radiation. The 140Ω impedance represents the maximum impedance that can be realised. To fit the feed network around the antenna, the lengths θ_1, θ_2, θ_3, θ_4 were constrained to an interval between $\pi/4$ and π.

The tolerance for $|V_2/V_4|$ was 1 ± 0.1 and for $\arg(V_2/V_4)$ was $90° \pm 4°$, so as to ensure good circular polarisation, while the tolerance for Γ_{in} was ± 0.02 in order to produce good matching conditions.
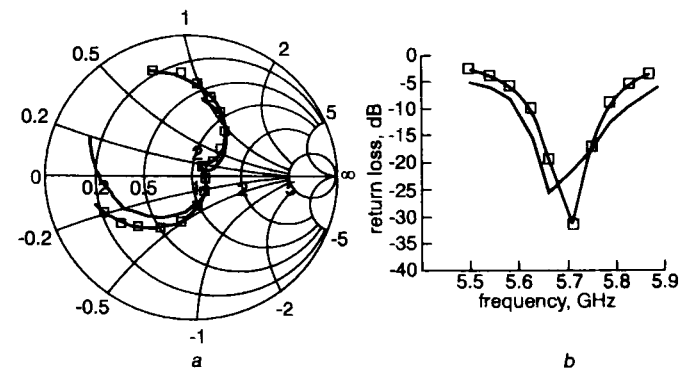
Fig. 2 *Simulated and practical results of dual-feed square microstrip patch antenna*

———— practical
—□— simulated
$h = 0.79$, $\varepsilon_r = 2.33$
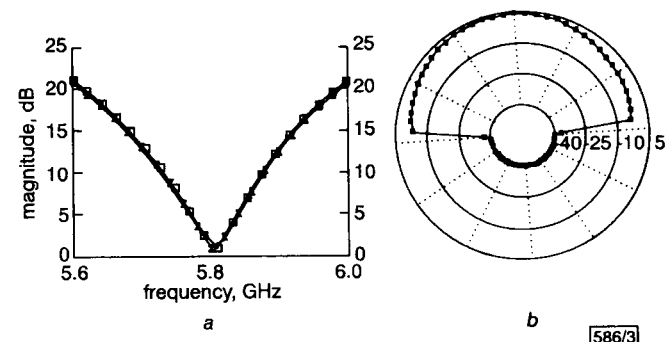
Fig. 3 *Simulated results for LHCP and RHCP designs*

a Axial ratio
b Radiation pattern
—□— LHCP
—X— RHCP

Results and discussion: The MGA approach, based on a nondominating sorting genetic algorithm [4], was developed to produce sets of feasible solutions. Selection was made from these solutions, using additional factors, such as a preference for similar characteristic impedance values of the feed line network.

The operating frequency of the patch antenna was 5.8GHz, and the feed network was optimised to produce left- and right-hand circular polarisation (LHCP and RHCP) with a 50Ω matched input impedance condition. The two sets of solutions for the optimised feed network are shown in Table 1.

Table 1: Two sets of solutions for optimised feed network

θ_1	Z_1	θ_2	Z_2	θ_3	Z_3	θ_4	Z_4	Z_{in}	$|V_2/V_4|$	$\arg(V_2/V_4)$	CP
2.31	135.0	1.96	132.4	0.8	135.2	1.16	134.3	50−0.5i	0.97	86	RH
1.2	137.4	0.74	137.1	2.3	135.7	1.97	138.6	49.5+0.5i	1.08	89.7	LH

As can be seen in Table 1, it is possible to use an average value of impedance for all four feed lines as this value is within the design and typical manufacturing tolerances. This makes the design particularly attractive as the effect of the step discontinuity is eliminated and also spurious radiation is reduced.

Practical and simulated (full-wave analysis software) results for the reflection coefficient of the LHCP solution using 137.2Ω are shown in Fig. 2 and indicate that a good matching condition at 5.8GHz has been obtained.

LHCP and RHCP designs are shown in Fig. 3 with a good axial ratio
and the expected radiation patterns.

Conclusion: It has been shown that the design of a dual-feed network for
a square patch antenna for circular polarisation involves eight variables
and that a closed form solution to the problem cannot be obtained. An
MGA with specified constraints has been successfully implemented to
optimise the design of a dual-feed network. A feed network with single
feed impedance has been realised. The practical and simulated results
for the return loss, axial ratio and radiation pattern show good agree-
ment and confirm the validity of the approach.

B. Aljibouri, E.G. Lim, H. Evans and A. Sambell (*Communication Systems
Research Group, University of Northumbria, United Kingdom*)

References

1   LIM, B., KOROLKIEWICZ, E., and SCOTT, S.: 'Optimised design of corner
     microstrip fed nearly square patch antenna for circular polarisation',
     Electron. Lett., 1996, **32**, pp. 610–612

2   HOWELL, J.Q.: 'Microstrip antennas', *IEEE Trans.,* 1975, **AP–23**, pp. 90–
     93

3   SOLIMAN, E.A., BREBELS, S., BEYNE, E., and VANDENBOSCH, G.: 'Circularly
     polarised aperture antenna fed by CPW and built in MCM-D
     technology', *Electron. Lett.,* 1999, **35**, pp. 250–251

4   DAY, P.I.: 'Transmission line transformation between arbitrary impedances
     using the smith chart', *IEEE Trans. Microw. Theory Tech.,* 1975, pp.
     772–773

5   SRINIVAS, N., and KALYANMOY, D.: 'Multiobjective optimization using
     nondominating sorting in genetic algorithms', *Evol. Comput.,* 1995, **2**,
     (3), pp. 221–248

Application of simulated annealing to design of serial feed sequentially rotated 2 × 2 antenna array

H. Evans, P. Gale, B. Aljibouri, E.G. Lim,
E. Korolkeiwicz and A. Sambell

A 5.8GHz circularly polarised 2 × 2 patch antenna array is presented, employing sequential rotation of dual-feed circularly polarised elements; appropriate phase-shifting and power splitting are achieved via a serial feed arrangement. The feed has been optimised using simulated annealing; the resulting structure has a voltage standing wave ratio 2:1 bandwidth of 9.8%. Results obtained by full wave simulation and practical measurement confirm the integrity of the design.

Introduction: Many modern communication systems use single-layer patch antenna arrays as they are light, low profile and inexpensive. One such system is a two-way digital communication link between a moving vehicle and a roadside beacon for traffic management applications. This array has been used in the roadside unit of a commercial system and also as a sub-array within a 4 × 4 arrangement resulting in a gain of 18.9dBi.

Sequential rotation of radiating elements, with suitable excitation phase-shifting, has been shown to improve the polarisation purity and radiation pattern symmetry over a wide range of frequencies. In addition, owing to the excitation phase-shifting by the feed, off frequency reflections from mismatched elements tend to cancel out at the feed point, leading to improved input impedance over a wider bandwidth [1 – 3]. These applications of sequential rotation all employ some form of corporate feed network.

This Letter presents a design that incorporates sequential rotation using a serial feed to provide appropriate phase-shifting and power splitting between the radiating elements. As it is not possible to obtain closed form expressions, the impedance elements within the feed network have been optimised using a simulated annealing algorithm.

Array description: The antenna configuration is shown in Fig. 1*a*. The radiating elements are dual feed left hand circularly polarised microstrip patches with an input impedance of 50 Ω [4], which are sequentially rotated by 90° with respect to each element's immediate neighbour. The serial feed compensates for this physical rotation by shifting the phase of each element's excitation by 90°.
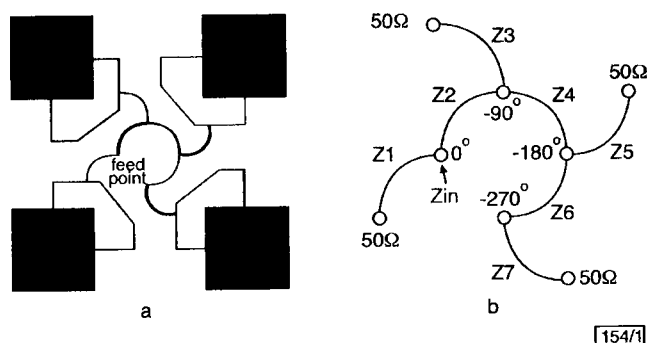
Fig. 1 *Antenna configuration and equivalent circuit*

a 2 × 2 antenna array incorporating sequentially rotated radiating elements excited by serial feed network
b Equivalent circuit for serial feed network

The radiating elements are spaced at 0.74λ as it has been shown that this minimises mutual coupling without substantial degradation of the radiation pattern by side lobes [5]. Smooth bends were used in the feed network as it has been shown that this can reduce feed radiation [6]. The use of high impedance elements in the feed network further reduces coupling and spurious radiation.

At the design frequency, the serial feed ensures that equal power is fed to each element. Off frequency, as the signal propagates along the feed, correct phase-shifting and power splitting progressively deteriorate. Although degradation of accurate power splitting dominates, the use of sequential rotation reduces this problem.

Feed optimisation: The equivalent circuit for the serial feed can be seen in Fig. 1*b*. λ/4 transformers are used to provide the necessary impedance matching and phase delays. The value of Z1 is fixed, as it must both divert a quarter of the power to the first patch while ensuring that

the input impedance to the whole structure is 50 Ω. There is no unique solution to the remaining impedances. However, to ensure Z5 and Z7 are at a maximum impedance, it is necessary to make Z6 the maximum impedance that fabrication constraints will allow, typically between 128 and 145 Ω.

An adaptation of iterated simulated annealing [7] has been implemented in C++ to optimise the feed network with the following five constraints. The minimum impedance was constrained to 70 Ω to reduce coupling and spurious radiation. In this Letter, solutions were found for a maximum impedance of 128 and 145 Ω. The target impedance was set to the maximum impedance value. The input impedance at the feed point, Z_{in}, was constrained to 50 Ω for this array, although it can be changed if the structure were used as a sub-array. The patch input impedance was set to 50 Ω for this design.

Results: Two sets of solutions for the feed network can be seen in Table 1. In both cases the optimisation algorithm has ensured that Z6 is at the maximum value, thus ensuring both Z5 and Z7 are also at maximum values; all impedances are within the specified constraints.

Table 1: Feed network solutions with maximum impedance restrained to 125 and 145 Ω

Z_{in}	Z1	Z2	Z3	Z4	Z5	Z6	Z7
Ω	Ω	Ω	Ω	Ω	Ω	Ω	Ω
50	100	80	120	96	80	128	80
50	100	90	135	115	85	145	85

The antenna was fabricated on 0.79mm 1/2 oz RT 5870 Duroid (ε_r = 2.33). The integrity of the design has been confirmed using full wave simulation [8] and experimental measurement. The voltage standing wave ratio (VSWR), radiation pattern and axial ratio can be seen in Fig. 2. Practical measurement confirms a VSWR 2:1 bandwidth of 9.8% although the axial ratio is not as wide band. The gain of the main lobe has been measured at 12.4dBi.
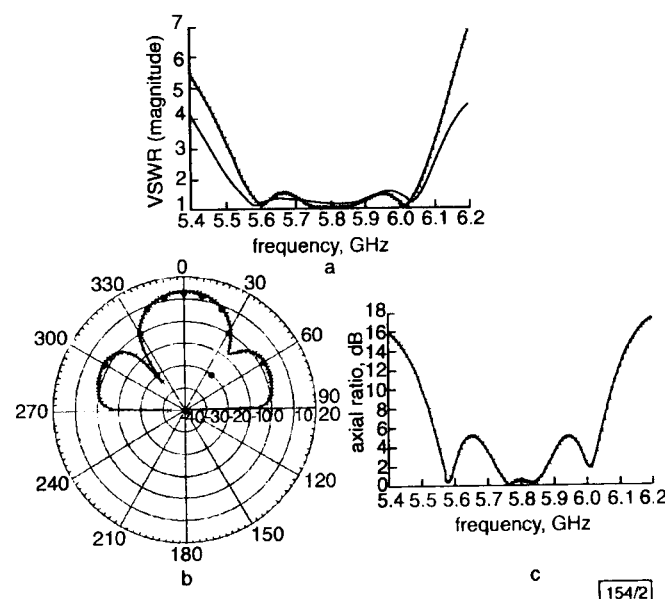
Fig. 2 *VSWR, radiation pattern and axial ratio*

a VSWR
—✕— full wave simulation
———— practical measurement
b Radiation pattern
—✕— full wave simulation
● practical measurements
c axial ratio
—✕— full wave simulation

Conclusion: A sequentially rotated 2 × 2 antenna array with a serial feed has been presented. Simulated annealing successfully optimised the feed network with a minimum of computational resources. The performance of the array has been confirmed both by full wave simulation and experimental measurement confirming a VSWR 2:1 bandwidth of 9.8%.

H. Evans, P. Gale, B. Aljibouri, E.G. Lim, E. Korolkeiwicz and A. Sambell
(*School of Engineering, University of Northumbria, Ellison Building, Newcastle Upon Tyne, NE1 8ST, United Kingdom*)

Huw.Evans@unn.ac.uk

References

1　TESHIROGI, T., TANAKA, M., and CHUJO, W.: 'Wideband circularly polarised array antenna with sequential rotation and phase shifts of elements'. Int. Symp. Antennas and Propag., ISAP 85, Tokyo, 1985

2　HALL, P.S.: 'Feed radiation effects in sequentially rotated microstrip arrays', *Electron. Lett.*, 1987, **23**, (17), pp. 877–878

3　HALL, P.S., DAHELE, J.S., and JAMES, J.R.: 'Design principles of sequentially fed, wide bandwidth, circularly polarised microstrip patch antennas', *IEE Proc. H*, 1989, **136**, (5), pp. 381–389

4　ALJIBOURI, B., LIM, E.G., EVANS, H., and SAMBELL, A.: 'Multiobjective genetic algorithm approach for a dual feed circular polarised patch antenna design', *Electron. Lett.*, 2000, **36**, (12), pp. 1005–1006

5　CHAN, T.K.: 'Development of a two way microwave communication system for traffic applications'. PhD thesis, University of Northumbria at Newcastle, June 1994

6　HALL, P.S., and HALL, C.M.: 'Coplanar corporate feed effects on microstrip patch array design', *IEE Proc. H*, 1988, **135**, (3), pp. 180–186

7　KIRKPATRICK, S., GELATT, C.D., and VECCHI, M.P.: 'Optimization by simulated annealing', *Science*, 1983, **220**, pp. 671–680

8　Ansoft Ensemble® V6. 1 - Method of Moments 2.5D EM field solver

Cavity model of circularly polarised cross-aperture-coupled microstrip antenna

B. Al-Jibouri, H. Evans, E. Korolkiewicz, E.G. Lim, A. Sambell and T. Viasits

Abstract: A cavity model is used to analyse an aperture-fed nearly square circularly polarised patch antenna. The form of the aperture is that of a symmetric cross-slot that couples the excitation between a single microstrip feed line and the patch antenna. Using equivalent magnetic current sources at the slots, the modal electric and magnetic fields under the patch are obtained, and hence analytical expressions for the patch admittances at the aperture are derived and used to obtain an equivalent circuit of the circular polarised antenna. Good agreement is obtained between the circuit modelling and practical results.

1 Introduction

An aperture-coupled feed structure is known to have a number of practical advantages. Since the feed network and radiating patch are on separate substrates, both the thickness and dielectric properties of each substrate can be independently chosen to meet requirements of the feed network to the radiation patch. The isolation of the patch from the feed network by the ground plane minimises spurious feed radiation. A compact structure can be realised using aperture coupling, and as the aperture is positioned below the centre of the patch, the symmetry ensures good circular polarisation [1, 2].

Aperture-coupled structures have been fully analysed using spectral domain [3, 4] and spatial solution [5] methods. These analyses can be used to examine the effects of the design parameters on the performance of the antenna with good accuracy. However, these approaches are numerically intensive and, because of the poor convergence of the reaction integrals and tabulation of Green's functions, can be time consuming and require expensive computations. In addition, these methods of analysis do not produce equivalent circuit models which are suitable for small-scale CAD computations.

Although not as rigorous as the above full-wave analyses, the cavity model [6, 7] can readily be used to derive equivalent circuit models of the antennas for implementation of small-scale CAD. It has been shown that in the cavity model the antenna substrate thickness must be much less than the free-space wavelength [8], a condition normally satisfied in the design of microstrip patch antenna structures.

In this paper the cavity model has been used to model a circularly polarised nearly square patch antenna, excited using a microstrip feed line via a symmetrical cross-slot

[1, 2, 9]. In contrast to a single slot structure the cross-slot structure allows the use of slot length greater than half the patch width; hence the matching condition is maintained over a wider bandwidth. In addition, the equal cross slots provide symmetry of excitation of the patch and ensure generation of circular polarisation with good axial ratio [2, 10]. An equivalent circuit model has been derived and used to determine the input impedance of the antenna and further, based on the derived equivalent circuit the conditions for producing a good axial ratio are also examined. It is shown that there is a close agreement between the practical results and those predicted by the cavity model approach.

2 Field distribution

The structure of the antenna using a symmetrical cross-slot is shown in Fig. 1, where it is assumed that the electric field distribution in each of the two orthogonal apertures is in the form of a single piece-wise sinusoidal mode [3]. The electric field in the aperture parallel to the y axis has only an x-directed component E_{ax}, given by

$$E_{ax} = \frac{V_{0y}}{W_a} \frac{\sin\left[k_a\left(\frac{L_a}{2} - \left|y - \frac{b}{2}\right|\right)\right]}{\sin\left(k_a \frac{L_a}{2}\right)} \quad \begin{array}{c} \frac{a-W_a}{2} \leq x \leq \frac{a+W_a}{2} \\ \frac{b-L_a}{2} \leq y \leq \frac{b-L_a}{2} \\ z = 0 \end{array}$$

$$= 0, \qquad\qquad \text{otherwise} \tag{1}$$

where V_{0y} is the voltage at the centre of the aperture parallel to the y axis and k_a is the wave number of the aperture determined by Cohn's method [11]. Similarly, the electric field in the aperture parallel to the x axis has only a y component E_{ay} given by

$$E_{ay} = \frac{V_{0x}}{W_a} \frac{\sin\left[k_a\left(\frac{L_a}{2} - \left|x - \frac{b}{2}\right|\right)\right]}{\sin\left(k_a \frac{L_a}{2}\right)} \quad \begin{array}{c} \frac{a-L_a}{2} \leq x \leq \frac{a+L_a}{2} \\ \frac{b-W_a}{2} \leq y \leq \frac{b-W_a}{2} \\ z = 0 \end{array}$$

$$= 0, \qquad\qquad \text{otherwise} \tag{2}$$

where V_{0x} is the voltage at the middle of the aperture parallel to the x axis.

IEE Proc.-Microw. Antennas Propag., Vol. 148, No. 3, June 2001

147

Fig. 1 *Design parameters of cross-aperture coupled microstrip antenna*
$a = 32.1\,\text{mm}$, $b = 34.5\,\text{mm}$, $W = 4.724\,\text{mm}$, $L_{os} = 9\,\text{mm}$, $L_a = 18\,\text{mm}$, $W_a = 2\,\text{mm}$, $\varepsilon_{ra} = 2.33$, $\varepsilon_{rf} = 2.33$, $d_a = 3.15\,\text{mm}$, $d_f = 1.575\,\text{mm}$, $\phi_s = \pm 45°$

The cavity models [12] assumes that the tangential magnetic field at the cavity side walls is zero to a good approximation, and, by the equivalence principle [12], the magnetic currents in each of the two apertures just above the ground plane are then given by

$$M_{ax} = -2E_{ay} \tag{3}$$

and

$$M_{ay} = 2E_{ax} \tag{4}$$

Fig. 2 *Equivalent magnetic currents replacing electric fields in aperture*

The equivalent magnetic current density excitation is assumed to be uniformly distributed in the cavity volume above the slot [13] as shown in Fig. 2. The corresponding current densities J_{mx} and J_{my} in the aperture cavities are therefore given by

$$J_{mx} = \frac{-2V_{0x}}{d_a W_a} \frac{\sin\left[k_a\left(\frac{L_a}{2} - |x - \frac{a}{2}|\right)\right]}{\sin\left(k_a \frac{L_a}{2}\right)} \quad \begin{array}{c} \frac{a-L_a}{2} \le x \le \frac{a+L_a}{2} \\ \frac{b-W_a}{2} \le y \le \frac{b+W_a}{2} \\ 0 \le z \le d_a \end{array}$$

$$= 0, \qquad \qquad \text{otherwise} \tag{5}$$

and

$$J_{my} = \frac{2V_{0y}}{d_a W_a} \frac{\sin\left[k_a\left(\frac{L_a}{2} - |y - \frac{b}{2}|\right)\right]}{\sin\left(k_a \frac{L_a}{2}\right)} \quad \begin{array}{c} \frac{a-W_a}{2} \le x \le \frac{a+W_a}{2} \\ \frac{b-L_a}{2} \le y \le \frac{b+L_a}{2} \\ 0 \le z \le d_a \end{array}$$

$$= 0, \qquad \qquad \text{otherwise} \tag{6}$$

The magnetic field H inside the cavity volume due to the magnetic current density J_m is given by Maxwell's equation

$$\nabla \times \nabla \times \boldsymbol{H} - k^2 \boldsymbol{H} = -j\omega\mu_0 \boldsymbol{J}_m \tag{7}$$

For the magnetic fields H_x, H_y which only have x and y components, eqn. 7 reduces to the following two differential equations:

$$\frac{\partial^2 H_y}{\partial x \partial y} - \frac{\partial^2 H_x}{\partial y^2} - k^2 H_x = -j\omega\mu_0 J_{mx} \tag{8}$$

$$\frac{\partial^2 H_x}{\partial x \partial y} - \frac{\partial^2 H_y}{\partial y^2} - k^2 H_y = -j\omega\mu_0 J_{my} \tag{9}$$

The solution of the above differential equations can be expressed in the following eigenfunction expansion form

$$H_x = \sum_m \sum_n B_{x,mn} \Psi_{x,mn} \tag{10}$$

$$H_y = \sum_m \sum_n B_{y,mn} \Psi_{y,mn} \tag{11}$$

where $B_{x,mn}$ and $B_{y,mn}$ are the unknown mode coefficients and $\Psi_{x,mn}$ and $\Psi_{y,mn}$ are the eigenfunction of eqns. 8 and 9. The eigenfunction must satisfy the associated homogenous equations and hence

$$\frac{\partial_2 \Psi_{x,mn}}{\partial x \partial y} - \frac{\partial^2 \Psi_{y,mn}}{\partial y^2} - k_{mn} \Psi_{x,mn} = 0 \tag{12}$$

$$\frac{\partial_2 \Psi_{y,mn}}{\partial x \partial y} - \frac{\partial^2 \Psi_{x,mn}}{\partial y^2} - k_{mn} \Psi_{y,mn} = 0 \tag{13}$$

where k_{mn} are the associated eigenvalues. The boundary conditions on the four magnetic walls are

$$\Psi_{x,mn} = 0 \text{ at } y = 0 \text{ and } y = b$$
$$\Psi_{y,mn} = 0 \text{ at } x = 0 \text{ and } x = a \tag{14}$$

The eigenfunctions are given by

$$\Psi_{x,mn} = A_{mn} . k_n . \cos(k_m x) \sin(k_n y) \tag{15}$$

$$\Psi_{y,mn} = A_{mn} . k_n . \cos(k_n y) \sin(k_m x) \tag{16}$$

with

$$A_{mn} = \sqrt{\frac{\chi_m \chi_n}{ab}}, \text{ where } \chi_p = \begin{cases} 1 & \text{if } p = 0 \\ 2 & \text{if } p \ne 0 \end{cases} \tag{17}$$

and

$$k_m = \frac{m.\pi}{a}, \qquad k_n = \frac{n.\pi}{b} \tag{18}$$

The mode coefficients $B_{x,mn}$ and $B_{y,mn}$ can be found by substituting for H_x and H_y from eqns. 10 and 11 into the non-homogeneous differential eqns. 8 and 9 to give

$$\sum_m \sum_n B_{x,mn}(k_{mn}^2 - k^2)\Psi_{x,mn} = -j\omega\varepsilon J_{mx} \tag{19}$$

and,

$$\sum_m \sum_n B_{y,mn}(k_{mn}^2 - k^2)\Psi_{y,mn} = -j\omega\varepsilon J_{my} \tag{20}$$

Multiplying eqn. 19 with the mode function $\Psi_{x,m'n'}$ and eqn. 20 by $\Psi_{y,m'n'}$ and integrating over the cavity volume of

148

IEE Proc.-Microw. Antennas Propag., Vol. 148, No. 3, June 2001

195

$$\sum_m \sum_n B_{x,mn}(k_{mn}^2 - k^2) \int_0^a \int_0^b \Psi_{x,mn} \Psi_{x,m'n'} dxdy$$

$$= -j\omega\varepsilon \int_0^a \int_0^b J_{mx} \Psi_{x,m'n'} dxdy \qquad (21)$$

and,

$$\sum_m \sum_n B_{y,mn}(k_{mn}^2 - k^2) \int_0^a \int_0^b \Psi_{y,mn} \Psi_{y,m'n'} dxdy$$

$$= -j\omega\varepsilon \int_0^a \int_0^b J_{my} \Psi_{y,m'n'} dxdy \qquad (22)$$

The orthogonal properties of $\Psi_{x,mn}$ and $\Psi_{y,mn}$ are

$$\int_0^a \int_0^b \Psi_{x,mn} \Psi_{x,m'n'} dxdy$$

$$= \begin{cases} k_n^2 & \text{if } m = m' \text{ and } n = n' \\ 0 & \text{otherwise} \end{cases} \qquad (23)$$

$$\int_0^a \int_0^b \Psi_{y,mn} \Psi_{y,m'n'} dxdy$$

$$= \begin{cases} k_m^2 & \text{if } m = m' \text{ and } n = n' \\ 0 & \text{otherwise} \end{cases} \qquad (24)$$

hence

$$B_{x,mn} = \frac{j\omega\varepsilon}{(k^2 - k_{mn}^2) \cdot k_n^2} \int_0^a \int_0^b J_{mx} \Psi_{x,mn} dxdy \qquad (25)$$

$$B_{y,mn} = \frac{j\omega\varepsilon}{(k^2 - k_{mn}^2) \cdot k_m^2} \int_0^a \int_0^b J_{my} \Psi_{y,mn} dxdy \qquad (26)$$

Substituting for J_{mx}, J_{my}, $\Psi_{x,mn}$ and $\Psi_{y,mn}$ integrating eqns. 25 and 26 gives

$$B_{x,mn} = \frac{-j\omega\varepsilon . A_{mn} V_{0x}}{d_a k_n \cdot (k^2 - k_{mn}^2)} \cdot$$

$$\frac{4 \operatorname{sinc}\left(k_n \frac{W_a}{2}\right) \sin\left(\frac{n\pi}{2}\right) \cos\left(\frac{m\pi}{2}\right)}{\sin\left(k_a \frac{L_a}{2}\right)} \cdot$$

$$\frac{k_a \left[\cos\left(k_m \frac{L_a}{2}\right) - \cos\left(k_a \frac{L_a}{2}\right)\right]}{k_a^2 - k_m^2} \qquad (27)$$

$$B_{y,mn} = \frac{-j\omega\varepsilon . A_{mn} V_{0y}}{d_a k_m \cdot (k^2 - k_{mn}^2)} \cdot$$

$$\frac{4 \operatorname{sinc}\left(k_m \frac{W_a}{2}\right) \sin\left(\frac{m\pi}{2}\right) \cos\left(\frac{n\pi}{2}\right)}{\sin\left(k_a \frac{L_a}{2}\right)} \cdot$$

$$\frac{k_a \left[\cos\left(k_n \frac{L_a}{2}\right) - \cos\left(k_a \frac{L_a}{2}\right)\right]}{k_a^2 - k_n^2} \qquad (28)$$

With the known mode coefficients the components of the magnetic field in the patch cavity are given by

$$H_x = \sum_m \sum_n A_{mn} B_{x,mn} k_n \cos(k_m x) \sin(k_n y) \qquad (29)$$

$$H_y = \sum_m \sum_n A_{mn} B_{y,mn} k_m \sin(k_m x) \cos(k_n y) \qquad (30)$$

Finally the electric field E_z can be determined from the Maxwell equation

$$E_{z(x,y)} = \frac{1}{j\omega\varepsilon}\left[\frac{dH_y}{dx} - \frac{dH_x}{dy}\right] \qquad (31)$$

giving

$$E_{z(x,y)} = \frac{1}{j\omega\varepsilon} \sum_m \sum_n A_{mn} C_{mn} \cos(k_m x) \cos(k_n y) \qquad (32)$$

where

$$C_{mn} = B_{x,mn} k_m^2 - B_{y,mn} k_n^2 \qquad (33)$$

Hence, the electromagnetic fields in the volume of the patch are now known and defined by eqns. 29, 30 and 32. The losses in the cavity can also be taken into account by replacing k by an effective wave number [5]

$$k_{eff}^2 = k_0^2 \varepsilon_r (1 - j\delta_{eff}) \qquad (34)$$

where δ_{eff} is the effective loss tangent, which includes the radiation and copper dielectric losses [14].

3 Input impedance

The admittances of the patch of the two orthogonal apertures can be evaluated using the energy conservation theorem [12] and are given by

$$Y_{x,ant} = \frac{\iiint_V H_x J_{mx}^* dv}{|V_{0x}|^2}$$

$$\text{and } Y_{y,ant} = \frac{\iiint_V H_y J_{my}^* dv}{|V_{0y}|^2} \qquad (35)$$

Substituting the expression for the magnetic field from eqns. 29 and 30 and the magnetic current density from eqns. 5 and 6, and performing the integration, the following analytical formulas are obtained for the admittance values of the antenna at the apertures:

$$Y_{x,ant} = \sum_m \sum_n \frac{16 \cdot j\omega\varepsilon \cdot A_{mn}^2}{d_a \left((k^*)^2 - k_{mn}^2\right)} \cdot$$

$$\left\{ \frac{\operatorname{sinc}\left(k_n \frac{W_a}{2}\right) \sin\left(\frac{n\pi}{2}\right) \cos\left(\frac{m\pi}{2}\right)}{\sin\left(k_a \frac{L_a}{2}\right)} \cdot \right.$$

$$\left. \frac{k_a \left[\cos\left(k_m \frac{L_a}{2}\right) - \cos\left(k_a \frac{L_a}{2}\right)\right]}{k_a^2 - k_m^2} \right\}^2 \qquad (36)$$

$$Y_{y,ant} = \sum_m \sum_n \frac{16 \cdot j\omega\varepsilon \cdot A_{mn}^2}{d_a \left((k^*)^2 - k_{mn}^2\right)} \cdot$$

$$\left\{ \frac{\operatorname{sinc}\left(k_m \frac{W_a}{2}\right) \sin\left(\frac{m\pi}{2}\right) \cos\left(\frac{n\pi}{2}\right)}{\sin\left(k_a \frac{L_a}{2}\right)} \cdot \right.$$

$$\left. \frac{k_a \left[\cos\left(k_n \frac{L_a}{2}\right) - \cos\left(k_a \frac{L_a}{2}\right)\right]}{k_a^2 - k_n^2} \right\}^2 \qquad (37)$$

The self-admittance of the aperture is obtained by considering it as two short-circuited slot lines of length $L_a/2$, and, is thus given by

$$Y_{ap} = -\frac{2j}{Z_{ca}} \cot\left(k_a \frac{L_a}{2}\right) \qquad (38)$$

Finally, the input impedance of the antenna is given by the following expression:

$$Z_{in} = \frac{n^2}{Y_{x,ant} + Y_{ap}} + \frac{n^2}{Y_{y,ant} + Y_{ap}} - jZ_f \cot(k_f L_{os}) \qquad (39)$$

where n is the turns ratio of the microstrip to aperture impedance transformation for the two orthogonal apertures, k_f is the wave number of the feed line [10, 13].
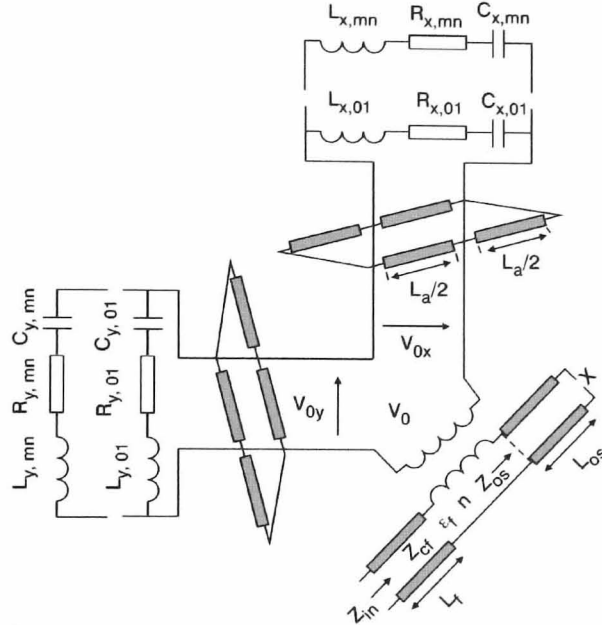

Fig. 3 *Equivalent circuit based on cavity model*

4 Equivalent circuit

Using the developed analytic expressions (see eqns. 36 and 37) for the patch admittances at the apertures, it is possible to draw an equivalent circuit of the cross-aperture coupled CP antenna based on the cavity method as shown in Fig. 3. Eqns. 36 and 37 can be written in the form

$$Y_{x,ant} = \sum_m \sum_n \frac{16 \cdot j\omega\varepsilon \cdot A_{mn}^2}{d_a[\omega^2 - \omega_{mn}^2]\left(1 + j\delta_{eff}\frac{\omega^2}{\omega_{mn}^2}\right)} \cdot$$
$$\left\{\frac{\text{sinc}\left(k_n \frac{W_a}{2}\right) \sin\left(\frac{n\pi}{2}\right) \cos\left(\frac{m\pi}{2}\right)}{\sin\left(k_a \frac{L_a}{2}\right)} \cdot \right.$$
$$\left. \frac{k_a\left[\cos\left(k_m \frac{L_a}{2}\right) - \cos\left(k_a \frac{L_a}{2}\right)\right]}{k_a^2 - k_m^2}\right\}^2 \qquad (40)$$

$$Y_{y,ant} = \sum_m \sum_n \frac{16 \cdot j\omega\varepsilon \cdot A_{mn}^2}{d_a[\omega^2 - \omega_{mn}^2]\left(1 + j\delta_{eff}\frac{\omega^2}{\omega_{mn}^2}\right)} \cdot$$
$$\left\{\frac{\text{sinc}\left(k_m \frac{W_a}{2}\right) \sin\left(\frac{m\pi}{2}\right) \cos\left(\frac{n\pi}{2}\right)}{\sin\left(k_a \frac{L_a}{2}\right)} \cdot \right.$$
$$\left. \frac{k_a\left[\cos\left(k_n \frac{L_a}{2}\right) - \cos\left(k_a \frac{L_a}{2}\right)\right]}{k_a^2 - k_n^2}\right\}^2 \qquad (41)$$

Each of these formulas corresponds to the expression of the

admittance of $m \times n$ series RCL circuits, which are all connected in parallel (see Fig. 3). The equivalent circuit of the patch admittance, as seen by the slot parallel to the y axis, have the following circuit elements:

$$L_{x,mn} = \frac{d_a}{16\varepsilon c^2 A_{mn}^2} \cdot$$
$$\left\{\frac{\text{sinc}\left(k_n \frac{W_a}{2}\right) \sin\left(\frac{n\pi}{2}\right) \cos\left(\frac{m\pi}{2}\right)}{\sin\left(k_a \frac{L_a}{2}\right)} \cdot \right.$$
$$\left. \frac{k_a\left[\cos\left(k_m \frac{L_a}{2}\right) - \cos\left(k_a \frac{L_a}{2}\right)\right]}{k_a^2 - k_m^2}\right\}^2$$

$$C_{x,mn} = L_{x,mn}^{-1} \frac{\varepsilon_{ra} k_{mn}^2}{c^2} \qquad R_{x,mn} = L_{x,mn} k_{mn} c \delta_{eff} \qquad (42)$$

Similarly, the equivalent circuit of the patch, as seen by the slot parallel to the x axis, have circuit elements:

$$L_{y,mn} = \frac{d_a}{16\varepsilon c^2 A_{mn}^2} \cdot$$
$$\left\{\frac{\text{sinc}\left(k_m \frac{W_a}{2}\right) \sin\left(\frac{m\pi}{2}\right) \cos\left(\frac{n\pi}{2}\right)}{\sin\left(k_a \frac{L_a}{2}\right)} \cdot \right.$$
$$\left. \frac{k_a\left[\cos\left(k_n \frac{L_a}{2}\right) - \cos\left(k_a \frac{L_a}{2}\right)\right]}{k_a^2 - k_n^2}\right\}^2$$

$$C_{y,mn} = L_{y,mn}^{-1} \frac{\varepsilon_{ra} k_{mn}^2}{c^2} \qquad R_{y,mn} = L_{y,mn} k_{mn} c \delta_{eff} \qquad (43)$$

5 Axial ratio

For the calculation of the axial ratio, the far field components of the antenna are first determined in the boresight. This is performed by replacing the electrical field at the edges of the patch by equivalent magnetic currents as given by [15]

$$\boldsymbol{M} = 2d_a \cdot E_{z(x,y)} \cdot \boldsymbol{z} \times \boldsymbol{n} \qquad (44)$$

where n is the outward normal unit vector to the magnetic wall at the edges of the patch. Substituting the expression of the electric field from eqn. 32 gives the following values of magnetic currents at the four edges of the patch:

$$M_{x(x,y=0)} = \frac{d_a}{j\omega\varepsilon} \sum_m \sum_n A_{mn} C_{mn} \cos(k_m x) \qquad (45)$$

$$M_{x(x,y=b)} = -\frac{d_a}{j\omega\varepsilon} \sum_m \sum_n A_{mn} C_{mn} \cos(k_m x) \cdot (-1)^n \qquad (46)$$

$$M_{y(x=0,y)} = \frac{d_a}{j\omega\varepsilon} \sum_m \sum_n A_{mn} C_{mn} \cos(k_n y) \qquad (47)$$

$$M_{y(x=a,y)} = -\frac{d_a}{j\omega\varepsilon} \sum_m \sum_n A_{mn} C_{mn} \cos(k_n y) \cdot (-1)^m \qquad (48)$$

The electrical field $E(r)$ caused by an infinitesimally small magnetic current element (dM) is obtained as

$$\boldsymbol{E}(\boldsymbol{r}) = \frac{jk_0 e^{-jk_0 r}}{4\pi r} \cdot \boldsymbol{r} \times d\boldsymbol{M} \qquad (49)$$

150

IEE Proc.-Microw. Antennas Propag., Vol. 148, No. 3, June 2001

current element to the observation point and r is the distance between the magnetic current and the observation point. The electric field radiated by the patch is obtained by integrating eqn. 49 along the edges of the patch. In the boresight, the components of the electric field are, therefore, given by

$$E_x = \frac{d_a k_0 e^{-jk_0 r}}{4\pi\omega\varepsilon r} \cdot \int_0^b \left(\sum_m \sum_n A_{mn} C_{mn} \cos(k_n y) \cdot \right.$$
$$\left. (-1)^m - \sum_m \sum_n A_{mn} C_{mn} \cos(k_n y) \right) dy$$

$$(50)$$

$$E_y = \frac{d_a k_0 e^{-jk_0 r}}{4\pi\omega\varepsilon r} \cdot \int_0^a \left(\sum_m \sum_n A_{mn} C_{mn} \cos(k_m y) \right.$$
$$\left. - \sum_m \sum_n A_{mn} C_{mn} \cos(k_m y) \cdot (-1)^n \right) dx$$

$$(51)$$

which simplify to

$$E_x = \frac{d_a k_0 e^{-jk_0 r}}{4\pi\omega\varepsilon r} \cdot \sum_m \sum_n A_{mn} C_{mn} \cdot [(-1)^m - 1]$$

$$(52)$$

$$E_y = \frac{d_a k_0 e^{-jk_0 r}}{4\pi\omega\varepsilon r} \cdot \sum_m \sum_n A_{mn} C_{mn} \cdot [1 - (-1)^n]$$

$$(53)$$

where,

$$C_{m0} = \begin{cases} -B_{y,m0} & \text{if } m \text{ odd} \\ 0 & \text{if } m \text{ even} \end{cases}$$

$$(54)$$

$$C_{0n} = \begin{cases} B_{x,0n} & \text{if } n \text{ odd} \\ 0 & \text{if } n \text{ even} \end{cases}$$

$$(55)$$

Therefore

$$E_x = \frac{d_a k_0 e^{-jk_0 r}}{4\pi\omega\varepsilon r} \cdot \sum_m A_{m0} B_{y,m0}$$

$$(56)$$

$$E_y = \frac{d_a k_0 e^{-jk_0 r}}{4\pi\omega\varepsilon r} \cdot \sum_n A_{0n} B_{x,0n}$$

$$(57)$$

The expressions for $B_{x,0n}$ and $B_{y,m0}$ can be written in the following form:

$$B_{x,0n} = V_{0x} \cdot B'_{x,0n}$$

$$(58)$$

$$B_{y,m0} = V_{0y} \cdot B'_{y,m0}$$

$$(59)$$

where

$$B'_{x,0n} = \frac{j\omega\varepsilon . A_{m0}}{d_a k_n \cdot (k^2 - k_n^2)} \cdot$$
$$\frac{4\operatorname{sinc}\left(k_n \frac{W_a}{2}\right) \sin\left(\frac{n\pi}{2}\right)}{\sin\left(k_a \frac{L_a}{2}\right)} \cdot \frac{k_a \left[1 - \cos\left(k_a \frac{L_a}{2}\right)\right]}{k_a^2} \quad (60)$$

$$B'_{y,m0} = \frac{j\omega\varepsilon . A_{0n}}{d_a k_n \cdot (k^2 - k_m^2)} \cdot$$
$$\frac{4\operatorname{sinc}\left(k_m \frac{W_a}{2}\right) \sin\left(\frac{m\pi}{2}\right)}{\sin\left(k_a \frac{L_a}{2}\right)} \cdot \frac{k_a \left[1 - \cos\left(k_a \frac{L_a}{2}\right)\right]}{k_a^2} \quad (61)$$

From the equivalent circuit, the voltages V_{0x} and V_{0y} can be expressed as

$$V_{0x} = V_0 \cdot \frac{(Y_{x,ant} + Y_{ap})^{-1}}{(Y_{x,ant} + Y_{ap})^{-1} + (Y_{y,ant} + Y_{ap})^{-1}}$$

$$(62)$$

$$V_{0y} = V_0 \cdot \frac{(Y_{y,ant} + Y_{ap})^{-1}}{(Y_{x,ant} + Y_{ap})^{-1} + (Y_{y,ant} + Y_{ap})^{-1}}$$

$$(63)$$

Substituting these results into the expressions for the electric field components in the boresight gives the computational formulas for the field components E_x and E_y

$$E_x = \frac{V_0 d_a k_0 e^{-jk_0 r}}{2\pi\omega\varepsilon r} \cdot$$
$$\frac{(Y_{x,ant} + Y_{ap})^{-1}}{(Y_{x,ant} + Y_{ap})^{-1} + (Y_{y,ant} + Y_{ap})^{-1}} \cdot \sum A_{m0} B'_{y,m0}$$

$$(64)$$

and

$$E_y = \frac{V_0 d_a k_0 e^{-jk_0 r}}{2\pi\omega\varepsilon r} \cdot$$
$$\frac{(Y_{y,ant} + Y_{ap})^{-1}}{(Y_{x,ant} + Y_{ap})^{-1} + (Y_{y,ant} + Y_{ap})^{-1}} \cdot \sum A_{0n} B'_{x,0n}$$

$$(65)$$

The amplitude error (A_e) and phase error (ϕ_e) required for the calculation of the axial ratio can be expressed as

$$A_e = \frac{|E_x|}{|E_y|} = \frac{|Y_{y,ant} + Y_{ap}|}{|Y_{x,ant} + Y_{ap}|} \cdot \frac{\left|\sum_m A_{m0} B'_{y,m0}\right|}{\left|\sum_n A_{0n} B'_{x,0n}\right|} \quad (66)$$

$$\phi_e = \angle\left(\frac{E_x}{E_y}\right) = \angle\left(\frac{Y_{y,ant} + Y_{ap}}{Y_{x,ant} + Y_{ap}} \cdot \frac{\sum_m A_{m0} B'_{y,m0}}{\sum_n A_{0n} B'_{x,0n}}\right)$$

$$(67)$$

Finally, the value of axial ratio is calculated by [12]

$$AR = \sqrt{\frac{1 + A_e^2 + [1 + A_e^4 + 2A_e^2 \cos(2\phi_e)]^{1/2}}{1 + A_e^2 - [1 + A_e^4 + 2A_e^2 \cos(2\phi_e)]^{1/2}}}$$

$$(68)$$

Eqns. 66 and 67, based on the resonant cavity model, provide a numerical means of determining the axial ratio of the cross-aperture coupled patch antenna at a given frequency when the design parameters shown in Fig. 1 are known.

6 Comparison of cavity method, full wave simulation and experimental results

The input impedance of the antenna with the dimensions in Fig. 1 has been calculated over a frequency range of 2.25–2.7GHz. It can be seen from Fig. 4 that the comparison for the input impedance between cavity model, full wave simulation Ensemble® [16] and experimental results are in good agreement. The impedance loci with the double resonance loop corresponding to the orthogonal modes also demonstrates that good circular polarisation has been achieved. Calculated resonant frequency from the cavity

151

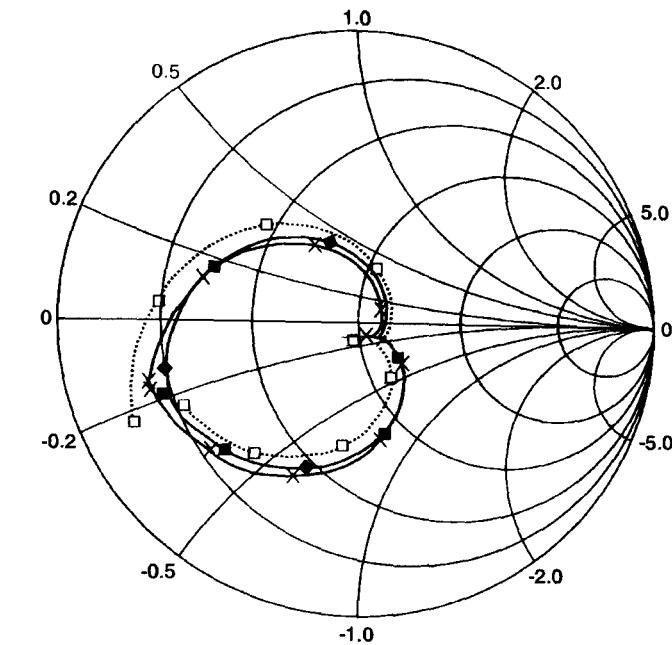...th that obtained experimentally and from full-wave simulation.

Fig. 4 *Input impedance of cross-aperture coupled antenna Fig. 1*
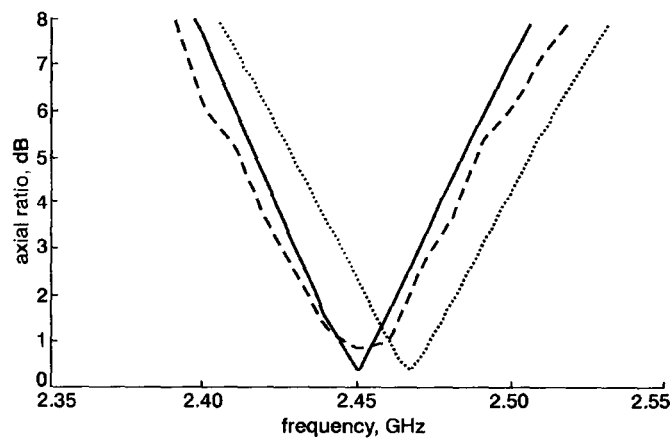- -☐- - cavity model
- ●— full-wave simulation
- —X— experimental results

Fig. 5 *Axial ratio of cross-aperture coupled antenna Fig. 1*
- ·········· cavity model
- ———— full-wave simulation
- — — — experimental results

The axial ratio (see Fig. 5) has also been evaluated using the cavity model, simulated using Ensemble and practically measured. The prediction of the frequency for the best axial ratio is accurate to about 2% while that prediction of the axial ratio bandwidth is within the range of 10%, when compared with experimental results.

7 Conclusions

Based on the cavity model of the equal cross-slots structure, this paper has presented a theoretical analysis to determine the modal fields under the patch antenna. Using these fields an equivalent circuit of the antenna has been derived which is then used to determine the input impedance and the axial ratio of the circular polarised antenna. This cavity model has been used successfully to design a circular polarised impedance matched antenna. The results based on the cavity model show a good agreement with full-wave simulation and practical results.

8 References

1   POZAR, D.M.: 'Microstrip antenna Aaperture coupled to a microstrip line', *Electron. Lett.*, 1985, 21, (2), pp. 49–50
2   TARGONSKI, S.D., and POZAR, D.M.: 'Design of widband circularly polarised aperture-coupled microstrip antennas', *IEEE Trans. Antennas Propag.*, 1993, 41, (2), pp. 214–220
3   SULLIVAN, P.L., and SCHAUBERT, D.H.: 'Analysis of an aperture coupling microstrip antenna', *IEEE Trans. Antennas Propag.*, 1986, AP-34, pp. 977–984
4   POZAR, D.M.: 'A reciprocity method of analysis for printed slot and slot-coupled microstrip antennas', *IEEE Trans. Antennas Propag.*, 1986, AP-34, (12), pp. 1439–1446
5   BARLATELY, L., SMITH, H.K., and MOSIG, J.R.: 'Printed radiating structures and transitions in multilayered substrates', *Int. J. Microw. Milimeter-Wave Computer-Aided Engineering*, 1992, 2, pp. 273–285
6   LO, Y.T., ENGST, B., and LEE, R.Q.: 'Simple design formulas for circularly polarised microstrip antennas', *IEE Proc.-H*, 1988, 135, pp. 213–215
7   AKSON, M.I., and CHUANG, S.L.: 'On slot-coupled microstrip antennas and their applications to CP operation-theory and experiment', *IEEE Trans. Antennas Propag.*, 1990, AP-38, (8), pp. 1224–1230
8   RICHARDS, W.F., LO, Y.T., and HARRISON, D.D.: 'An improved theory for microstrip antennas and applications', *IEEE Trans. Antennas Propag.*, 1981, AP-29, pp. 38–46
9   TASO, C.H., HWANG, Y.M., KILLBURG, F., and DIETRICH, F.: 'Aperture-coupled patch antennas with wide-bandwidth and dual polarisation capabilities', *IEEE Antennas Propag. Symp. Dig.*, 1988, pp. 936–939
10 ALJIBOURI, B., VLASITS, T., KOROLKIEWICZ, E., SCOTT, S., and SAMBELL, A.: 'Transmission line modelling of the crossaperture-coupled circular polarised microstrip patch antenn', *IEE Proc. Microw., Antennas Propag.*, 2000, 147, (2), pp. 82–86
11 CHON, S.B.: 'Slot line on a dielectric substrate', *IEEE Trans. Microw. Theory Techn.*, 1969, 17, (10), pp. 786–778
12 BALAINS, C.A.: 'Antenna theory: analysis and design' (Wiley & sons, 1989)
13 HIMDI, M., DANIEL, J.P., and TERRENT, C.: 'Analysis of aperture-coupled microstrip antenna using cavity method', *Electron. Lett.*, 1991, 27, (5), pp. 455–457
14 THOUROUDDE, D., HIMDI, M., and DANIEL, J.P.: 'Cad-oriented cavity model for rectangular patches', *Electron. Lett.*, 1990, 26, (13), pp. 842–844
15 CARVER, K.R, and MINK, J.W.: 'Microstrip antenna technolog', *IEEE Trans. Antennas Propag.*, 1981, AP-29, (1), pp. 2–24
16 ANSOFT Corporation, Ensemble 5.1, 1998

152

199

Performance of 4 × 4 sequentially rotated patch antenna array using series feed

H. Evans, P. Gale and A. Sambell

A new 4 × 4 sequentially rotated patch antenna array using an out-of-line series feed network is presented. The use of a series feed is shown to increase input impedance bandwidth and axial ratio bandwidth compared with a corporate feed when used in this sequentially rotated array. Performance is confirmed by full-wave simulation and experimental measurement, demonstrating a voltage standing wave ratio 2:1 bandwidth of 14.7% and a 3 dB axial ratio bandwidth of 12.4%.

Introduction: Microstrip arrays, due to their very thin profiles, offer three main advantages over other types of antenna array: low weight, low profile with conformability and low manufacturing costs. However, these advantages are offset by inherent limitations such as small bandwidth (<5%) and relatively high feed line losses [1].

Sequential rotation of radiating elements has been shown to increase the input impedance bandwidth, polarisation purity and the radiation pattern symmetry of microstrip patch antenna arrays [2]. Much work has since been undertaken on the design and application of sequential rotation using a corporate feed network [3–5].

Within a traditional corporate feed network, both power splitting and excitation phase remain equal away from design frequency, as the distance from each radiating element to the feed point is equal. This is no longer the case when a corporate feed is used in a sequentially rotated array because of the delays in excitation that are required to compensate for the physical rotation of each radiating element.

Series-fed patch antenna arrays have the advantages of being less complex, requiring less real estate and often having lower loss than corporate feed networks. However, it is more problematic to maintain equal excitation amplitude and phase away from the design frequency. Despite these disadvantages, practical designs have been shown to demonstrate very good performance [6].

In this Letter we present a new series-fed 4 × 4 antenna array constructed from sequentially rotated 2 × 2 sub-arrays that demonstrates improvement in both input impedance and axial ratio bandwidth over the same array using a corporate feed. This array has been used as part of a high-speed two-way digital communication link between a moving vehicle and a roadside beacon in a commercial traffic management system.
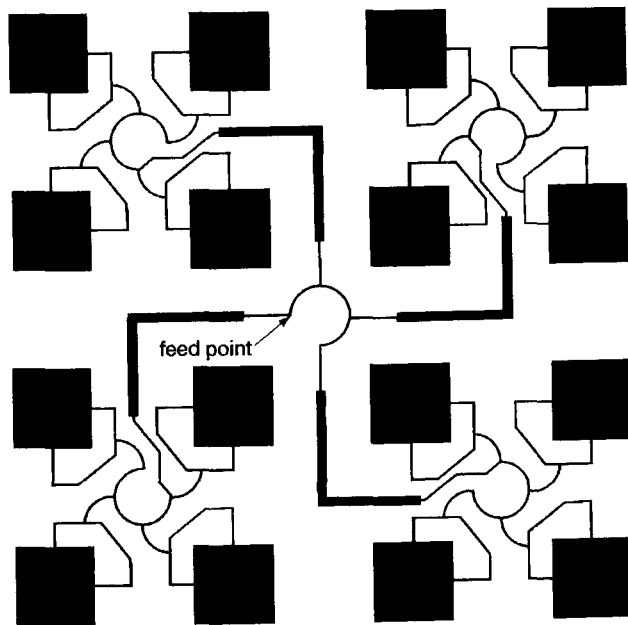

Fig. 1 *Configuration of 4 × 4 sequentially rotated antenna array with dual feed radiating elements and series feed*

Array configuration: The 4 × 4 circularly polarised sequentially rotated patch antenna array is shown in Fig. 1. Non-isolated dual feed circular polarised radiating elements with an input impedance of 50 Ω [7] are spaced at 0.74λ. These radiating elements are sequentially rotated to form the 2 × 2 sub-arrays using the design parameters detailed in [8]. Both power splitting and the necessary phase delay in

each element's excitation are achieved using an out-of-line series feed. Using the same series feeding technique, each 2 × 2 sub-array is then sequentially rotated to form the 4 × 4 array.

The feed network needs to ensure correct excitation phase and equal power distribution to each patch while maintaining impedance matching at the design frequency. These constraints do not uniquely define values for the impedance elements within the feed network, allowing investigation of solutions with other desirable features. As no closed form expression exists, an adaptation of simulated annealing was used to optimise the feed network for minimum track width [8].

Results: A comparison between the series and corporate feed has been made using a parallel RLC circuit (assuming an unloaded Q of 47) to represent each orthogonal mode of radiation for each radiating element and calculating the return loss and axial ratio using standard transmission line theory [9]. From Fig. 2 it can be seen that the calculated voltage standing wave ratio (VSWR) 2:1 bandwidth of the series-fed array is almost twice that of the array using the corporate feed described in [4], while Fig. 3 shows the calculated 3 dB axial ratio increases by more than a factor of 2. This improvement is due to a more favourable phase relationship between the internal reflections within the series feed network away from design frequency.
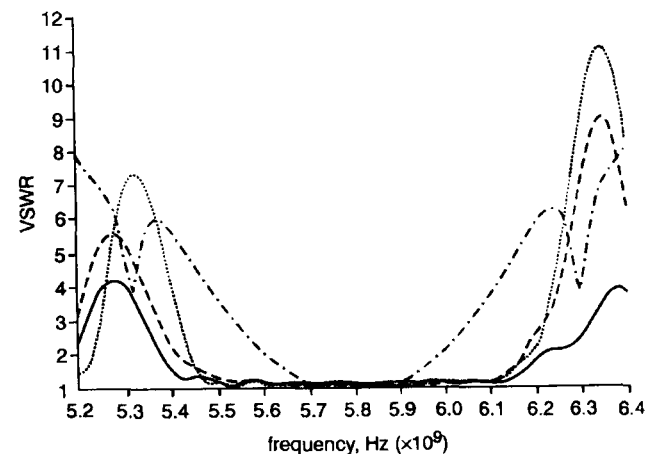

Fig. 2 *Input impedance*

- – – – 4 × 4 corporate-fed array calculated using transmission line theory
- · · · · · · 4 × 4 series-fed array calculated using transmission line theory
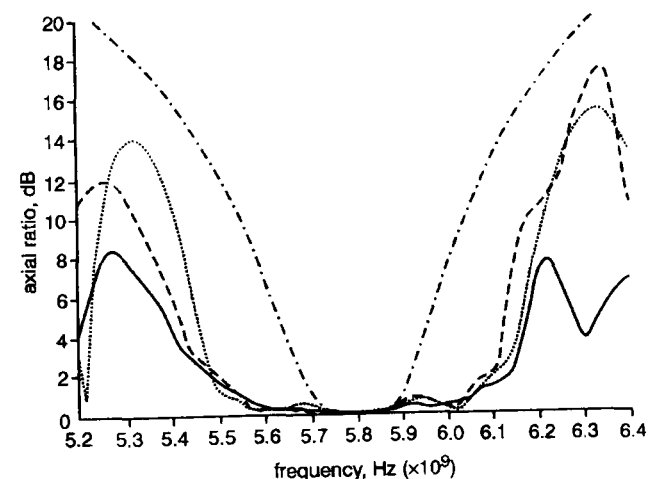- – – – – 4 × 4 series-fed array simulated
- ——— 4 × 4 series-fed array measured

Fig. 3 *Boresight axial ratio*

- – – – 4 × 4 corporate-fed array calculated using transmission line theory
- · · · · · · 4 × 4 series-fed array calculated using transmission line theory
- – – – – 4 × 4 series-fed array simulated
- ——— 4 × 4 series-fed array measured

The series-fed 4 × 4 antenna array was fabricated using 0.79 mm 1/2 oz RT 5870 Duroid ($\varepsilon_r = 2.33$), the integrity of the design was confirmed using full-wave simulation [10] and practical measurement. A VSWR 2:1 bandwidth of 14.7% was measured between 5.38 and 6.23 GHz as seen in Fig. 2 and a 3 dB axial ratio bandwidth of 12.4% was measured between 5.44 and 6.16 GHz as seen in Fig. 3. Both

simulated and measured results are in good agreement with the results calculated using transmission line theory. The normalised radiation pattern of the array can be seen in Fig. 4, with the gain of the mainlobe measured at 18 dBi.
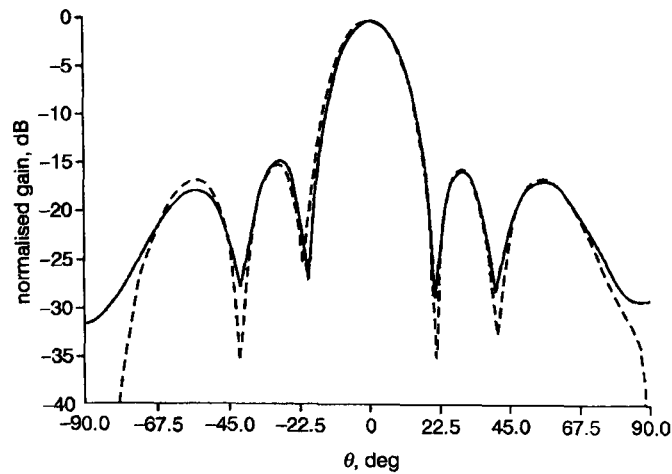

Fig. 4 *Radiation pattern*

- - - - - 4 × 4 series-fed array simulated
———— 4 × 4 series-fed array measured

Conclusion: A 5.8 GHz circular polarised 4 × 4 antenna array composed of sequentially rotated 2 × 2 sub-arrays with a series feed network has been presented. The use of an out-of-line series feed allows a compact structure with enhanced input impedance and axial ratio over a corporate feed when used in this array. The performance of the array has been confirmed both by full-wave simulation and experimental measurement confirming a VSWR 2:1 bandwidth of 14.7% and a 3 dB axial ratio bandwidth of 12.4%.

H. Evans, P. Gale, and A. Sambell (*School of Engineering, University of Northumbria, Ellison Building, Newcastle Upon Tyne, NE1 8ST, United Kingdom*)

E-mail: huw.evans@unn.ac.uk

References

1   HUANG, J., and POZAR, D.M.: 'Advances in microstrip and printed antennas' (John Wiley & Son, 1997), p. 123
2   TESHIROGI, T., TANAKA, M., and CHUJO, W.: 'Wideband circularly polarised array antenna with sequential rotation and phase shifts of elements'. Int. Symp on Antennas and Propagation, ISAP 85, Tokyo, Japan, 1985
3   HALL, P.S., DAHELE, J.S., and JAMES, J.R.: 'Design principles of sequentially fed, wide bandwidth, circularly polarised microstrip patch antennas', *IEE Proc. H*, 1989, **136**, (5), pp. 381–389
4   HALL, P.S.: 'Application of sequential feeding to wide bandwidth, circularly polarised microstrip patch arrays', *IEE Proc., H*, 1989, **136**, (5), pp. 390–398
5   HALL, P.S., and HALL, C.M.: 'Coplanar corporate feed effects in microstrip patch array design', *IEE Proc., H*, 1989, **135**, (3), pp. 180–186
6   POZAR, D.M., and SCHAUBERT, D.H.: 'Comparison of three series-fed micro-strip array geometries'. IEEE Int Symp. Antennas and Propagation Dig., CA, USA, June 1993, pp. 728–731
7   ALJIBOURI, B., LIM, E.G., EVANS, H., and SAMBELL, A.: 'Multiobjective genetic algorithm approach for a dual feed circular polarised patch antenna design', *Electron. Lett.*, 2000, **36**, (12), pp. 1005–1006
8   EVANS, H., GALE, P., ALJIBOURI, B., LIM, E.G., KOROLKEIWICZ, E., and SAMBELL, A.: 'Application of simulated annealing to design of serial feed sequentially rotated 2 × 2 antenna array', *Electron. Lett.*, 2000, **36**, (24), pp. 1987–1988
9   YIP, P.: 'High frequency circuit design and measurement' (Chapman and Hall, 1990)
10   Ansoft Ensemble® V6.1—Method of Moments 2.5 D EM field solver

4. NUMERICAL RESULTS

We straightforwardly apply the proposed algorithm to analyze a typical rectangular microstrip antenna, which is shown in Figure 3.

The excitation is a point-voltage source with a wave form of a Gaussian pulse, which can be written as

$$V_s(t) = \exp\left[-\left(\frac{t - t_0}{T}\right)^2\right], \qquad (3)$$

where the time step used is $\Delta t = 0.441$ ps, the pulse width $T = 15$ ps, and the time delay $t_0 = 3T$. Table 1 shows the two different cases of spatial-grid size tested to compare the error resulting from the numerical dispersion. The size of a unit spatial cell of Case 2 is four times that of Case 1.

Far-field patterns of the rectangular patch of Figure 3 are plotted in Figure 4(a) and (b) for the H-plane and E-plane, respectively. The $S24$ results were computed with Case 2 at a far-field distance $R > 2D^2/\lambda$, for a computational domain of 86 × 42 × 42 unit cells. On the other hand, results from the near-to-far field transformation technique were computed using a unit cell with Case 1, which is much finer than that of the $S24$ computation. It is apparent that the two patterns compare favorably and both are close to that of the cavity model.

5. CONCLUSION

The higher-order FDTD method has the advantages of lower numerical dispersion and its ability to maintain accuracy within an acceptable range. When an electromagnetic wave crosses a PEC boundary, the $S24$ algorithm must be corrected by the PEC shielding process. Using the higher-order FDTD method to analyze the far-field pattern of an antenna allows more flexibility than the near-to-far field transformation technique. The methodology is very simple and existing computer programs can be easily updated by modifying only a small portion of code.

REFERENCES

1. K.S. Yee, Numerical solution of initial boundary value problem involving Maxwell's equations in isotropic media, IEEE Trans Antennas Propagat AP-14 (1966), 302–307.
2. M.F. Hadi and M. Piket-May, A modified FDTD (2,4) scheme for modeling electrically large structure with high-phase accuracy, IEEE Trans Antennas Propagat 45 (1997), 254–264.
3. G. Dolmans, Applicability of higher-order FDTD schemes with Berenger's ABC for indoor fading channels, IEEE Antennas Propagat Soc Int Symp 3 (1997), 1900–1903.
4. O.M. Ramahi, Near- and far-field calculation in FDTD simulations using Kirchhoff surface integral representation, IEEE Trans Antennas Propagat 45 (1997), 753–759.
5. K. Lan, Y. Liu, and W. Lin, A higher-order scheme for reducing dispersion in FDTD algorithm, IEEE Trans Electromagn Compat 41 (1999), 160–165.
6. N.V. Kantartzis and T.D. Tsiboukis, A higher-order FDTD technique for the implementation of enhanced dispersionless perfectly matched layer combined with efficient absorbing boundary conditions, IEEE Trans Magnetics 34 (1998), 2736–2739.
7. A. Taflove, Computational electrodynamics: The finite-difference time-domain method, Artech House, Boston, MA, 1995.

WIDEBAND 2 × 2 SEQUENTIALLY ROTATED PATCH ANTENNA ARRAY WITH A SERIES FEED

H. Evans and A. Sambell
School of Engineering
University of Northumbria
Ellison Building
Newcastle Upon Tyne, NE1 8ST, UK

ABSTRACT: *A new wideband 2 × 2 patch antenna array operating at 5.8 GHz with an out-of-line series feed is presented. Input impedance bandwidth and axial ratio bandwidth are shown to be significantly increased for this new array, which employs a sequential rotation of series-fed, circularly polarised, aperture-coupled radiating elements. The array also maximises the available space on the feed substrate for microwave circuitry. A VSWR 2:1 bandwidth of 22.8% and a 3-dB axial ratio of 17.5% are confirmed by full-wave simulation and experimental measurement.* © 2004 Wiley Periodicals, Inc. Microwave Opt Technol Lett 40: 292–294, 2004; Published online in Wiley InterScience (www.interscience.wiley.com). DOI 10.1002/mop.11356

INTRODUCTION

Microstrip patch antenna arrays are an attractive choice for many modern communication systems due to their light weight, low profile with conformability, ease of manufacture, and compatibility with MMIC designs. A major operational disadvantage is the very narrow frequency bandwidth of the radiating elements, which is only a few percent for a typical patch radiator [1].

One response to this problem is to increase the bandwidth of the individual patch radiators, for example, using a method of aperture coupling in which the radiating patch and feed network are implemented on different substrate materials, thus allowing a patch with a lower Q [2].

Sequential rotation of radiating elements within an array has also been shown to increase both radiation pattern symmetry and the polarization purity of microstrip patch antenna arrays. Furthermore, due to the phase delays necessary in the feed network, these structures also benefit from an increased input impedance bandwidth, as reflections from mismatched radiating elements tend to cancel at the feed point [3, 4].

In a traditional array, a corporate feed is usually favored over a series feed because both the power distribution and excitation phase remain equal away from the design frequency, as the distance from each radiating element to the feed point remains equal. This is not usually the case when a corporate feed is used in a sequentially rotated array because of the delays in excitation that are required to compensate for the physical rotation of each radiating element. Indeed, it has been shown that the use of a series feed in a sequentially rotated array can result in an improvement of both input impedance and axial-ratio bandwidth over a corporate feeding system [5].

This paper presents a new configuration that combines aperture-coupled radiating elements with an out-of-line series feeding system to form a 2 × 2 sequentially rotated left-hand circularly polarised array operating at 5.8 Ghz. This novel combination leads to a compact structure with dramatically increased array bandwidth. Wideband array performance is confirmed by both full-wave simulation and practical measurement.
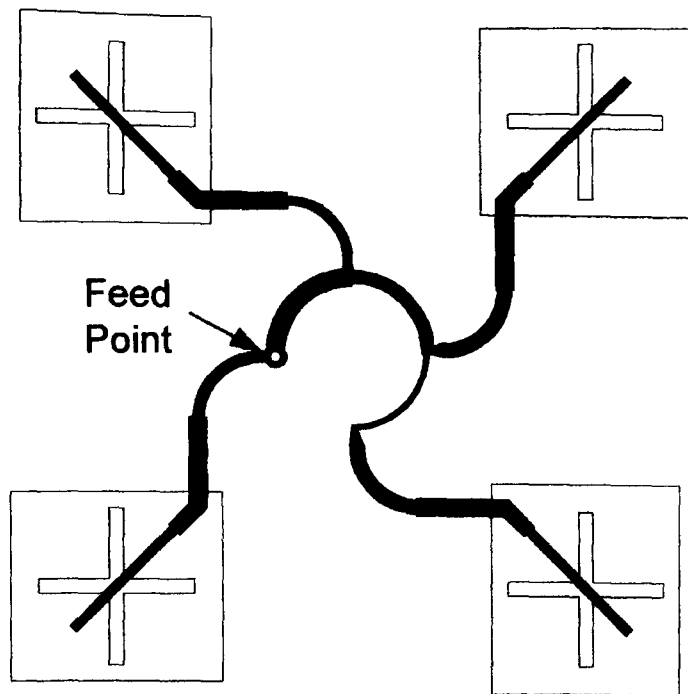
Figure 1 Configuration of the aperture-coupled patch array for left-hand circular polarisation

ARRAY DESCRIPTION

The configuration of the antenna array is shown in Figure 1.

The choice of radiating element is a left-hand circularly po-larised, single-feed, cross-slot, aperture-coupled, nearly square patch antenna that uses air for the antenna substrate [6]. An adaptation of the cavity model [7] was used to generate the design parameters detailed in Figure 2. The bandwidth of the radiating element can be increased further by using an aperture closer to resonance [8], however, this leads to more back radiation and may necessitate the use of another ground plane below the aperture [9] or a microstrip reflector element [10] to remove this unwanted radiation.

Each radiating element is spaced at 0.74λ and sequentially rotated 90° with respect to its immediate neighbour. The series feed compensates for this physical rotation by shifting the phase of each element's excitation by 90° while distributing the power equally to each element and maintaining an input impedance of 50Ω at the feed point at the design frequency. As there is no unique solution and no closed-form expression exists, the values of the feed impedances are optimised for minimum track width via an adaptation of simulated annealing [11].

As the feed network and radiating patch are implemented on separate substrates, both the thickness and dielectric properties of each substrate can be optimised independently in order to accommodate their conflicting requirements. While the thin feed substrate has a permittivity of 2.33, the thicker antenna substrate (air) has a lower permittivity of 1, thereby reducing spurious radiation from the feed and increasing the bandwidth of the radiating patch. The cross aperture is positioned below the centre of each patch, as this excitation symmetry helps to maintain good polarisation purity. The patch is isolated from the feed network by a ground plane, thus minimising the contribution of spurious feed radiation to the main radiation pattern, shown to be a potential problem in sequentially rotated arrays [12]. Using single-feed aperture-coupled radiating elements within an array excited by this compact series-feed network also maximises the space available when incorporating microwave circuitry on the low-loss feed substrate.

FABRICATION

The feed network was fabricated using a 0.79-mm 1/2-oz. RT 5870 Duroid. The nearly square patches were etched onto a standard 0.8-mm 1/2-oz. FR4 PCB radome. Using M2 nylon bolts, the radome is supported 2.6 mm above the apertures, which are etched into the ground plane of the feed substrate.

RESULTS

The integrity of the design has been confirmed over a frequency range of 4.5–7.5 GHz, using both full-wave simulation [13] and practical measurement. Measurements of input impedance were made using an Anritsu 37347C vector network analyser, confirming a VSWR 2:1 bandwidth of at least 22.8% from 5.28 to 6.6 GHz, as shown in Figure 3(a). Measurement of boresight axial ratio confirms left-hand circular polarisation with a 3-dB axial-ratio bandwidth of 17.5% between 5.44 and 6.45 GHz, as shown in Figure 3(b).

The radiation pattern at 5.8 GHz is shown in Figure 3(c), and the gain of the main lobe has been measured at 14.25 dBi with a 3-dB beam width of 30°. There is 14.5-dB difference between the main beam and side lobes seen at ±60° with nulls at 42° from boresight. At the extremities of the VSWR 2:1 bandwidth, radiation pattern symmetry deteriorates as correct power distribution and excitation phase deteriorate within the feed network.

This novel array configuration is shown to increase the input impedance bandwidth by a factor of 2.5 and the axial-ratio bandwidth by a factor of 6, compared with the monolithic 2 × 2 array using dual-feed radiating elements presented in [11].

CONCLUSION

A new wideband sequentially rotated 2 × 2 antenna array with an out-of-line series feed and aperture-coupled radiating elements has been presented. The use of aperture coupling with this compact series-feed network has increased both input impedance and axial-ratio bandwidth, while increasing the amount of real estate available for microwave circuitry. The performance of the array has been confirmed by full-wave simulation and experimental measurement, confirming a VSWR 2:1 bandwidth of 22.8% and a 3-dB axial-ratio bandwidth of 17.5%, a significant improvement over conventional designs.
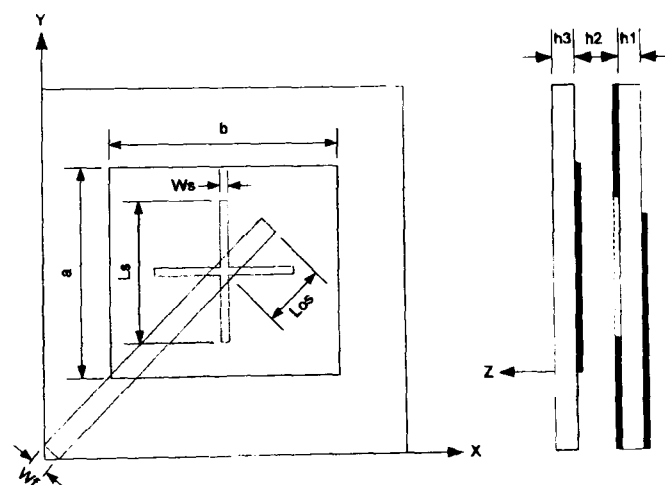

Figure 2 Radiating element design parameters $a = 15.3$, $b = 17.1$, $Ls = 12.5$, $Ws = 1$, $Los = 4.8$, $Wf = 0.5$, $h1 = 0.79$, $h2 = 2.6$, $h3 = 0.8$ (all dimensions in mm)
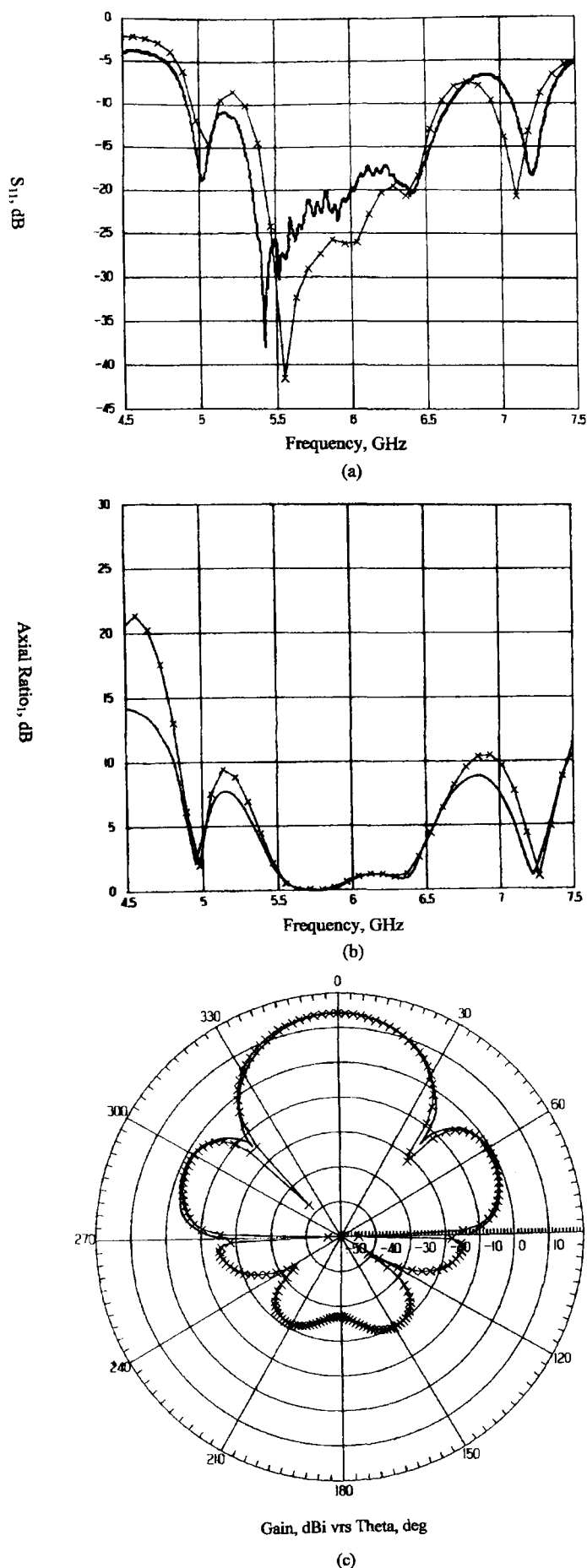
203

Gain, dBi vrs Theta, deg

(c)

━X━X━X━ Simulated
━━━━━ Measured

Figure 3 (a) Input impedance; (b) boresight axial ratio; (c) radiation pattern at 5.8 GHz

REFERENCES

1. C.A. Balanis, Advanced engineering electromagnetics, Wiley, New York, 1989, p. 722.
2. D.M. Pozar, A microstrip antenna coupled to a microstrip line, Electron Lett 21 (1985), 49–50.
3. T. Teshirogi, M. Tanaka, and W. Chujo, Wideband circularly polarised array antenna with sequential rotation and phase shifts of elements, Int Symp Antennas Propagat, ISAP 85, Tokyo, 1985.
4. P.S. Hall, J.S. Dahele, and J.R. James, Design principles of sequentially fed, wide bandwidth, circularly polarised microstrip patch antennas, IEE Proc H 136 (1989), 381–389.
5. H. Evans, P. Gale and A. Sambell, Performance of 4 × 4 sequentially rotated patch antenna array using series feed Electron Lett 39 (2003), 493–494.
6. T. Vlasits, E.K. Korolkiewicz, A. Sambell, and B. Robinson, Performance of a cross-aperture coupled single feed circularly polarised patch antenna, Electron Lett 32 (1996), 612–613.
7. B. Al-Jibouri, H. Evans, E.K. Korolkiewicz, A. Sambell and T. Vlasits, Cavity model of circularly polarised cross-aperture-coupled microstrip antenna, IEE Proc Antennas Propagat 148 (2001), 147–152.
8. S.D. Targonski and D.M. Pozar, Design of wideband circular polarised aperture coupled microstrip antennas, IEEE Trans Antennas Propagat 41 (1993), 214–220.
9. S.B. Chakrabarty, F. Klefenz, and A. Dreher, Dual-polarised wideband stacked microstrip antenna with aperture coupling for SAR applications, IEEE Antennas Propagat Symp Dig, Salt Lake City, UT, 2000, pp. 2216–2219.
10. S.D. Targonski, R.B. Waterhouse, and D.M. Pozar, Wideband aperture coupled microstrip patch array with backlobe reduction, Electron Lett 33 (1997).
11. H. Evans, P. Gale, B. Al-Jibouri, E.G. Lim, E. Korolkeiwicz and A. Sambell, Application of simulated annealing to design of serial feed sequentially rotated 2 × 2 antenna array, Electron Lett 36 (2000), 1987–1988.
12. P.S. Hall, Feed radiation effects in sequentially rotated microstrip arrays, Electron Lett 23 (1987), 877–878.
13. Ansoft Ensemble® V6.1, Method of Moments 2.5D EM field solver.

© 2004 Wiley Periodicals, Inc.

ON PATTERN STABILITY OF THE CROSSED PLANAR MONOPOLE

M. J. Ammann, R. Sierra Cordoba, M. Uzelac, J. A. Evans, and A. T. Schwarzbacher
School of Electronic & Communications Engineering
Faculty of Engineering
Dublin Institute of Technology
Kevin St., Dublin 8, Ireland

ABSTRACT: *It is shown that a significant improvement in the radiation pattern stability with frequency can be achieved for the wideband planar monopole antenna. This is realised by the addition of a second orthogonal element, while maintaining the same overall surface area.* © 2004 Wiley Periodicals, Inc. Microwave Opt Technol Lett 40: 294–296, 2004;

INTRODUCTION

As present and future digital communications systems develop, the demand on antenna parameters also increases. Heavy demands have been placed on antenna size, bandwidth, gain, patterns, and intermodulation performance. The quarterwave monopole antenna